DOCTOR OF PHILOSOPHY

Amino acids in oral drug delivery

salts, ion-pairs and transcriptomics

Amr Elshaer

2013

Aston University

AMINO ACIDS IN ORAL DRUG DELIVERY: SALTS, ION-PAIRS AND TRANSCRIPTOMICS

AMR MOHAMED MOHAMED KAMEL ABDELFATAH ELSHAER

Doctor of Philosophy

ASTON UNIVERSITY

December 2012

Aston University

Amino acids in oral drug delivery: salts, ion-pairs and transcriptomics

Amr Mohamed Mohamed Kamel Abdelfatah ElShaer
Doctor of Philosophy

Thesis Summary

Oral drug delivery is considered the most popular route of delivery because of the ease of administration, availability of a wide range of dosage forms and the large surface area for drug absorption via the intestinal membrane. However, besides the unfavourable biopharmaceutical properties of the therapeutic agents, efflux transporters such as P-glycoprotein (P-gp) and multiple resistance proteins (MRP) decrease the overall drug uptake by extruding the drug from the cells. Although, prodrugs have been investigated to improve drug partitioning by masking the polar groups covalently with pre-moieties promoting increased uptake, they present significant challenges including reduced solubility and increased toxicity.

The current work investigates the use of amino acids as ion-pairs for three model drugs: indomethacin (weak acid), trimethoprim (weak base) and ciprofloxacin (zwitter ion) in an attempt to improve both solubility and uptake. Solubility was studied by salt formation while creating new routes for uptake across the membranes via amino acids transporter proteins or dipeptidyl transporters was the rationale to enhance absorption. New salts were prepared for the model drugs and the oppositely charged amino acids by freeze drying and they were characterised using FTIR, ^{1}HNMR, DSC, SEM, pH solubility profile, solubility and dissolution. Permeability profiles were assessed using an *in vitro* cell based method; Caco-2 cells and the genetic changes occurring across the transporter genes and various pathways involved in the cellular activities were studied using DNA microarrays.

Solubility data showed a significant increase in drug solubility upon preparing the new salts with the oppositely charged counter ions (ciprofloxacin glutamate salt exhibiting $2.9x10^{3}$ fold enhancement when compared to the free drug). Moreover, permeability studies showed a 3 fold increase in trimethoprim and indomethacin permeabilities upon ion-pairing with amino acids and more than 10 fold when the zwitter ionic drug was paired with glutamic acid. Microarray data revealed that trimethoprim was absorbed actively via OCTN1 transporters while MRP7 is the main transporter gene that mediates its efflux. The absorption of trimethoprim from trimethoprim glutamic acid ion-paired formulations was affected by the ratio of glutamic acid in the formulation which was inversely proportional to the degree of expression of OCTN1. Interestingly, ciprofloxacin glutamic acid ion-pairs were found to decrease the up-regulation of ciprofloxacin efflux proteins (P-gp and MRP4) and over-express two solute carrier transporters; (PEPT2 and SLCO1A2) suggesting that a high aqueous binding constant (K_{11aq}) enables the ion-paired formulations to be absorbed as one entity.

In conclusion, formation of ion-pairs with amino acids can influence in a positive way solubility, transfer and gene expression effects of drugs.

Key words: Oral drug delivery, solubility, permeability, efflux transporters, ion-pairs, microarrays.

Acknowledgements

I would like to record my gratitude to Dr Afzal R Mohammed and Peter Hanson for their supervision, advice, availability, guidance and continuous support from the very early stage of this research as well as for the trust Dr Mohammed put on me to decide the direction of the research.

I gratefully acknowledge Dr Tony Worthington for his great contribution to the microbiology section and for his inspiring passion for science. And thanks to Noreen Akhtar for providing help during some of the compaction studies.

Special thanks goes to Mr Jiteen Kansara, Dr Michael Davis and Aston University technical staff for their technical support and assistance throughout my research.

Many thanks to Laine Wallace, Nil Turan and Dr Ayesha Rahman, I greatly benefited from their advice and they kindly made all the resources available to me at Birmingham University, genomic facility.

I would also like to thank Dr Defang Ouyang for his great help to perform the simulation studies of our ciprofloxacin salts.

It is also pleasure to pay tribute to my colleagues at Aston labs who created a friendly atmosphere during the research time.

Dedication

I dedicate my work to my family. With a special feeling of gratitude to my loving mother Kamilia Gad who encouraged me not only during my master program, but throughout my studying life, her push for tenacity and words of encouragements ring in my ears.

My sisters, Ola and Sammer and my brother Ahmed who never left my side. They are my role-model for personal sacrifices and are my emotional anchors through my entire life.

The memory of my father M. ElShaer who instilled in me the hard work, confidence, being tolerant and modest.

List of contents

List of tables

List of figures

Abbreviation list

IND	Indomethacin
TMP	Trimethoprim
CIP	Ciprofloxacin
A_n	Absorption number
D_n	Low dissolution number
APIs	Active pharmaceutical agents
GIT	Gastro Intestinal Tract
Py	Yield pressure
pK_a	Dissociation constant
ATP	Adenosine triphosphate
HUGO	Human Genome Organisation
ABC	ATP-binding cassette
SLC	Solute carrier transporters
P-gp	P-glycoprotein
NBD	Nucleoside-binding domains
MRP	Multi-drug resistance associated protein
ABCP/ ABCG2	Placenta specific ABC transporter
LAT	L-type amino acid transporter
BCCT	Betaine/Carnitine/Choline transporter
AGCS	Alanine/Glycine/Cation symporter
PEG 400	Polyethylene glycol
TEER	Transepithelial electrical resistance
ADMET	Absorption, distribution, metabolism, excretion and toxicity
SNP	Single nucleotide polymorphism
CGH	Comparative genomic hybridization
TMA	Tissue microarrays
D_2O	Deuterated water
TGA	Thermogravimetric analysis
FT-IR	Fourier Transform infra-red spectroscopy
DCPD	Dicalcium phosphate dehydrate
Fc	Crushing force
ε	Porosity
ρ_d	Bulk density
ρ_t	True density
σ_o	Zero porosity
VMD	Volume median diameter
Y	Yield strength
P_Y	Yield pressure
g	Gram
HCl	Hydrochloric Acid
HPLC	High Performance Liquid Chromatography
hr	Hour
kV	Kilovolt
L	Litre
log	Logarithm
mA	Milliampere
min	Minutes
mg	Milligram

µg	Microgram
Kg	Kilogram
ANOVA	Analysis of variance
DoE	Design of experiment
DSC	Differential scanning calorimetry
FDA	Food and Drug Administration
PM	Phyical mixture between the drug and amino acid
SM	Salt mixture between the salt form of the drug and amino acid

Thesis publications

Peer-reviewed articles

1. **Amr ElShaer**, Peter Hanson and Afzal R Mohammed., (2013). A systematic and mechanistic evaluation of aspartic acid as filler for directly compressed tablets containing trimethoprim and trimethoprim aspartate. *European Journal of Pharmaceutics and Biopharmaceutics. In press.*

2. **Amr ElShaer**, Peter Hanson, Tony Worthington, Peter Lambert and Afzal R. Mohammed., (2012). Preparation and Characterization of Amino Acids-Based Trimethoprim Salts. Pharmaceutics, 4, 1, 179-196

3. **Amr ElShaer**, Defang Ouyang, Peter Hanson and Afzal R Mohammed., (2012). Application of molecular simulation studies in the development of amino acid based pharmaceutical salts of ciprofloxacin. *Submitted*.

4. **Amr El Shaer**, Peter Hanson and Afzal R Mohammed., (2011). Improving the drug properties of chemotherapeutic agents through using amino acids. *UKICRS newsletter*.

5. **Amr ElShaer**, Sheraz Khan, Dhaya Perumal, Peter Hanson and Afzal R Mohammed (2011). Use of amino acids as counter ions improves the solubility of the BCS II model drug, indomethacin. *Curr Drug Deliv.* 8, 4, 363-372.

Book chapters

Afzal R. Mohammed, **Amr M. ElShaer**, Rhys J. Jones, Sheraz Khan, Craig A. Russell (2011). Drug Bioavailability and Gene Profiling: Challenges and Opportunities for Pharmaceutics and Personalised Medicine. *Handbook of Personalized Medicine: Advances in Nanotechnology, Drug Delivery and Therapy.*

Conference proceedings

1. **Amr ElShaer**, Peter Hanson and Afzal Mohammed. The use of amino acid based tablet fillers as solubility and permeability enhancers for BCS IV drugs., *UK Pharmasci*

2. **Amr ElShaer**, Peter Hanson and Afzal Mohammed., 2012. Ion pairing a BCS IV model drug with amino acids as solubility and permeability enhancers. UKICRS conference, Aston University, Birmingham, UK.

3. **Amr ElShaer**, Sheraz Khan, Ayesha S. Rahman, Peter Hanson, Yvonne Perrie, Afzal R. Mohammed., 2011., System biology evaluation of drug formulation: A tale of drug transporters., UKICRS, conference, Queen's university, Belfast, Northern Ireland.

4. **Amr ElShaer**, Peter Hanson, Tony Worthington, Peter Lambert, Afzal R Mohammed. 2011. Amino acids salts and drug resistance of chemotherapeutic agents. Aston University PG. Birmingham, UK.

5. **Amr M ElShaer**, Peter Hanson and Afzal R Mohammed., Feasibility of using amino acids as counter ions to study the solubility of indomethacin through salt formation. PG Day. Aston University, Birmingham, UK.

Oral presentations

Could amino acid salts fool fussy bacteria to improve antibiotics uptake? *UKICRS, Queen's University Belfast, April 2011*

Chapter 1

Introduction

Papers relating to chapter 1

Afzal R. Mohammed, **Amr M. ElShaer**, Rhys J. Jones, Sheraz Khan, Craig A. Russell (2011) Drug Bioavailability and Gene Profiling: Challenges and Opportunities for Pharmaceutics and Personalised Medicine. *Handbook of Personalized Medicine: Advances in Nanotechnology, Drug Delivery and Therapy.*

1.1. Introduction

Oral drug administration is considered the most popular route of delivery (Fig. 1.1.1) due to various factors including ease of administration, availability of large surface area for drug absorption and the wide range of dosage forms that can be designed to deliver active pharmaceutical ingredient/s (Sastry, et al., 2000). Despite the several advantages, physiological barriers such as degradation in the acidic environment of the stomach, presence of luminal digestive enzymes and most importantly the biopharmaceutical properties of the drug molecule limit oral drug bioavailability (Hunter & Hirst, 1997). Biopharmaceutical properties have gained significant attention after the introduction of high throughput drug discovery programmes which generate large numbers of new chemical entities (NCE) with unfavourable properties primarily due to the use of lipophilic screens in generating lead candidates. Therefore, improving biopharmaceutical properties and developing new methods to accurately predict these properties have gained considerable attention within the pharmaceutical industry.

Figure 1.1.8:- Contribution of various routes of administration in UK market (Aulton, M. E. 2002)

1.2. Biopharmaceutical classification system

Amidon et al. (1995) recognised that the rate and extent of oral bioavailability is controlled by aqueous solubility and gastro-intestinal permeability which led to the development of a

Biopharmaceutical Classification System (BCS) that categorizes all the drugs into four classes according to their permeability and solubility profile (table 1.1.1).

In 2000, the BCS system was accepted by the FDA as a scientific model to waive the *in vivo* bioequivalence and bioavailability testing for class 1 drugs that exhibit rapid dissolution and permeability (FDA guidelines). The main objective of BCS is to predict in *vivo* pharmacokinetics of drugs by measuring permeability and solubility characteristics. According to the BCS, a highly soluble drug is a substance which at its highest dose strength is soluble in 250 mL or less of aqueous media over a pH range of 1-7.5 at 37 ^{o}C while a highly permeable drug is a substance which exhibits an absorption profile of ≥ 90% of the total administered dose.

Class I (high solubility/high permeability drugs): drugs in this class dissolve rapidly when administered and are transported rapidly across the gastrointestinal membrane. The rate limiting step to drug absorption is the drug dissolution or the gastric emptying rate (when the dissolution is very fast).

Class II (low solubility/ high permeability drugs): drugs in this class are characterised by a high absorption number (A_n) and low dissolution number (D_n) and *in-vivo* drug dissolution is the rate limiting step. As the intestinal membrane and intestinal luminal contents vary along the intestine, the dissolution profile must be determined at 4-6 time points and at different physiological pH's. Examples of class II drugs include griseofulvin, indomethacin and ibuprofen (Wu & Benet, 2005).

Figure 1.1.9:- Classification of marked drugs and NCEs according to the Biopharmaceutical classification system (BCS) Aulton (2002).

Class III (high solubility/low permeability drugs); permeability is the rate limiting step in drug absorption. Therefore, it is important for class III drugs to be released rapidly from their formulations in order to maximise the residence time in the gastro-intestinal tract thereby improving their permeability.

Class IV (low solubility/low permeability); drugs in this class are characterised by poor permeability and poor solubility and as a result have very poor oral bioavailability. Use of a prodrug is a common approach to overcome this problem.

Table 1.1.12:- Biopharmaceutical classification system substrates adapted from Wu & Benet, (2005)

	High solubility		**Low solubility**	
High permeability	**Class 1** Acyclovir Amiloride [S,I] Amitryptyline [S,I] chloroquine [S,I] Diltiazem [S,I] Fluoxetine [I] Verpamil [I]	 Imipramine [I] Levofloxacin [S] Levodopa [S] Midazolam [S,I] Nifedipine [S] Quiniidine [S,I]	**Class 2** Azithromycin [S,I] Carbamazepine [S,I] Ciprofloxacin [S] Cyclosporine [S,I] Indinavir [S] Indomethacin	 Erythromycin [S,I] Talinolol [S] Spiranolactone [I] Ketoconazole [I] Digoxin [S] Cisapride [S]
Low permeability	**Class 3** Acyclovir Amoxicillin [S,I] Atenolol Cimetidine [S] Cloxacillin Famotidine Folinic acid	 Penicillins Methotrexate Trimethoprim [S] Metoformin Pravastatin Tetracyclin	**Class 4** Amphotercin B Colistin Ciprofloxacin [S] Hydrochlorothiazide Mebendazole Neomycin	 Methotrexate Furosamide

1.3. Factors affecting oral drug delivery

1.3.1. Physiological factors in the gastrointestinal tract that affect drug bioavailability

Gastrointestinal tract (GIT) physiology has a major effect on the bioavailability of active pharmaceutical ingredients (APIs). Physiological factors such as surface area, pH, gastric emptying rate, gastric motility and food are among the major factors influencing the rate and extent of drug bioavailability.

The surface area available for oral drug absorption varies along the gastrointestinal tract as shown in table (1.1.2). The small intestine is composed of three regions: duodenum, jejunum and ileum which posses the largest surface area for absorption. Therefore, the majority of oral absorption occurs in the small intestine. On the other hand, the small surface area of the stomach and colon limits the absorption in these organs.

Table 1.1.13:- Comparison of various physiological factors of the different regions of the gastrointestinal tract, which can affect the absorption of active drug ingredients. Adapted from Washington et al. 2001.

Section	Length (m)	Surface Area (m^2)	pH	Residence Time
Oesophagus	0.3	0.02	6.8	>30 seconds
Stomach	0.2	0.2	1.8-2.5	1-5 hours
Duodenum	0.3	0.02	5-6.5	>5 minutes
Jejunum	3	100	6.9	1-2 hours
Ileum	4	100	7.6	2-3 hours
Colon	1.5	3	5.5-7.8	15-48 hours

Another factor that influences oral bioavailability is the gastrointestinal pH. The pH of the gastrointestinal fluid varies from one region to another (between 1.8-7.8) along the GIT. Stomach has the most acidic environment (pH 1.8-2.5) because of the high concentration of hydrochloric acid secreted from the parietal cells of the stomach (Widmaier et al., 2011). The secretion of bicarbonate increases down the gastrointestinal tract and neutralizes the effect of hydrochloric acid and hence more alkaline conditions are observed along the small and large intestine (Aulton, 2002). pH influences ionisation and chemical stability of the therapeutic

agent depending on the acidity and basicity of the surrounding environment in the GIT (Aulton, 2002). The rate at which an API leaves the stomach and reaches the duodenum is called the gastric emptying rate. As the small intestine is the major site for oral drug absorption, reducing the rate of gastric emptying will delay the availability of the active drug at the absorption site which in turn will delay the onset of therapeutic effect. Besides, the dosage forms are believed to affect the rate of gastric emptying as for instance solid dosage forms have a pronounced influence when compared to the aqueous solutions (Gidal, 2006).

Intestinal motility is another physiological factor that affects drug bioavailability as it controls the residence time in the small intestine. Propulsive and mixing movements are the two types of motions encountered along the gastrointestinal tract. The propulsive movement is responsible for moving the materials through the GIT with slower propulsive movement increasing residence time in the small intestine. Mixing movements have a profound role in the fed state as it enables mixing the different food components which affect the residence time in the GIT and the dissolution rate of the drugs from solid dosage forms (Aulton, 2002).

Food has a direct and indirect effect on oral absorption and bioavailability of active pharmaceutical agents. Food consumption could reduce the gastric emptying rate and in turn delay drug uptake. Food also could stimulate the secretion of gastric fluids and enzymes which might degrade certain active ingredients. Moreover, dietary components might complex with the active drug to form a resultant bigger complex with reduced absorption characteristics leading to decrease in bioavailability. For instance tetracycline antibiotics form a non-absorbable complex with calcium (found in dairy products) which requires patient counseling to prevent reduced drug efficacy (Aulton, 2002). Similarly, the viscosity of gastrointestinal contents increases after food consumption which reduces drug dissolution and decreases oral bioavailability.

1.3.2. Effect of dosage form on drug bioavailability

The pharmaceutical dosage form and its method of manufacture may have an impact on oral bioavailability of the therapeutic agents. Maximum bioavailability is exhibited by aqueous dosage forms as the active pharmaceutical ingredients (APIs) are available in solution and ready for absorption into the systemic circulation. Nevertheless, it is not possible to formulate most APIs as oral solutions because of stability related issues and inherent properties of the drugs which affect their aqueous solubility.

Aqueous suspensions are placed in the second position after solutions. High bioavailability is achieved due to the larger surface area of drug presented to the gastrointestinal fluid which provides the necessary conditions for drug dissolution and absorption into the systemic circulation. There are various factors which affect drug release from aqueous suspensions including the crystalline form of the drug, particle size and effective surface area of the suspended drug particles, viscosity of the suspension in the gastrointestinal fluid and the inclusion of any surfactants (Aulton, 2002).

Hard gelatin capsules are rated below suspensions and are a suitable delivery system for poorly soluble API as they provide large effective surface area for the drug in the gastrointestinal fluid. Hydrophilic diluents such as lactose are added into hard gelatin capsules in order to enhance dissolution of API. Other factors such as the nature and quantity of the diluents, surfactants or any added lubricants also determine the bioavailability of the drug.

Among the dosage forms listed above, tablets are rated at the bottom of the table. Compression of the API with various pharmaceutical excipients into tablets results in a significant reduction in effective surface area of an active drug ingredient due to the manufacturing process. The reduction in the effective surface area has a negative impact on drug bioavailability as it becomes more difficult to produce a suspension of fine drug particles

from the compressed form. Before active ingredients undergo dissolution and become available for absorption from tablets, they undergo disintegration to form aggregates or granules followed by deaggregation to form suspension of drug particles. Tablet excipients and the manufacturing cycle have a significant impact on drug release from compressed formulations and affect bioavailability of the drug.

Despite providing less bioavailability when compared against aqueous solution, suspensions and hard capsule dosage forms, tablets have achieved tremendous success since their introduction because of the various advantages they provide. Tablets can be easily handled, manufactured by various methods, produced at low cost, have more enhanced chemical, mechanical and microbiological stability than liquid formulations and can be modified to provide differing dissolution profiles.

The tablet manufacturing cycle usually includes weighing, milling, granulation, blending, lubrication and compression. Direct compression is considered the simplest process in tablet manufacture as it requires no heat or moisture. However, the physical properties of the active ingredient and pharmaceutical excipients such as compactibility limit the use of direct compression especially for drugs of low potency where a high dose is required

1.3.2.1. Excipients used in tablet manufacture

Tablets contain a mixture of various excipients in addition to the active pharmaceutical ingredients (API). The inclusion of various excipients ensures the success of the tablet manufacturing process and the quality of the final product. Therefore, appropriate selection of the excipients including accurate concentrations is critical in the tableting process. Most commonly used excipients include fillers (diluents), binders, lubricants, glidants, disintegrants, colorants and flavouring modifiers.

1.3.2.1.1 Diluents

Diluents/fillers are usually added into the tablet mix to bulk up the formulation for processing and handling. The diluents should have an acceptable taste, be chemically inert and non hygroscopic (Aulton, 2002). Lactose, sucrose, microcrystalline cellulose and glucose are among the commonly used diluents. Various grades of these fillers are commercially available and each grade has its characteristic physical properties which can be exploited depending on the requirements of the finished dosage form. For instance, fine grades of lactose are used for milling and wet granulation as they enhance the performance of milled excipients (Aulton, 2002). Lactose is widely used as a tablet filler because of its pleasant taste, its ability to dissolve readily in water and good compactability properties. It is available in both amorphous and crystalline form and the former is prepared by spray drying while the latter by precipitation.

Microcrystalline cellulose, also known as Avicel is a widely used filler. Avicel is a depolymerised cellulose prepared by treating cellulose with mineral acids. Besides, being used as filler, it is used as a binder and disintegrant in tablet manufacture (Aulton, 2002).

1.3.2.1.2. Binder

In order to improve cohesive and adhesive forces between different ingredients within the powder mixture and to ensure the formulation of an intact tablet, a binder (adhesive) is added to the formulation mixture. The binder should be able to cohere various excipients without impairing the disintegration and dissolution properties of the tablets. Sucrose, gelatine and starch are the most commonly used binders in the concentration range between 2- 10% w/w (Aulton, 2002).

1.3.2.1.3. Disintegrants

A disintegrant is usually added to tablets to overcome the impaired cohesion during the compression process and in turn facilitate tablet disintegration. Disintegration takes place in

two stages; during the first step the liquid wets the solid surface of the tablet and penetrates through the tablet pores, which results in the second phase of tablet disaggregation. Various mechanisms of disintegration have been proposed including wicking, enhanced wettability and swelling (Alderborn, 2002).

1.3.2.1.4. Lubricants

High friction between the tablet and die wall emerges as a result of the high compression force applied during tablet compaction. This high friction results in a series of problems such as capping and even tablet fragmentation. Incorporation of a lubricant in the tablet mix forms an intermediate film of low shear strength between the die wall and the tablet interface which facilitates tablet ejection and reduces tablet deformation (Alderborn , 2002).

Magnesium stearate is the most widely used lubricant at a concentration range between 0.25-0.5% and sometimes up to 1%. Nevertheless, using lubricants can have negative effects on tablet manufacture. Lubricants can interfere with the bonding properties of the binder which could impair tablet hardness. Moreover, the majority of the used lubricants are hydrophobic in nature, thus they retard tablet disintegration and dissolution.

1.3.2.1.5. Glidants

Glidants may be required in tablet manufacture especially when high production speed is employed. Glidants are fine particles which are mixed with the powder in the dry state before compression. Collidal silica, talc and starch are examples of the glidants.

1.3.2.2. Tablet characterisation

Directly compressed tablets are prepared by applying high pressure onto a bed of powder which results in the formation of new bonds between particles or granules forming a coherent

compact. Both the manufacturing process and the properties of used materials affect the characteristics of the resultant tablets e.g. disintegration time, mechanical strength and drug release profile.

1.3.2.3. Tablet preparation

During powder compression, the bulk volume of the powder decreases as the air between the particles is displaced. Reduction in the amount of air enables the particles to get closer to each other and promotes bond formation by an exothermic process (Rowling et al., 1995; Coherin Beach and Hollenbelk, 1985).

Joiris et al. (1998) presented insights into the commonly applied terminology in tablet preparation. Compressibility was defined as the ability of the material to undergo a volume reduction upon exposure to pressure. Plotting tablet porosity against compaction pressure produces a compressibility profile of the material. Similarly, compactability describes the entire process, and was defined as the ability of material to produce tablets with sufficient hardness after densification. Compactability can be represented by plotting tablet tensile strength against porosity. Finally, the ability of materials to form a tablet of specified mechanical strength under the effect of compaction force was known as tabletability.

When compressing a powder bed at low compaction pressure, the particles rearrange themselves to form a closely packed structure. As the compression pressure increases further, the particles fail to undergo further rearrangement and volume reduction is achieved by elastic and plastic deformation or fragmentation of the particles (Train, 1956; Duberg & Nystrom, 1986).

Plastic deformation results in permanent change of particle shape as it is an irreversible process, while elastic deformation is a reversible process and particles can resume their

original shape. Brittle particles which cannot undergo plastic or elastic deformation break down into smaller units (fragmentation).

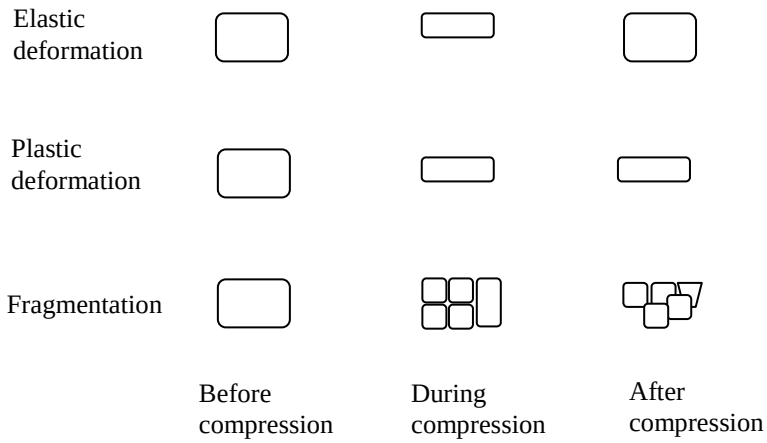

Figure 1.1.10:- Diagram showing various types of deformation occurring during powder compaction.

Both mechanical properties and mechanism of volume reduction affect the degree of volume reduction. For instance, brittle particles which fragment extensively produce tablets with high porosity as it creates more bonding points which prevent further volume reduction. However, ductile materials produce tablets with relatively low porosity as a high degree of plasticity enables particles to move close to each other and results in less a porous structure.

To describe the volume reduction behaviour of a powder, various mathematical equations were developed including the Heckel, Kawakita and Cooper-Eaton equations. These equations evaluate the effect of applied pressure on the porosity changes of the tablets.

The Heckel analysis (Heckel, 1961a; Heckel, 1961b) is considered one of the most valuable methods to describe powder behaviour during compaction. In the Heckel equation, the material constant K measures material plasticity and can be calculated from the slope of the linear portion of Heckel plot. The reciprocal of the material constant is known as the yield

pressure (Py). Initial filling of the die and rearrangements of the particles are represented by constant A.

$$\ln(1/(1-D)) = KP + A$$

Where D is the tablet relative density at pressure P, K is a material constant

Two methods can be used for Heckel analysis; the in-die and out-of-die method. For the in-die method (at-pressure) the relative density is calculated at the applied load. Despite being suitable for materials that have difficulties in forming intact compacts (due to capping), the elastic deformation affects the K values and hence the Py value is the apparent mean yield pressure.

The out-of-die method (zero-pressure) measures the relative density after tablet ejection from the die. Therefore, materials are pressed at different compression forces to construct a plot between D and P. The only drawback for the out-of-die method is the laborious and time consuming experimental set up (York, 1979; Duberg & Nystrom, 1986).

1.3.2.4. Bonding mechanisms

The five main types of bonding mechanisms include formation of solid bridges, bonding due to movable liquids, non-freely movable binder bridges, shape-related bonding and attraction between solid particles. During powder compaction, it is believed that the bonding is restricted to formation of solid bridges, intermolecular forces and shape related bonding (mechanical interlocking) (Alderborn, 2002).

Solid bridges are formed in materials with mobility in the contact area. The movement is either due to the dissolved state under the effect of multi molecular solvent sorption layer or from the fused state under the effect of heat. The strength of the formed solid bridges depends on the internal strength of the particles and separation of the resultant aggregates is irreversible.

On the other hand, mechanical interlocking occurs when materials are able to hook and twist together. This kind of bonding depends on the shape and surface features of the particles and is predominant in needle shaped fibres and irregular particles that have a higher tendency to twist and hook during compaction.

1.3.3 Effect biopharmaceutical drug properties on oral bioavailability

Biopharmaceutical properties such as aqueous solubility and drug permeability across the intestinal membrane are believed to be the main determinants of oral drug bioavailability.

1.3.3.1 Solubility

Both aqueous solubility and dissolution are important factors which affect bioavailability as insoluble drug candidates which show poor solubility during their transit of the GIT are eliminated without entering the systemic circulation (Aungst, 1993). Currently, there is a general consensus in the pharmaceutical industry that the majority of new drug candidates are poorly water soluble (Lipinski et al., 1997; Lipinski, 2000) with intrinsic solubility values of less than 1 µg/mL (Li et al., 2005). Various physical techniques such as particle size reduction, complexation with cyclodextrins or surfactants and dispersing a drug into a carrier have been adapted in order to improve drug solubility. Chemically modified drugs (salts and prodrugs) have also been shown to enhance solubility.

1.3.3.1.1 Physical modification to improve drug solubility.

Many studies have demonstrated that particle size reduction can increase the rate of dissolution and oral bioavailability of poorly soluble drugs such as progesterone (Hargrove et al., 1989), estradiol and estrone (Englund and Johansson, 1981), oxfendazole (Shastri et al., 1980) proquazone (Nimmerfall and Rosenthaler, 1980) and nitrofurantoin (Watari et al., 1983). Size reduction results in increasing the specific surface area and consequently the dissolution rate (Noyes and Whitney, 1897). However, agglomeration could take place upon milling

especially with hydrophobic drugs such as aspirin and phenobarbitone. The formed aggregates decrease the effective surface area and reduce the bioavailability. Ball milling, micronization (using impact mills and fluid energy mills) and spray drying are commonly used techniques in size reduction.

Solid dispersion formation is another technique for improving drug solubility. The first generation of solid dispersion was first described in the early sixties by Sekiguchi & Obi (1961) when it was observed that formation of eutectic mixtures improved drug bioavailability by reducing the drug particle size and improving its wettability in the eutectic mixture. This was followed by the application of urea as a water soluble carrier for poorly soluble drugs such as chloramphenicol (Sekiguchi & Obi, 1964) and sulfathiazole (Sekiguchi & Obi, 1961). In the mid sixties, Goldberg et al., (1966) demonstrated that crystalline carriers such as mannitol and crystalline sugars release the drug as microcrystals which possess higher solubility.

Studies conducted by Simonelli et al., (1969); Chiou & Riegelman (1969) found that solid dispersions using crystalline carriers are thermodynamically stable and less effective. Therefore, the use of new amorphous carriers such as polymers was investigated and was later referred to as second generation solid dispersions. Synthetic polymer carriers such as povidone, polyethyleneglycol or natural polymers such as cellulose derivatives (Vasconecelos et al., 2007) were investigated in the formation of solid dispersion compacts (Van Drooge et al., 2006).

Recently, it has been suggested that inclusion of carriers with surface activity or self emulsifying properties could have a greater impact on the dissolution profile of poorly soluble drugs. Consequently, the third generation of solid dispersions were formulated which included surfactants like intutec SPI and inulin (Van Drooge et al., 2006).

Inclusion complexes (host-guest complexes) were found to exert a profound effect on the physicochemical properties of their guest molecules since the guest molecules are caged and locked inside the host cavity. These properties include; taste masking, controlled drug release,

control of sublimation and volatility, stabilization of labile guest and importantly enhancing the solubility of highly insoluble guests (Del Valle, 2004). Cyclodextrins are commonly used as hosts due to their ability to form inclusion complexes with a wide range of guest molecules including gaseous, liquid and solid compounds. Cyclodextrins are cyclic oligosaccharides consisting of eight, seven and six α (1, 4) linked glycosyl units to form α, β, γ-cyclodextrins respectively. There are two key factors which determine the ability of cyclodextrins to form the inclusion complex; steric factors which depend on the relative size of guest molecules or functional groups within the guest molecules and secondly, the thermodynamic interaction between the different components (cyclodextrin, solvent, guest) (Del Valle, 2004).

1.3.3.1.2. Chemical modifications to improve drug solubility

Various approaches have been investigated to improve drug properties without altering therapeutic activity. Chemical based approaches which work on the principle of drug derivatization were very effective in improving drug efficacy. A commonly used chemical approach which utilises reversible derivatives is the synthesis of a prodrug. Prodrugs (proagents) were first discussed by Albert in the late 1950s and the technique gained significant attention in 1975 as a tool to optimise and enhance the clinical application of drugs (Amidon, 2000). The theory behind prodrug synthesis is based on the addition of a functional group on to the structure of the poorly water soluble drug to enhance its solubility. This functional group is modified chemically or enzymatically *in-vivo* to release the parent drug. A commonly used functional moiety is a phosphate group by linking directly or through a linker to the parent drug (Stella, 1996). The main advantage of using a phosphate group is its good chemical stability and rapid quantitative *in-vivo* cleavage by alkaline phosphatase (Burstein et al., 1999). Stella et al., (2005) utilised phosphate group to prepare a phosphoryloxymethyl ether prodrug of propofol (general anaesthesia) which is believed to be pain free and avoids any hyperlipidemia problems when prepared in a purely aqueous vehicle. The Hemi-succinate

group is another promoiety which was used to prepare prodrugs of chloroamphenicol, prednisone and methylprednisone (Kauffman et al., 1981).

During the last few decades amino acids have been investigated widely as promoieties to improve the aqueous solubility of poorly soluble amine and alcohol based drugs (Kovach et al., 1975; Amidon et al., 1980; Aggarwal et al., 1990; Upshall et al., 1990). In 1995 Pochopin et al., investigated the solubility and stability of dapsone upon conjugation with alanine, lysine, leucine, glycine and phenylalanine. The study concluded that all the amino acid prodrugs showed at least a 2 fold increase in solubility. The lysine prodrug exhibited the highest solubility (greater than 65 mg/mL) which was attributed to its γ–amine which becomes protonated at physiological pH (Pochopin et al., 1995). Another successful study was carried out by Hatchinson et al., (2002) which included conjugating benzothiazoles with lysine and alanine that converts the highly lipophilic benzothiazoles into water soluble prodrugs.

1.3.3.1.2.1. Salt formation

As discussed above, most of the NCE's possess poor mechanical and physicochemical properties which present significant formulation challenges (Forbes et al, 1995). Salt formation is considered a potential solution to optimise properties for drug candidates which have ionisable groups. Both the physicochemical characteristics and biological performance of the drug differ considerably for the salt form when compared to the free drug (Bighley et al., 1996). However, the selection of counter ions (salt forming ions) is carried out empirically based on a range of criteria including ease of crystallization, percentage yield, hygroscopicity and flowability (Berge et al., 1977).

Many studies have investigated the relationship between salt properties and the counter ions used. Yet, to date no successful predictive tool for estimating the effect of the salt former on the behaviour of the parent compound has been reported. Stahl & Wermuth, (2002) suggested

that the dissociation constant (pK_a) is the most important property of the drug that influences salt formation and the selection of the counter ion is based on the difference in pKa between the parent molecule and the counter ion (minimum difference between the salt former and counter ion should be 3 pK_a units).

Salt formers are divided into different categories according to their functionality and purpose. Table 1.1.3 summarises some of the commonly used potential salt formers.

Table 1.1.14:- Classification of common pharmaceutical salts (adapted from Bastin et al., 2000).

Salt class	examples
	Anions
inorganic acids	hydrochloride, hydrobromide, sulfate, nitrate, phosphate
sulfonic acids	mesylate, esylate, isethionate tosylate, napsylate, besylate*g*
carboxylic acids	acetate, propionate, maleate, benzoate, salicylate, fumarate
anionic amino acids	glutamate, aspartate
hydroxyacids	Citrate, lactate, succinate, tartrate, glycollate
fatty acids	hexanoate, octanoate, decanoate, oleate, stearate
insoluble salts	pamoate (embonate), polystyrene sulfonate (resinate)
	Cations
organic amines	triethylamine, ethanolamine, triethanolamine, meglumine, ethylenediamine, choline
insoluble salts	procaine, benzathine
metallic	sodium, potassium, calcium, magnesium, zinc
cationic amino acids	arginine, lysine, histidine

Hydrochloride is one of the popular salt formers used for weakly basic drugs because of its low pKa value. However, hydrochloride salts could salt out and in turn reduce the optimal solubility, causing high acidity in the formulations and greater corrosion risk (Bastin et al., 2000). Due to the limitation on the use of inorganic ions, alternative counter ions have been explored lately. Pellegate, (1993) investigated lysine, ornithine and arginine to prepare novel salts of furosemide. The prepared salts exhibited very high solubility up to 560 mg/mL for the lysinate salt which was much higher than furosemide itself and even its sodium counterpart. In another study, L-arginine was used to solubilise ionosine and lysine was tested for salt formation with ibuprofen (Tung et al., 1991)

1.3.3.2. Permeability

Oral drug bioavailability is an important parameter for new drug candidates under the drug discovery investigation programme. Once the new drug candidate is identified based on its pharmacological response, the following critical stage is to investigate its *in vitro* permeability. Further development is unlikely to take place if the drug is found to have poor permeability or absorption and as a result a great deal of interest is dedicated to study and enhance drug permeability (Egan and Lauri., 2002).

1.3.3.2.1. Anatomy and physiology of the small intestine.

The human small intestine ranges between 2-6 m in length and is divided mainly into three parts; duodenum, jejunum and ileum. Around 90% of the gastrointestinal tract absorption takes place in the small intestine. The intestinal surface has a unique structure which makes it suitable for absorption. The surface is covered by villi and microvilli which increase the intestinal surface area by 30 and 600 fold respectively (Balimane, et al., 2000).

The main role of the small intestine is to serve as a site of absorption for nutrients. It also works as a barrier which prevents the entry of any foreign substance or digestive enzymes. The absorptive cells or enterocytes are the most common epithelial cells which are differentiated into apical and basolateral membrane and separated by tight junctions (Balimane, et al., 2000).

1.3.3.2.2. Mechanisms and transport routes of drug absorption in the gastrointestinal tract

After the drug enters into the solution form that is suitable for absorption across the gastrointestinal membrane, a number of transport routes are available for drug permeation from the apical to the basolateral side. The major routes of drug uptake include transcellular, paracellular, efflux and metabolism based drug absorption as illustrated in Figure 1.1.4.

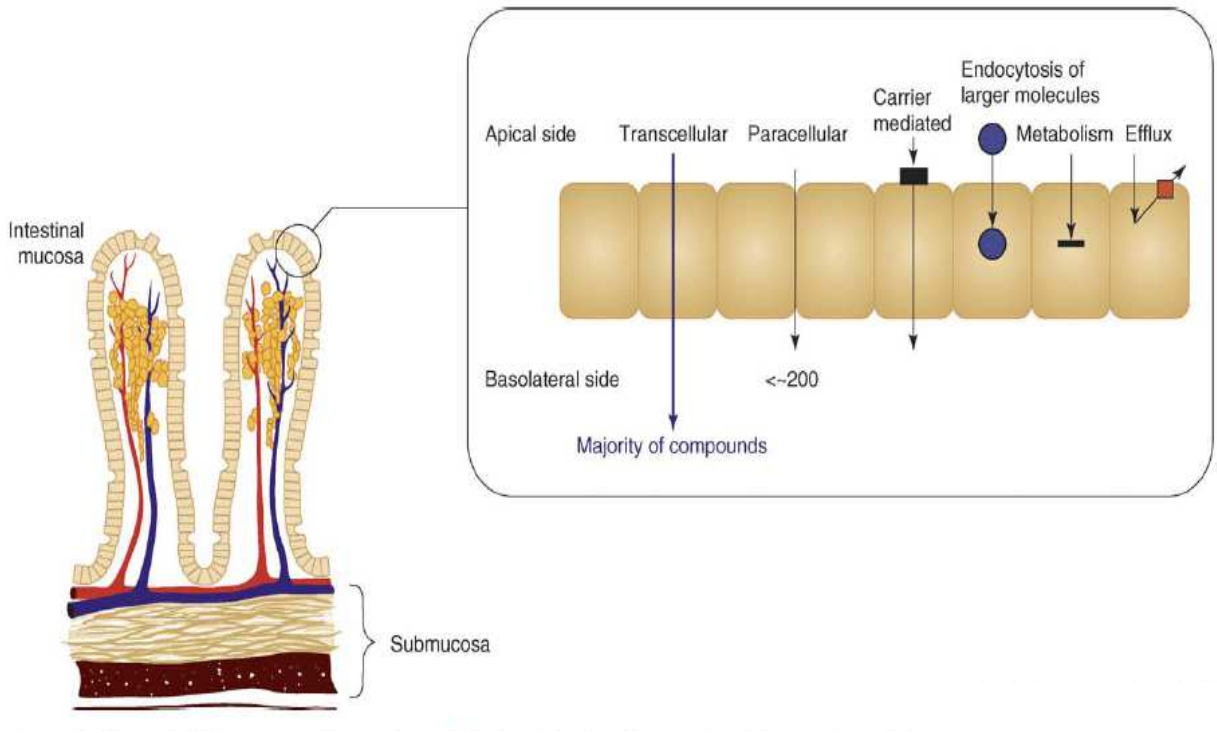

Figure 1.1.11:- Structure of intestinal wall showing the various mechanisms of oral absorption, adapted from Hamalain & Frostell-Karlsson, (2004).

The majority of the therapeutic agents are absorbed through the transcellular route by passive diffusion through the lipid membranes of the intestinal mucosa. Drug molecules with smaller molecular mass (<500 Daltons) capable of forming hydrogen bonds and exhibiting high lipophilicity move from regions of high concentration to lower concentration i.e. down the concentration gradient before entering into the blood circulation.

Another known passive diffusion mechanism for drug uptake is through the paracellular route. Drug candidates reach the basolateral side by travelling through the water filled pores between the tight junctions of the adjacent epithelial cells. Molecules transported via this route should be polar with a molecular weight less than 250g/mol (Dressman et al., 2010).

Drugs can also be transported against their concentration gradient via a transporter route known as active transport. Adenosine triphosphate (ATP) provides the energy required for absorption by the active transporters which involves binding of the drug with the carrier that

results in conformational changes in the cellular membrane and helps in the transport of the drug into cell lumen (Dressman et al., 2010).

Large drug molecules such as antibodies, hormones and proteins which cannot bind to transporter carriers or enter the cells via transcellular or paracellular routes get absorbed via endocytosis. The drug molecule is enclosed by the lipid membrane on the apical side to form a vesicle which travels across the cell and exits by fusing with the lipid membrane on the basolateral side (Dressman et al., 2010).

1.3.3.2.3. Carrier mediated transporters

The majority of the previous studies investigating drug absorption across the intestinal membrane suggested that drug transportation occurs predominantly via paracellular transport and passive transcellular mechanisms (Stenberg et al., 2000) in which the lipid solubility of the drug is the critical determinant. However, water soluble compounds such as amino acids, sugars, monocarboxylic acids, organic cations and anions, phosphates and water-soluble vitamins were found to cross cell membranes via specialized carrier mediated transporter (Ling and Thompson, 1974)

Human gene sequence analysis has demonstrated the presence of 406 genes which encode for ion channels and 883 genes which encode for transporters (350 of which encode for intracellular transporters). The Human Genome Organisation (HUGO) has approved 52 ATP-binding cassette (ABC) genes and 229 solute carrier transporters (SLC). More than 200 of these genes have been cloned and characterised including peptide transporters, amino acid transporters and neurotransmitter transporters (Shin et al., 2003)

Membrane transporter proteins are classified into channels and carrier mediated transporters. Carriers are further classified into facilitated diffusion, primary and secondary active transporters according to the energy requirements (Stenberg et al., 2000).

Primary active transporters extrude the substrates from the cell against its concentration gradient utilising energy derived from the conversion of ATP into ADP by ATPase. On the other hand, secondary active transporters (solute carrier transporters) utilize the energy generated by ion pumps (Na^+/K^+ ATPase) during transportation of Na^+ and Ca^{+2} ions across the membrane.

Membrane Transporters

1.3.3.2.3.1. ATP-binding cassette Transporters (ABC)

ABC transporters were first discovered as drug-resistance proteins (Gottesman et al., 2002) and a correlation between expression of ABC transporters and cancer drug resistance has been known for more than 25 years (Huang and Sadee, 2006). A diverse number of substrates are transported across the cell membrane by ABC transporters. To date, around 52 ABC transporter genes have been identified and grouped according to their structural homology into seven groups (from A to G). ABC transporters are classified according to their predicted two-dimensional structure into four classes (Figure 1.1.5). The first class was defined after the discovery of P-glycoprotein (P-gp) in 1976 (Juliano & Ling, 1976).

Transporters in the first class consist of two identical halves and each half contains 6 putative transmembrane segments and two cytoplasmic nucleoside-binding domains (NBD); these two domains bind and enable the hydrolysis of ATP and N-glycosylation occurs in the first extracellular loop of P-gp. The second class has a similar structure to that of the first and the only difference is the N-glycosylation site as it takes place in the fourth extracellular loop. This class includes transporters such as MRP4 and MRP5 (mammalian). The third class has

additional 5 putative transmembrane segments towards the N-terminus. Additional glycosylation takes place on the new extracellular loop. Recently, a new ABC transporter known as BCRP was discovered which was found to have a single intracellular ATP binding site at N-terminus, followed by 6-putative transmembrane segments with N-glycosylation on the last extracellular loop. Due to its unique conformation and arrangement in the plasma membrane, BCRP is also known as a half-transporter (Figure. 1.1.5).

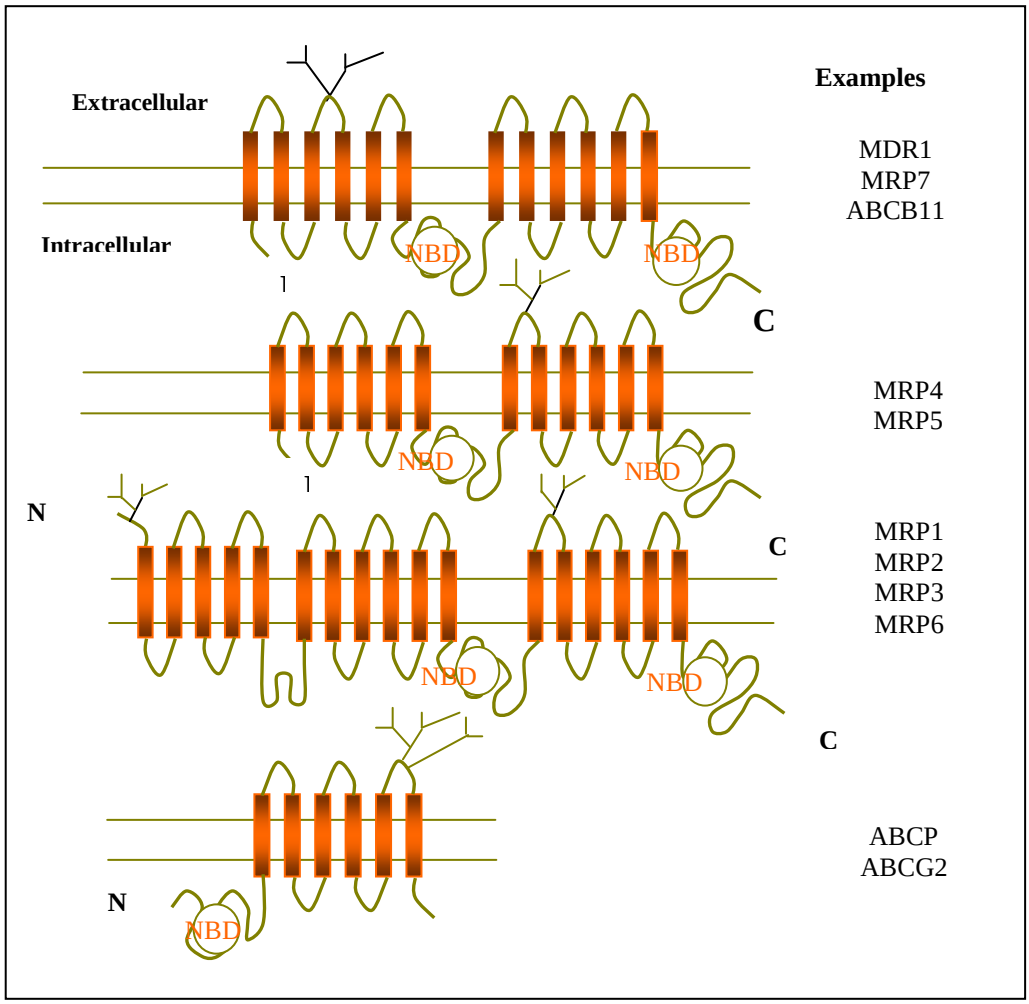

Figure 1.1.12:- Structure of ABC transporters which confer drug resistance adapted from Mohammed et al., 2012.

1.**3.3.2.3.1.1. P-glycoprotein**.

P-gp is also known as ABCB1 or MDR1 and is the first and most characterised ABC transporter. P-gp is expressed in the blood brain barrier, apical membranes of excretory cells such as hepatocytes and the epithelial cells in kidney proximal tubules and luminal membrane of the small intestine (Giacomini et al., 2010). The mRNA levels of P-gp increase longitudinally along the intestine with the lowest level in the stomach and highest levels in the colon (Wacher et al., 1998). P-gp drew great attention when it was found to interact with multiple anticancer drugs and mediated the efflux of a wide range of therapeutic drugs across biological membranes. Polyaromatic hydrophobic drugs with positive or neutral charges are common substrates for P-gp (Huang and Sadee, 2006). Not only conventional anti-cancer drugs (e.g. methotrexate), but newly developed drugs such as geldanamycin (Huang et al., 2004) and gleevec (Mahon et al., 2003) were found to be effluxed by P-gp. Talinolol (intermediate lipophilic B-blocker) is an extensively studied P-gp substrate. Although the metabolic clearance of talinolol is negligible and the drug is excreted unchanged in faeces and urine, talinolol oral bioavailability is just over 50% which suggests that the drug is not completely absorbed from the gastro-intestinal tract (GIT). Despite the acceptable physico chemical properties and in vitro permeability profile of talinolol, the basolateral to apical flux was greater by 10 fold compared to apical to basal flux (Wetterich et al., 1996). The efflux pattern was reduced upon inclusion of P-gp inhibitors such as verapamil providing further evidence of the efflux mechanism of talinolol. P-gp knockout mice were used in a study carried out by Schinkel et al to evaluate the role of P-gp in limiting the oral bioavailability of its substrates (Schinkel et al., 1997). The results showed that the wild type mice had an oral bioavailability of less than 5% for UK-22,671 (new compound) while P-gp knockout mice resulted in a higher bioavailability (22%).

In order to improve the permeability of P-gp substrates, its activity is inhibited or modulated through the use of drugs or chemicals. P-gp modulation is achieved either indirectly, by inhibiting; the hydrolysis of ATP, binding to ATP or directly through interaction with P-gp binding sites. The indirect method is not feasible as the chemical agent could adversely affect other ATPases. Pharmacokinetic interactions of P-gp substrates were reported and the number is on the rise as, for instance cardiac patients who are on digitoxin and quinidine could show digitoxin toxicity as the plasma concentration of digitoxin (which has a narrow therapeutic window) increases by at least three fold (Shin et al., 2003). P-gp substrates and inhibitors are summarised in Table 1.1.4.

Since P-gp is not expressed in all multi-drug resistance cells, research groups have explored other efflux transporters which resulted in the discovery of a protein referred as multi-drug resistance associated protein1 (MRP1). MRP1 (ABCB1) was found to confer resistance to anionic and neutral hydrophobic natural products such as vinca alkaloids and anthracyclines (Kruh and Belinsky 2003). Glutathione is a MRP1 substrate and is believed to play a major role in MRP1 activity (Leslie et al., 2001). Despite showing potential *in vitro*, isoxazoles (MRP1 inhibitors) exhibit limited *in vivo* effects due to their side effects and low bioavailability. Further investigation of MRP homologues led to the discovery of eight new members of MRP sub families including MRP-2 to MRP9 (Huang and Sadee, 2006).

Another cancer resistance protein that has been investigated is ABCG2 known as placenta specific ABC transporter (ABCP). ABCG2 mediates the transportation of negatively and positively charged hydrophobic molecules such as topotecan, flavopiridol, mitoxantrone, methotrexate and rhodamine (Doyle & Ross 2003). Interestingly, ABCG2 was found to exhibit polymorphism which in turn affects its interaction with the substrates. For instance, ABCG2 shows more resistance to mitoxantrone and anthracyclines upon its mutation. Yet, mutated

ABCG2 fails to transport methotrexate (Volk & Schneider 2003). Table 1.1.4 summarises other members of the ABC transporter family which have been shown to confer drug resistance.

Table 1.1.15:- Location and functions of ABC transporters (Huang and Sadee, 2006).

1.3.3.2.3.2. Solute carrier transporter (SLC)

Solute carrier transporters are another super family of membrane transporters. Approximately, 300 SLCs genes have been cloned and clustered into 43 families. SLCs mediate the transportation of hydrophilic moieties such as sugars, organic cations, anions, phosphates,

metals, monocarboxylic acids, water soluble vitamins and drugs with structures that resemble natural substrates (Huang and Sadee, 2006).

Folate transporter (SLC19 family) was the first reported SLCs to be studied in conjunction with anti-cancer drugs. Resistance to antifolate drugs such as methotrexate was reported *in vitro* in cancer cells; these cells have showed loss of SLC19A1 activity due to mutation. Also, the expression of SLC19A3 was found to be down regulated in breast cancer cells and as a result these cells were resistant to doxorubicin (Liu et al., 2003).

Nucleoside transportation also takes place through SLCs mainly via the SLC28 family; concentrative CNTs and SLC29 family. The former is distributed in tissues such as renal and intestinal epithelia, liver and macrophages (Huang and Sadee, 2006). SLC28 consists of three members (SLC28A1-A3) which transport Na^+ concentration dependant synthetic and natural nucleoside analogues and take part in synthesizing nucleic acid through salvage pathways (Rauchwerger et al., 2000). On the other hand, SLC29 consists of four members SLC29A1-A4 which are distributed widely in mammalian cells and tissues. Similar to SLC28, they take part in cellular transport of nucleosides and nucleoside salvage.

Interestingly, SLC29A1 down regulation confers resistance to nucleoside drugs by effluxing the drug, while SLC28 proteins mediate drug influx (Baldwin et al., 2004). Therefore nucleoside drug resistance could be overcome by using SLC29A inhibitors which do not affect SLC28.

Amino acids are essential for mammalian cells and tissues as they serve as building blocks for glutathione and protein synthesis and also are essential in energy metabolism. Amino acids are transported through SLC carriers and are subdivided into small families according to their substrate selectivity and Na^+ dependence (Amo et al., 2008). The L-type amino acid transporter; LAT1 (SLC7A5) was first cloned by Kanani et al. in 1998 which was followed by the

discovery of LAT2 in the subsequent year by Segawa et al., (1999). Previous studies have demonstrated that SLC7A5 plays a major role in transporting aromatic, branched, long chain and essential amino acids. As such these transporters were found to be highly expressed in rapidly growing cells such as tumors (Huang and Sadee, 2006). LAT1 is distributed mainly in dividing/growing cells such as the brain, placenta and tumors. However, LAT2 is distributed in colon, intestine and kidney (Amo et al., 2008).

Interestingly, amino acids have a full transporter system in prokaryotes as well. For instance, *Pseudomonas aeruginosa* has a branched chain amino acid cation symporter (LIVCS) family which transport branched chain amino acids. Similarly, the BCCT (betaine/carnitine/choline transporter) family was found in Gram negative bacteria. BCCT functions as a membrane transporter of amino acids with quaternary amino groups. Amino acid transporters were also found in Gram positive bacteria such as AGCS (alanine/glycine/cation symporter) which transport glycine and alanine in symport with monovalent cations like H^+/Na^+ (Reizer et al., 1994) Eukaryotes also have a full amino acid transporter system. Solute:Sodium Symporter (SSS family) transports exist in bacteria, archaea and animals as well (Saier,M.H., 2000).

Further examples of SLCs are summarised in Table 1.1.5.

Table 1.1.16:- **functions of SLC transporters (Huang and Sadee, 2006).**

1.3.3.2.4. Techniques for improving drug permeability

Prodrug synthesis has been studied to improve both drug solubility and permeability. The pre moieties mask any polar groups on the compounds which results in drug partitioning across the membranes to increase its absorption. One of the most commonly employed groups of compounds is carboxylic acid esters and amino acids. Amino acid ester prodrugs of nucleosides were found to improve their permeability as for instance valacyclovir which is 5-L-valyl ester of acyclovir was shown to exhibit 3 to 5 fold increase in systemic bioavailability when compared to the parent drug (Weller et al., 1993). These results could be attributed to the enhanced intestinal absorption of L-amino acid nucleosides prodrugs via PEPT1 transporters as suggested by Han et al., (1998). Despite being successful as a permeability enhancer, most of the prepared prodrugs have low solubility which self limits their use as bioavailability enhancing strategy (Majumdar et al., 2004).

Other studies suggested that ion-pairing (neutral species formed by electrostatic attraction between oppositely charged ions in solution) can be used to improve drug permeability. The interaction between the two opposite charges results in burying of the charge in the drug molecule and hence alters its physical properties. A study conducted by Irwin et al., (1969) demonstrated that the rate and efficacy of an ionic drug isopropamide was improved upon ion-pairing with an exogenous counter ion such as trichloroacetate. However, the mechanism of ion-pairing is still not clear and the permeability increase could be attributed to the direct effect of the counter ion i.e. binding to mucosal membrane, lowering the interfacial tension of the gut wall and causing mucosal erosion (Quintanar-Guerrero et al., 1997).

Interestingly, ion-pairing of methotrexate with L-arginine was found to enhance the nasal permeability of the drug 24 times when compared to the drug alone (Ivaturi and Kim., 2009).

Other approaches used to improve drug permeability include; use of polymers which could disturb the epithelial cell tight junctions (Kotze et al., 1998), the use of microspheres and nanoparticles (Hodges et al., 1995) and membrane fluidizing agents (Manganaro, 1997).

Since carrier mediated transport is believed to play a more important role than previously appreciated, research emphasis has shifted to blocking multi drug resistance (MDR) transporters using pharmacological reversal agents such as verapamil, quinidine, cyclosporine and valspodar (Donnenberg & Donnenberg, 2005).

Interestingly, some studies have demonstrated that various formulation excipients can inhibit the efflux function of P-gp and in turn improve the overall intestinal absorption. In 2002, Hugger et al. suggested that Pluronic P85 and Polyethylene glycol [PEG 400] have a direct effect on P-gp function and also could work indirectly by changing the Caco-2 monolayer membrane fluidity or buffer osmolarity. Another study conducted by Rege et al., (2002) suggested that Tween 80 and Cremophor EL increase apical-basolateral permeability and decreased basolateral to apical permeability of a P-gp substrate (rhodamine 123). Other excipients such as Labrasol, Acconon E, Miglyol, Solutol HS 15, sucrose monolaurate, polysorbate 20, TPGS and polysorbate 80 were also found to decrease P-gp efflux function (Cornaire et al., 2004).

1.3.3.2.5. Method for assessing drug permeability

Human intestine is not only the site for drug absorption but also functions as a barrier (physical and biochemical) for drug uptake for orally administrated drugs. The tight junctions between the enterocytes in the intestine and the hydrophobic nature of the cell membranes represent the physical barrier that the drug faces, while the degradation enzymes and the efflux transporter proteins account for the biochemical barriers in the intestine.

Various methods have been proposed to assess the permeability function of the intestinal membrane including in *vivo, in vitro* and *in silico* analysis. *In vivo* models use living animals or humans in order to track the permeability of the therapeutic agents while the *in vitro* models mimic *in vivo* conditions in order to estimate the permeability of oral drugs (Worth & Balls, 2002). Nevertheless, *in vivo* and *in vitro* correlation analysis is important to ensure the validity of data produced by *in vitro* experimentation.

1.3.3.2.5.1. In vitro Assessment of Permeability

In vitro models include a variety of different methods including physicochemical assays, membrane based assays, cell based assays and excised tissue assays.

1.3.3.2.5.1.1. Physiochemical Assessment of Permeability

The most common physicochemical descriptor used to predict drug absorption across the intestinal membrane is the octanol/water partition coefficient (log P). There are numerous methods to measure the log P values including the shake-flask method, slow stirring method, methanol-water gradient and micellar/microemulsion method. Table (1.1.6) summarises the advantages and disadvantages of the various method used in determining the log P.

Table 1.1.17:- Various methods used in determining the log P values.

Method	Advantage	Disadvantage	Reference
Direct			
Shake-flask	Most realistic method, reliable	Time consuming, requires high quantity of product used, formation of octanol emulsions in water, not reliable for highly lipophilic compounds	OECD (1995)
Slow stirring method	Avoid the formation of emulsions, reliable	Time consuming, quantity of product used	Brooke et al. (1986) and de Bruijn et al. (1989)
Chromatographic methods			
Classical HPLC approach	Quick and cheap, does not require chemical quantification	Different retention mechanisms; has poor reproducibility; just work between pH 2-7.5	Finizio et al. (1997),
Micellar and microemulsion electrokinetic chromatography	Quick and not expensive	Requires the establishment of solvation parameter model	Poole and Poole (2003)
Methanol–water gradient and a short octadecylpoly(vinyl alcohol) column	Good correlation with shakeflask method		Donovan and Pescatore (2002)
Others			
Filter probe method	Rapid; well adapted to construct a logD/pH profile	Expensive, hard to set up	Leo (2000)

1.3.3.2.5.1.2. Excised Tissue Permeability Assays

Excised tissues for instance intestinal segments, intestinal rings and mucosal sheets can be used to assess drug permeability. Intestinal segments are isolated and everted prior to filling by a small volume of the buffer solution free from the drug. The two ends of the segment are tied off and immersed in an Erlenmeyer flask that contains large volume of the buffer solution with the drug of interest solubilised in it. The flask is continuously supplied with oxygen and agitated and samples from the buffer solution inside the segment are taken to assess drug permeability.

1.3.3.2.5.1.3. Cell Based and Membrane Based Permeability Assays

One of the major drawbacks of using excised tissues for assessing oral absorption is the technical difficulties it poses which resulted in the introduction of the different cell lines. Human cell lines such as intestinal adenocarcinoma cell lines (Caco-2), HT29 (Huet et al., 1987) and T84 (Dias and Yatscoff 1994) and animal cell lines like MDCK (Madin Darby Canine Kidney), CHO (Chinese Hamster Ovary) (Tavelin et al., 1999) have been used widely in laboratories around the world to assess oral permeability.

Caco-2 monolayers were first isolated from a colon adenocarcinoma of a 72-year-old patient (Fogh et al. 1977). Upon culturing, Caco-2 differentiates continuously and produces the structural and functional patterns of enterocytes (Pinto et al. 1983). Caco-2 cells can reach confluency after 3-6 days and become completely differentiated within 20 days (Pinto et al. 1983). After differentiation, the cells express alkaline phosphatase, sucrase isomaltase and aminopeptidase which are characteristic for enterocyte brush border microvilli.

The barrier function of the differentiated Caco-2 monolayers is judged by the transepithelial electrical resistance (TEER) values which range between 200-600 Ωcm^2. Caco-2 monolayers have been extensively used to study passive paracellular permeability (Artursson et al. 1993; Artursson et al. 1996), passive transcellular absorption (Artursson 1990), carrier mediated uptake of B-lactam antibiotics (Inui et al. 1992), amino acids (Thwaites et al. 1995), amino acids analogue (Hu and Borchardt 1990) and efflux transport (Eneroth et al. 2001, Tran et al. 2002).

Table 1.1.18:- Some of the transporter proteins expressed in Caco-2 monlayers

Membrane transporter	Location	Substrate	Inhibitor	Reference
P-gp (MDR1)	apical	Talinolol Digoxin	Verapamil Guinidine Verapamil	Augustijns and Mols, 2004 Greiner et al. 1999 Collett et al. 2005
MRP1	basolateral	Methotrexate Estradiolglucor.	Probenecid MK571	Endres et al. 2006
MRP2	apical	Grepafloxacin Vinblastine	MK571, Furosemide Indomethacin	Lowes and Endres et al. 2006
MRP3	basolateral	Methotrexate Estradiolglucor.	Hydroxycotinine *O*-glucuronide	Endres et al. 2006 Létourneau 2005
MRP4	apical	Estradiolglucor.	Probenecid	Endres et al. 2006
MRP5	basolateral	Methotrexate	Probenecid, MK571	Pratt et al. 2006
MRP6	basolateral	Mercaptopurine	Probenecid, Indomethacin	Endres et al. 2006 Boraldi et al. 2004
MCT1	apical	Salicylic acid Ketoprofen	Fluorescein L-lactic acid	Konishi et al. 2002 Choi et al. 2005
OATP-B	apical	Estrone-3-sulphate Pravastatin	Pravastatin	Ito et al. 2005 Kobayashi et al. 2003
BCRP	apical	Topotecan	GF120918	Jonker et al. 2000
hPepT1	apical	Cefixime Valacyclovir Gly-Sar	Nifedipine cephalosporines	Duverne et al. 1992, Behrens et al. 2004

Table 1.1.19:-Summary table of *in vitro* permeability models and their advantages and limitations (Worth & Balls 2002).


Aston University
Illustration removed for copyright restrictions

1.3.3.2.5.2. *In vivo* Assessment of Permeability

The majority of the in *vivo* studies (Table 1.1.9) use animals as models to predict oral absorption in humans. The main advantage of conducting *in vivo* studies is that it provides the all the necessary biological parameters that could influence drug absorption and as such an accurate full picture of permeability assay can be obtained. Summary of the various models that are available are presented below.

Table 1.1.20:- Summary table for *in vivo* permeability models (Worth & Balls 2002).

1.3.3.2.5.3. *In silico* Assessment of Permeability

Due to the increase in the development of NCE over the last couple of decades, there has been a growing demand to predict drug performance at an early stage of development phase which has seen the emergence of predictive *in silico* techniques to estimate drug absorption, distribution, metabolism, excretion and toxicity (ADMET). *In silico* models comprise of a group of mathematical models which examine compound descriptors such as hydrogen bonding, molecular size and lipophilicity and estimate the biological activity based on their physicochemical properties.

The advantage of using *in silico* models is that they do not require access to the actual compound and produce results faster which means that the permeability studies of a compound could be predicted even before the synthesis of the compound. However, the major limitation of applying *in silico* models is that the obtained results account for passive transcellular permeability and do not take into account other routes such as active transport and efflux.

Table (1.1.10) provides a summary of the major physiochemical characteristics used in predictive absorption models.

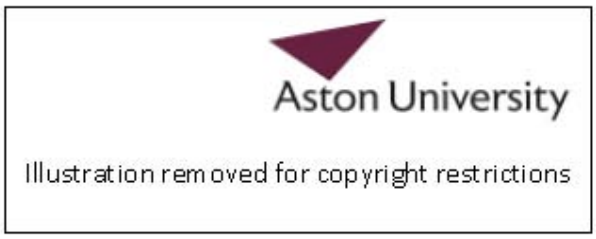

Figure 1.1.13:- Comparison of how much research has been performed using, *in silico, in vitro* and *in vivo* techniques during the last decade (2001- 2010) Mohammed et al., 2012.

Table 1.1.21:- Summary table for in silico Permeability models (Stenberg et al., 2000)

1.4. Microarrays

Carrier transporter proteins have broad substrate specificity and various drugs from different pharmacological classes interact during the process of permeation. Moreover, there could be a partial overlap between these transporters' substrates and as a result the pharmacodynamics and pharmacokinetics of a drug can be affected by more than one efflux protein (Taipalensuu et al., 2001). Thus, a systematic/holistic investigation of the efflux proteins is vital to get a broad picture of carrier expression profiles that affect drug/formulation permeability.

Interestingly, many physiological changes that take place at the cellular level are reflective of their level of gene expression. Genes are up or down regulated under different physiological conditions such as disease state, drug metabolism, exposure to toxins and response to treatment. This has paved the way for modern biomedical research that prompted the biologist to develop gene expression matrices that would allow identification of specific gene sets involved in a defined process, disease condition or cellular differentiation. Analysis of gene expression at m-RNA levels was first discussed by Alwine et al. (1977) using Northern blotting but was limited to the study of small sets of genes. The second major development by Liang and Pardee (1992) was differential displaying technology which succeeded in measuring multiple differences of gene expression in parallel. Yet, this method was qualitative and screening was dependent on the length of mRNA rather than its identity. The introduction of microarrays in 1995 revolutionised the research arena relying on gene expression profiling. The technique addressed the various limitations in studying gene expression and was associated with high sensitivity and throughput. Microarrays allow for the use of low amounts of starting material and the small size of the arrays improves the sensitivity and enables the screening of vast number of genes simultaneously (Hal et al., 2000).

A microarray is defined as a collection of microscopic spots orderly arranged onto the surface of a solid support. It is a modern technique comprising of thousands of genes automatically spotted on specially treated glass slides. Spots or probes are designed in such a way that each probe binds to a specific fluorescently labeled nucleic acid (target) during the hybridization reaction. The binding between probe and target is analyzed via measuring the emitted fluorescence by the hybridized target during scanning. The principle difference between conventional hybridization and a microarray is the capability of arrays to monitor multiple genes on a single array which results in simultaneous profiling of genes in an organism.

1.4.1. Types of microarrays

Microarrays are arrangements of samples or probes in specific order onto a matrix. According to the probe used, microarrays are broadly divided into two types; nucleic acid and tissue microarrays.

Nucleic acid microarrays are prepared by spotting nucleotide probes onto a support matrix and base-pairing principles are used to bind the complementary targets (Southern et al., 1999). Glass slides are commonly used as a support matrix for the microships, however materials such as nylon, silicon and nitrocellulose membranes have also been used. The probes used for nucleotide microarrays could be DNA, cDNA or oligonucleotides which are printed onto the slides via robotics or could be built in directly onto the array by inkjet techniques or photolithography (Lockhart et al., 1996).

cDNA microarray is an example of transcriptomic arrays which enables large scale comparison of the whole genome of two samples. RNA is extracted from the test sample followed by reverse transcription to get cDNA that is labelled by fluorochrome. Both the normal (control) and target samples are mixed and incubated with the cDNA microarray and the slide is analysed using image analysis systems. The obtained data represent the transcriptional affinity for the whole genomes on the grid. The large amount of data obtained makes it impossible to point the genes that characterise the molecular pathobiology of certain disease; hence data processing is considered the bottleneck of microarray technologies.

Another category of nucleotide microarrays is single nucleotide polymorphism (SNP) microarray which is a genomic array that detects polymorphism or mutation that might occur in a population. SNPs usually take place in non-coding regions of the DNA and occur throughout the genome. The main advantage of using SNPs is to determine disease susceptibility and therefore tailoring the efficiency of drug therapy for an individual which is also known as personalized medicine. It might be in the near future when physicians can

screen patients for susceptibility to certain disease by analyzing their DNA for specific SNPs profiles.

A third category of nucleotide microarrays is comparative genomic hybridization (CGH) microarray which identifies genomic losses and gains in certain diseases. Most of the solid tumours are characterised by genetic instabilities which cause chromosomal re-arrangements. Until recently, it was difficult to characterise solid tumours by using chromosomal re-arrangements because of the high chromosomal instability. Studies using CGH have shown that solid tumours undergo frequent losses and gains and different tumour types have distinct CGH patterns. Nevertheless, the lack of spatial resolution of CGH arrays makes it difficult to conclude that different tumour types or tumours at different stages of evolution have distinct pattern of gains and losses.

The final type of microarray is called tissue microarrays (TMA). A number of novel markers have been identified recently by molecular biologists. These markers are believed to have prognostic, diagnostic and therapeutic significance especially in the field of cancer. The introduction of TMA enables rapid and cost effective validation of these markers rather than the use of conventional histo pathological techniques.

1.4.2. Procedure for setting up Microarray studies

The microarray experiment starts with isolation of the RNA from both the control sample and the treated sample (test sample). The cDNA probes are prepared separately through reverse transcription which are labelled using fluorescence dyes; Cy3 (control sample) and Cy5 (test sample). The labelled probes are mixed together and hybridized for 17 hours on the array slide which is followed by washing and imaging of fluorescence to record the different levels of expression of genes.

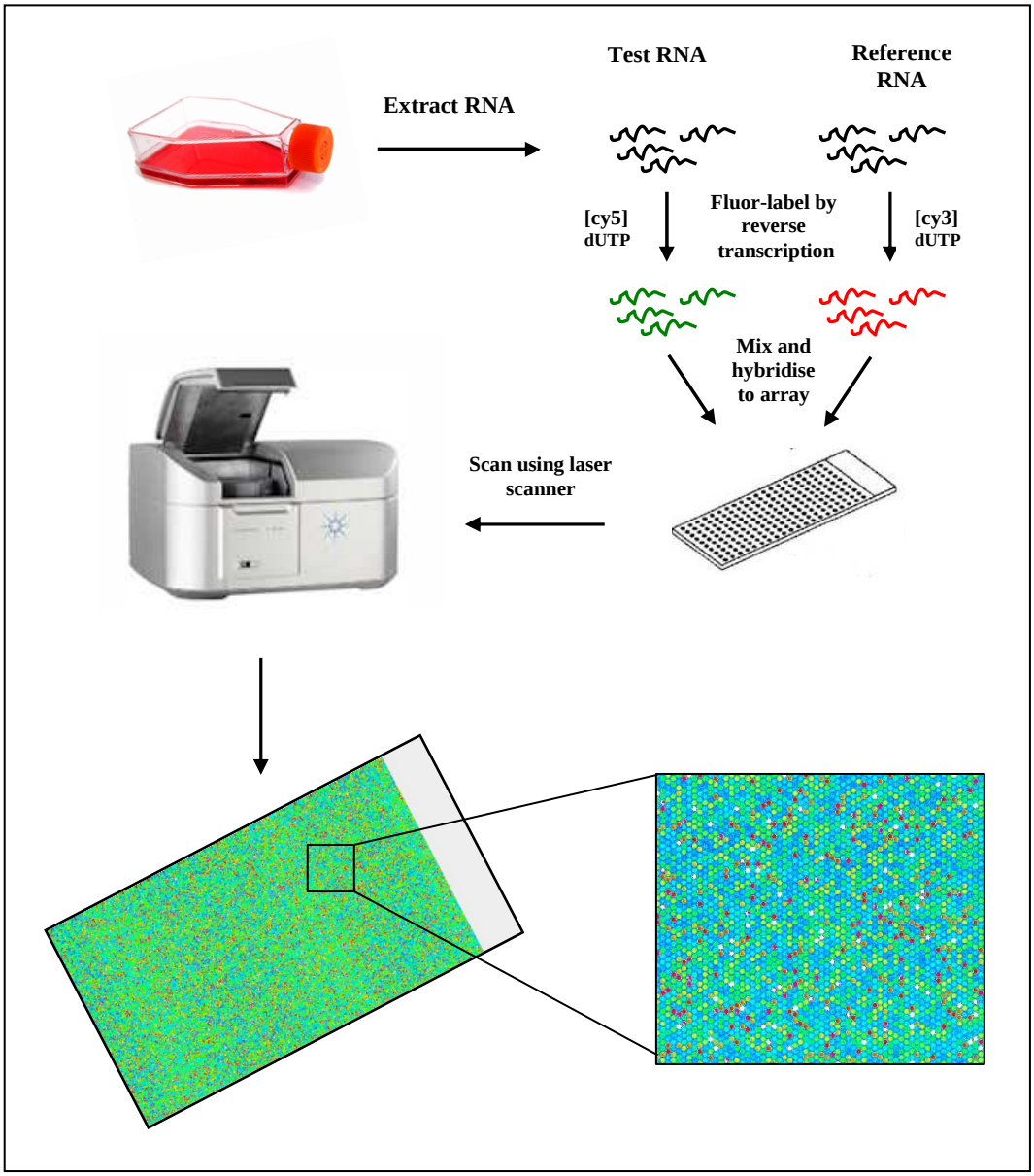

Figure 1.1.14:- **Schematic representation of the procedures followed to setup microarrays studies. Samples (control and test samples) are labeled with different fluorescent dyes (Cy3 and Cy5) and competitively hybridized to the same array. Final imaging requires a fluorescent scanner that can excite and detect at multiple wavelengths.**

2.1. Aims and Objectives

Despite the several advantages of oral drug delivery, the unfavourable biopharmaceutical properties of drugs (i.e. low solubility and low permeability) decrease drug bioavailability across the oral route. Although prodrugs have been formulated to alter the biopharmaceutical properties, they present significant challenges including the requirement for complete drug profiling, potential toxicity and stability issues. On the other hand, ion-pairs could be a potential solution to address both solubility as well as permeability.

The overarching aim of this thesis is to study the application of charged amino acids as both solubility as well as permeability enhancing agents through formation of ion-pair complexes. The content in this thesis investigates and addresses for the first time both solubility and drug uptake through the inclusion of a single agent i.e. amino acids. For this purpose, three model drugs were selected; indomethacin (weak acid, BCS II), trimethoprim (weak base, BCS III/IV) and ciprofloxacin (zwitter ion, BCS IV). All the selected drugs carry charges so that they could bind electrostatically with the oppositely charged counter ions. In addition, trimethoprim and ciprofloxacin are known to be substrates to efflux transporter proteins and possess limited permeability. The objectives of this thesis include:

1. Preparation of physical mixtures and salts for the different model drugs using oppositely charged amino acids to evaluate their influence upon changes in concentration, structure and physico-chemical properties.
2. Systematic investigation of multi-functionality of amino acids in dosage form preparation to determine their suitability in translation of results into clinic.
3. Evaluating the permeability of model drugs across Caco2 monolayers and identifying the genomic signature for drug transport of model drugs in the presence of oppositely charged counter ions.

Chapter 3

Indomethacin

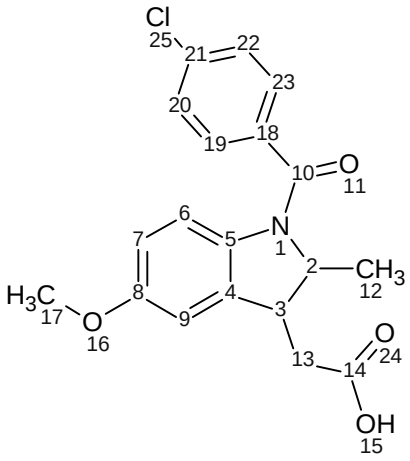

Papers relating to chapter 3

Amr ElShaer, Sheraz Khan, Dhaya Perumal, Peter Hanson and Afzal R Mohammed., (2010) Use of amino acids as counter ions improves the solubility of the BCS II model drug, indomethacin. *Current drug delivery*.

3.1. Salt preparation and characterisation for indomethacin using cationic amino acids

3.1.1. Introduction

Both solubility and permeability are considered key determinants for drug bioavailability. Lately, the number of poorly soluble drugs has increased greatly especially after the introduction of combinatorial chemistry and high throughput screening to the drug discovery cycle and around one third of these new compounds have aqueous solubility less than 20 µg/mL (Li et al., 2005). Therefore, formulating oral dosage forms of these poorly soluble drugs becomes a great challenge for the formulation pharmacist (Leuner and Dressman, 2000).

Salt formation is a commonly used technique to modify the characteristics of new chemical entities (NCE) in order to overcome the undesirable characteristics of the parent drug (Anderson and Conradi, 1985). Both the physicochemical characteristics and biological performance of the drug differs dramatically from the salt form (Bighley et al., 1996). Most of the salt forming agents are selected empirically; many issues such as ease of crystallization, percentage yield, hygroscopicity and flowability are considered prior to selecting the salt former (Berge et al., 1977). Many studies tried to investigate the relationship between the salt properties and the counter ions used. Yet, until now no successful way of predicting the effect of salt former on the behaviour of the parent compound has been reported. Stahl & Wermuth suggested that the dissociation constant (pK_a) is the most important piece of information to gather about NCE (Stahl and Wermuth, 2002), then a number of counter ions can be selected to form a stable form (minimum difference between the salt former and counter ion should be 3 pK_a units). After selecting a number of potential counter ions, further physicochemical tests should be carried out to evaluate the crystallinity, polymorphism and melting point. Amino acids have shown great success as potential salt formers: Pellegate (1993) utilised lysine,

ornithine and arginine to prepare novel salts of furosamide (Pellegata R., 1993). The prepared salts exhibited very high solubility up to 560 mg/mL for the lysinate salt which was much higher than furosemide itself and even its sodium salt. Another study conducted by Fujisawa et al have prepared new cephalosporin salts with arginine and lysine, the prepared amino acid salts were claimed to be less painful when administered parentally (Fujisawa et al., 1976). Other studies have succeeded to prepare novel salts of arginine with acidic drugs such as benzoquinolizine-2-carboxylic acids (Deshpande et al., 2007) and inosine (Kurauchi et al., 2004). While lysine managed to form new salts with ibuprofen (Tung et al., 1991) and 4-diphenylacetic acid (Giuseppe, 1989).

On the other hand, poor permeability of NCE makes the drug unsuitable for further development and great efforts are exerted to avoid getting a potent non-absorbed drug (Egan and Georgio, 2002). It is strongly believed that nutrient transporters play a major role in transporting nutrients as well as various therapeutic agents (Oh et al., 1999). Interestingly, amino acids succeeded in improving the drug permeability of poorly permeable drugs such as gemcitabine and other anticancer agents by ester linkage and mediate the transportation through hPEPT1 transporters (Song et al., 2004). Moreover, amino acids have been used in the past to improve aqueous solubility of alcohol and amine drugs through prodrug formation (Aggarwal et al., 1990; Upshall et al., 1990). Therefore, amino acids were chosen in the current study to improve the solubility of a BCS II model drug through a salt formation technique as the first stage prior to investigating the effect of using these amino acids to improve drug permeability via amino acids mediated transporter and ion-pairing mechanisms.

Indomethacin (IND) was selected as a model drug for this study as it has an acidic carboxyl group which acts as a potential salt former, moreover its transportation is mediated by P-glycoprotein transporter. According to the Biopharmaceutical classification system (BCS), IND is classified as a poorly soluble highly permeable drug (i.e Class II). IND is a non-steroidal anti-

inflammatory drug (NSAID) which is widely used to reduce pain associated with rheumatoid arthritis, osteoarthritis, bursitis and headache (Sweetman, 2005).

3.1.2. Materials and methods

3.1.2.1 Materials

Indomethacin (TLC ≥ 99%), L-Arginine (non-animal source), L-Histidine (Reagent plus ™, L-Lysine and Potassium bromide (99% FT-IR grade) all were purchased from Sigma Aldrich, UK. D_2O (99.9% min) was purchased from Coss scientific instrument Ltd, DMSO-D6 (98.8% min) was purchased from MERCK (Darmstadt, Germany).

3.1.2.2 Methods

3.1.2.2.1 Analytical technique

The amount of indomethacin (IND) dissolved in the solution samples was quantified by HPLC using a Dionex 1100 system with autosampler (AS50), gradient pump (GP50), UV detector (UVD 170U) and RP-C18 analytical column (Phenomenex 110A, 150x4.6 mm, 5µm). The analysis method was adapted from Song et al., (2004). IND was eluted using acetonitrile (60%) and 0.1 M acetic acid (40%) as a mobile phase and pumped at 1.0 mL/min flow rate. UV detector was adjusted at λmax of 248 nm (predetermined using Unicam UV-Visible Spectrophotometer). The retention time was 6.5±0.12 min and a rectilinear calibration curve was established at concentration range between 10-500µg/mL with 0.99 correlation coefficient (For more details see appendix 1).

3.1.2.2.2 Phase solubility diagram

Phase solubility diagram was established by measuring the saturated solubility of IND free acid with various concentrations of basic amino acids (L-arginine,L-lysine and L-histidine). Excess IND was added into screw-capped tubes containing serial dilutions of the amino acids solutions

and agitated at room temperature (Stuart SB 162 stirrer) for 24 h. After equilibrium the supernatant was filtered through 0.45 µm filters and analysed by HPLC to determine indomethacin concentration. The pH of amino acid solutions was monitored using Xisherbrand Hydrus 500 pH meter.

3.1.2.2.3 Salt preparation

Equimolar amounts of IND and the free amino acid (L-arginine, L-lysine, L-histidine) were solubilised in water and the solutions were mixed and stirred until equilibration then filtered. The filtrate was transferred into vials and freeze dried for 48 h using Modulyo freeze dryer at -40^{o}C shelf temperature and under vacuum created by an E2M5 Edwards pump then samples were collected and kept at 40^{o}C oven for 4h using Gallenkamp vacuum oven.

Despite the low yield of the freeze drying technique, it was preferred over the salt preparation method adapted by Anderson & Conradi using organic solvent (Berge, 1977). Lyophilized products are highly pure and devoid of the formation of any solvates. Generally, salts prepared by an organic solvent method do not behave well in an aqueous environment as they could convert to the free acid or base, exhibit low solubility and stability and their use becomes limited (Chauhan et al., 2004).

3.1.2.2.4 Thermogravimetric analysis (TGA)

Moisture content and decomposition temperature of indomethacin and its prepared salts were determined using a thermogravimetric analyser (Pyris 1 TGA, Perkin Elmer). 5-10 mg of samples were added to an open pan and analysed at temperature range 30-300 ^{o}C at 10 ^{o}C/min scanning rate and under nitrogen stream. The resultant thermograms were analysed using Pyris Manager Software (version 5.00.02)

3.1.2.2.5 Differential scanning calorimetry

Differential scanning calorimeter (Pyris Diamond DSC) was used to investigate the melting point and the crystallization exotherms of the prepared salts. Approximately, 2-5 mg of the salts were weighed and transferred to an aluminium sample pan (50 µL capacity) then a pierced aluminium top was crimpled in place in order to seal the pan. Intra cooler 2P system was used to initially cool the samples to 50 ^{o}C and then the sample was heated to 300 ^{o}C at a rate of 10 ^{o}C/min. Nitrogen was used as a purge gas at a flow rate of 20 mL/min, Indium and Zinc were used to calibrate the heat flow and melting point onset (156.6 ^{o}C for Indium and 419.47 ^{o}C for Zinc). The obtained thermograms were analysed using Pyris Manager Software (version 5.00.02). The experiment was performed in triplicate and an empty aluminium pan, sealed in the same way of the samples, was used as a reference cell for all the measurements.

3.1.2.2.6 FT-infrared (IR) spectroscopy

FTIR absorbance spectra of IND and its salts were obtained with Nicolet IR 200 spectrometer (Thermo electron corporation) using KBr discs technique. Crystalline KBr was dried at 65^{o}C over night before use. Samples were prepared by mixing IND or its salts with dry KBr at 1:100 (w/w) ratio and pressed at 8 tones for 5 min (using Specac tablet presser) to form KBr discs. 64 scans were done over wavelength 4000- 400 cm^{-1} for each sample. EZ OMNNIC 7.0 software was used to interpret the IR spectrum.

3.1.2.2.7 ^{1}HNMR

Samples were analysed with Bruker Avance DPX-250 NMR (at 250.1 MHz) and Bruker Topspin software was used to analyse the data. Approximately, 1-2 mg of the salts were dissolved in 1 mL of deuterated water (D_2O) and placed in sample capillary vial up to 5-10 cm height.

3.1.2.2.8. pH solubility profile

pH solubility studies were determined by using the Ledwidge & Corrigan method (Ledwidge and Corrigan, 1998). Saturated solutions of the salts and acids were prepared by dissolving an excess of the drug in deionised water. The solutions were agitated constantly using (Stuart SB 162) stirrer at ambient temperature. pH was adjusted to values below and above these of the saturation solutions by adding HCl or the appropriate base (L-arginine). After 2 hours intervals an aliquot was withdrawn and filtered through 0.45 µm filter, then analysed using HPLC (see section 3.1.2.2.1)

3.1.2.2.9. Solubility studies

Solubility studies were carried out using Hugchi and Connor's method (Higuchi and Connors, 1965) excess amount of IND or its salts are added to capped test tubes with 5 mL of deionised water and stirred for 24 hours at room temperature until equilibrium is reached. Subsequently, the suspension is filtrated through 0.45µm syringe filters and suitably diluted and the concentration was measured by HPLC.

3.1.2.2.10. Conventional tablet preparation and dissolution studies

Conventional tablets weighing 500 mg and containing 50 mg of IND or equivalent amounts of the prepared salts were prepared for dissolution studies. Starch was used as a tablet binder and anhydrous lactose was used as a diluent in 1: 8 ratio respectively. All the excipients were geometrically mixed with the active ingredients and 500 mg were weighed and compressed using a Specac tablet presser at 8 tones pressure for 10 minutes.

USP II paddle method (ERWEKA DT-600) was used to perform the *in vitro* dissolution studies. The prepared tablets were placed into dissolution vessels containing 900 mL of phosphate buffer (pH 7.2) and the dissolution medium was maintained at $37^{o}C \pm 0.5^{o}C$ and stirred at 50 rpm. 5mL of samples were collected at a predetermined time intervals (1, 5, 10, 20, 30, 45, 60

and 90 min) then filtered through 0.45 µm Millipore filters. The dissolution media was replaced by 5mL of fresh dissolution fluid in order to maintain a constant volume. After proper dilution samples were analysed by HPLC as mentioned above.

3.1.3. Results and discussion

3.1.3.1 Phase solubility diagram

Before preparing IND salts, a phase solubility diagram was first constructed between IND and three basic amino acids namely; L-arginine, L-lysine and L-histidine. The phase solubility diagram gives preliminary data about the ability of the counter ions to dissociate IND free acid and also provides data about the extent of improvement of solubility upon using these counter ions.

The results showed that increasing the basic amino acid concentrations resulted in improving IND solubility significantly (Fig. 3.1.1). Such an increase in solubility could be attributed to the ability of the amino acids to increase pH of the medium upon increasing their concentration which in turn enables the dissociation of IND free acid (ionised form) resulting in an increase in solubility.

L-arginine has a basic side chain with a pKa of 12.48 for $–NH_2$ group; this value is much higher than the pKa of IND (pKa= 4.5). This in turn results in IND free acid giving up its proton to $–NH_2$ group to form $–NH_3^+$ cation and hence IND acts as a strong acid in L-arginine solution. Since a linear relationship between IND solubility and L-arginine concentration was observed (R^2= 0.998), therefore it is believed that IND is 100% dissociated in arginine solution. Hence an electrostatic interaction is possible between the two ionised species to form a salt.

Although the pKa of the $–NH_2$ side chain of L-lysine (pKa= 10.53) is lower than that of arginine, the solubility of IND in L-lysine was significantly higher and this could be possibly because of self-association between IND and lysine which inhibits the rate of nucleation of the final salt (Ledwidge and Corrigan., 1998; Serajuddin and Mufson, 1985; Serajuddin and Jarowski, 1985).

Such self-association was not observed in IND-arginine salt probably because of the large numbers of H-donor groups in arginine and the very low number of H-acceptor groups, therefore the possibility of arginine self-association is low and instead arginine would interact intermolecularly with the H-acceptor groups of IND. However, lysine has 2 H-donor groups and one H-acceptor group and there would be a high probability of intermolecular interaction between lysine molecules and hence a higher chance for IND to self-associate and to inhibit the nucleation rate.

On the other hand, the basic amino group of L-hisitidine has a pK_a of 6 (slightly higher than IND) which possibly results in weaker degree of dissociation of indomethacin in histidine (Fig. 3.1.1). As a consequence, only a small ratio of IND exists in the ionised form (i.e. IND acts as a week acid in histidine solution) and results in poor yield of the salt.

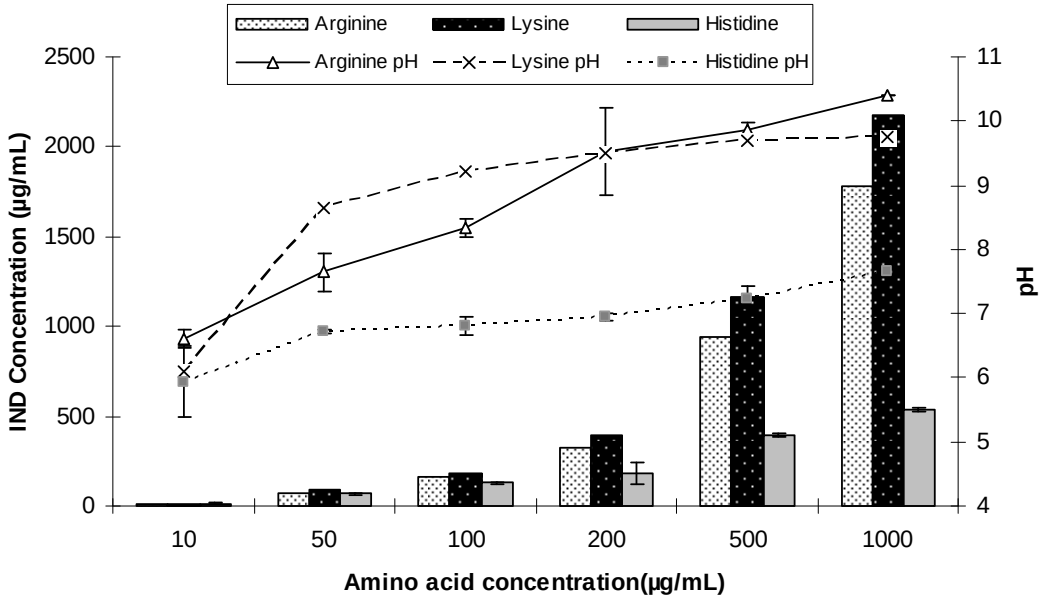

Figure 3.1.15:- Phase solubility diagram between IND, L-arginine, L-lysine and L-histidine. The figure also shows pH measurements of various concentrations of the amino acids (n=3).

3.1.3.2 Characterisation of the salt form

After evaluating the degree of dissociation of IND with the various basic amino acids, three salts were prepared by lyophilisation and further characterised by Fourier transform infra-red,

differential scanning calorimetry, thermo-gravimetric analysis and ^{1}H nuclear magnetic resonance.

3.1.3.2.1 Differential scanning calorimetry and Thermo-gravimetric analysis

Fig 3.1.2 shows the DSC and TGA scans of IND and its prepared salts. IND showed an endothermic peak at 162.67 ^{o}C, corresponding to its melting point (onset 161.07 ^{o}C). The IND melting enthalpy of fusion was very high (1133.69 J/g) reflecting the strong crystal lattice of the drug. Interestingly, thermal characterisation of IND-arginine salt revealed that the prepared salt was in the amorphous form as DSC data have shown a crystallization exotherm at 118.93 ^{o}C where the amorphous form starts to crystallize and these formed crystals exhibited melting at 209.73 ^{o}C. Similarly, the IND-lysinine salt was found to exist in an amorphous form and showed a weak crystallization exotherm at a lower temperature 79 ^{o}C followed by a melt at 223.26 ^{o}C. Interestingly, after 2-week of storage under ambient conditions; IND-lysine crystallization exotherm disappeared which possibly suggests that the salt converted from the amorphous form into the crystalline form upon storage and this could be attributed to the relatively low crystallization temperature. However the arginine salt remained in its amorphous form under similar conditions.

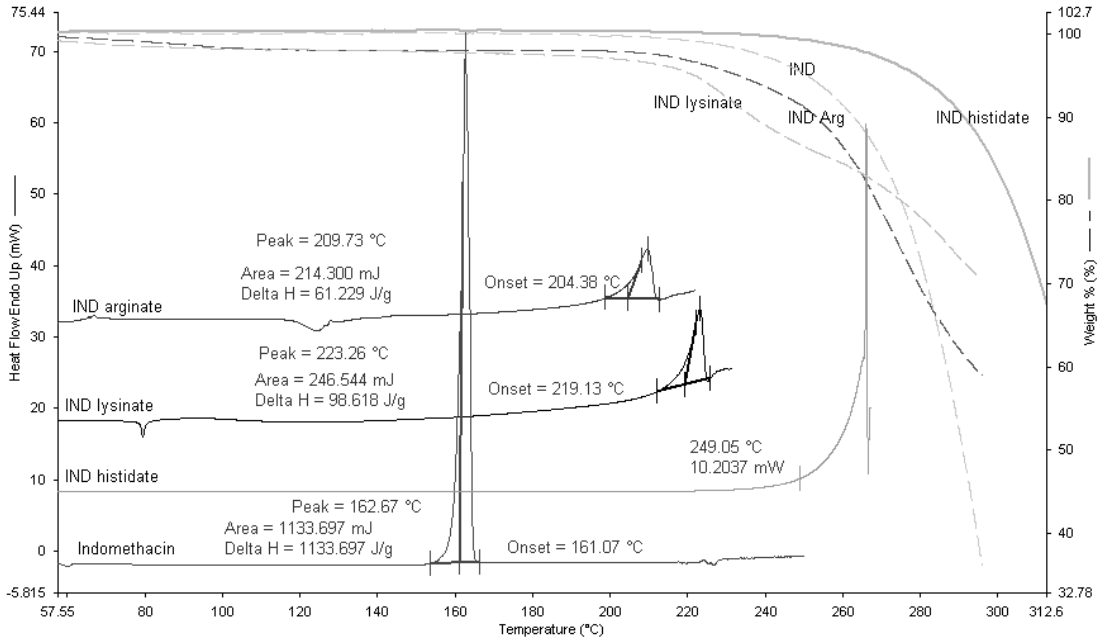

Figure 3.1.16 :- DSC and TGA scans for IND free acid, IND-Hisidatine, IND-Lysinate salt, and IND-Arginate salt. 2- 5 mg of the sample was heated to 300^{o}C at rate of 10 ^{o}C/min (n=3)

On the other hand, L-histidine did not form a salt with IND and DSC shows a melt at 249.05 ^{o}C which degrades before complete melting. A similar peak was obtained upon thermal analysis of L-histidine free base. This result suggest that there was no salt formation and these results were further confirmed with FT-IR and ^{1}HNMR studies (sections 3.1.3.2.2 & 3.1.3.2.3)

TGA scans revealed that the prepared salts degrade a few degrees above their melt and the % weight loss increased greatly after the decomposition point due to the volatility of the degradation products. The moisture content was very low in all the prepared salts and maximum moisture of 1.2% was found for IND-lysine salt (Fig. 3.1.2).

3.1.3.2.2 Fourier Transform infra-red spectroscopy (FT-IR)

FT-IR spectra were used to characterize the possibility of interaction between IND and the amino acids counter ions. Using FT-IR, the IND salt formation could be established by (1) Absence of non-hydrogen bonded carboxylic acid peak νC=O at 1717 cm^{-1} (Silverstein and Webster., 1998). (2) Appearance of absorption bands at 3350-3150 cm^{-1} corresponding to NH_3^+ stretching of amino acids salts (Socrates, 1994).

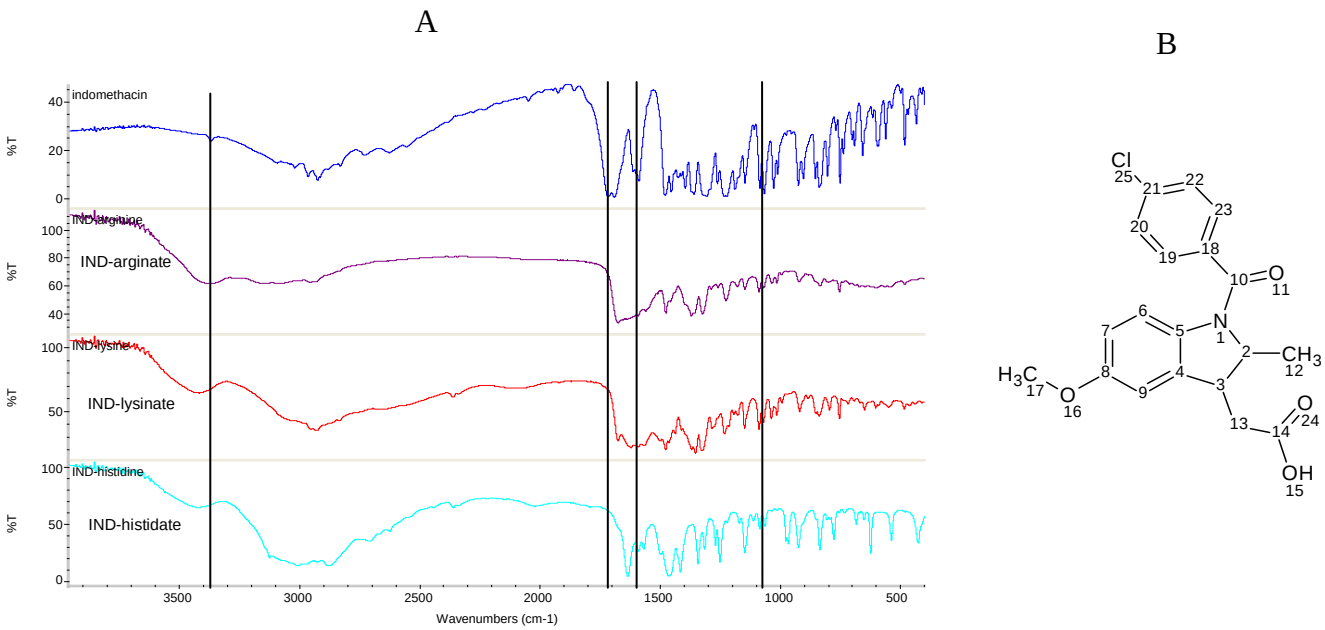

Figure 3.1.17 :- (A) The characteristic FT-IR absorption bands of IND, IND-arginate, IND-lysinate and IND-histidate (from top to bottom), (B) chemical structure of indomethacin.

IND FT-IR spectra (Fig. 3.1.3A) showed characteristic absorption bands at 3021 cm^{-1} which can be assigned for C-H aliphatic chains, 1717 cm^{-1} corresponding to carbonyl stretching of the acid v (C14=O) and at 1691 cm^{-1} for bezoyl C10=O as previously described by (Tong and Zografi, 2001). Interestingly, upon adding L-arginine to IND free acid, the absorption band of non-hydrogen bonded C14=O was eliminated, possibly due to proton loss and involvement of the carboxylic group in the salt formation with the basic amino group of the amino acid. While, the benzoyl carbonyl stretches at around 1691 cm^{-1} shifted slightly to 1675 cm^{-1} for both arginate and lysinate salt. Such a shift could be attributed to the effect of the local dielectric constant change between the ionised form and non-ionised form of IND (Tong and Zografi, 2001). On the other hand, both benzoyl and carbonyl stretching for IND free acid v(C=O) were absent in IND-histidine and an absorption band was observed at 1635 cm^{-1} which corresponds to carboxylic vC=O of histidine (Petrosyan, 2007). These results suggest that histidine could not

form a salt with IND and this could be attributed to the low dissociation ability of IND in histidine solution as discussed above for the phase solubility diagram.

Table 3.1.22: Major band (peak) positions and assignments for IND and its salts in the region of 4000-400 cm-1

compound	Infrared (cm-1)	Assignment
IND	3371	C-H aliphatic
	3021	OH group
	1717	Asymmetric acid νC=O
	1691	Benzoyl (amide) νC=O
IND-arginate	3381	N-H stretching
	3089	C-H alphatic
	1675	Benzoyl (amide) νC=O
	1584	Asymmetric COO^-
IND-histidine	3418	N-H stretching
	3009, 2881	C-H alphatic
	1635	Carboxylic νC=O of histidine
IND-lysinate	3417	N-H stretching
	2932	C-H alphatic
	1675	Benzoyl (amide) νC=O
	1590	Asymmetric COO^-

3.1.3.2.3 ^{1}HNMR

^{1}HNMR spectroscopy was also used to confirm the salt formation and determine the molar ratio of interaction between IND free acid and the anionic amino acids by counting the hydrogen integrals. DMSO was used to dissolve IND while, deuterated water (D_2O) was used to solubilise the salts.

Fig 3.1.4 shows the ^{1}HNMR of IND free acid, at 7.6 ppm frequency the 4H of IND halogenated aromatic ring which appeared as multiplet. While, the hydrogens of the methoxy aromatic ring; C^7(1H) doublet, C^9 (1H) doublet and C^6 (1H) singlet appeared at 6.9, 6.94 and 7.04 ppm respectively. (3H) of the methoxy group ($OC^{17}H_3$) appeared as singlet at 3.6 ppm, while (3H) of methyl group ($C^{12}H_3$) appeared as singlet at lower frequency (2.21 ppm) as it is less shielded. Similar results were reported by Chauhan et al., (2004). The total integrated H count for IND was 15 (Fig. 3.1.4).

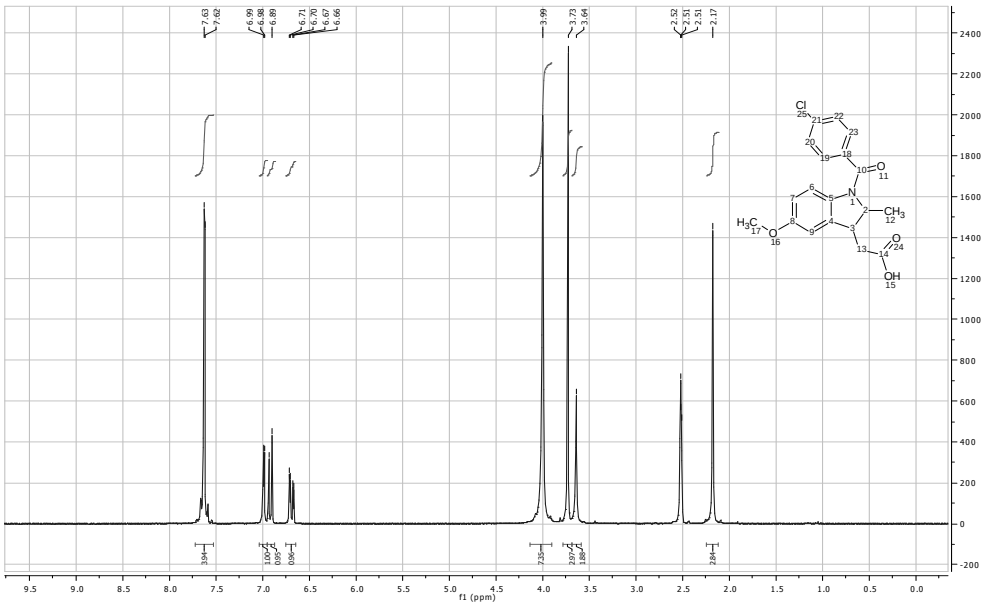

Figure 3.1.18:- ^{1}HNMR spectra of indomethacin free acid in DMSO

IND-arginine salt showed a slight chemical shift (δ) for IND bands and 7H assignments appeared between 1.44 to 3.00 ppm which represent $C^{33}H_2$, $C^{32}H_2$, $C^{31}H_2$ and $C^{29}H$ groups of the aliphatic chain of L-arginine. The total integration of (H) was 22, which confirms the formation of IND-arginate salt with 1:1 molecular ratio as the new 7H assignments correspond to one arginine molecule (Fig. 3.1.5).

Interestingly, DMSO dissolved IND and IND-arginine salt and (H) atom of IND carboxylic OH group appeared at 12.38 ppm and disappeared in IND-arginine salt (data not shown) which further confirms the loss of carboxylic proton as previously discussed in FT-IR section.

Similarly, the ^{1}HNMR data for IND-lysine salt (Fig. 3.1.6) showed the appearance of new 9H assignments corresponding to $C^{32}H_2$ (multiplet), C^{33}H2 (triplicate), $C^{34}H_2$ (triplicate), $C^{31}H_2$ and $C^{29}H_1$ (triplicate) at 1.31, 1.55, 1.72, 2.84, 3.57 ppm respectively. The formed lysine salt was in the 1:1 ratio. However, IND-histidine samples revealed histidine characteristic bands with the absence of IND bands (Fig. 3.1.7) and this could be attributed to very low dissociation of IND and its inability to form a salt with histidine.

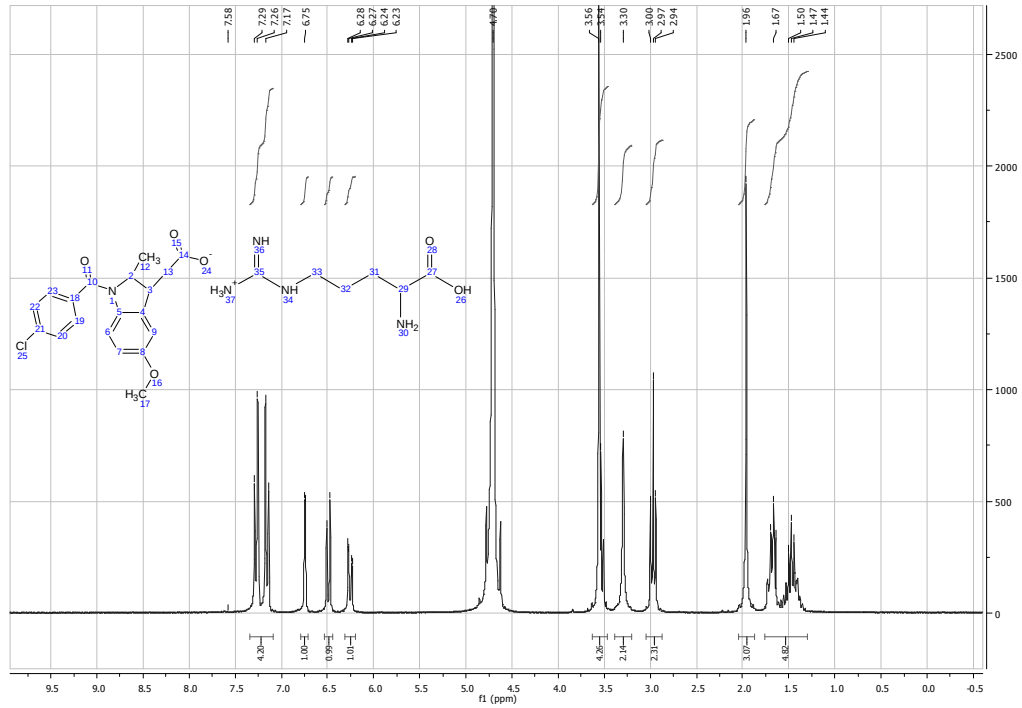

Figure 3.1.19:- ^{1}HNMR spectra for IND-arginine salt dissolved in D_2O.

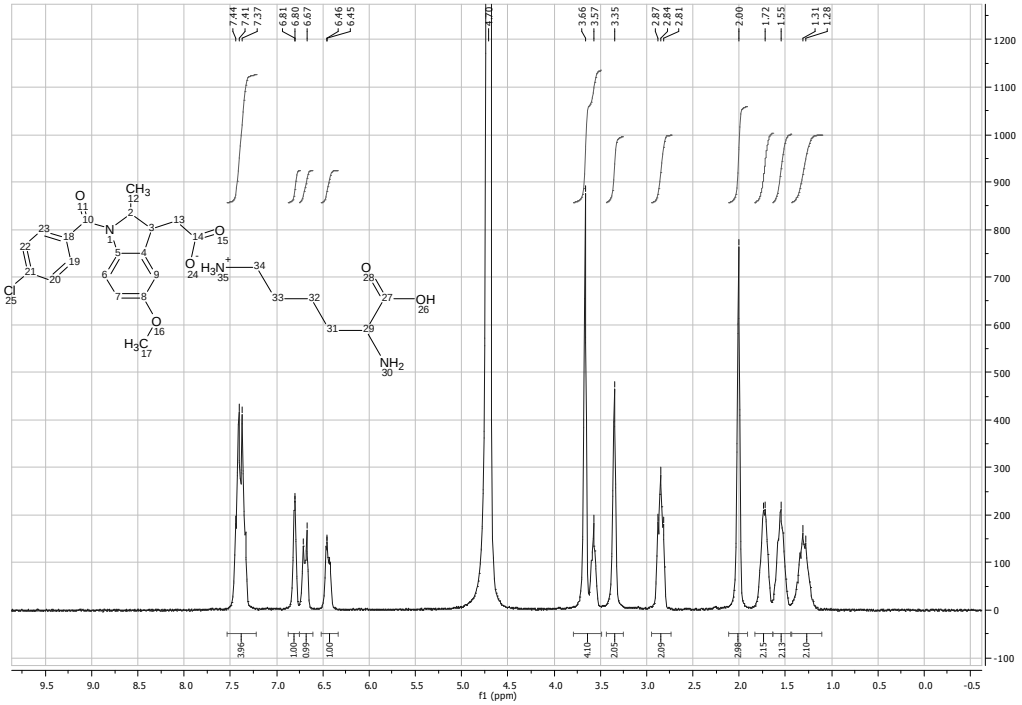

Figure 3.1.20:- ^{1}HNMR spectra for IND-lysine salt dissolved in D_2O.

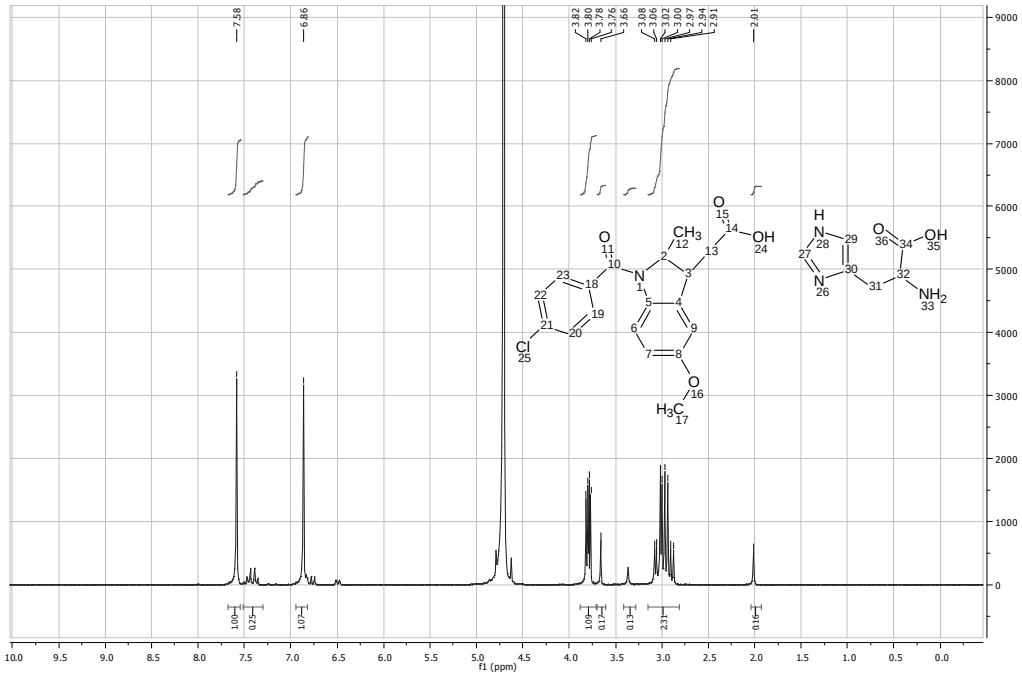

Figure 3.1.21:- **^{1}HNMR spectra for IND-histidine dissolved in D_2O**.

3.1.3.3. Aqueous solubility determination.

IND aqueous solubility is a prerequisite for its dissolution rate as compounds with aqueous solubility lower than 100µg/mL cause dissolution limitations to drug absorption (El-Badry et al., 2009). IND is practically insoluble at acidic pH (0.33 µg/mL at pH 4.5) and slightly soluble at pH 7; 40 µg/mL (Chauhan et al., 2004). IND aqueous solubility was 0.244 µg/mL at pH 4.95 while the IND-arginine salt exhibited the highest solubility among the prepared salts and improved the solubility by 10^4 fold to 34.8mg/mL. IND-lysine increased the solubility by $2x10^3$ fold corresponding to 7.8 mg/mL. The high solubility exerted by arginate salt could be attributed to its stable amorphous form and in turn low energy is required to solubilise the salt. On the other hand, lysinate salt was in the crystalline form requiring higher energy to disrupt the crystal structure and in turn resulting in lower solubility values.

3.1.3.4. Dissolution study.

In vitro drug release profile of IND free acid and its salt are shown in Fig. 3.1.8. The prepared salts showed greater dissolution rates than the free acid.

The highest dissolution rate was exhibited by the IND-arginine salt and 69.4±5.02% of IND was released within the first 10 min and up to 94.3±2.9 % after 30 min, followed by IND-lysinate salt which released 59.88±5.6% and 88.4±0.42 % of the drug after 10 and 30 min respectively. Nevertheless, only 37.9±12.4% of IND was released from the free acid formulation during the first 10 min and 93.2±1.8% in 60 min.

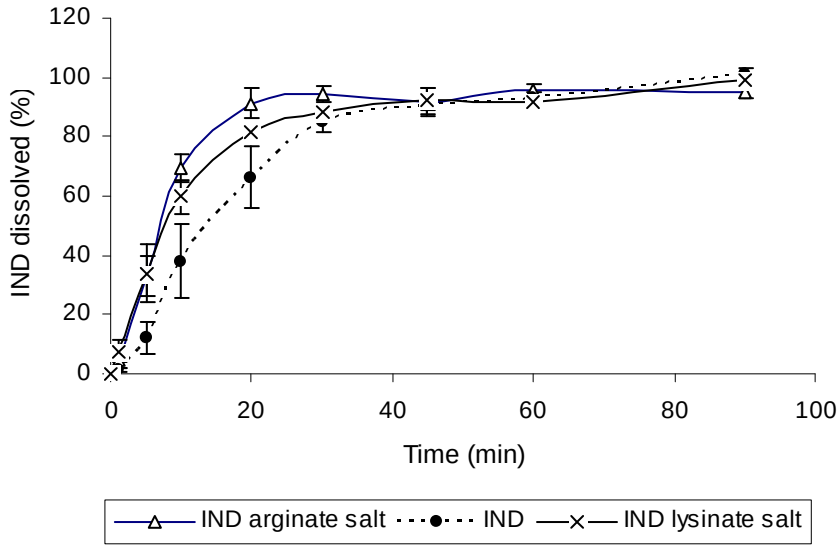

Figure 3.1.22:- Dissolution profile for IND free acids and its salts in phosphate buffer pH 7.2. Data are mean± SD (n=3).

It is obvious that changing the salt form has an influence on the dissolution rate despite using similar bulk pH (phosphate buffer pH 7.2) for all the studied samples. Such changes in the dissolution profile could be attributed to the ability of IND-arginine and IND-lysine salts to exert a self-buffering action, yielding different pH values at the dissolving surface in the diffusion layer (Forbes et al., 1995). It is possible that the IND-arginine salt has a high buffering capacity and produces higher pH at the diffusion layer and in turn higher dissolution rate. Moreover, the arginine salt was in the amorphous form and it is well-known that the amorphous form represents the ideal case for faster dissolution (Hancock and Zografi, 1997).

Despite the high solubility exhibited by IND L-arginine and IND L-lysine salts, a slight improvement in dissolution rate was observed and this could be attributed to the different micro-environmental pH surrounding the surface of the formulation in the solubility and dissolution studies where deionised water and phosphate buffer were used respectively. These results come in line with Stahl et al findings which conclude that the aqueous solubility may not always be a good indicator which form would have the optimum dissolution rate and the dissolution profile of the salt could be higher, equal or even lower than the free form of the drug depending on the micro-environmental pH surrounding the surface of the formulation (Stahl and Wermuth, 2002).

3.1.3.5. pH- solubility profile.

Classical pH-solubility profile of weak acids consists of two main regions; region I and region II. The excess solid in equilibrium with saturated solution in region I represent the free acid and the total solubility is described by Kramer and Flynn equations (Kramer and Flynn, 1972).

$$S_T, acid(pH < pH_{\max}) = [HA](1 + \frac{K_a}{H_3O^+})$$

$$= [AH](1 + 10^{pH - Pka}) \quad \textbf{Equation 3.1.1}$$

Where S is the total solubility at given pH, [HA] is the intrinsic solubility of free acid, K_a is the acid dissolution constant.

On the other hand, the excess solid in equilibrium with the saturated solubility in region II represents the salt and the total solubility is described by

$$S_T, salt(pH > pH_{\max}) = [A^-](1 + \frac{H_3O^-}{K_a})$$

$$= [A^-](1 + 10^{pka - pH}) \quad \textbf{Equation 3.1.2}$$

$$S = (1 + \frac{[H^+]}{K_a})\sqrt{K_{sp}} \quad \textbf{Equation 3.1.3}$$

Where [A^-] is the saturation solubility of the salt, K_{sp} is the solubility product of the salt.

For weekly acidic drugs when pH less than pK_a by 2 units, the solubility is practically independent on the pH and remains constant at the intrinsic solubility (So). At pH >pKa the log solubility increases linearly with pH (i.e solubility increases exponentially with pH).

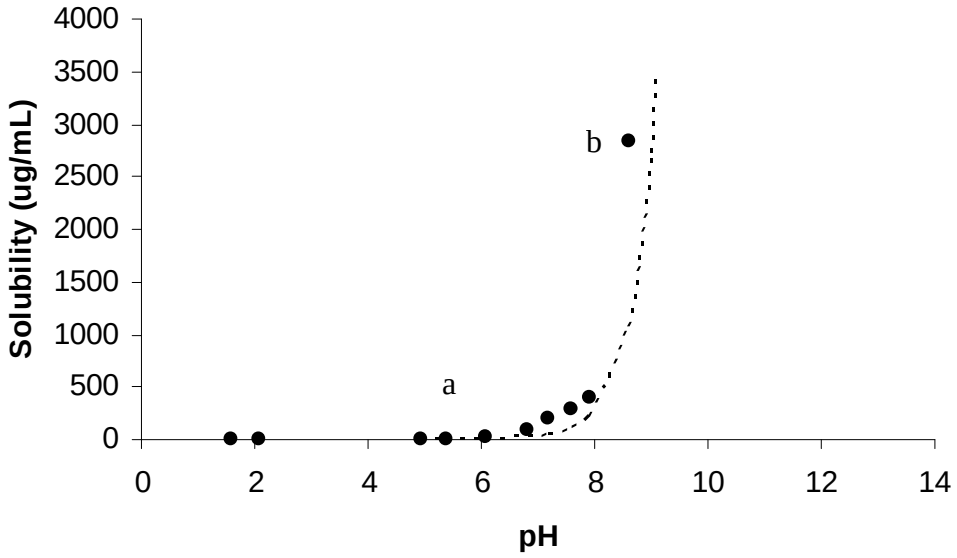

Figure 3.1.23:- pH solubility profile of indomethacin free acid (circles) titrated with L-arginine at ambient conditions.Point a represents the saturation solubility of the free acid. The theoretical curve (dotted lines) was fitted using Eq 3.1.1.

pH solubility profile of indomethacin is presented in figure (3.1.9) and follows equation (3.1.2) with R^2= 0.94. Indomethacin acid has a solubility of 0.24 µg/mL at pH 4.95 in water (point a) reducing the pH to 2 using 0.1N HCl gave an estimation of 0.09 µg/mL for intrinsic solubility [HA]. Indomethacin solubility increased exponentially with pH upon titrating with L-arginine free base reaching a maximum solubility of 2837.8 µg/mL at pH 8.6 (point b) and this was attributed to the formation of IND-arginate salt which has higher solubility.

Excess IND-arginate salt was dissolved in water with saturation solubility 34833.22 µg/mL at pH 8.45, addition of 0.1 N HCl to this saturated solution dropped the solubility to 0.55µg/mL at pH 2.25 due to the precipitation of indomethacin as a free acid, these results comes in line with Ledwidge and Corrigan (1998).

3.1.4. Conclusion

The ability of basic amino acids to forms salts with indomethacin was evaluated in this study. Both L-arginine and L-lysine dissociate IND and then interacted electrostatically to form two novel salts. However, IND failed to dissociate in L-histidine solution. These results were further confirmed by FT-IR and ^{1}HNMR. The two prepared salts showed very high solubility and dissolution profile when compared with the free acid. Na, K and Li IND salts have been previously prepared, however using amino acids as counter ions will provide number of advantages such as suitability with hypertensive patients and painfulness injection. Future work will investigate the effect of using these amino acid salts on the drug permeability across Caco-2 cells.

Prediction of compaction properties of binary mixtures of indomethacin and indomethacin-arginine with arginine

3.2.1. Introduction

Salt formation studies have shown 10^4 fold increase in IND solubility. However, the high dissociation of the salt form could deteriorate the drug ability to partition across the intestinal membrane. Adding excess of the counter ion would act as a common ion and could reduce IND dissociation by shifting equilibrium towards the undissociated form. To put this into a practical solution, the current study aims at investigating the feasibility of using arginine as a tablet filler and upon reaching the absorption site the tablet will disintegrate and an excess of arginine will be available around the drug and might be able to keep the salt form undissociated for absorption.

Tablets are the most commonly used dosage form nowadays. Many components are involved during the tablet manufacture in order to improve the quality of the product. The compaction of all the ingredients into one tablet is a complex process. The main reason behind such complexity is the involvement of various physical characteristics of each pharmaceutical powder during the compaction process. Therefore, most of the scientific research was devoted to studying the compaction behavior of individual powders.

Compaction behavior of binary mixtures was investigated by many studies (Sheikh-Salem and Fell., 1981; Humber-Droz et al., 1983; Van Veen et al., 2000; Zheng et al., 1995; Ramaswamy et al., 1970; Jetzer, 1986; Ilkka and Paronen, 1993; Fell J., 1996). However, no simple relationship was observed between the properties of tablets prepared from binary mixtures to tablets prepared of single components. Three relationships have been discussed in the literature; linear, positive and negative relationships. The study carried out by Newton et al., (1977*)*

found that tablets prepared of dicalcium phosphate dihydrate (DCPD) and phenacetin had a higher tensile strength than tablets prepared from either individual alone (Newton et al., 1977). The study suggested that the positive relationship is probably because the bonds formed between DCPD-phenacetin are stronger than the bonds between individual materials *(*Newton et al., 1977*)*. Similar results were later found by Cook and Summers (Cook and Summers, 1985) when DCPD was co-compressed with aspirin. Although porosity, punch force and elastic recovery showed a linear relationship, the tensile strength of the prepared tablets showed a positive relationship (Cook and Summers, 1985). Linear relationship was reported by Newton et al., (1977) and Fell (1996) for different types of lactose. Such a good correlation was attributed to the similarity in the compaction properties and the bonding mechanisms of the two components. On the other hand, mixtures of brittle lactose and plastic sodium chloride had negative relationship. This was attributed to the ability of lactose to undergo brittle fracture resulting in higher proportion of lactose-lactose bonding which is believed to be weaker than that of sodium chloride (Sheikh-Salem and Fell, 1981).

Despite the large number of studies conducted on binary mixtures only a few studies managed to propose a model to predict the mechanical properties of compacted mixtures (Leuenberger, 1985; Van Veen et al., 2004). Percolation theory is widely used to explain the change of properties exhibited by binary mixtures. For instance, in binary mixture of materials A and B if powder B exists in a small fraction it will form isolated inclusions and form a dispersed phase. While the A powder will form the continuous phase. Because of the localized tension caused by the presence of a small amount of B, the behavior of powder A will change. Increasing the amount of B in the mixture will result in aggregate formation and at certain point in the concentration increasing of B, a network of B particles appears and this concentration represents the percolation threshold. Furthermore, during the compaction of A and B three kinds of interactions can take place: (1) A prefer bonding with A and B bonds preferentially

with B, or (2) the affinity of A-A or B-B bonding is similar to the affinity of A-B bonding or (3) A bonds preferentially with B.

Indomethacin (IND) is a non-steroidal anti-inflammatory drug (NSAID) which is widely used to reduce pain associated with rheumatoid arthritis, osteoarthritis, bursitis and headache (Sweetman, 2005). The compaction properties of IND solid dispersion with crosspovidone was evaluated by (Shibata et al., 2005), and the study found that better tablets are obtained upon using microcrystalline cellulose and magnesium stearate. While the studies conducted by Tahvanainena *et al* (2012) found that IND can form good tablets with acceptable tensile strength upon loading with thermally oxidized mesoporous silicone microparticles (Tahvanainena et al., 2012), these tablets were found to have higher dissolution and permeability profile than the free IND. Although many studies evaluated the compaction properties of formulations containing IND, none of them investigated the densification mechanism of this anionic drug alone.

Most of the active pharmaceutical ingredients (API) have poor compaction properties therefore pharmaceutical excipients such as tablets fillers, binders and disintegrants are incorporated in the formulation in order to improve the properties of the manufactured tablets. The first aim of this work is to characterise the compaction properties of three individual powders namely; IND, as a module drug and IND arginine salt (as its salt form) and arginine (as a tablet filler for the free drug and the salt form), The second stage of this work will utilize Response Surface Modeling (RSM) to predict the characteristics of binary mixtures between the free drug and arginine (PMs) and the IND salt form with arginine (SMs) and compare the predicted results against the experimental data.

3.2.2. Materials and methods

3.2.2.1. Materials

Indomethacin (TLC ≥ 99%), L-Arginine (non-animal source) and magnesium stearate were purchased from Sigma Aldrich (Dorset, UK). Ethanol was purchased from Fisher Scientific (Loughborough, U.K.)

3.2.2.2. Methods

3.2.2.2.1. Physical mixtures (PMs) and salt preparations.

PMs of IND with various molar ratios of arginine were prepared by weighing accurate amount of TMP and mixed by KitchenAid (Michigan, USA) at mixing speed of 3 for 5 minutes with the various ratios of of arginine. IND arginine salt was prepared using the ElShaer et al method (2011). Equimolar amounts of IND and the free amino acid were solubilised in water and the solutions were mixed and stirred until equilibration then filtered. The filtrate was transferred into vials and freeze dried for 48h using a Modulyo freeze dryer at -40^{o}C shelf temperature and under vacuum created by (E2M5 Edwards pump) then samples were collected and kept at 40^{o}C for 4h using a Gallenkamp vacuum oven. Salt excess amino acid mixtures (SMs) were prepared by the same way as PMs.

3.2.2.2.2. Tap density and Powder flow (Hausner's ratio and Carr's index)

USP I apparatus (Sortax tap density tester) was used to measure the true density of the powders. 15 gm of the powders was weighed and poured into a 100 mL measuring cylinder and the initial volume of the powder was recorded as zero tap (bulk volume). The machine was allowed to vibrate at 50, 100, 150, 200 and 250 taps and the final volume after each tapping was recorded.

Carr's compressibility index was used to study the flow characteristics of the powders and was calculated from equation (3.2.1).

$$Carr's = \frac{\rho_t - \rho_p}{\rho_t} \times 100$$ **Equation 3.2.4**

While the Hausner ratio was used to evaluate the ease of powder flow and equation (3.2.2) was used to work it out.

$$Hausner = \frac{\rho_t}{\rho_p}$$ **Equation 3.2.5**

Where ρ_t is the tapped density and ρ_p is the poured density.

Table 3.2.23:- Flowability based on Hausner ratio, Carr's Index and angle of repose according to BP guidelines (British Pharmacopoeia 2011).

3.2.2.2.3. Particle Size Distribution Analysis (Sieve method)

A set of sieves (Retsch AS 200) of diameter 710 µm, 355 µm, 250 µm, 125 µm, 90 µm, 75 µm and 63µm arranged in a decreasing order of their diameter were used to measure the powders' particle size distribution. 15 gm of the powders were accurately weighed and placed on the top sieve and then allowed to shake for 12 minutes at amplitude of 60. The powder retained in each pan was weighed and the cumulative weight undersize was calculated and plotted against sieve diameter. This test was not carried out for the salts and their mixtures because of the small sample sizes

3.2.2.2.4. Tablet preparation

Tabets of IND, its arginine salt and physical mixtures with excess of the amino acid counter ions at (1:1), (1:2), (1:4) and (1:8) molar ratios were prepared to study tableting properties. The powders were compacted using an uniaxial hydraulic press (Specac tablet presser) and split die which prevents mechanical failure by allowing triaxial decompression. Magnesium stearate in ethanol (5% w/v) was used to lubricate the die walls and punch surfaces. Powders were compressed at 5, 10, 20, 30, 40 and 60 kN and at dwell time of 30 sec.

The prepared tablets were cylindrical with a diameter of 13 mm and weight of around 500 mg. Tablets were left in desiccators for 24 h prior to performing any mechanical testing.

Tablet characterization

3.2.2.2.5. Tensile strength measurements

The force required to crush the prepared tablets was measured using a tablet hardness apparatus (Schleungier 4M, Thun, Switzerland). The measured force was used to determine the tablet tensile strength using equation (3.2.3).

$$\sigma = \frac{2F_c}{\pi dt}$$ **Equation 3.2.6**

Where σ is the tablet tensile strength, *Fc* is the crushing force required to break the tablet, *d* is the tablet diameter and *t* is the tablet thickness. All measurements were done in triplicate.

3.2.2.2.6. Heckel analysis

The Heckel equation (3.2.4) was used to analyze tablets' compression data (Heckel, 1961a).

$$\ln(1/(1-D)) = KP + A$$ **Equation 3.2.7**

Where D is the tablet relative density at pressure P, K is a material constant (slope of the straight line portion of Heckel plot) and is 1/3 of the yield strength. 1/K value is used to express

the mean yield pressure. A is a function of the initial bulk volume and is calculated from the intercept of the straight line of the Heckel plot.

3.2.2.2.7. Apparent, bulk particle density and porosity measurements

Bulk density was determined by using 10 ml cylinder to measure the volume (V) of a pre-weighed sample. Apparent particle density was measured using a helium pycnometer (Multipycnometer Quantachrome Instruments, Hampshire, UK). Both bulk and true density values were used to determine the powder porosity according to equation (3.2.5).

$$\varepsilon = 100(1 - \rho_d / \rho_t)$$ **Equation 3.2.8**

Where ε is the porosity and ρ_d is the bulk density and ρ_t is the true density. All the measurements were done in triplicate.

3.2.2.2.8. Disintegration time studies

Disintegration time is the time required for tablets to disintegrate completely without leaving any solid residue. *In vitro* disintegration time was evaluated using US pharmacopoeia monograph (<701> disintegration). Erweka ZT3, Appartebau, GMBH was used in this study as a disintegration apparatus and distilled water (800 ml) as disintegration medium; the disintegration medium temperature was maintained at 37 °C by thermostat. Six tablets were placed in the basket rack assembly and covered by a transparent plastic disk. The disintegration time was taken as the time required for tablets to disintegrate completely without leaving any solid residue. All the measurements are carried out in triplicate and presented as (mean ± standard deviation).

3.2.2.2.9. Design of the experiment

MODDE software version 8 (Umetrics inc., USA) was used to design the statistical experiment for this study. Three levels full factorial design response surface modelling (RSM) with total runs of 24 of which three replicated centre points was selected for this study.

The effect of two independent variables; compaction force (F) and arginine percentage (R) on three dependant variables (responses); porosity (P), tensile strength (S) and disintegration time (T) was studied.

3.2.3. Results and discussion

3.2.3.1. Powder characterisation

Physical mixtures (PMs) of IND and arginine and salt mixtures (SMs) of IND salt and arginine were prepared in ratios of 1:1, 1:2, 1:4 and 1:8. The prepared PMs, SMs and individual powders of IND and arginine were characterised in terms of particle size distribution, flowability, bulk, true, tapped density and porosity.

3.2.3.1.1. Particle size analysis

Particle size analysis showed that IND:arginine 1:1 PM has the most uniform particle size distribution with its median of around 175 µm. Around 90% of 1:8 and 1:4 physical mixtures had particle size <350 µm. whilst the 1:2 and 1:1 ratios had 70% and 30% of the particles <350 µm respectively. Particle size distribution of IND and arginine was comparable as 60% of IND molecules having a particle size <350 µm, and 70% of arginine particles having a particle size <350 µm (Fig. 3.2.1).

The particle size analysis suggests that the IND dry powder and 1:2 physical mixture should have good flowability because of their large particle size. Whilst particles with particle size

lower than 100 µm are cohesive and flow problems occur (Staniforth, 2007). Therefore, it was interesting to carry out flowability studies for the individual powders and the physical mixture.

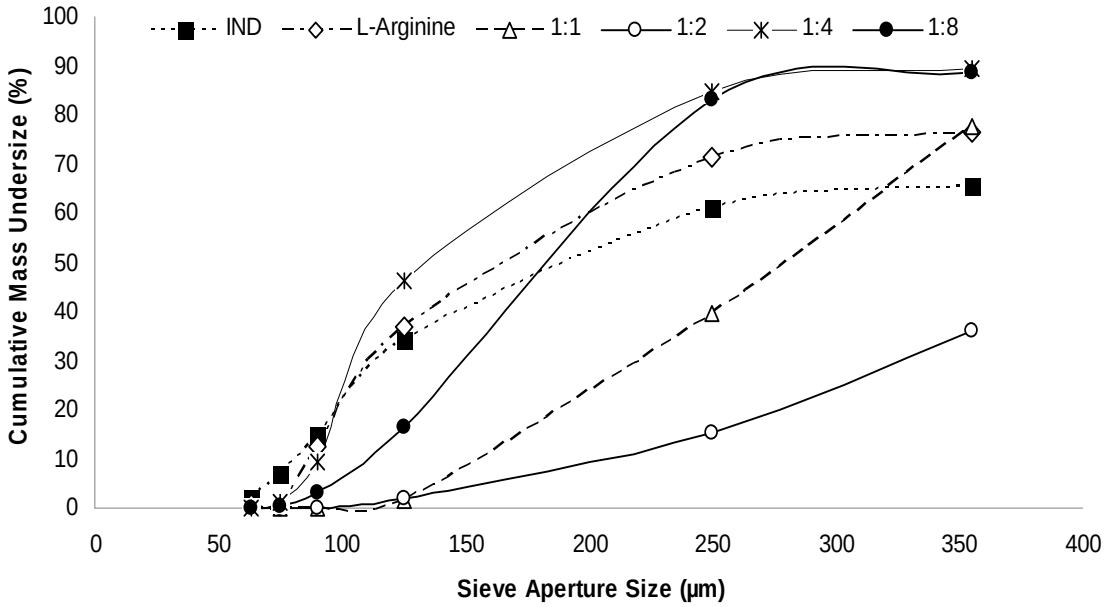

Figure 3.2.24– Particle size analysis of Indomethacin, L-Arginine and physical mixtures (n=3).

3.2.3.1.2. Flowability studies.

In this study the flow properties for IND, its salt, PMs and SMs were evaluated using angle of repose (Table 3.2.2).

Table 3.2.24– Hausner Ratio, Carr's Index and angle of repose for Indomethacin, L-Arginine and their PMs and SMs.

Formulation	Angle of Repose (Mean ± SD, n=3)	Hausner Ratio	Carr's Index	Formulation	Angle of Repose (Mean ± SD, n=3)
IND	36.89 ± 3.28	3.54	71.77		
L-Arginine	29.4 ± 0.84	2.70	63.00	IND arg Salt	36.00 ± 1.92
PM 1:1	42.82 ± 0.07	3.11	67.88	SM 1:1	37.06 ± 3.56
PM 1:2	41.44 ± 3.20	2.94	66.03	SM 1:2	24.83 ± 0.86
PM 1:4	33.86 ± 4.30	3.36	70.23	SM 1:4	25.40 ± 0.37
PM 1:8	29.85 ± 2.40	3.44	70.92	SM 1:8	26.60 ± 2.31

Angle of repose measurements showed that IND has fair flowability (angle of repose= 36.89 ± 3.28), whilst, arginine had excellent flowability (angle of repose= 29.4 ± 0.84). Although SEM images show large particle size of IND (Fig. 3.2.2), the drug showed fair flowability characteristics and this may be attributed to the positive surface charge carried by IND. This positive charge increases the adhesiveness to the surfaces and in turn deteriorates the flow of the powder as suggested by Soppelaa et al., (2010). On the other hand, SEM has shown elongated rods for arginine with rough surface which are believed to be the reason behind the good flowability of this amino acid.

Interestingly, the flow properties dropped ($p<0.05$) upon mixing IND and arginine at 1:1 and 1:2 ratios. This is possibly because of significantly electrostatic interactions forming between the negative and positive charge on IND and arginine respectively which results in increasing the co-adhesion between the two binary mixtures. Beyond these two ratios increasing arginine concentration resulted in increasing the overall negative charge on the mixture and hence the flowability of the powder mixture (Table 3.2.2) improved from passable at 1:1 and 1:2 ratios into excellent flowability (29.85 ± 2.40) at 1:8 ratio.

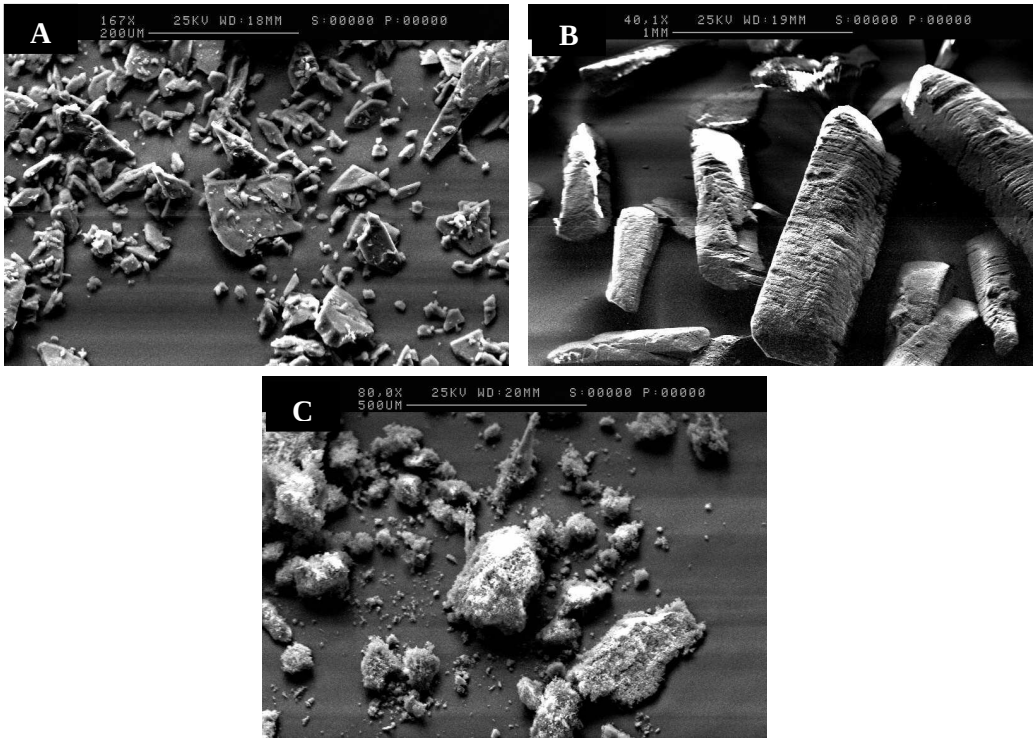

Figure 3.2.25:- SEM images for (A) IND and (B) ar ginine, (C) IND arginine salt.

On the other hand, flow properties for all the powders were found to be poor upon using the Hausner ratio and Carr's index methods (Table 3.2.2). Such variation between the two methods is possibly because the Hausner ratio and Carr's index are one-point determinations that do not take into account the ease or speed with which consolidation of the powder occurs (Staniforth, 2007). Materials with high index which are supposed to have low flowability were found to consolidate quickly and hence had more uniform filling on tablet machines. The study conducted by Li *et* al found a similar trend in that powders which showed good flowability according to Hausner ratio exhibited poor flowability when tested using the bin-flow test and vice versa (Li et al., 2004).

The flowability characters of IND arginine salt and SMs were studied as well by measuring the angle of repose of the powders. Haunser ratio and Carr's index were not carried out because of the low amount of the salt obtained via freeze drying.

Although IND arginine salt has zero net charge on its surface, yet its flowability (AOR= 36.00 ± 1.92) was similar to that of IND free acid. The poor flowability of the salt form is possibly because of the agglomerate like structure of its particles formed during its freeze drying as suggested by Soppelaa et al., (2010) and Alhusban et al., (2011). In contrast to the PMs, salt binary mixtures showed increase in the flowability characteristics as the amount of arginine increased in the mixture (Table 3.2.2) probably because no co-adhesion occurs between the cationic arginine as the salt carries no charges on its surface. Hence, increasing the ratio of the amino acid in the mixture resulted in increasing the negative charge and enhancement of flowability.

Table 3.2.25:- Weight, volume Bulk Density, True Density and Porosity of IND, arginine and their PMs

Formulation	Weight (g) (M± SD, n=3)	Volume (cm^3) (Mean ± SD, n=3)	Bulk Density (g/cm^3) (Mean ± SD, n=3)	True Density (g/cm^3) (Mean ± SD, n=3)	Porosity (Mean ± SD, n=3)
IND	1.01 ± 0.01	2.43 ± 0.15	0.41 ± 0.03	1.44 ± 0.04	0.71 ± 0.02
L-Arginine	1.01 ± 1.01	2.10 ± 0.10	0.48 ± 0.02	1.50 ± 0.31	0.67 ± 0.09
PM 1:1	1.01 ± 0.00	2.67 ± 0.06	0.38 ± 0.01	1.58 ± 0.14	0.76 ± 0.02
PM 1:2	1.01 ± 0.01	2.60 ± 0.10	0.39 ± 0.02	1.52 ± 0.34	0.74 ± 0.06
PM 1:4	1.01 ± 0.00	2.23 ± 0.15	0.45 ± 0.03	1.54 ± 0.21	0.70 ± 0.06
PM 1:8	1.01 ± 0.00	2.30 ± 0.10	0.44 ± 0.02	1.50 ± 0.14	0.71 ± 0.03

3.2.3.1.3. Porosity studies

Bulk density, true density and porosity were measured for the individual powders and physical mixture and are summarised in Table (3.2.3). IND bulk density was found to be 0.41 ± 0.03 whilst that of arginine was 0.48 ± 0.02. Upon preparing physical mixtures of IND and arginine, the bulk density dropped significantly ($p<0.01$) to 0.38 ± 0.01 which is lower than that of IND and arginine alone. A similar trend was observed in ElShaer et al (in press) studies with TMP/aspartic acid physical mixture (chapter 4.2) and as suggested, it may be because of the overall reduction of the repulsion force between similar by charged molecules in the same powder with such reduction caused by the addition of counter ions which carry opposite

charge (ElShaer et al., 2012). Nevertheless, the true density and powder porosity were the same for all the formulations and no significant difference was found between any of them (Table 3.2.3).

Table 3.2.26:- Weight, volume, bulk density, true density and porosity of IND salt and the SMs

Formulation	Weight (g) (M±SD, n=3)	Volume (cm^3) (M±SD, n=3)	Bulk Density (g/cm^3) (M±SD, n=3)	True Density (g/cm^3) (M±SD, n=3)	Porosity (M±SD, n=3)
IND arg Salt	0.50 ± 0.00	3.07 ± 0.06	0.16 ± 0.00	2.13 ± 0.06	0.92 ± 0.00
SM 1:1	0.50 ± 0.00	1.80 ± 0.01	0.28 ± 0.02	1.80 ± 0.05	0.85 ± 0.01
SM 1:2	0.50 ± 0.00	1.77 ± 0.06	0.28 ± 0.01	1.96 ± 0.05	0.86 ± 0.01
SM 1:4	0.50 ± 0.00	1.50 ± 0.10	0.33 ± 0.02	2.08 ± 0.12	0.84 ± 0.00
SM 1:8	0.50 ± 0.00	1.53 ± 0.32	0.34 ± 0.06	1.95 ± 0.02	0.83 ± 0.02

Analysis of bulk density for SM suggested that an increase in bulk density decreases the porosity although statistically there was no difference found between any of the formulations in bulk density, true density and porosity data shown in Table 3.2.4 ($p>0.05$).

Powder characterisation has shown better bulk densities and porosity for the salt form and the SMs when compared to the free drug and its PMs which could be attributed to the way the salt form was prepared as the lyophilized salt would have a highly porous structure and in turn higher bulk density (Alhusban et al., 2011).

3.2.3.2. Densification properties of individual powders

After the full powder characterisation, the compaction properties of each individual powder were studied in order to understand their densification mechanisms prior to conducting the RSM and experimental studies for the binary mixtures.

The reduction of the material volume that accompanies an applied pressure is known as compressibility (Joiris et al., 1998). The compressibility behaviour of pharmaceutical powders is evaluated by plotting the tablet porosity against the compaction force (Joiris et al., 1998). For a pharmaceutical powder to form a strong compact, the material should be highly compressible, i.e. have smaller porosity upon compression in order to enable particles to get closer to each

other and increase the bonding area between the particles. Fig. 3.2.3 shows the compressibility profile of the three individual powders; IND, arginine and IND arginine salt. Generally, increasing the compression force resulted in a decrease in the tablets' porosity. The highest compressibility profile was exhibited by the salt. Probably because of the highly porous structure of the salt form obtained during the freeze drying cycle which might have resulted in poor packing due to cohesiveness of the powder as reflected by its flowability. The high compressibility profile of the salt form would enable the formation of strong tablets because of the high interparticulate bonding area created upon densification of this highly compressible powder. On the other hand, IND free acid showed the lowest compressibility profile as the tablet porosity was 0.52±0.01 at 5 kN and slight dropped to 0.46 upon doubling the compression force then no significant ($P>0.05$) change was observed even at the very high compression forces. Arginine compressibility was between that of the free acid and the salt form (Fig. 3.2.3).

In order to understand the densification mechanism of the individual powders, Heckel analysis was carried out.

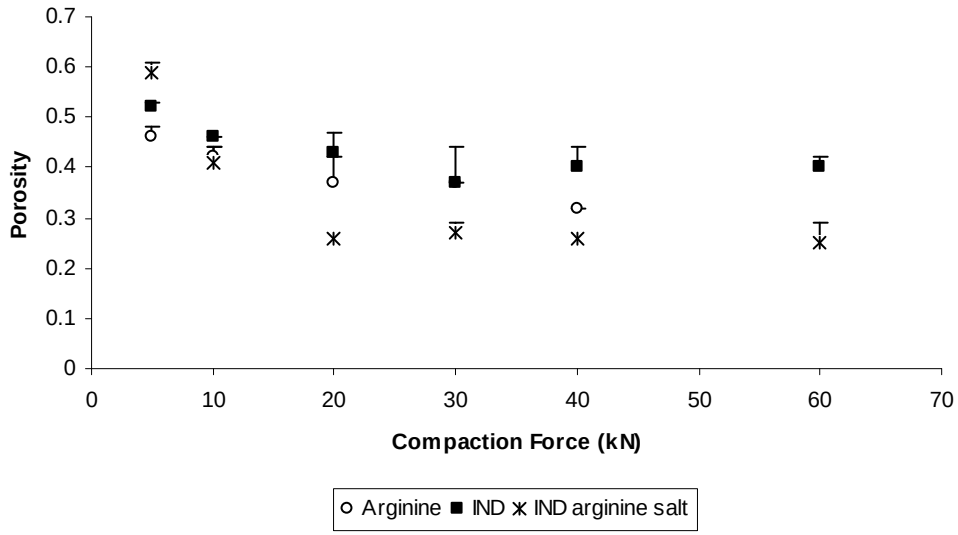

Figure 3.2.26:- Plots of tablet porosity against compaction pressure, showing the compressibility of IND, arginine, IND arginine salt (n= 3).

It is known that the plastic properties of pharmaceutical powders play an important role during the densification of the powder. Therefore, Heckel analysis was carried out and both the yield strength and yield pressure were calculated using Heckel equation (Equation 3.2.4) and summarised in Table (3.2.5). Heckel graphs for the powders showed initial curvature representing the particle fragmentation and rearrangement in the die. This is followed by a linear relationship between compaction force and -ln porosity, the slope of which indicates the degree of plastic deformation and consequently yield strength (Staniforth, 2007). Heckel analysis showed that IND arginine salt and arginine have yield strengths of 43.85 and 28.01 respectively. Which reflects the high plasticity of the two powders especially arginine. Nevertheless, the analysis showed a very low plastic characteristics and high elastic deformation of IND that take place during compaction as the yield strength was found to be 208.33. The high elastic behaviour of IND affected the integrity of its prepared tablets and problems such as capping, lamination and breakage were observed.

Table 3.2.27:- Summary of Heckel analysis and tensile strength at zero porosity (σ_0) for IND, arginine, IND arginine salt, PMs and SMs.

Formulation	σ_0	Yield pressure	Yield strength	Formulation	σ_0	Yield pressure	Yield strength
IND	1.13	625	208.3333	Salt	3.35	131.5789	43.85965
Arginine	381	84.03361	28.0112	SM 1:1	4.12	208.3333	69.44444
PM 1:1	1289.9	185.1852	61.7	SM 1:2	29.33	166.6667	55.55556
PM 1:2	223.9	72.46377	24.15459	SM 1:4	147.12	188.6792	62.89308
PM 1:4	217.65	62.5	20.83333	SM 1:8	588.54	109.8901	36.63004
PM 1:8	n/d	107.5269	35.84229				

The ability of pharmaceutical powders to form a strong tablet during densification is known as compactability and can be represented by plotting the tensile strength against porosity.

The compactability profile of IND, IND arginine salt and arginine were studied and are summarised in Fig. 3.2.4. As suggested by Ryshkewitch, (1953) an exponential correlation between tablets tensile strength and porosity was observed for both arginine and the IND arginine salt, i.e. increasing the tablet porosity resulted in an exponential decrease in the tablets' tensile strength. However for unknown reasons IND showed a weak correlation (Fig. 3.2.4). The highest compactability was exhibited by arginine and because the compactability reflects the strength of bond formation, this suggests that strong bonds are formed during the densification of arginine. In contrast to IND which showed the lowest compactability indicating, the weak bond formation under the compaction. In order to calculate the tablets' tensile strength at zero porosity the Ryshkewitch equation (Equation 3.2.6) was used and results are summarised in (Table 3.2.5).

$$\sigma = \sigma_0 e^{-b\varepsilon}$$ **Equation 3.2.9**

Where σ is the tensile strength σ_0 is the tensile strength at zero porosity, ε is the porosity and *b* is a constant.

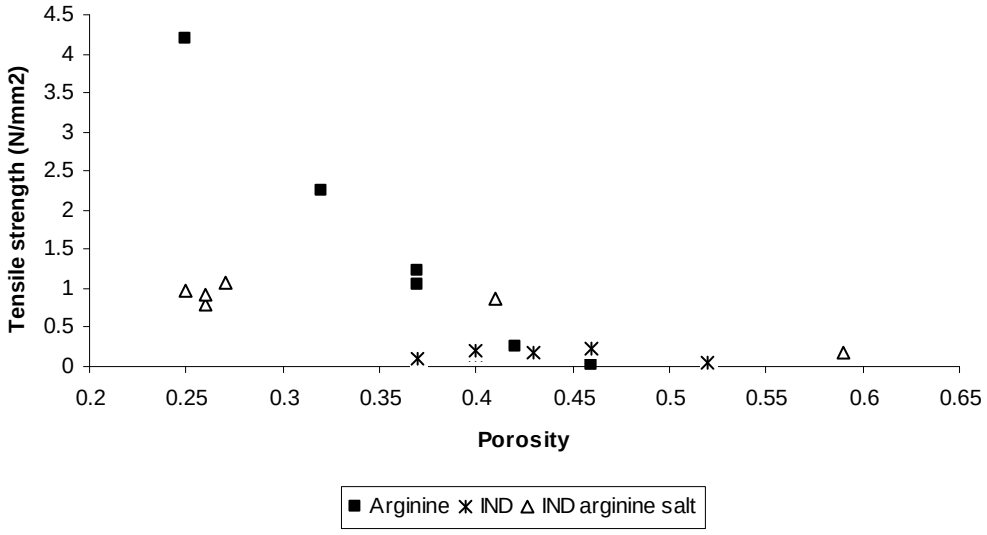

Figure 3.2.27:- Plots of tablet tensile strength against porosity, showing the Compactability of IND, arginine, IND arginine salt (n= 3).

Another property is tabletability which is known as the ability of powder to form a tablet of specific strength while exposed to compaction pressure. The tabletability profile of a pharmaceutical powder can be expressed by plotting tablet tensile strength against compaction force (Sun and Grant, 2001). Both powder compressibility, which affects the bonding area and compactability properties of the powder which reflects the strength of bond formation determine the tabletability characteristics of the pharmaceutical powder. Figure 3.2.5 shows that increasing the compaction force results in increasing the tensile strength for the tablets. IND powder showed the lowest tensile strength (0.21±0.05) at 60 kN. This result was expected as Heckel analysis revealed the high elasticity of IND while the compactability data showed weak bond formation. On the other hand, the cationic amino acid tablets showed the highest tensile strength and IND arginine salt tablets had good tabletability. Although the salt form showed better compressibility, its tabletability was not as great as the arginine. This assumes that compactability of the powder is the main determinant of the compacts strength.

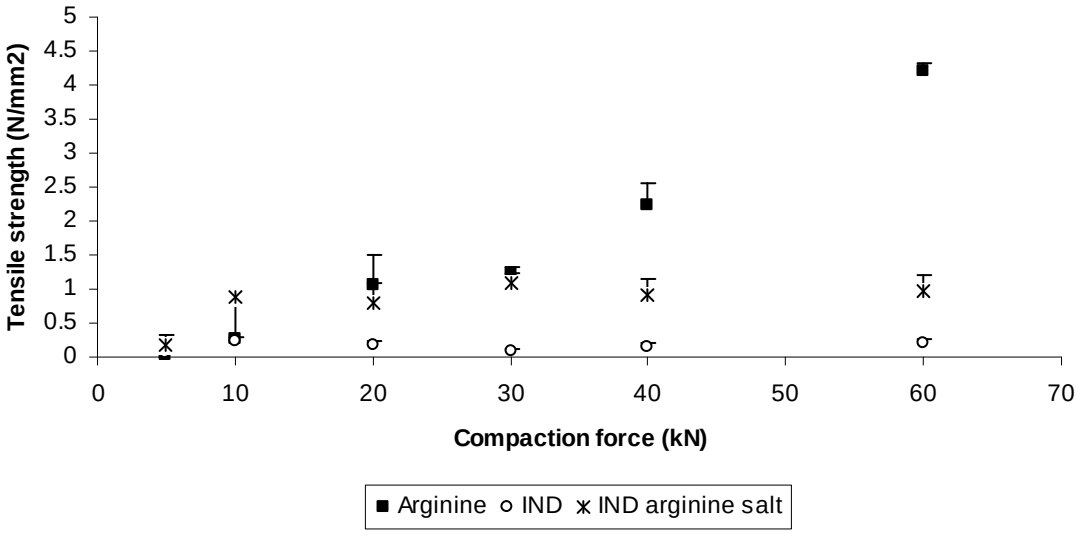

Figure 3.2.28:- Plots of tablet tensile strength against compaction pressure, showing the tabletability of IND, arginine, IND arginine salt (n= 3).

The ability of the tablets to disintegrate in water was evaluated and the disintegration results revealed that increasing the compaction force deteriorates the tablets' disintegration time. Although compressibility data revealed the high porosity of IND, the free acidic drug showed a very poor disintegration and the drug failed to disintegrate even after 20 minutes (Fig 3.2.6). The high lipophilicity of IND could be the reason behind its poor disintegration. Hansch and Leo reported the log P value of IND to be 3.8 (Hansch and Leo, 1979) which reflects its low hydrophilicty, low wettability (Fukami et al., 2005) and hence the extended disintegration time.

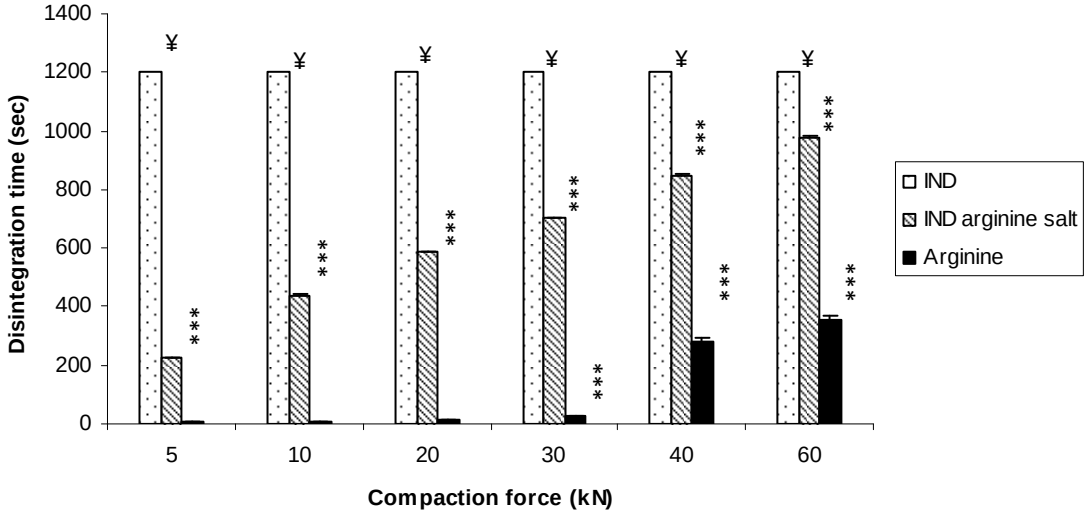

Figure 3.2.29:- Disintegration time for IND, arginine and IND arginine salt (n=3) (¥; tablets failed to disintegrate within 20 minutes), (* p<0.001).**

However, arginine tablets showed very rapid disintegration time (25.3±2 s) for tablets compressed at 30 kN despite having high tensile strength (1.23±0.09). Probably because of the high hydrophilicity of arginine as it has low log P value of 0.69 (Kennedy et al., 2000) and therefore high wettability and fast disintegration. Although the salt form was found to be highly hydrophilic (ElShaer et al., 2011), the disintegration time was not as low as that of arginine and this might be attributed to the very low porosity of the salt tablets as suggested by the compressibility data. Low porosity results in poor water penetration into the tablets and hence a longer disintegration time is required.

3.2.3.3 Comparison between the predicted and experimental data for binary mixtures

3.2.3.3.1. Compressibility characterisation of the binary mixtures

The characterisation of the individual powders showed that arginine has very high bonding capacities and its tablets disintegrate quickly. This means that incorporating the amino acid into the formulations, should improve the tablets' characteristics. Moreover, studies carried out in our lab showed that adding arginine to the formulation improves anionic drugs dissolution and absorption through intestinal membranes (data discussed in the next chapter).

Therefore, an experimental design was used to predict the effect of incorporating arginine to IND, which showed very poor compaction and disintegration characteristics, and IND arginine salt in an attempt to fit a model that could predict the compaction properties of the binary mixtures and compare it against the experimental data.

The compaction force is an important factor that affects the porosity and tensile strength of the tablets. Hence the compaction force (F) was selected as an independent variable and compaction force was changed between 5-60 kN. The arginine ratio (R) –ranging between 0-100%- in the binary mixture was the second variable and was selected for the reasons mentioned above. The effect of these two independent variables on tablet porosity (P), tensile strength (S) and disintegration time (T) was studied using response surface modelling (RSM). RSM was preferred over screening modelling because the aim of the study is to predict effect of both the compaction force and arginine ratio on the tablets characteristics. A full factorial design with each factor varied at three levels was selected, and the model was fitted to the multiple linear regression (MLR) because the total number of responses was not more than 3. The significance of the quadratic model (linear, interactive and polynomial) on the dependent variables was carried out using analysis of variance (ANOVA) and the quantitative effects of the independent variables on the responses was considered significant at a 95% confidence level ($p< 0.05$). A high degree of reproducibility was obtained for most of the responses (Fig. 3.2.7), which suggest that the three responses are strongly dependent on the two independent variables.

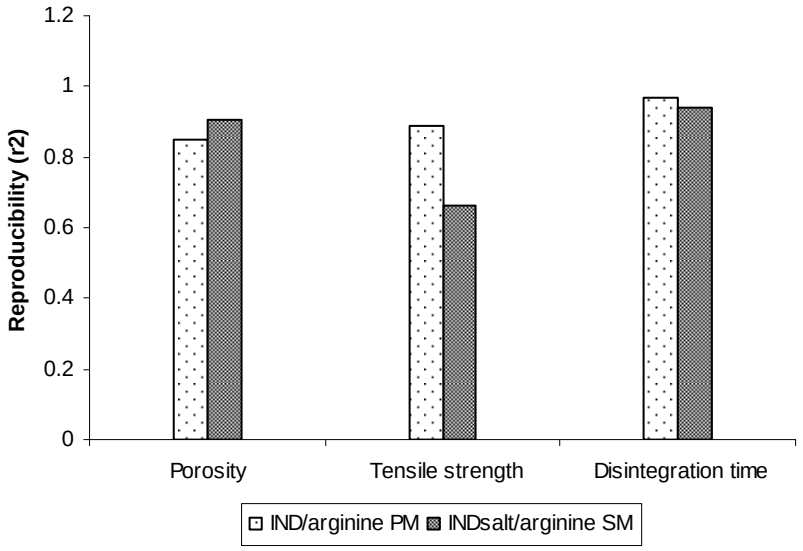

Figure 3.2.30:- Reproducibility of the results for all three responses which represents the variation of the response under the same conditions (pure error) compared with the total variation of the response.

Table (3.2.6) summarise the effect of each independent factor on the responses; the sign of the effect represents the trend while the values indicate the magnitude of this effect. The data show that both the compaction force (F) and arginine ratio (R) have a significant (P< 0.001) influence on IND tablet porosity. Figure (3.2.8A) shows that increasing the compaction force and arginine ratio causes a decrease in the tablets porosity. Nevertheless, the effect of compaction force (0.16) was twice that of arginine ratio (0.08). Interestingly the interactive term FR was found to have an antagonistic effect as the magnitude of decrease in the tablet porosity (P) was less than the effect of each single term.

Table 3.2.6:- The quantitative factor affecting tablets porosity and their associated p value for the responses.

	Porosity			
term	IND		IND arginine salt	
	Effect	*p* value	Effect	*p* value
F	-0.1598	<0.001	-0.3045	<0.001
R	-0.07805	0.001176	-0.0175	0.578895
F^2	0.154053	<0.001	0.25403	<0.001
R^2	-0.02275	0.46393	0.2332	<0.001
FR	-0.06226	0.0217	0.06554	0.100594

Looking at IND-arginine salt/arginine binary mixtures (Fig. 3.2.8B, Table 3.2.6) showed that only the compaction force influences the porosity of the tablets (0.3), while incorporating

arginine had no significant effect on the porosity (p>0.05). This is probably because of the high compressibility of the salt form which was found to be higher than the cationic amino acid and hence masked the effect of arginine which appeared to be significant upon mixing with low compressible IND.

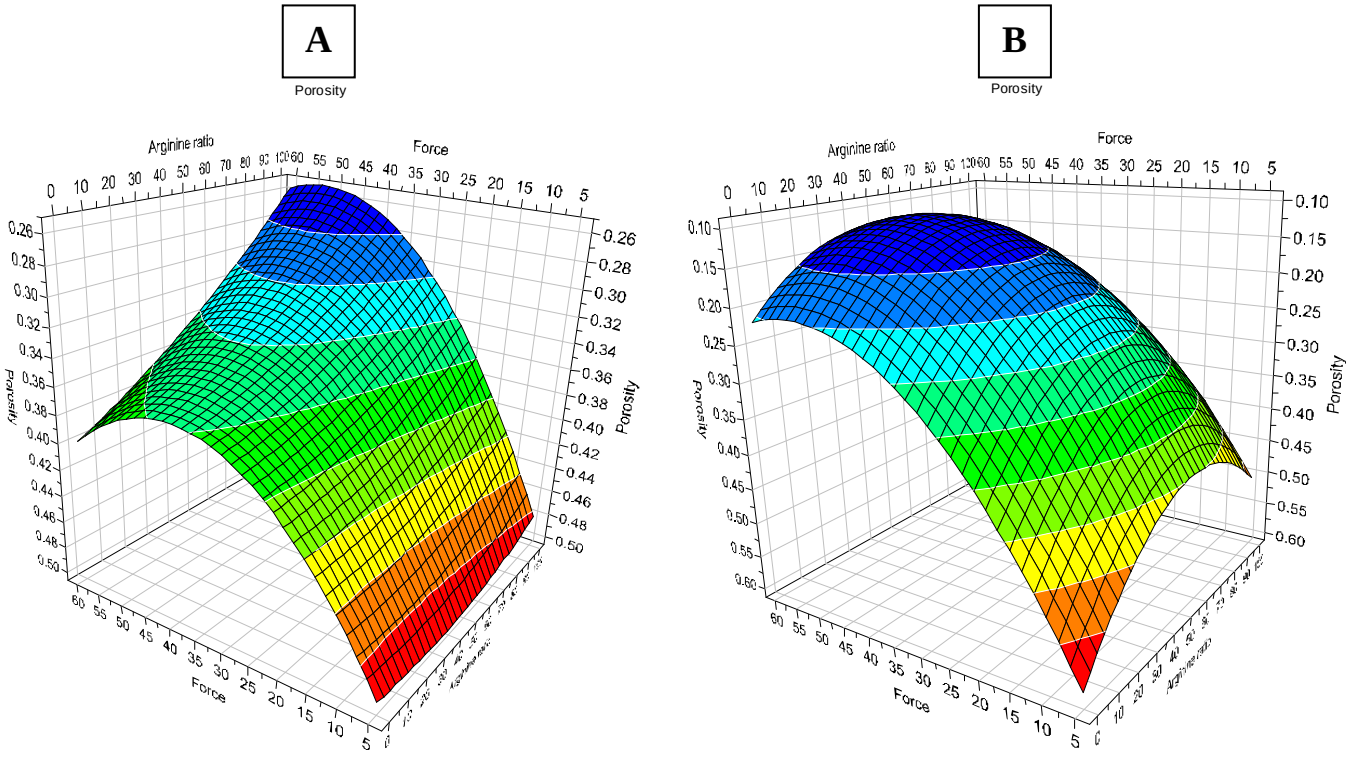

Figure 3.2.31:- Surface response plot showing the effect of compaction force and arginine ratio on tablets porosity for (A) IND/arginine binary mixtures, (B) IND salt/arginine binary mixtures

The MLR was used to fit the mathematical equation and the response surface plots (3D) which could be used to predict the tablet porosity by inputting the experimental conditions using the two independent variables; F and R.

The mathematical expression for working out the porosity of IND/arginine binary mixtures is equation (3.2.7)

$$P_{Ind} = 0.343 - 0.159F - 0.078R + 0.15F^2 - 0.062FR \qquad \textbf{Equation 3.2.10}$$

While that for the salt form is expressed in equation (3.2.8)

$$P_{Salt} = 0.15 - 0.3F + 0.25F^2 + 0.23R^2$$ **Equation 3.2.11**

Where P_{Ind} is the porosity for IND/arginine PMs, P_{Salt} the porosity of IND salt/arginine SMs, F is the compaction force and R is arginine percentage in the binary mixture.

The compressibility profile for IND and the salt with various ratios of arginine was studied in order to compare the experimental findings against the predicted data (Table 3.2. 6).

Figure (3.2.9A) shows the compressibility profile for IND/arginine binary mixtures. Similar to the individual powders, increasing the compaction force resulted in decreasing the tablet porosity. The highest compressibility was exhibited by arginine> PM 1:4> PM 1:2> PM 1:1> IND Heckel analysis (Table 3.2.5) showed that PM 1:4 has the highest plasticity as its yield strength was found to be (20.83) and the elasticity of IND (yield strength of 208.33) dropped significantly upon incorporating arginine into the formulations (yield strength of 61.7 at PM 1:1). These results confirm the quadratic model findings which suggested the significant role of adding arginine on the tablet porosities.

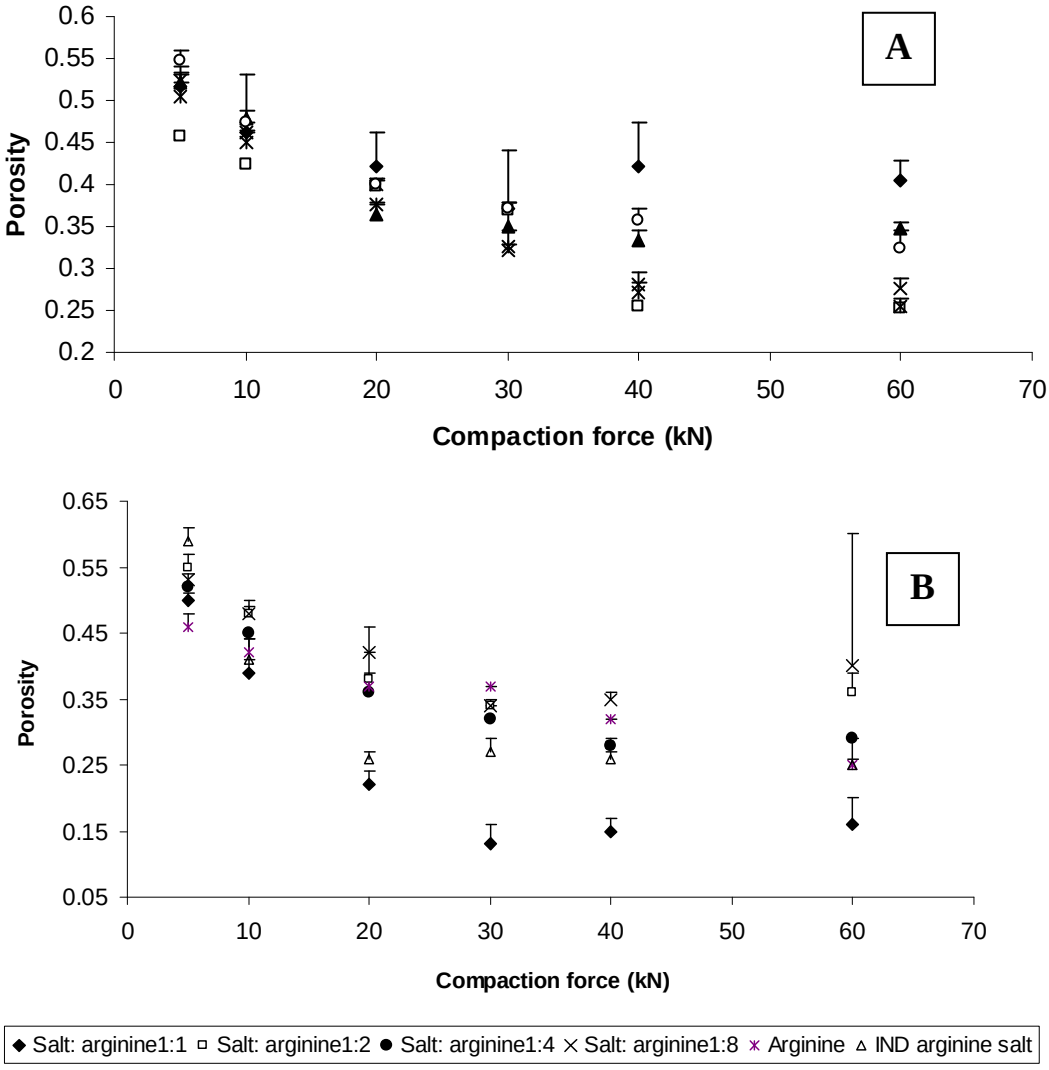

Figure 3.2.32:- Plots of tablet porosity against compaction pressure, (A) Compressibility of IND, L-arginine and PM's and (B) Compressibility of IND salt and SM's (n=mean±SD and n=3).

On the other hand, studying the compressibility profile for IND salt/arginine mixtures (SMs) showed that only SM at 1:1 (50 % arginine) ratio had higher compressibility than the salt form while other has not been significantly affected when adding the amino acid. Moreover, Heckel analysis revealed that there is no big difference between the yield strength of the salt form and the salt mixtures with arginine (Table. 3.2.5) which reflects the low changes in the compressibility profile upon incorporating arginine. The porosity for most of the ratios

dropped significantly upon increasing the compaction pressure which suggests that the compaction force is the main determinant of the compressibility profile for the SMs. These results go in line with the RSM model.

3.2.3.3.2. Tabletabiliy characterisation

In order to predict the ability of arginine binary mixtures with IND and the salt to form a tablet of specific strength while exposed to compaction pressure (tabletability), RSM was carried out and figures (3.2.10A) and (3.2.10B) were generated for IND/arginine PMs and salt/arginine SMs respectively.

Tensile strength was the second response evaluated in this study and the predicted data showed that IND tablets tensile strength was significantly ($P< 0.001$) increased upon increasing both the compaction force (F), arginine ratio (R) and their interactive term (FR). The compaction force (F) and arginine ratio (R) were found to have the same magnitude of effect on the tablets' tensile strength; 1.73 and 1.79 respectively (Table 3.2.7).

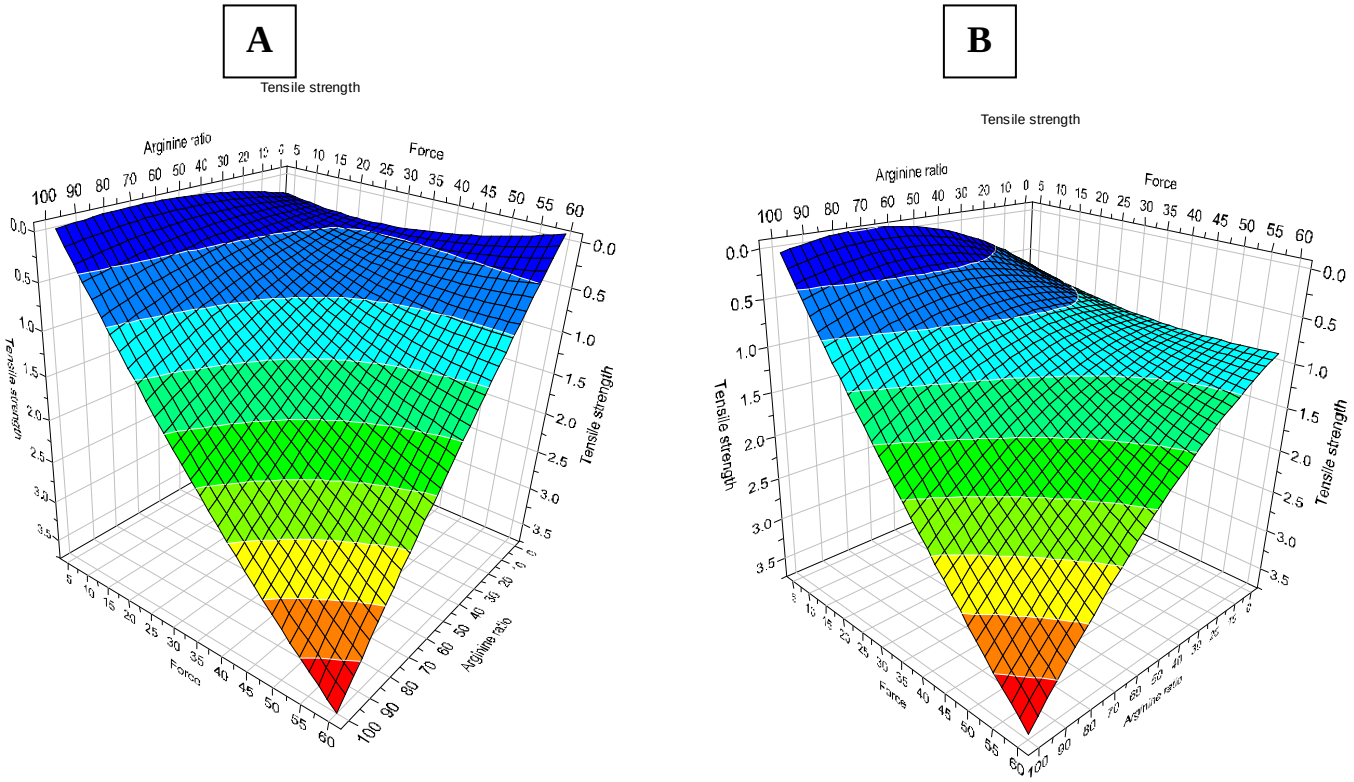

Figure 3.2.33:- Surface response plot showing the effect of compaction force and arginine ratio on tablets tensile strength for (A) IND/arginine binary mixtures and (B) IND salt/arginine binary mixtures.

Interestingly, combining both factors (FR) during the preparation of the tablets was found to have a synergistic effect (2.032) on the tablets' strength. This effect could be explained by the ability of arginine to improve the compressibility of IND tablets which in turn improves the interparticulate bonding area. Besides, its ability to enhance the bond formation during densification as reflected by the compactability studies. Because both compressibility and compactability are pre-determinant of tablet strength, hence an increase in the tensile strength was observed. Moreover, this synergistic effect could reflect strong bonding between IND and arginine which achieved highest value at 50% of arginine (PM 1:1) as suggested by the high (σ_0) value as early suggested by Sheikh-Salem and Fell., (1981). None of the polynomial terms (F^2 or R^2) were found to be effective ($p>0.05$) on the tablets hardness.

Table 3.2.28:- The quantitative factor affecting tablets tensile strength and their associated p value for the responses.

	Tensile strength			
term	IND		IND arginine salt	
	Effect	*p* value	Effect	*p* value
F	1.73733	<0.001	1.938	<0.001
R	1.79459	<0.001	1.0815	0.02527
F^2	-0.4075	0.289239	-0.2607	0.702288
R^2	0.28075	0.45716	0.72462	0.28989
FR	2.0324	<0.001	1.711	0.00544

Similarly, incorporating arginine to the salt formulations showed similar trends and the tablets' tensile strength was increased upon increasing the compaction force and arginine ratio. Nevertheless, the compaction force was the main determinant of the tablets' hardness for the SMs as the magnitude of effect exhibited by the compaction force (F) was twice (1.938) that of arginine ratio (1.08) (R). Moreover, the interactive term (FR) was found to antagonise the effect of compaction force as combining the two factors was found to be less effective (1.71) than the compaction force alone (1.94). Mathematical equations (3.2.9 and 3.2.10) and response surface plots were generated after the model was fitted to MLR, and could be used to predict the tablets tensile strength if the compaction force and arginine ratio are known.

$$S_{Ind} = 1.022 + 1.73F + 1.79R + 2.03FR$$ **Equation 3.2.12**

$$S_{Salt} = 1.083 + 1.938F + 1.08R + 1.711FR$$ **Equation 3.2.13**

Where S_{ind} is the tensile strength for IND/arginine PMs, S_{salt} is the tensile strength for IND salt/arginine SMs, F is the compaction force and R is the arginine percentage.

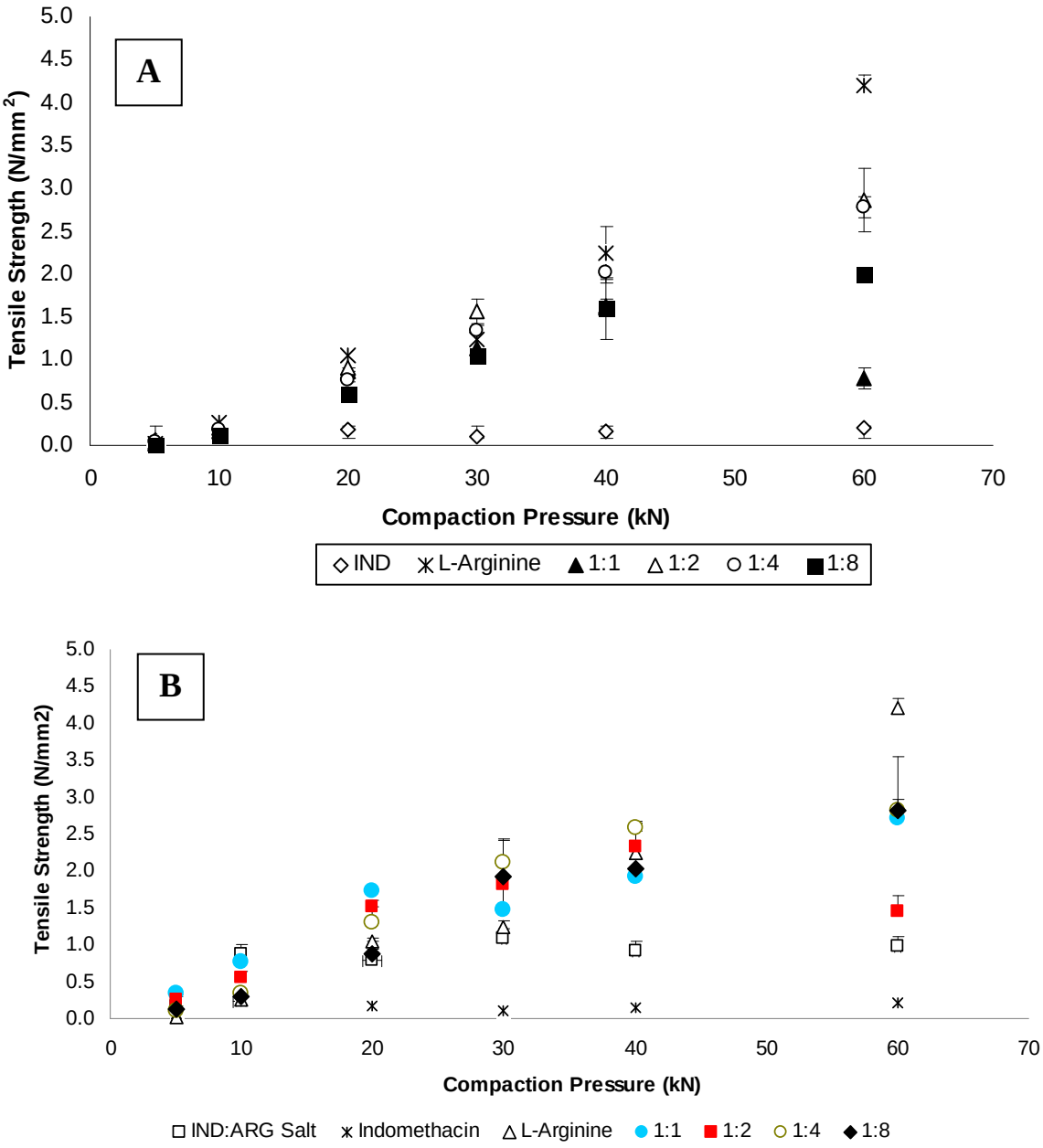

Figure 3.2.34:- :- Plots of tablet tensile strength against compaction pressure showing (A) Tabletability of IND, ARG and PM's, (B) Tabletability IND salt and SM's (n=3).

Experimental studies of the effect of compaction force and arginine ratios on the tensile strength for PMs and SMs were studied and summarised in Fig. 3.2.11.

Similar to individual powders, a linear relationship was observed between the tablets tensile strength and compaction force, i.e. increasing the compaction force resulted in increasing the tensile strength for all the formulations. The highest tabletability was shown by arginine> PM

1:2≈ PM 1:4> PM1:8 >PM 1:1. While IND free acid which showed the lowest tabletability properties among the PMs (Fig. 3.2.11A). The compressibility and compactability similarities between 1:2 and 1:4 PMs might be behind their similar tabletability.

Fig. 3.2.11B shows the tabletability profile of the SMs, again it was clear that increasing the compaction force increased the tablet tensile strength. However, SM at 1:2 showed a drop in the tablets' strength at very high compaction force (Fig. 3.2.11B) which could be because of the over-compaction.

The highest tabletability was exhibited by arginine> SM 1:8> SM 1:4 > SM 1:1≈ SM 1:2:> salt. The practical data shows clearly that the compaction force has a strong effect on the tablet strength for both the IND and the salt mixture as suggested by the RSM model. Furthermore, the effect of arginine ratio in salt binary mixture is believed to go in line with the data suggested by the model. Nevertheless, IND/arginine physical mixtures data has not demonstrated similar trend and the effect of arginine ratio on the tablet hardness of the PM was not clear.

3.2.3.3.3. Disintegration studies

Disintegration time was the last response to be evaluated in this study. The significant terms which were found to affect the disintegration time for IND/arginine PMs tablets were identified as compaction force (F), arginine ratio (R), the interactive term (FR) and the polynomial term of arginine ratio (R^2). Increasing the compaction force (F) was found to increase the disintegration time by a magnitude of (262.16) while increasing the ratio of arginine in the mixtures were found to decrease the time required for the tablets to disintegrate significantly ($p< 0.001$) and even by higher magnitude when compared to the compaction force (F). Although the arginine ratio had higher impact on the disintegration time than the compaction force, the interactive term (FR) was found to delay the tablets disintegration for the PMs.

Table 3.2.29:- The quantitative factor affecting tablets disintegration time and their associated p value for the responses.

	Disintegration time			
term	IND		IND arginine salt	
	Effect	*p* value	Effect	*p* value
F	262.167	<0.001	509.167	<0.001
R	-1069.51	<0.001	-513.834	<0.001
F^2	-43.4425	0.57141	-162.128	0.0259
R^2	250.25	0.00352729	-127	0.0706917
FR	170.137	0.0119061	-192.515	0.00218

On the other hand, RSM showed that both the compaction force and the arginine ratio have similar magnitude of effect on the disintegration time of salt/ arginine SMs. Nevertheless, the compaction force (F) was found to increase the disintegration time while the arginine ratio was found to speed up the tablets' disintegration (Table 3.2.8). The interactive term (FR) was found to decrease the disintegration time for the SMs.

Equations (3.2.11) and (3.2.12) can be used to describe the effect of the two independent factor; compaction force and arginine ratio on the effect of disintegration time for PMs and SMs, respectively.

$$T_{Ind} = 556.055 + 262.16F - 1069.51R + 250.25R^2 + 170FR \quad \textbf{Equation 3.2.14}$$

$$T_{Salt} = 504.647 + 509.16F - 513.83R - 162.12F^2 - 192.5FR \quad \textbf{Equation 3.2.15}$$

Where T_{ind} is the disintegration time for IND/arginine PMs, T_{salt} is the disintegration time for IND salt/arginine SMs, F is the compaction force and R is the arginine ratio. The three dimensional surface plots were generated using the software and simulates the effect of compaction force and arginine ratio, individually and simultaneously, on the disintegration time for the PM (Fig. 12A) and SMs (Fig. 3.2.12B).

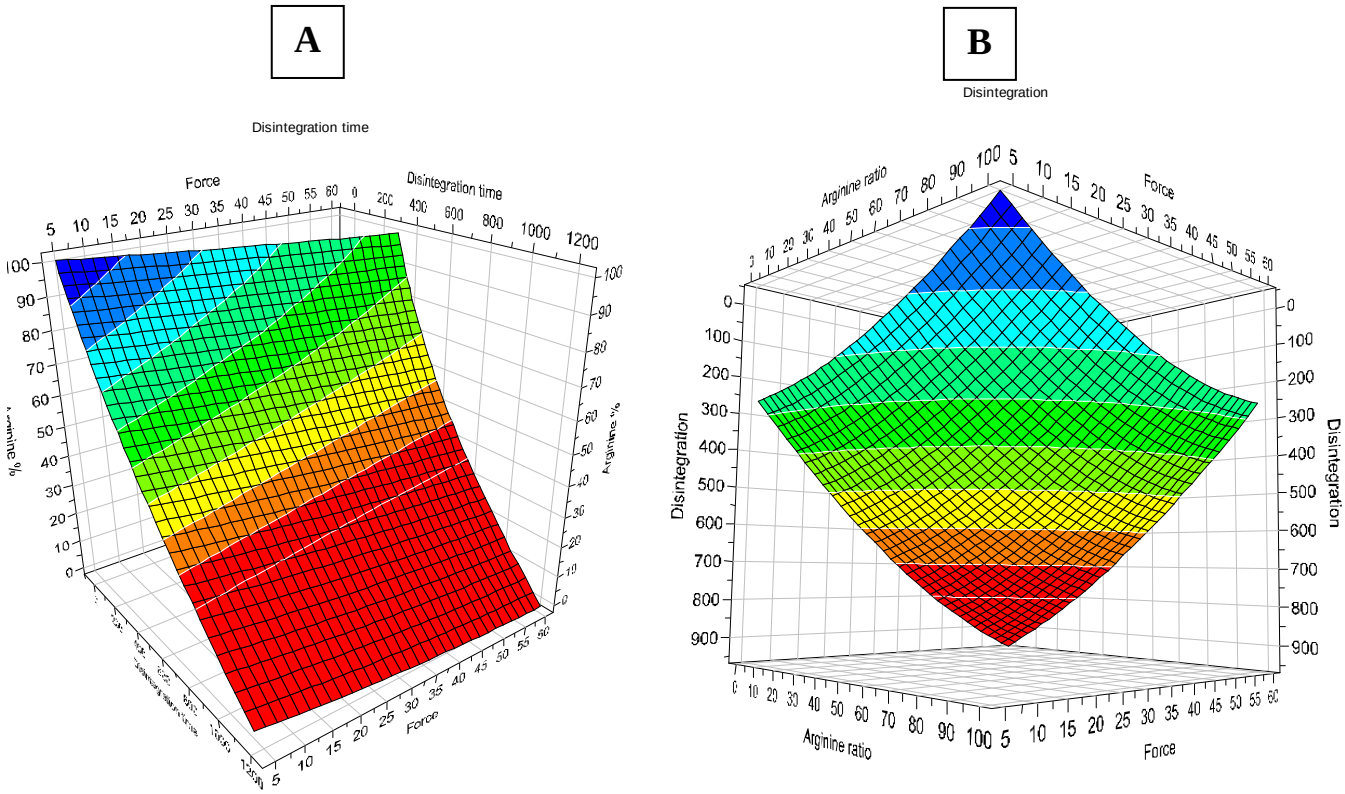

Figure 3.2.35:- Surface response plot showing the effect of compaction force and arginine ratio on tablets disintegration time for (A) IND/arginine binary mixtures and (B) IND salt/arginine binary mixtures

The experimental data for the effect of compaction force and arginine ratio on the disintegration time for the PMs and SMs are summarised in Figures 3.2.13A and 3.2.13B respectively.

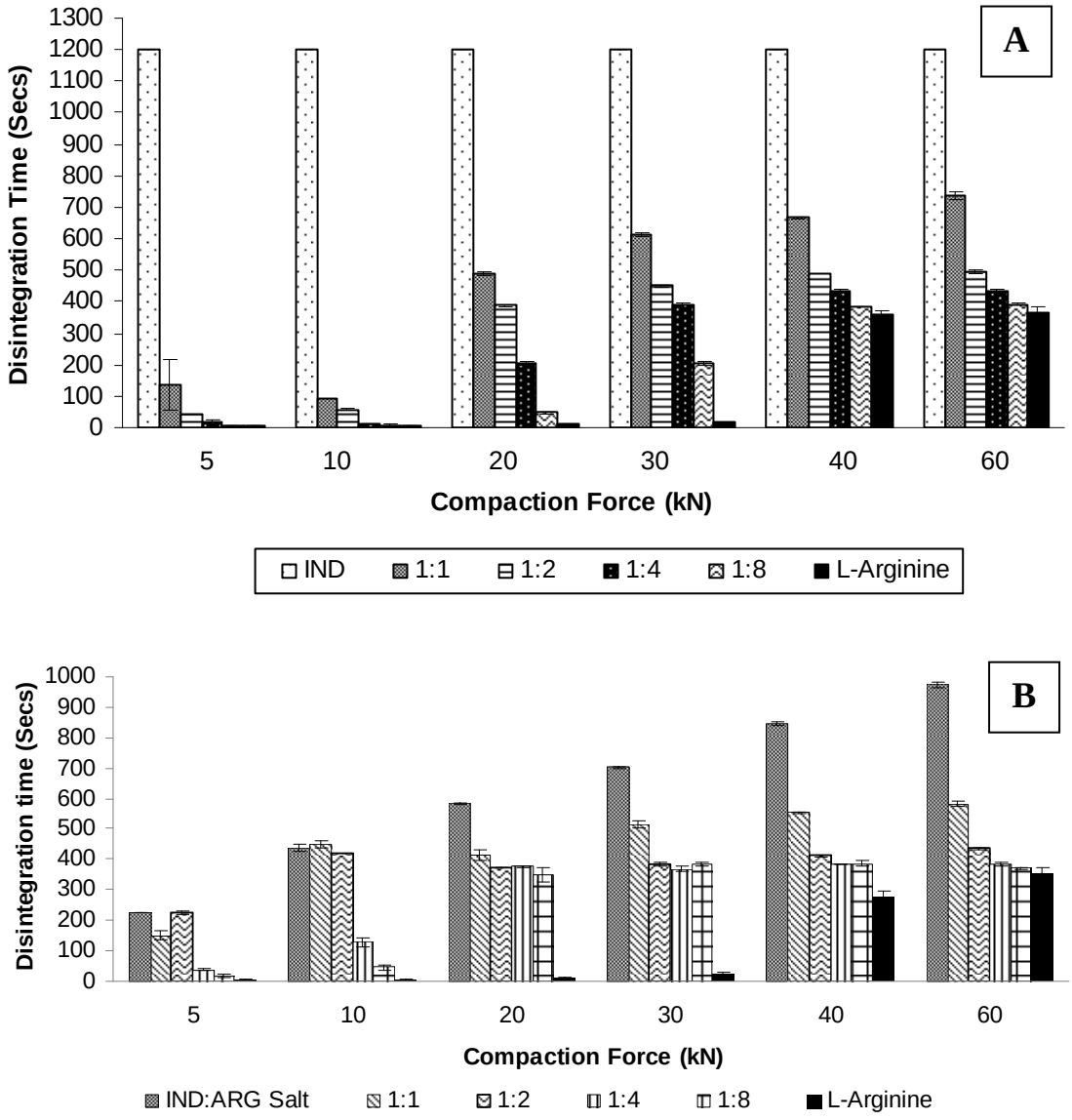

Figure 3.2.36:- (A) Disintegration time for IND, ARG and PM's (B) Disintegration time for IND salt and SM's

The addition of arginine to IND tablets was found to drop the disintegration time significantly (Fig. 3.2.13A). It usually takes more than 20 minutes for IND tablets (compressed at 5 kN) to disintegrate and upon adding 50% arginine (PM 1:1) to the formulations the disintegration time was dropped to 195±117 sec. Moreover, increasing the ratio of arginine in the formulation was found to significantly decrease the disintegration time (Fig 3.2.13A). The effect of compaction force (F) on the disintegration time was significant upon applying low

forces and up to 30 kN. Beyond 30 kN the effect of force was insignificant. These data comes on line with the RSM findings which suggested that the arginine percentage is the more determinant as it has higher magnitude than that of the compaction force (Table 3.2.8).

Studying the disintegration profile of IND arginine salt and SMs showed a similar profile to that of the PMs. Generally, increasing the compression force resulted in increasing the disintegration time (Fig. 3.2.13B). At most of the compression forces, the disintegration time was decreased in the order IND salt>1:1SM>1:2SM>1:4SM>1:8SM i.e. as the L-arginine ratio increase. Interestingly, the disintegration time of the SM 1:1 was faster than the salt form although the former had lower porosity than the latter as early observed in (Fig. 3.2.9B). This suggests that the incorporation of arginine in the formulation has a great impact on the disintegration time as suggested by the RSM.

The correlation between the predicted values and the actual values of tablets' porosity, tensile strength and disintegration times were compared (Fig. 3.2.14). A strong correlation (R^2= 0.89) was observed between the predicted and actual values for tablets' porosity. While weak correlation was observed for that of tablets' tensile strength and disintegration time R^2= 0.77 and 0.61 respectively. This suggest that RSM can be used to predict tablets' porosity for binary mixtures but not tablets' tensile strength or disintegration time probably other factors may be involved during the process of tablet disintegration and tabletability.

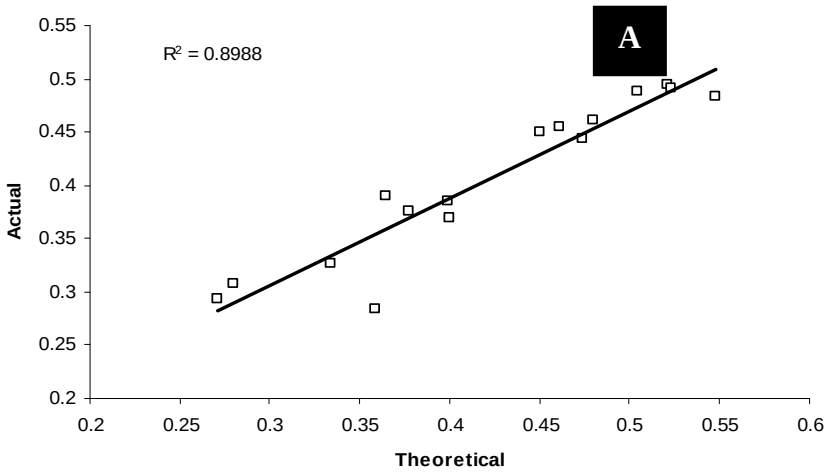
A
R² = 0.8988
Actual
Theoretical
0.55
0.5
0.45
0.4
0.35
0.3
0.25
0.2
0.2
0.25
0.3
0.35
0.4
0.45
0.5
0.55
0.6

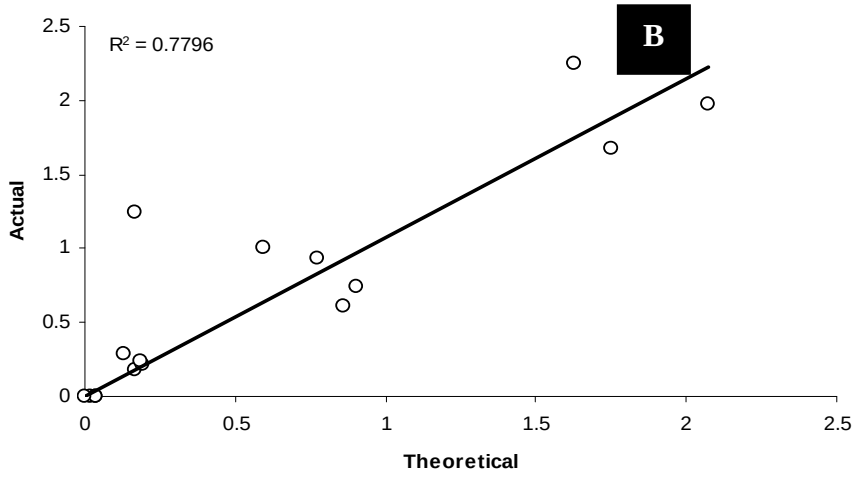
B
R² = 0.7796
Actual
Theoretical
2.5
2
1.5
1
0.5
0
0
0.5
1
1.5
2
2.5

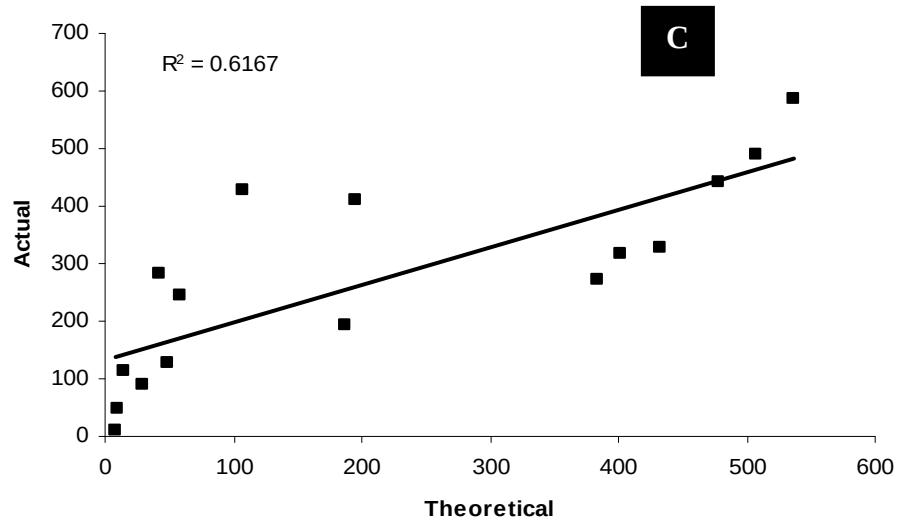
C
R² = 0.6167
Actual
Theoretical
700
600
500
400
300
200
100
0
0
100
200
300
400
500
600

Figure 3.2.37:- Correlations between actual and theoretical values for measuring (A) tablets' porosity, (B) tablets' tensile strength and (C) tablets' disintegration time.

3.2.3. Conclusion

Individual powder characterisation showed good flowability properties of arginine as it had low angle of repose of (29.4 ± 0.84) mainly because of its large particle size and rough surface of its particles. Moreover, the tablet characterisation showed that arginine could be used successfully as a tablet filler, binder and disintegrant because of it's good compressibility, compactability and low disintegration time. RSM showed that both compaction force and arginine ratio could have a significant impact on tablets' porosity, tensile strength and disintegration time. Nevertheless, RSM could not be used to predict the tensile strength and disintegration time of the tablets probably because of the involvement of other factors such as the type of forces formed at various ratios of the binary mixtures.

The effect of ion-pairing indomethacin with arginine/lysine on its permeability profile across Caco-2 cells

3.3.1. Introduction

Indomethacin (IND) is a non steroidal anti-inflammatory drug which is used for the treatment of rheumatoid arthritis. IND was first introduced in 1962 as a treatment for inflammation. IND is a weakly acidic drug (pKa= 4.5) and has poor solubility because of its hydrophobic nature (log P=3.1). Nevertheless, IND diffuses quickly and is completely absorbed through the intestinal membrane after oral ingestion and can therefore be classified as a class II drug under the biopharmaceutical classification system (BCS).

pH partitioning theory for charged drug candidates states that lipid membrane bilayers only allow the absorption of unionised (molecular form) drug candidates while the charged species do not pass through the membrane (Shore et al., 1957) . However, investigations over the last couple of decades on oral drug absorption have demonstrated the role of other factors in drug absorption. Daniel et al. (1985) and McEwain and Lucas (1990) suggested that the acidic microclimate of the drug at the surface of the epithelium has an effect on the passive uptake of uncharged weakly acidic drugs which was known as pH shift (Winne, 1977). Although passive diffusion is the main mechanism of absorption for majority of drugs, carrier mediated transporters, found in mucosal and serosal membranes can be involved in the transport of acidic drugs. Tsuji et al., (1994) investigated the mechanism of absorption of monocarboxylic acid drugs through various ion channel transporter systems. The results showed that carboxylic acid drugs were primarily carried across the intestinal cells through H^+ gradient dependant transporter systems when compared to Na^+ dependent carrier systems. Although the study by Tsuji et al., (1994) identified the role of a specific carrier system in the transport of acidic

drugs, the contribution of active influx to net transport of the drug was not clear suggesting the wider role of alternative/complimentary carrier systems in the absorption of weakly acidic drugs. The next set of studies published by Ganapathy et al., in 1995 identified H^+ coupled oligopeptide transporters (PEPT)-1 (SLC15A1) expressed in human small intestine and was shown to mediate the absorption of anionic angiotensin converting enzyme inhibitors and B-lactam antibiotics. Similarly, monocarboxylic acid transporter (MCT)-1 also known as SLC16A1 was believed to play an essential role in the rapid transport of monocarboxylates. Recent studies by Kobayashi et al., 2003 identified another super family of organic anion transporting polypeptide (OATP)-B expressed in the apical membrane of the small intestine with a specific role for the transport of anionic molecules across the gut.

The current investigation focuses on the permeability profile of the weakly acidic model drug indomethacin (IND). IND was selected for this study as it is metabolically stable at intestinal pH and previous studies from our lab (ElShaer et al., 2011) showed a substantial improvement in solubility and dissolution upon addition of cationic amino acids (lysine and arginine). The primary hypothesis of this study was to explore the role of ion-pairing IND with cationic amino acids (arginine and lysine) on drug uptake across Caco-2 cells. Arginine and lysine were selected for this study because they carry positive charge upon ionisation which could interact electrostatically with the anionic carboxylic group of IND to form ion-pairs. Moreover, arginine and lysine have a full transporter system on the epithelial cells hence an alternative transporter system would be created for IND and higher absorption profile could be achieved. Solute carrier transporter SLC3A1 ($b^{0,+}$) is the major transporter of the cationic amino acids and expressed mainly in the apical membrane of the small intestine (Broer, 2008).

Caco-2 cells are human colorectal carcinoma cell lines and posses microvillus structure, hydrolysis enzymes and carrier mediated transporters and have been used to evaluate parallel

transport routes including passive and active transport (Dantzig & Bergin, 1990; Hilgers et al., 1990; Chen et al., 1994).

3.3.2. Materials and methods

3.3.2.1. Materials

Indomethacin (TLC ≥ 99%), L-Arginine (non-animal source), L-Lysine, 1-octanol (ACS spectrophotometric grade ≥ 99%) and ninhydrin reagent (2% solution) were purchased from Sigma Aldrich, UK.

Acetonitrile, glacial acetic acid and absolute ethanol were purchased from Fisher Scientific UK.

Dulbecco's modified Eagle's medium (DMEM), fetal bovine serum (FBS), Nonessential amino acids (NEAA), 1% pencillin-strepotomycin, 2mM glutamine and Hank's balanced salt solution (HBSS) were purchased from Bio Sera, UK. 1% Trypsin–EDTA was obtained from Gibco Lab. UK.

3.3.2.2. Methods

3.3.2.2.1. Preparation of pre-saturated solution of 1-octanol and de-ionised water.

1000 ml of de-ionised water was added to 4 mL of 1-octanol. The mixture was shaken for few minutes and left overnight. The de-ionised water was separated from 1-octanol using 1000 mL separating funnel.

3.3.2.2.2. Octanol- water partitioning experiment

500 µg of IND was added to 100 mL octanol-saturated deionised water with molar excess of arginine/lysine (in ratios 1:1, 1:2, 1:4 and 1:8). 5 mL of the aqueous phase was allowed to equilibrate with 5mL of octanol at room temperature and stirred for 24 hours using a magnetic stirrer. The two phases were then separated by centrifugation and IND concentration $[IND_t]_{Aq}$ in the aqueous phase was measured using HPLC. Mass balance was used to calculated IND concentration in octanol phase $[IND_t]_{Oct}$ using equation (3.3.1).

$[IND_t]_{Oct}$ = total drug put into the system- $[IND_t]_{Aq}$ Equation 3.3.16

The apparent distribution coefficient D_A could be calculated using equation (3.3.2)

$$D_A = [IND_t]_{Oct}/[IND_t]_{Aq}$$ **Equation 3.3.17**

3.3.2.2.3. HPLC method to study the concentration of indoemthacin

The amount of indomethacin (IND) dissolved in the solution samples was quantified by HPLC using a Dionex 1100 system with autosampler (AS50), gradient pump (GP50), UV detector (UVD 170U) and RP-C18 analytical column (Phenomenex 110A, 150x4.6 mm, 5µm). The analysis method was adapted from Song et al., (2004). IND was eluted using acetonitrile (60%) and 0.1 M acetic acid (40%) as a mobile phase and pumped at 1.0 mL/min flow rate. UV detector was adjusted at λmax of 248 nm (predetermined using Unicam UV-Visible Spectrophotometer). The retention time was 5.09±0.02 min and a rectilinear calibration curve was established at concentration range between 1-500µg/mL with 0.99 correlation coefficient.

3.3.2.2.4. Ninhydrin analysis

Ruhemann (1911) found that reacting ninhydrin with alanine under condensation of ammonia with hydrantoin (reduced form of ninhydrin) produced a blue coloured compound (diketohydrindylidene diketohydrindamine) known as Ruhemann purple (Fig. 3.3.1). Ruhemann found that the colour is produced upon reacting ninhydrin reagent with any acidic compounds that has α-NH_2 side chain e.g amino acids, proteins and peptides. Therefore this method was used to determine the concentration of compounds containing α-NH_2 photo-metrically.

The concentrations of arginine and lysine in octanol/water partitioning studies were quantified using the ninhydrin method. In order to construct a calibration curve, serial dilutions of the amino acids were prepared and 1 mL of the prepared samples was mixed with 0.5 mL of ninhydrin reagent and vortexed for 20 seconds. The samples were heated in a pre-warmed water bath at 80 ^{o}C for 20 minutes. The samples were removed from the water bath and left

to cool. The intensity of the coloured Ruhemann purple was analysed using a UV spectrophotometry at a wavelength of 560 nm.

Calibration curves were constructed with regression coefficient of 0.99 and 0.94 for arginine and lysine respectively. After constructing the calibration curves, the concentrations of the amino acids in the aqueous layer were determined using the linear curve equations (3.3.3) and (3.3.4) for arginine and lysine respectively.

Y=0.421x **Equation 3.3.18**

Y=0.0481x **Equation 3.3.19**

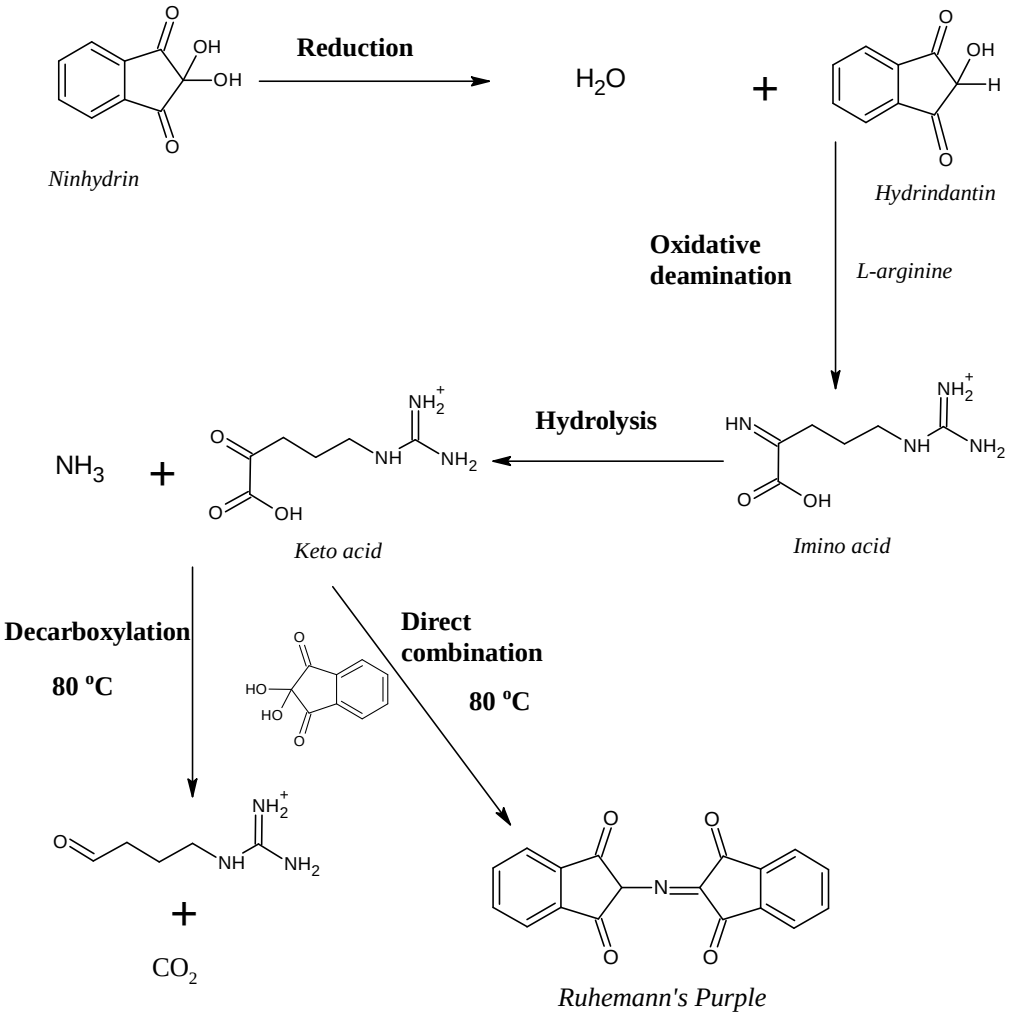

Figure 3.3.38:- Schematic representation of ninhydrin reaction.

3.3.2.2.5. Procedure for Caco-2 cell culture

Caco-2 cells at passage 48 were gifted from Huddersfield University and used at passages 50-80. Cells were allowed to grow in 75cm² T-flasks and maintained using Dublecco's modified Eagle's medium (DMEM) with 10% fetal bovine serum (FBS), 0.5% pencillin-streptomycin, 2mM glutamine and 1% nonessential amino acids (NEAA). Culture medium was changed every 2 to 3 days and cells were grown at a temperature of 37°C and 5% CO_2. The cells were passaged by 5 mL trypsin-EDTA when they reach 90% confluence. Transepithelial transport assay was carried out using Khan et al., (2011) methods, 2 x 10^5cells/cm² were seeded on polycarbonate-coated membranes (6-well transwell plates, 24mm, 4.7cm²) and were allowed to grow for 21 days and the media in both apical and basal compartments were changed every 2-3 days. Transepithelial electrical resistance (TEER) was measured at the start and end of every study.

3.3.2.2.6. Indomethacin permeability study

Caco-2 monolayers were used 19-21 days after seeding. Apical to basolateral permeability of IND and IND PM formulations was assessed. The transwells were rinsed and incubated for 15 minutes with drug-free transport medium (Hanks balanced salt solution; HBSS). Following incubation, HBSS was removed and 1.5 mL of the medium containing IND alone (500 µg/mL) and IND with various molar ratios of the cationic amino acids (1:1, 1:2, 1:4 and 1:8) were introduced to the apical side. Sample aliquots (300µL) were taken from the basolateral side at given time intervals (0, 5, 10, 15, 20, 30, 60 and 90 minutes). After each sampling, an equal volume of fresh transport buffer (pre-warmed at 37°C) was added to the receiver compartment (basal side) and kept the cells at a temperature of 37°C and 5% CO_2 during experiment. Samples were subsequently analyzed by HPLC. In order to confirm the mass balance, samples were taken from both apical and basolateral compartments at the last time point (90 mins). All experiments were performed at 37°C (n = 5).

Apparent permeability coefficient P_{app} (cm/s) was calculated using (equation 3.3.5)

$$P_{app} = dQ / dt \times 1 / AC_0$$ **Equation 3.3.20**

Where *dQ/dt* is the rate of appearance of the drugs on the basolateral side (nmol s^{-1}), C_o is the initial concentration on the apical side and *A* is the surface area of the monolayer (4.7 cm^2).

The data presented was validated using HPLC measurement of drug transfer during the process of permeability.

3.3.2.2.7. Recovery

The amounts of IND recovered from both apical and basolateral compartments at the end of the experiment were calculated using equation (3.3.6) and results are summarised in tablet (3.3.1).

$$\text{Recovery (\%)} = \frac{C_{R90\,\min} \times V_R + C_{D90\,\min} \times V_D}{C_{D0\,\min} \times V_D} \times 100$$ **Equation 3.3.21**

Low recovery data are attributed to entrapment of the compounds into the cell monolayers or adsorption to the device surface which in turn results in error calculating the transport rate (Aungst et al., 2000)

3.3.3. Results and discussion

Partitioning studies

3.3.3.1. Octanol-Water partitioning.

As mentioned above, the majority of the acidic drugs are transported mainly by passive diffusion. The surface area of brush border membranes is more than 1000 fold larger than the surface area available for paracellular transport (Pappenheimer, 1987) which leaves the passive transcellular route as the main mechanism of absorption for most of the drugs. Many studies were carried out to predict passive absorption across intestinal membrane based on various physico-chemical properties of the drugs. Various properties such as desolvation energy (Burton, 1992), hydrogen bonding capacity (Young, 1988; Conradi, 1991), molecular surface area (Barlow, 1994), surface activity (Seelig, 1994) and octanol/water partitioning coefficient (Martin, 1981) were studied to correlate drug absorption across cell membranes. Although using a single physico-chemical property to predict the permeability properties of drug molecule was an easy and simple tool to investigate, the outcomes showed a reasonable correlation to transcellular passive drug absorption.

The most widely used predictor for drug absorption is the octanol/water partitioning (log P). As octanol has lipophilicity that resembles that of cell membranes, log P values are used to predict the capacity of drug molecules to partition into cell membrane.

Our earlier work utilized hydrophilic amino acids as ion-pairs with the lipophilic IND to improve its solubility and dissolution profile. As suggested by the pH partitioning theory, lipid membrane bilayers only allow the absorption of uncharged drug species while the charged species do not pass through the membrane (Shore et al., 1957). In our current study, it was expected that the ion-paired IND amino acid (salt form) (AB) would ionise in the aqueous medium into its respective ionic species (A^-) and (B^+) raising that prospect of unfavourable/poor transcellular absorption of the drug. Having studied the fundamental

principle of ionisation (Fig. 3.3.2), we decided to add excess of the basic counter ion (arginine and lysine amino acids in this study) to shift the equilibrium of salt ionisation towards the non-ionised form of the salt (Fig. 3.3.2). Therefore, excess of the cationic amino acids were ion-paired with the salt forms.

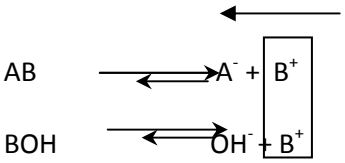

Figure 3.3.39:- schematic representation of the ionization of the salt form and the effect of adding excess of the basic counter ion on the ionisation equilibrium.

The goal of this current study was to investigate whether incorporating hydrophilic amino acids at various molar ratios with the prepared salt forms, have an effect on the permeability profile of IND .

Assuming that ion-pair formation between IND (acidic drug) and the basic amino acids (arginine/ lysine) in octanol-water mixture, at equilibrium conditions, there would be formation and destruction of ion-pairing and partitioning process between octanol-water. Miller, (2009) and Connors, (1987) and Grant and Higuchi (1990) defined the association constant for ion-pair formation in the aqueous phase K_{11aq} in equation (3.3.7).

$$K_{11aq} = \frac{[AB]_{aq}}{[A]_{aq}[B]_{aq}} \quad \textbf{Equation 3.3.22}$$

Where $[A]_{aq}$, $[B]_{aq}$ and $[AB]_{aq}$ are the concentrations of the acidic drug IND, basic counter and the ion-pair in the aqueous phase respectively.

The total amount of IND in octanol would exist only as an ion-pair which means that $[A_t]_{oct}$ equals $[AB]_{oct}$ and the apparent octanol aqueous distribution coefficient of IND can be calculated from equation (3.3.8).

$$D_A = \frac{[AB]_{oct}}{[A]_{aq} + [AB]_{aq}} \quad \textbf{Equation 3.3.23}$$

Where $[A]_{aq}$ represents the concentration of IND free drug in the aqueous phase and [At]aq is the total concentration of IND in the aqueous phase $[A_t]_{aq}= [A]_{aq}+[AB]_{aq}$.

The intrinsic partition coefficient of the ion-pair in octanol-water, P_{AB} is defined as the ratio between the ion-pair concentration in octanol to its concentration in water equation (3.3.9).

$$P_{AB} = \frac{[AB]_{oct}}{[AB]_{aq}}$$ **Equation 3.3.24**

Upon combining equations (3.3.7)(3.3.8) and (3.3.9), a common equation is obtained.

$$\frac{1}{D_A} = \frac{1}{K_{11aq} P_{AB} [B]_{aq}} + \frac{1}{P_{AB}}$$ **Equation 3.3.25**

The concentration of IND was determined using the HPLC method while the concentration of the cationic amino acids in the aqueous phase was calculated using the ninhydrin test. Upon plotting the double reciprocal of the apparent octanol-water distribution coefficient of IND as a function of the basic amino acid concentration (i.e plotting $1/D_A$ Vs $1/[B]_{aq}$), both K_{11aq} and P_{AB} can be calculated from the double reciprocal curves or the curve equations.

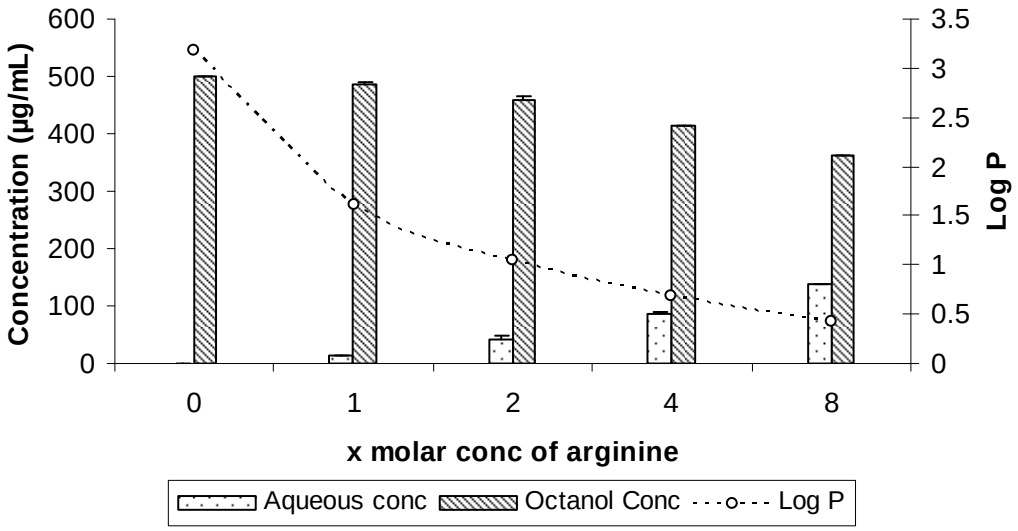

Figure 3.3.40:- IND concentrations in aqueous and octanol layers and its corresponding Log P values at various concentrations of arginine.

The partitioning behaviour of IND at various molar ratios of arginine were studied and summarised in Fig. (3.3.3). The experimental data showed that IND has a log P value of 3 which is in line with the literature findings (Siissalo et al., 2010). Such high log P value reflects the

hydrophobic nature of IND which in turn deteriorates its solubility. The ratio of the cationic amino acid counter ions was increased while IND concentration was held constant. Increasing the concentration of arginine in the formulations was found to increase the aqueous solubility of IND and reduce its partitioning in the lipophilic layer. IND log P value dropped significantly by 1.5 units upon adding arginine at 1:1 ratio. Further increase in arginine concentration resulted in a gradual drop of Log P until it reached 0.5 at 1:8 molar ratio of IND to arginine respectively.

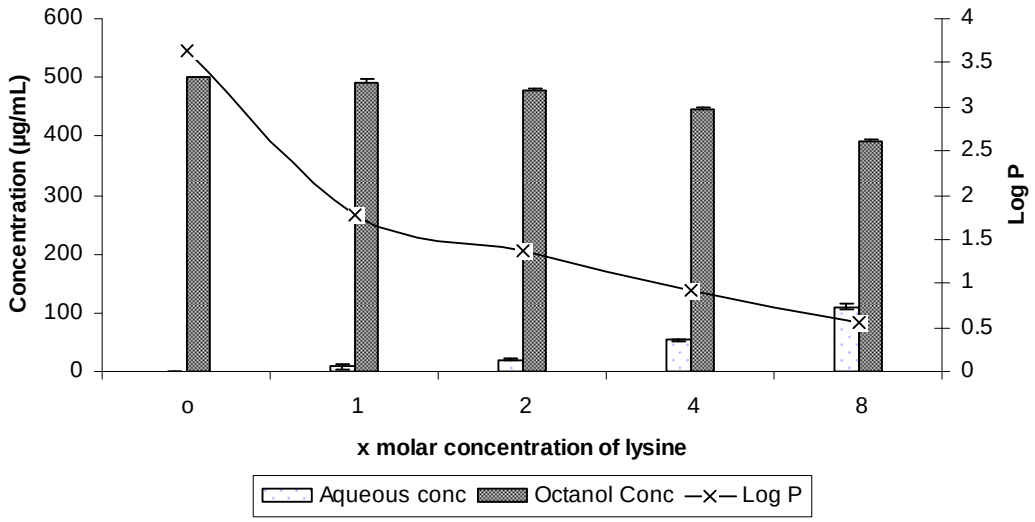

Figure 3.3.41:- IND concentrations in aqueous and octanol layers and its corresponding Log P values at various concentrations of lysine.

Similar trend was observed upon using lysine as counter ions: this is probably because both arginine and lysine have very close pKa values of 12.48 and 10.53 respectively.

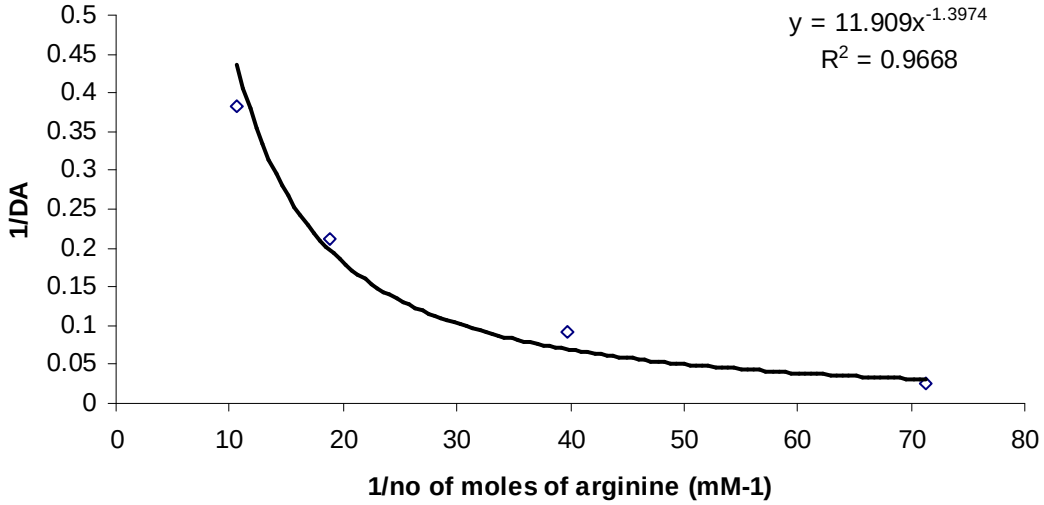

Figure 3.3.42:- Double reciprocal plot of the apparent octanol-water distribution coefficient of IND as function of arginine molar concentration.

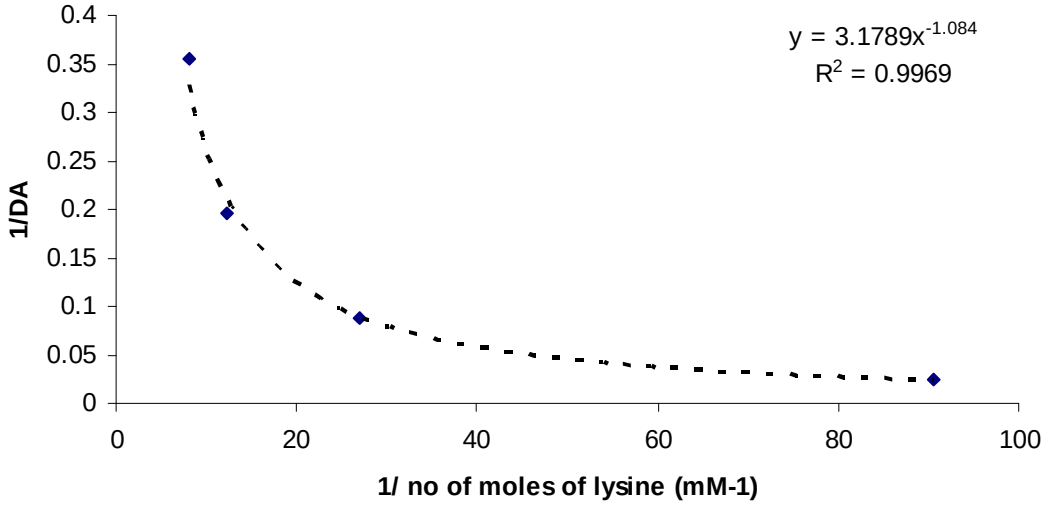

Figure 3.3.43:- Double reciprocal plot of the apparent octanol-water distribution coefficient of IND as function of lysine molar concentration.

The double reciprocal plots of apparent octanol/water distribution coefficients of IND as function of the molar concentrations of arginine and lysine are shown in figures (3.3.5 and 3.3.6) respectively. The double reciprocal plots showed weak linear relationships (R^2 of 0.81 for arginine and R^2 of 0.61 for lysine). Nevertheless, the double reciprocal plots showed strong

negative exponential relationships for both the amino acids suggesting that increase in the molar concentration of the amino acids will decrease the partitioning coefficient of IND exponentially. pH solubility profile studied earlier by ElShaer et al., (2011) for IND showed that increasing arginine concentration results in increasing the ionisation of IND and its solubility exponentially. The exponential increase in ionisation will result in an exponential drop in D_A values as the ionized species cannot partition into octanol as suggested by Shore et al., (1957). Studies carried out by Maller et al (2010) showed linear relationship which could be attributed to the small range of concentration of the counter ions used in the study. The high inherent hydrophilicity of arginine (Log P=-4.2) and lysine (Log P=-3.02) is the main reason behind the drop of the D_A values for IND.

The exponential curve equations (3.3.11, 3.3.12) were used to describe the correlation between the D_A values and the molar concentrations of arginine and lysine respectively. These two equations were used to work out the intrinsic octanol water partitioning (P_{AB}) and the aqueous phase binding constant ($K11_{aq}$).

$Y = 11.909\,x^{-1.397}$ **Equation 3.3.26**

$Y = 3.17\,x^{-1.084}$ **Equation 3.3.27**

The $K11_{aq}$ was calculated for IND-arginine and IND-lysine and found to be 1084 M^{-1} and 520 M^{-1} respectively. The aqueous phase binding constant for IND-arginine was stronger than that of IND-lysine which reflects the higher intermolecular complexation between IND and arginine. Two major bonds are involved during ion-pair formation; ionic and hydrogen bonds. The ΔpKa values between IND and arginine was 8 units while that between IND and lysine was 6 units, which suggests that the degree of ionic bonding is higher in IND-arginine when compared to its lysine counterpart. Moreover, our previous studies (ElShaer et al., 2011) suggested that arginine has more H-donors and H- acceptors than lysine (13 vs 9) and possibly results in

greater H-bonding between IND-arginine. Which further explains the stronger aqueous binding constant for lysine.

3.3.3.2. Permeability studies

Prior to conducting the permeability studies, the transepithelial resistance (TEER) was monitored for 22 days (Fig. 3.3.7). TEER resistance for Caco-2 cells was 221±20 Ω/cm^2 after 3 days of seeding the membranes and started to increase steadily until it reached 589±26 Ω/cm^2 on day 12. TEER remained constant after 12 days of seeding which suggests the formation of integral monolayers.

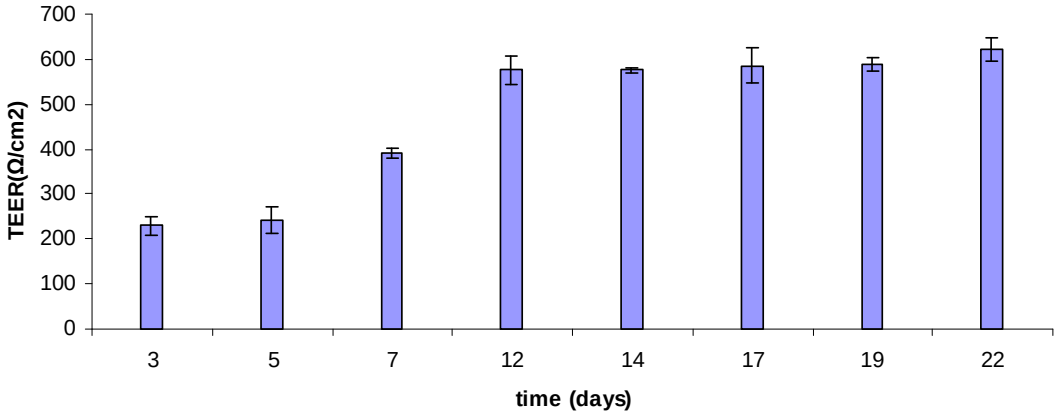

Figure 3.3.44:- TEER measurements of Caco-2 cells for 22 days of seedings (n= 3).

Upon formation of intact monolayers, the cells are washed and incubated with HBSS buffer. The effect of incubation time with HBSS on Caco-2 monolayers TEER values was also studied. It was noticed that incubating the cells for too long with HBSS would not have a significant effect the integrity of the cells (Fig. 3.3.8). For all subsequent experiments, Caco-2 cells were incubated for 15 minutes with the buffer prior to carrying out the permeability studies.

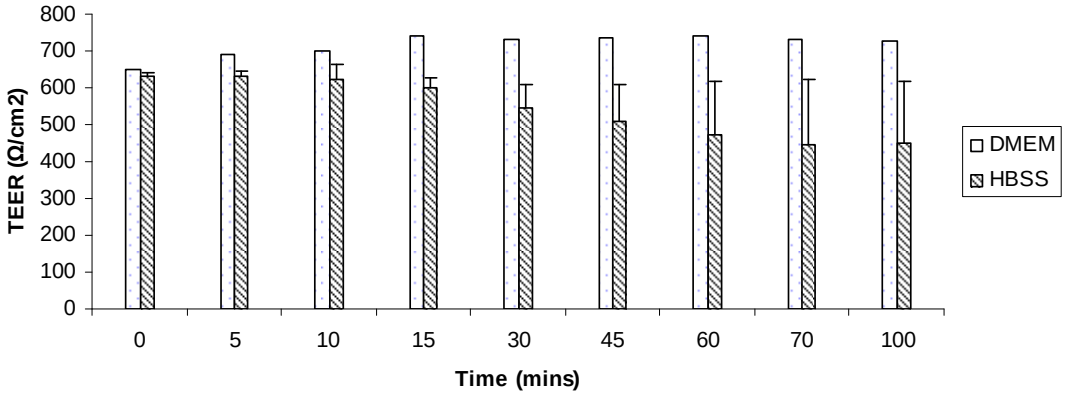

Figure 3.3.45:- Effect of inoculation time with HBSS and DMEM on the TEER values of Caco-2 cells (n=3).

The permeability profiles of IND with increasing ratio of arginine and lysine were studied and summarised in Fig. 3.3.9 and 3.3.11. In all the experiments the concentration of IND was constant and the concentration of the amino acids was changed. TEER values were measured before and after the run of the experiments and all the values were above 300 (Table 3.3.1) which demonstrates full integrity of the monolayes and their tight junctions.

Table 3.3.30:- TEER measurements for IND formulations before and after the permeability assay (n=5)

Formulation	TEER measurements (Ω/cm^2) Before	TEER measurements (Ω/cm^2) After	Recovery (%)
IND	555.66±12.7	421.66±28.4	71.4
IND-arg 1:1	611.33±19.73	450.66±21.12	89
IND-arg 1:2	571.66±31.33	438±11.5	98.15
IND-arg 1:4	595±14.9	457.66±26.1	72.7
IND-arg 1:8	577.66±15.04	440.66±8.1	97
IND lysine salt			
IND-lys 1:1	387.66±10.69	337±33.45	99
IND-lys 1:2	349±3.60	345.66±4.16	89.7
IND-lys 1:4	410.33±59.5	352.33±49.34	80.1
IND-lys 1:8	412±13.1	386±22.34	76

Generally amount of drug absorbed increased with time, regardless of the formulations. Equation 3.3.5 was used to calculate the apparent permeability (P_{app}). The percentage of IND absorbed from IND free acid formulations was 5.7±0.26 % after 5 minutes and increased steadily to 31±3.8% after 90 minutes. Adding arginine to IND at 1:1 ratio showed no significant effect on the absorption profile of IND. In contrast, IND-arginine 1:2 (P_{app}= 24.3x10^{-6} cm/sec)

and 1:4 (P_{app}= $22x10^{-6}$ cm/sec) ratios showed a significant increase in IND permeability especially after 60 minutes of starting the permeability assay.

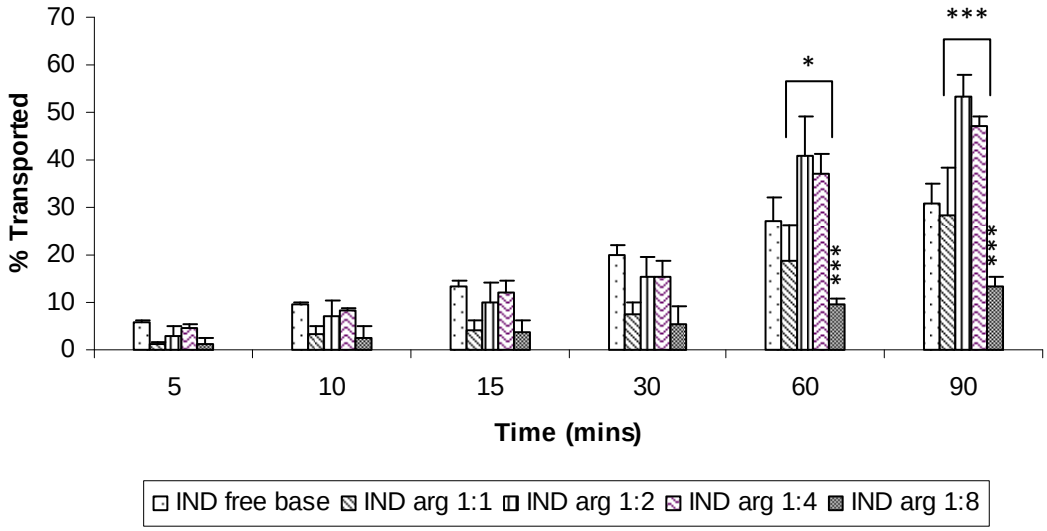

Figure 3.3.46:- Percentage of IND transported across Caco-2 monolayers at various molar ratios of arginine (n=5). One way analysis of variance (ANOVA) and pair-wise multiple comparisons method (Tukey test) against drug alone at each time point were used for statistical analysis and probability values of (P< 0.05, * and P<0.001,*) were used to determine the significant difference.**

As discussed above, the partitioning studies showed that the log P values of IND decreased as arginine ratio in the formulations was increased which would suggest that there would be a drop in the overall IND permeability profile. However the results demonstrated unexpected and interesting trends with a substantial increase in permeability especially for the 1:2 and 1:4 ratio of IND:counter ion. Two possible scenarios could explain such improvement of the absorption profile. Firstly, it is possible that the increase in solubility and dissolution profile (Fig. 3.1.8**)** with increasing the concentration of the cationic amino acids resulted in the drug being readily available in the solution faster than that of the formulations containing IND alone.

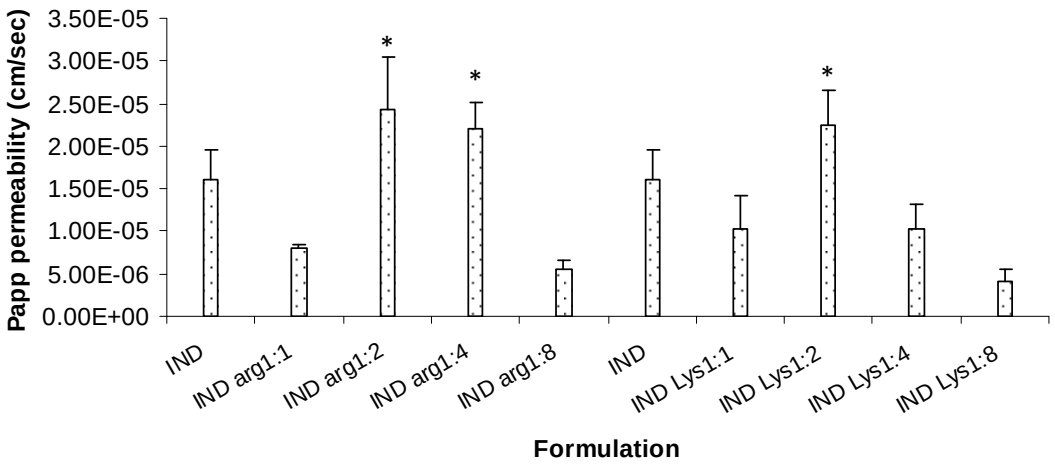

Figure 3.3.47:- P_{app} permeability values at 60 minutes for IND alone and IND at various molar ratios of arginine and lysine. One way analysis of variance (ANOVA) and pair-wise multiple comparisons method (Tukey test) against drug alone at each time point were used for statistical analysis and probability values of (P< 0.05, * and P<0.001, *) were used to determine the significant difference (n=3).**

The second scenario is that active transportation via carrier transporters for amino acids such as peptidyl or anionic transporters might have played a role in drug transport. Interestingly, IND-arginine 1:8 ratio showed a significant drop (P<0.001) in the percentage of IND permeated (13.5±1.76 %) when compared to formulations containing IND alone (31±3.8 %) after 90 minutes. Although the former had a much higher dissolution profile than the latter (Fig. 3.1.8) the results suggest that the permeability improvement is not because of the increase in the dissolution profile or deterioration in the Log P values but possibly due to increase in active transcellular carriage of the drug. At very high concentrations of the amino acids (1:8 ratio) the amino acids transporters might have been saturated with the excess arginine and hence the over all uptake of IND was decreased. While on the other hand, at smaller molar ratios of arginine, the receptors did not get saturated quickly and IND uptake is facilitated by active transporters.

Studying the effect of lysine molar ratio on the permeability profile of IND showed similar trend. IND-lysine formulations at 1:2 ratios had a significant impact (P_{app}= 22.4±4)10^{-6} on

percentage of IND absorbed across the Caco-2 monolayers and beyond this ratio the permeability started to decline.

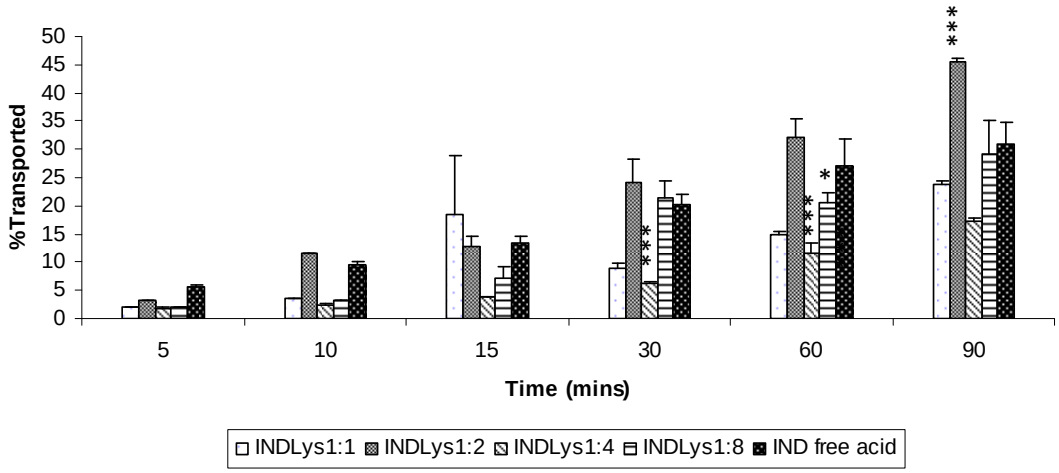

Figure 3.3.48:- :- Percentage of IND transported across Caco-2 monolayers at various molar ratios of lysine (n=5). One way analysis of variance (ANOVA) and pair-wise multiple comparisons method (Tukey test) against drug alone at each time point were used for statistical analysis and probability values of (P< 0.05, * and P<0.001,*) were used to determine the significant difference.**

Conclusion

After improving the solubility and dissolution profile of IND using cationic amino acids (Chapter 3.1), it was interesting to evaluate the effect using IND ion-paired formulations on its permeability across Caco-2 cells. High solubility and dissolution of IND reflects the high ionisation of the salt form hence excess amount of the counter ions were added in a trial to shift the salt ionisation equilibrium towards the non-ionised form of the salt. Octanol/water partitioning studies revealed the greasy nature of IND (log P=3) and increasing the molar ratio of the cationic amino acids results in significant drop in the partitioning capacities of IND in octanol organic layer. Nevertheless permeability data showed a significant increase in IND absorption especially for PMs of 1:2 molar ratios. This suggests that active carrier might have been involved in the uptake of IND ion-paired formulations as drug partitioning has decreased.

Chapter 4

Trimethoprim

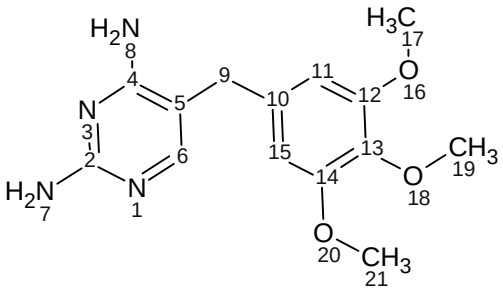

Papers relating to chapter 4

Amr ElShaer, Peter Hanson, Tony Worthington, Peter Lambert and Afzal R. Mohammed., (2012). Preparation and Characterization of Amino Acids -Based Trimethoprim Salts. *Pharmaceutics*, 4(1), 179-196.

Amr ElShaer, Peter Hanson and Afzal R Mohammed (2013) A systematic and mechanistic evaluation of aspartic acid as a filler for directly compressed tablets containing trimethoprim and trimethoprim aspartate., *European Journal of Pharmaceutics and Biopharmaceutics*. In press.

Could amino acid salts fool fussy bacteria to improve antibiotics uptake? *UKICRS, Queen's University Belfast, April 2011.* Oral presentation.

Preparation and characterisation trimethoprim salts with anionic counter ions

4.1.1. Introduction

Trimethoprim (Figure 4.1.1) [2,4-diamino-5-(3,4,5-trimethoxybenzyl)pyrimidine], is a synthetic antibacterial agent belonging to a group of compounds known as diaminopyrimidines. It was first synthesized as a dihydrofolate reductase inhibitor (DHFR) and used mainly in combination with sulfonamides to treat pneumonia and urinary tract infections. TMP is administered through various routes including intramuscular, intravenous and oral and has high gastro-intestinal tolerability and low side effects. However, low aqueous solubility of TMP (Manius, G., 1978) reduces the bioavailability from oral formulations. In order to improve TMP dissolution profile, a study conducted by Li et al utilised β-cyclodextrin to form a complex with TMP (Li et al., 2005). The study concluded that the high surface area of contact between TMP and the cyclodextrin along with reduction in drug crystallinity were responsible for improvement in TMP solubility (Li et al., 2005). Nevertheless, the solubility improvement achieved by this study was 2.2 fold. Besides, high doses of β–cyclodextrin are not recommended and can cause diarrhea and bloating as they are degraded and fermented by bacteria in the colon (Del Valle., 2004). Therefore, investigation of alternative approaches to improve the solubility of TMP would have a high impact on oral administration of the drug.

Interestingly, TMP has a basic nature (pKa 7.3) and a soluble derivative of the antibiotic can be obtained by reacting TMP with acids resulting in salt formation. Around 50% of the prepared salts of basic drugs are hydrochloride salts. Yet, hydrochloride salts salt out easily and in turn reduce the optimal solubility. Furthermore, hydrochloride salts usually cause high acidity in the formulations and high risk of corrosion (Bastin et al., 2000), while the loss of volatile HCl could affect the stability of weak bases especially over the long-term (Stahl and Wermuth, 2002). Due to the limitations of hydrochloride salts, alternative counter ions that have been explored include citric acid, acetic acid, fumaric acid and maleic acid Stahl and Wermuth., 2002;

Hemamalini et al., 2003 ; Raj et al., 2003). Another class of counter ions that can potentially address the solubility of basic drugs includes acidic amino acids. Fabrizio & Vetere utilized aspartic acid to prepare a water soluble salt of erythromycin. The obtained salt was used to prepare parenteral formulations of erythromycin and was found to be highly tolerable and less toxic (Fabrizio and Vetere, 1973). Glutamic acid was used to prepare water soluble salts of chitosan and the glutamate salt was found to improve the apparent permeability of many drugs such as naproxen (Maestrelli et al., 2004) and rokitamycin (Gavini et al., 2010) when compared to chitosan alone.

The present study aims to improve the solubility of TMP through salt formation with anionic amino acids, namely glutamic acid and aspartic acid and to characterize the prepared salts using FT-IR spectroscopy, proton nuclear magnetic resonance (^{1}HNMR), differential scanning calorimetry (DSC) and thermogravimetric analysis (TGA). The study also investigates the effect of different amino acid isomers on the salt characteristics and evaluates the inhibitory effect of the amino acids salts on intrinsically resistant bacteria.

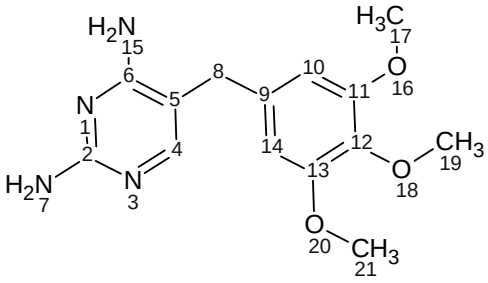

Figure 4.1.1. Trimethoprim chemical structure.

4.1.2. Materials and methods

4.1.2.1. Materials

Trimethoprim 98% TLC, L-glutamic acid, L-aspartic acid, D-aspartic acid (99%), D-glutamic acid (minimum 99% TLC) and Potassium bromide (99% FT-IR grade) were purchased from Sigma Aldrich, UK.

D_2O (99.9% min) was purchased from Goss scientific instrument Ltd (Cheshire, UK). DMSO-D6 (98.8% min) was purchased from Merck (Darmstadt, Germany). Tryptone Soya Broth (TSB) and Muller Hinton Broth (MHB) were purchased from Oxoid Ltd, Hampshire, England.

4.1.2.2. Methods

4.1.2.2.1. Analytical technique

The amount of Trimethoprim (TMP) dissolved in the solution samples was quantified using the HPLC (Dionex 1100 system) method reported by Gallego and Arroyo (Gallego and Arroyo., 2002). HPLC was operated at 25^{o}C on RP-C18, (Phenomenex 110A, 150x4.6 mm, 5µm) column using acetonitrile-NaH_2PO_4 buffer (10 mM) (70:30, v/v) (pH 3) as mobile phase which was pumped at 1.0 mL/min flow rate using gradient pump (GP50). UV detector (UVD 170U) was used and the analysis was monitored at 230 nm. The retention time was 1.74±0.04 min and a rectilinear calibration curve was established at concentrations ranging between 10- 500µg/mL (R^2 of 0.99). LOD and LOQ were calculated using standard deviation of response and slope and were found to be 0.109 and 0.364 respectively. For more details see appendix (1).

4.1.2.2.2. Phase solubility diagram

Phase solubility diagram was established by measuring the saturated solubility of TMP free base with various concentrations of acidic amino acid (L-aspartic acid and L-glutamic acid).

Excess TMP was added into screw-capped tubes containing serial dilutions of the amino acid solutions and agitated at room temperature (Stuart SB 162 stirrer) for 24 h. After equilibrium, the supernatant was filtered through 0.45 µm filters and analysed by HPLC to determine TMP concentration. The pH of amino acid solutions was monitored using an Xisherbrand Hydrus 500 pH meter.

4.1.2.2.3. Salt preparation

Equimolar amounts of TMP and the free amino acids (L-aspartic acid and L-glutamic acid) were solubilised in water and the solutions were mixed and stirred until equilibration was achieved. The filtrate was transferred into vials and freeze dried for 48 h using a Modulyo freeze dryer at -40^{o}C shelf temperature and under vacuum. The samples were collected and kept in 40^{o}C oven for 4h using a Gallenkamp vacuum oven.

Despite the low yield with freeze drying, it is a preferred technique unlike organic solvent methods adapted by Anderson & Conradi (1985), as lyophilized products have a high degree of purity and are devoid of the formation of any solvates.

4.1.2.2.4. Thermogravimetric analysis (TGA)

A thermogravimetric analyser (Pyris 1 TGA, Perkin Elmer) was used in this study to measure the moisture content and decomposition temperature of TMP and its prepared salts. 5- 10 mg of samples were loaded on to an open pan and analysed between temperature range 30- 300 ^{o}C at 10 ^{o}C/min scanning rate and under nitrogen stream. Pyris Manager Software (version 5.00.02) was used to analyse the resultant thermograms.

4.1.2.2.5. Differential scanning calorimetry

Differential scanning calorimeter (Pyris Diamond DSC) was used to explore thermal events of TMP and its salts. Approximately 2-5 mg of the samples were weighted and transferred to an

aluminium sample pan (50 µL capacity). Intra cooler 2P system was used to initially cool the samples to 50 ^{o}C and then sample heated to 300 ^{o}C at a rate of 10 ^{o}C/min. Nitrogen was used as a purge gas at a flow rate of 20 mL/min. Indium and Zinc were used to calibrate the heat flow and melting point onset (156.6 ^{o}C for Indium and 419.47 ^{o}C for Zinc). The obtained thermograms were analysed using Pyris Manager Software (version 5.00.02). The experiment was performed in triplicate and an empty aluminium pan was used as a reference cell for all the measurements.

4.1.2.2.6. FT-infrared (IR) spectroscopy

FTIR absorbance spectra of TMP and its salts were obtained with Nicolet IR 200 spectrometer (Thermo electron corporation) using KBr discs. Crystalline KBr was dried at 65^{o}C over night before use. Samples were prepared by mixing TMP or its salts with dry KBr at 1:100 (w/w) ratio and pressed at 8 tonnes for 5 minutes (using a Specac tablet presser) to form KBr discs. 64 scans were done over a wavelength range of 4000- 400 cm^{-1} for each sample. EZ OMNNIC 7.0 software was used to interpret the IR spectrum.

4.1.2.2.7. ^{1}HNMR

Samples were studied with Bruker Avance DPX-250 NMR (at 250.1 MHz) and Bruker Topspin software was used to analyse the data. Approximately, 1-2 mg of the salts was dissolved in 1 mL of deuterated water (D_2O) and placed in sample capillary vial. Sample vials were placed into the NMR machine and analysed for the presence of hydrogen atoms (^{1}H-NMR)

4.1.2.2.8. pH solubility profile

pH solubility studies were determined by using the Ledwidge & Corrigan method (Ledwidge and Corrigan, 1998). Saturated solutions of the salts and acids were prepared by dissolving excess of the drug in deionised water. The solutions were agitated constantly using a stirrer

(Stuart SB 162) at ambient temperature. pH was adjusted by adding NaOH or the appropriate acid (L-aspartic acid or L-glutamic acid). After 2 hour interval an aliquot was withdrawn and filtered through 0.45 µm filter, then analysed using HPLC (see section 2.2.1)

4.1.2.2.9. Solubility and dissolution studies

Solubility studies were carried out using Hugchi and Connor's method (Higuchi and Connors., 1965). An excess amount of TMP or its salts was added to capped tubes with 5 mL of deionised water and stirred for 24 hours at room temperature until equilibrium was reached. Subsequently, the suspension was filtered through 0.45µm syringe filters and suitably diluted and the concentration was measured by HPLC.

Hard gelatin capsules were filled with 200 mg of TMP or equivalent amounts of the prepared salts for dissolution studies. USP II paddle method (ERWEKA DT-600) was used to perform the in-vitro dissolution studies. The prepared capsules were placed into dissolution vessels containing 900 mL of distilled water (pH 7.2) and the dissolution media was maintained at $37^{o}C \pm 0.5^{o}C$ and stirred at 50 rpm. 5mL of samples were collected at a predetermined time intervals (1, 5, 10, 20, 25, 30, 45 and 60 min) then filtered through 0.45 µm Millipore filters. The dissolution media was replaced by 5mL of fresh dissolution media in order to maintain a constant volume. After proper dilution samples were analysed by HPLC as mentioned above.

4.1.2.2.10. Microbiological studies

Two Gram-negative bacterial strains; *Escherichia coli* NCTC 10418 and *Pseudomonas aeruginosa* ATCC 9027 were used for this study. Freshly inoculated bacteria agar plate was prepared one day before the experiment by spreading colony suspension on Trypticase-soy agar plate and incubating for 18 to 24h.

Zone of inhibition study was performed using Agar plates prepared using Trypticase-soy agar plates. Loopful of bacteria was spread gently on the surface of the agar plates. Six small holes

were perforated on the agar plates and filled with 20µl of 0.5mM TMP or equivalent concentration of TMP salts. In order to evaluate any inhibitory effect of the amino acids on the bacterial growth, free amino acids were used as controls for this study.

The bacterial minimum inhibitory concentration (MIC) of TMP and its prepared salts against the same two species of Gram negative bacteria were performed using micro-dilution method and following the national committee for clinical laboratory standards (NCCLS) specifications.

The bacterial inoculum was established by direct colony suspension method from 18 to 24h Trypticase-soy agar plates, standardized and counted by Pharmacia spectrophotometer (Pharmacia LKB, Novaspec II). Around $5x10^6$ CFU/mL was suspended in Tryptone Soya Broth and used in our study.

50 µl of the bacterial inoculum was transferred to 100 µl of Muller Hinton Broth (MHB) at final concentration ranging between 0.5- 0.00024 mM prepared by two fold dilution.

Inoculated plates were incubated at 37^oC for 18- 24 h. The lowest concentration of the antibacterial agent that inhibits the growth of bacteria was determined by visual turbidity when compared against control.

4.1.2.2.11. Statistical analysis

Graph Pad Instat® software was used for the statistical analysis study. Data groups were compared using one way analysis of variance (ANOVA) and pair-wise multiple comparisons method (Tukey test). Standard deviation (SD) was used to report the error in the figures and texts. Probability values of 95% ($P< 0.05$) were used to determine the significant difference.

4.1.3. Results and discussion

4.1.3.1. Phase solubility diagrams

Prior to preparing TMP salts, a solubility phase diagram was first constructed between TMP and two acidic amino acids; aspartic acid and glutamic acid as previously discussed by ElShaer et al (2011). Figure 4.1.2 shows that increasing the anionic amino acid concentrations results in lowering of the solution pH and in turn improving the solubility of TMP. Aspartic acid has an acidic (-COOH) side chain with pKa of 1.88 which is 5 units lower than the pKa of TMP (pka 7.3). Therefore TMP could potentially act as a strong base in aspartic acid solution capable of deprotonating the –COOH acidic group. Interestingly, a linear relationship (R^2= 0.93) between TMP solubility and aspartic acid concentration was observed which suggests that complete ionisation of TMP in aspartic acid solution was achieved suggesting the feasibility of salt formation.

On the other hand, despite the slightly higher pk_a of the acidic side chain (-COOH) of glutamic acid (pKa = 2.19) a similar trend in solubility improvement was achieved possibly due to the ionisation of TMP in solution. These results suggest that both glutamic and aspartic acid can be used in preparing novel salts of TMP.

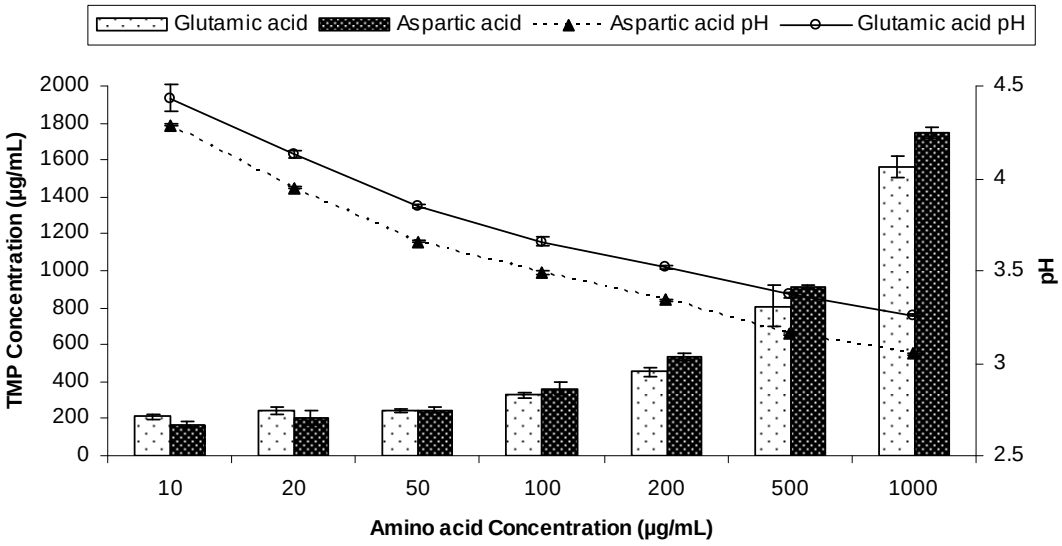

Figure 4.1.2. Phase solubility diagram of TMP in the presence of different concentrations of glutamic acid and aspartic acid at different pH (n=3).

4.1.3.2. Characterization of salt form

In order to evaluate the effect of the isomer form on the salt characteristics, D and L isomers of glutamic and aspartic acid were used to prepare TMP salts. The prepared salts were further characterised by Fourier transform infra-red, differential scanning calorimetry, thermo-gravimetric analysis and ^{1}H nuclear magnetic resonance.

4.1.3.2.1. Fourier Transform Infrared Spectroscopy (FT-IR)

FT-IR was performed in order to assess any possible interaction between TMP and the acidic amino acids during salt formation and to investigate any possible changes that could occur due to the use of different isomeric forms of amino acids.

The FT-IR spectra of TMP, TMP L-aspartate and TMP D-aspartate are shown in Figure 4.1.3. TMP has characteristic bands at 1634.3 and 1594.7 cm^{-1} which account for deformation of NH_2 group and stretching of aromation ring respectively. Deformation of $C^{9}H_2$ group appeared at

1458.7 cm^{-1}, while the vibration of C^6=N of the aromatic primary appeared at 1263.71 cm^{-1}. – OCH_3 aromatic groups had characteristic bands at 1128.68 cm^{-1}, as reported by Garnero et al. (2010).

Assessment of TMP L-aspartate salt showed that TMP bands corresponding to NH_2 and C-H aromatic stretching vibration were difficult to analyse due to overlapping with NH_2 and CH aliphatic of the amino acid (Figure 4.1.3A). Interestingly, the C=N in the amine aromatic primary became very weak and a new band appeared at 1664.53 cm^{-1} corresponding to νC=O stretching which confirms that the cationic nitrogen has interacted with the carboxylic group of aspartic acid. In contrast, OCH_3 aromatic groups did not show any changes in the formed salt.

Upon comparing the FT-IR spectra of the L-aspartate and D-aspartate salt, no difference was spotted between the two isomers (Figure 4.1.3A & B).

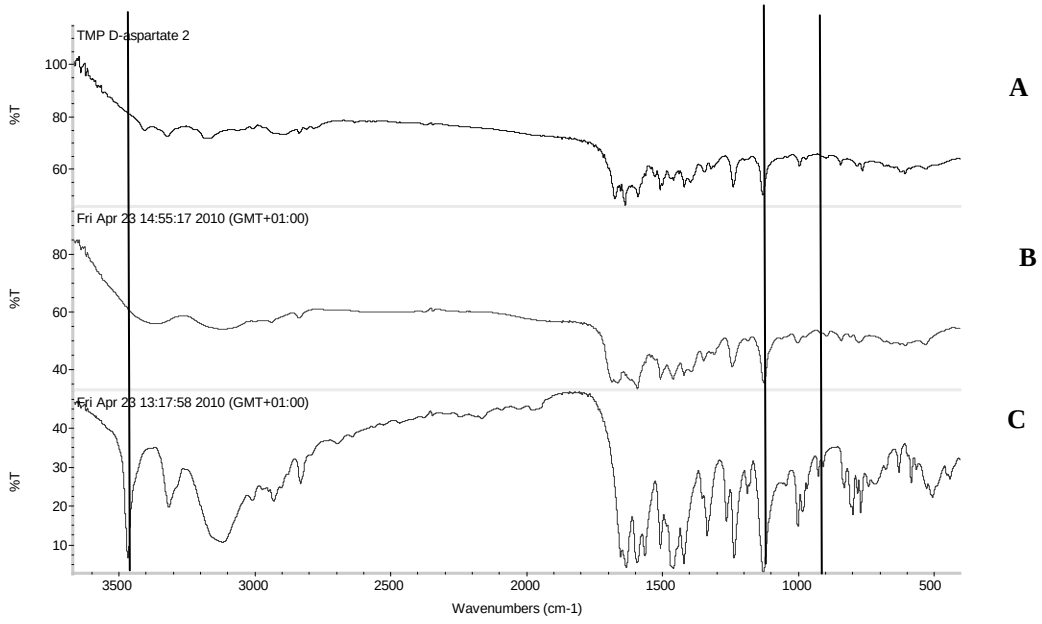

Figure 4.1.3. FTIR spectra of (A)trimethoprim D-aspartate, (B) trimethoprim L-aspartate and (C) trimethoprim.

Figure 4.1.4 shows the FT-IR for TMP L-glutamate and TMP D-glutamate. Similar to the results obtained for aspartate salts, a new band appeared at 1656.87 cm^{-1} and 1654.74 cm^{-1} for TMP

L-glutamate and TMP D-glutamate respectively. This band corresponds to the vC=O of the amino acid carboxylic group which when deprotonated potentially interacts electro-statically with the protonated amino group of TMP prymidine ring. Both the L and D salts had similar FT-IR spectra and no significant difference was observed.

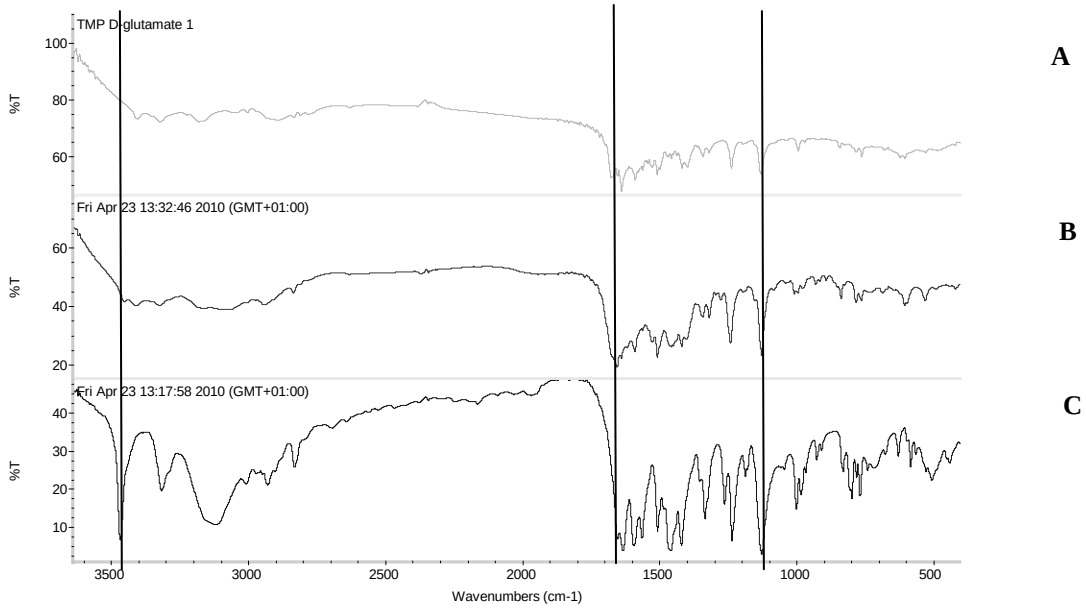

Figure 4.1.4. FTIR spectra of (A) trimethoprim D-glutamate, (B) trimethoprim L-glutamate and (C) trimethoprim.

4.1.3.2.2 Differential scanning calorimetry and Thermogravimetric analysis.

Figure 4.1.5 shows the TGA and DSC scans for TMP and L-glutamic acid. TMP had one single endothermic peak at 204.22 ^{o}C with an enthalpy of fusion of 166.7 J/g. TGA data revealed that TMP starts to degrade after around 30 ^{o}C of its melting.

TMP L-glutamate salt was found to be in the crystalline form as no crystallization exotherm was observed in the DSC scans (Figure 4.1.5). At around 130^{o}C, TMP L-glutamate had an endothermic peak which could possibly correspond to moisture loss. Another two endothermic peaks appeared at 197.22 ^{o}C (ΔH = 20.22 J/g) and 233.47 ^{o}C (ΔH= 150.02 J/g). This data suggest that we might have two enantiotrophs or monotrophs. A second scan was run after cooling down and the first thermal event was found to be irreversible and hence this

strongly suggests that these are monotrophs rather than enantiotrophs. Interestingly, coupling the DSC scans with TGA has showed a weight loss (4.03%) at 196 ^{o}C which means that this thermal event can not be a phase transition because polymorphic transitions are not associated with weight loss. ^{1}HNMR data (discussed in details in section *3.3.3*) has not picked up any impurities in the spectra and strongly suggest that this 4.03% weight loss is probably due to highly associated water molecules within the crystalline structure of the salt. The water 2H appear at 4.7 ppm and interfering with D_2O peaks (Gottlieb et al., 1997).

On the other hand, the TMP D-glutamate salt is partially crystalline and the amorphous portion of the salt starts to crystallize at 140 ^{o}C. Moisture loss appeared as an endothermic hump at around 80 ^{o}C corresponding to 1.62%. Similar to TMP L-glutamate, TMP D-glutamate showed hydrate loss at 197.22 ^{o}C (ΔH= 18.16 J/g) appeared as small peak reflecting the small amount of the hydrate crystals formed during the freeze drying while the rest of the salt was in the amorphous state and crystallizes at 140 ^{o}C as discussed before. After dehydration, the salt started to melt at 231.74 ^{o}C (Figure 4.1.5) similar results were suggested by Sichina, (2011).

The thermal events of TMP L-aspartate and TMP D-aspartate were studied using TGA and DSC (Figure 4.1.6). TMP L-aspartate showed an up drafted base line between 100- 150 ^{o}C which corresponds to moisture loss and the salt converted from the amorphous form to the crystalline form at 160 ^{o}C followed by crystal melt at 184.22 ^{o}C.

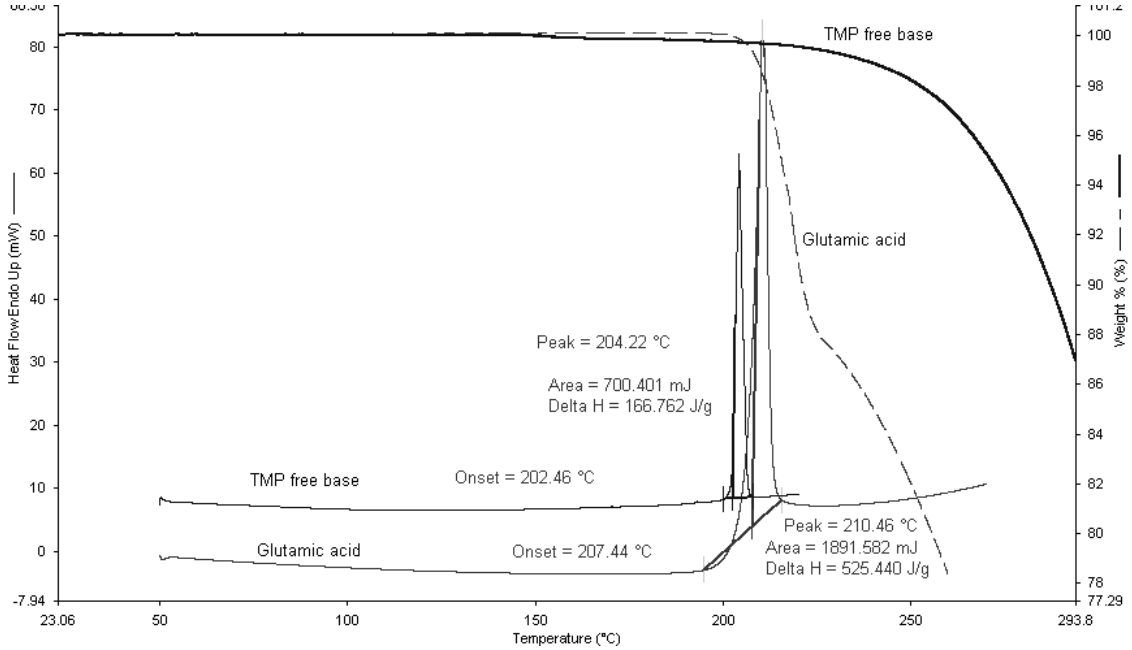

Figure 4.1.5. TGA and DSC scans for L- glutamic acid and TMP free base.

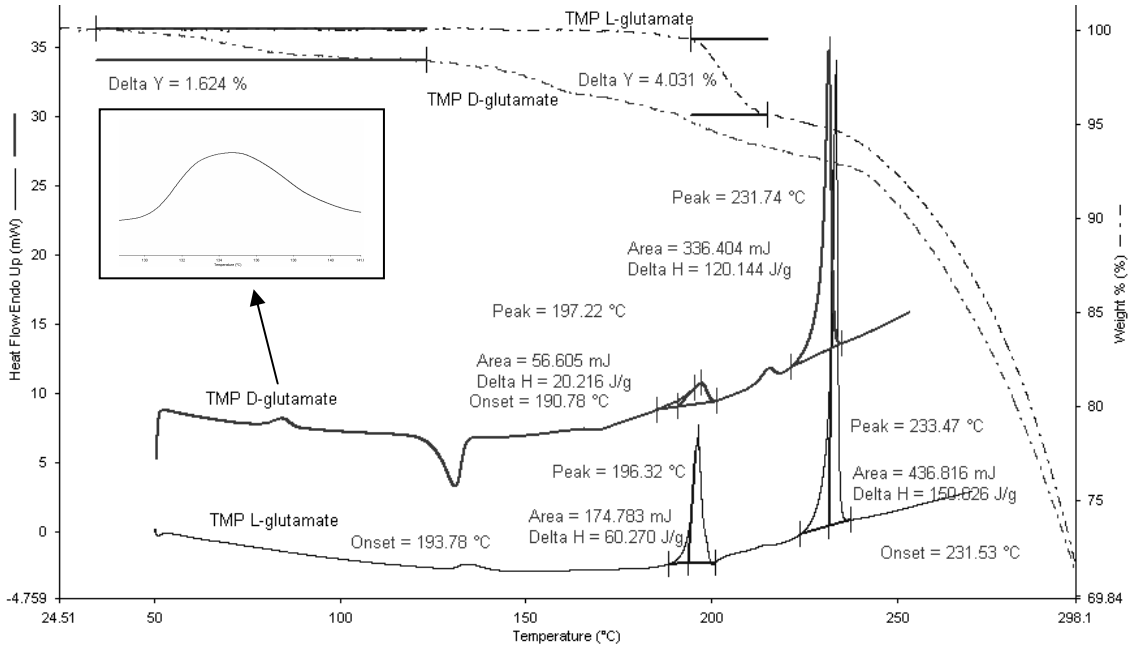

Figure 4.1.6. DSC and TGA scans for TMP D-glutamate and TMP L-glutamate salts. 2- 5 mg of the sample was heated to 300°C at rate of 10 °C/min (n=3).

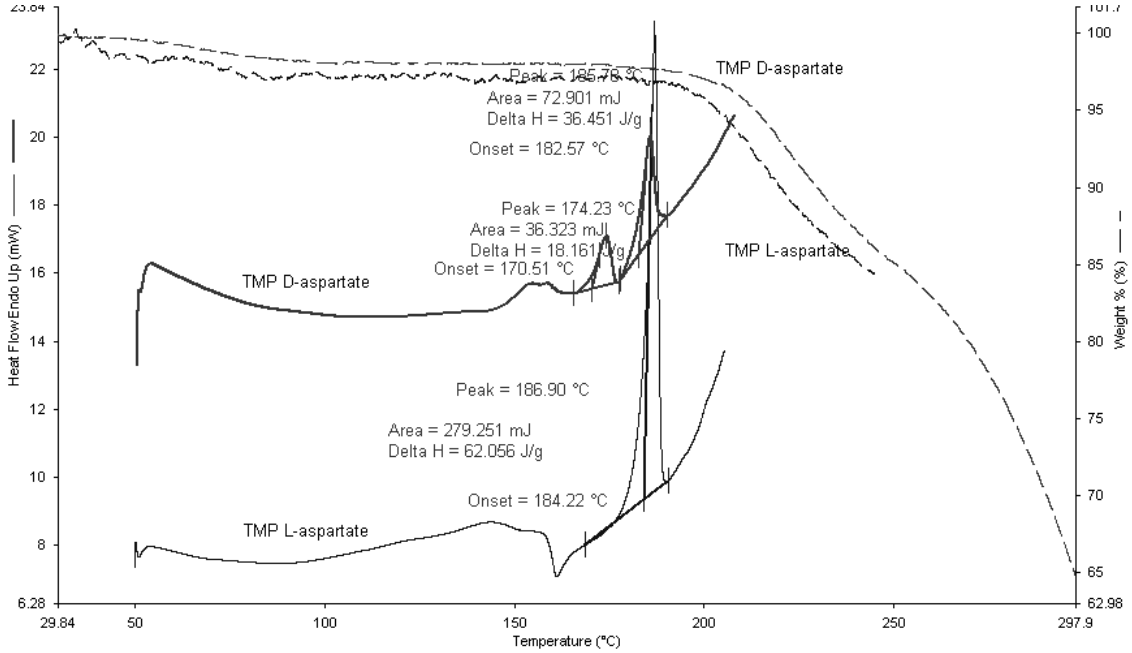

Figure 4.1.7. DSC and TGA scans for TMP D-aspartate and TMP L-aspartate. 2- 5 mg of the sample was heated to 300°C at rate of 10 °C/min (n=3).

4.1.3.3.3 ^{1}HNMR studies

The electronic and chemical environment of protons are affected during salt formation which could be reflected by the changes in δ. ^{1}HNMR is considered a powerful tool in studying salt formation as it provides insight in to the ratio of molar interaction between the two moieties. Figure 4.1.8 shows the ^{1}HNMR of TMP free base (solubilised in DMSO). At 7.53 ppm frequency one proton of TMP heterocyclic ring $C^{4}H$ appeared as singlet and the two protons on the aromatic ring $C^{10}H$ and $C^{14}H$ appeared at 6.56 ppm. The nine hydrogens of OCH_3 groups appeared as two different peaks; (6H) appeared as a singlet at 3.73 ppm as they have the same surrounding environment, while the other (3H) appeared as a singlet at 3.63 ppm. The two hydrogens of aliphatic ($C^{8}H_2$) appeared as singlet at 3.54 ppm while two singlet bands appeared at 5.7 and 6.2 which correspond to $N^{5}H_2$ and $N^{7}H_2$ respectively. The total integrated H count for TMP was 18 (Figure 4.1.8).

TMP L-aspartate salt (solubilised in D_2O) showed new (3H) assignment at 2.6 corresponding to ($C^{27}H_2$) and a highly deshielded $C^{25}H$ group at 3.75 ppm, which represents the aliphatic chain of L-aspartic acid. As D_2O was used as a solvent for TMP salts, NH_2 groups were masked and the total integration of TMP aspartate salt was 17 instead of 21. These results confirm that one mole of L-aspartic acid interacts with 1 mole of TMP to form the salt (i.e 1:1 ratio) as shown in Figure 4.1.9.

On the other hand, TMP L-glutamate had 5 new protons representing the aliphatic chain of the amino acid. ($C^{28}H_2$, $C^{27}H_2$) appeared at 1.96 and 2.2 ppm, while the third $C^{25}H$ group appeared at around 3.6 ppm due to the deshielding by NH_2 group. The total integration also shows that 1 mole of L-glutamic acid interacts with 1 mole of TMP (Figure 4.1.10).

^{1}HNMR studies of TMP D-aspartate and TMP D-glutamate salts did not reveal any difference in the spectra between the L and D isomers (Figure A2.1& A2.2 Appendix 2). The high similarity of the salts formed despite using different isomers suggest that water used to solubilise the amino acids during the preparation step might provide free space for the rotation of the molecules and potentially catalyze racemisation as suggested by Feng et al., (2011).

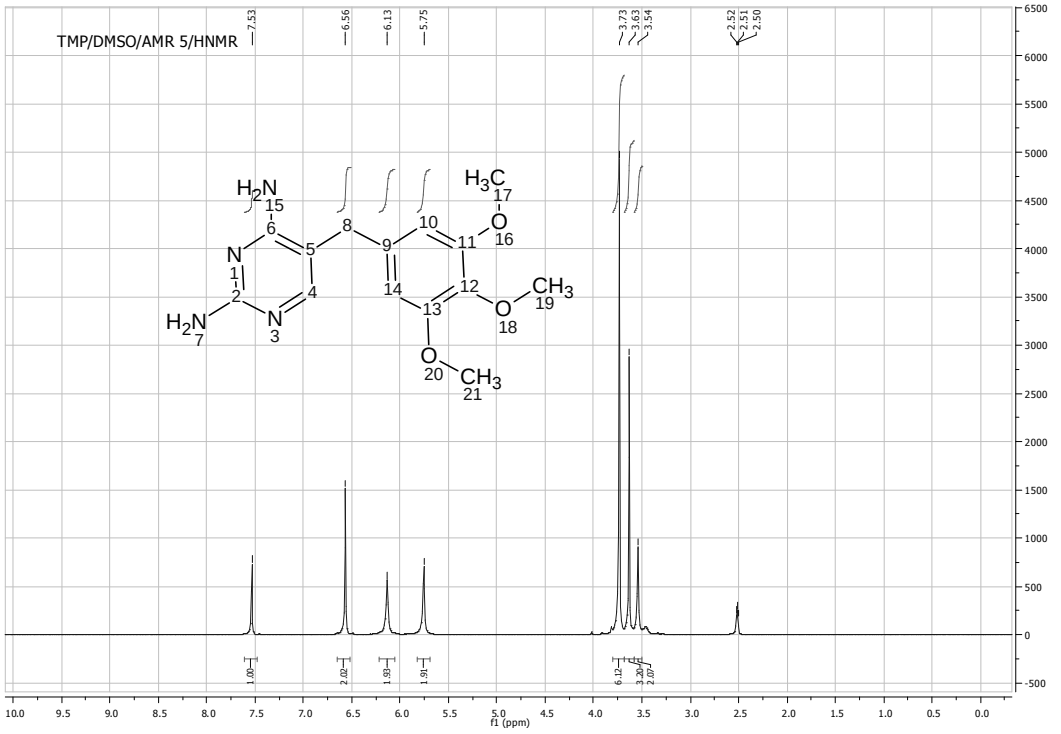

Figure 4.1.8. ^{1}HNMR spectra of trimethoprim free base solubilised in DMSO.

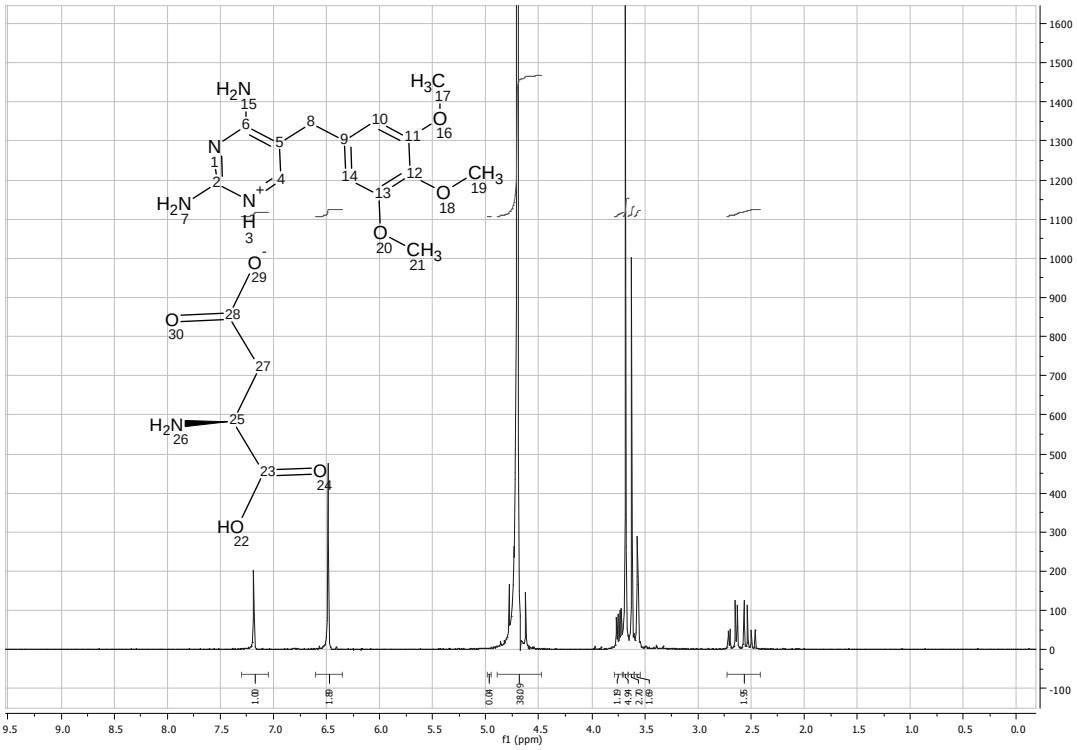

Figure 4.1.9. ^{1}HNMR spectra of trimethoprim L-aspartate solubilised in D_2O.

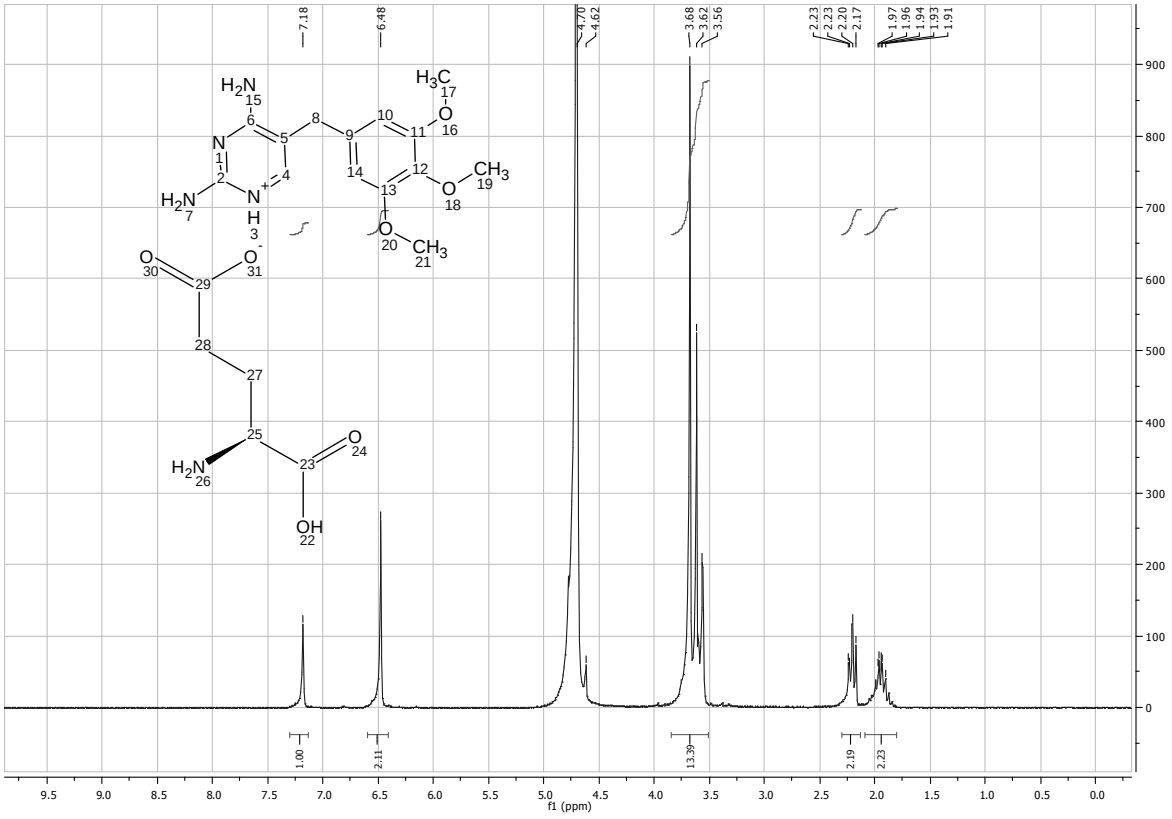

Figure 4.1.10. ^{1}HNMR spectra of trimethoprim L-glutamate solubilised in D_2O.

4.1.3.3.4. Aqueous solubility and dissolution Studies

TMP is usually used in combination with sulfonamides in various formulations such as suspension, tablets and solution dosage forms. Therefore TMP solubility and dissolution are important determinants for its bioavailability.

Solubility studies in our laboratory have found that the saturation solubility of TMP free base was 0.217 mg/mL in water. Using acidic amino acids counter ions improved the solubility of the drug by around 280 fold when compared against the free drug. The solubility of the prepared salts was around 55 mg/mL with no significant difference between the L and D isomers for both the counter ions (Figure 4.1.11).

The dissolution profile of TMP and its different salts was also studied (Figure 4.1.12). Dissolution studies show a significant improvement of the salt form when compared to the free base. Around 70% of the TMP was released from aspartate and glutamate salt form after only 10 minutes of the dissolution experiment while only 10% release was seen from TMP free form (Figure 4.1.12). Such changes in the dissolution profile could be attributed to the ability of TMP salts to exert a self-buffering action, which yield different pH values at the dissolving surface in the diffusion layer (Forbes and York, 1995). No significant difference was observed between the two salts, which suggest that both salts might have similar buffering capacity and hence similar pH at the diffusion layer.

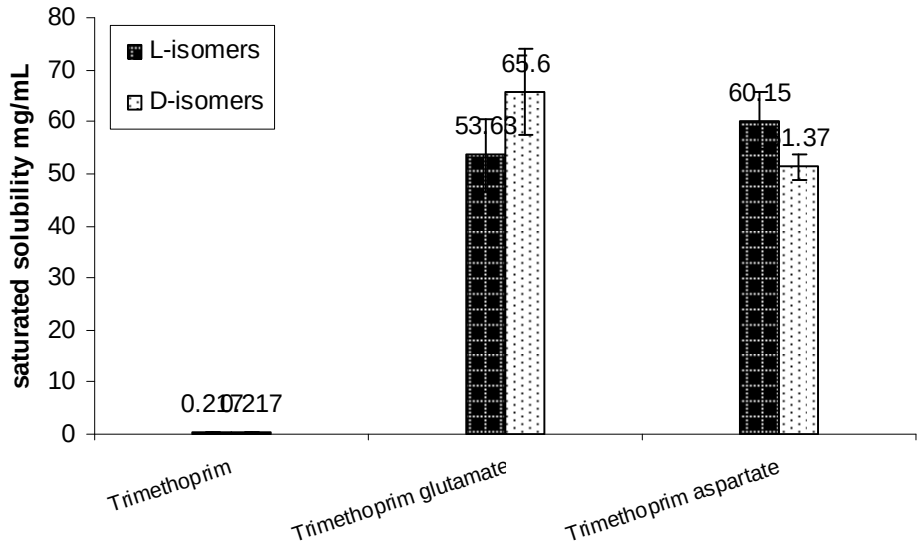

Figure 4.1.11. Solubility of trimethoprim and its prepared L & D aspartate and glutamate salts mean ±SD (n=3).

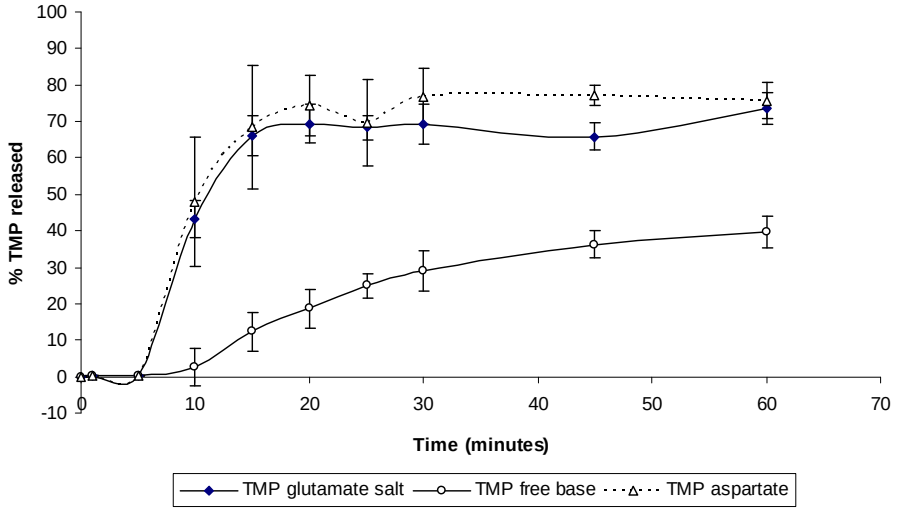

Figure 4.1.12. Dissolution profile for TMP free base and its salts in deionised water. Data are mean± SD (n=3).

Table 4.1.31:- pH measurements during solubility and dissolution studies.

		Formulation		
		TMP free base	TMP Aspartate	TMP glutamate
pH measurement	Solubility study (Equilibrium)	7.7±0.05	5.075±0.06	5.2±0.11
	End of dissolution study	8.6±0.07	5.37±0.08	5.88±0.05

4.1.3.3.5. pH- solubility profile

TMP pk_a and intrinsic solubility are 7.3 and 0.19 mg/mL respectively. Figure 4.1.13 shows the pH solubility profile of TMP when TMP glutamate salt and TMP free base were used as starting materials for determination of solubilities. The intrinsic solubility (Bs) was first determined by increasing the pH of TMP solution to 11.28 using NaOH and Bs was found to be 0.266 mg/mL. When TMP was used as a starting material the solubility was found to increase exponentially upon titrating with glutamic acid (Figure 4.1.13). TMP solubility increased from 0.37 mg/mL at pH 7.7 (point a) to 13.8 mg/mL at pH 4.23.

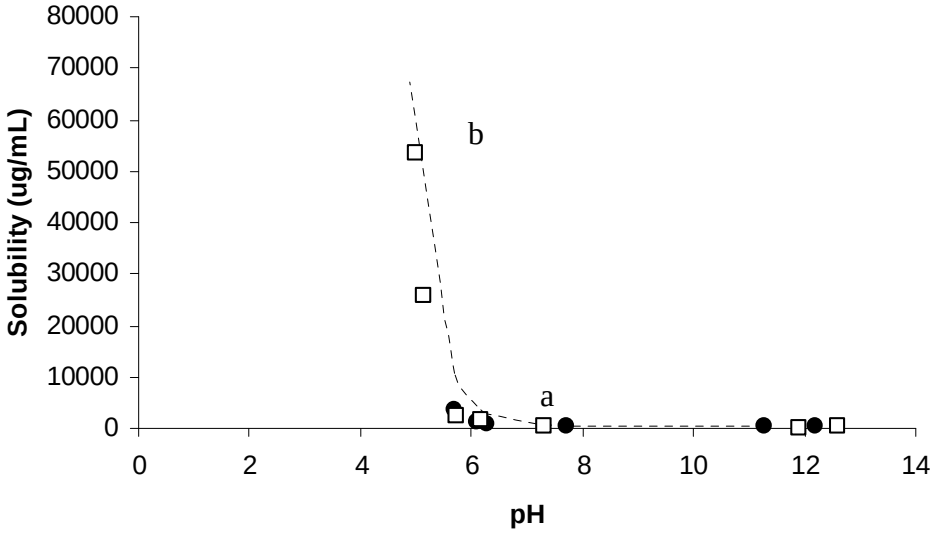

Figure 4.1.13. pH solubility profile of TMP and TMP-glutamate salt at ambient conditions using free acid (circles) and TMP-glutamate salt (squares) as starting materials. Points b and a represent the saturation solubility of the salt and TMP free base respectively. [Bs]= 266.35µg/mL and pKa=7.3.

On the other hand, when TMP glutamate salt was used as a starting point, the solubility started to decrease upon titrating with NaOH. TMP glutamate solubility was 53.6 mg/mL at pH 5 and decreased to 0.194 mg/mL at pH 11.9. A similar trend was observed upon titrating TMP with aspartic acid (data not shown). Generally, a good agreement was observed between the experimental values (squares and circles) and the theoretical predicted values (dotted line) see table (2). Theoretical calculations were carried out using Kramer and Flynn (1972) (Equation 4.1.1).

$$Ka = \frac{[B][H_3O^+]}{[BH^+]}$$

$$S_t base(pH > pH_{\max}) = B_s(1 = \frac{H_3O^+}{K_a})$$

$$= B_s(1 + 10^{Pka - pH}) \qquad \textbf{(Equation 4.1.28)}$$

Where S_t is the total solubility at given pH, $[B_s]$ is the intrinsic solubility of the free base and K_a is the acid dissociation constant.

Table 4.1.32. Theoretical calculations of pH solubility profile using (Equation 4.1.1). [Bs]= 266.35µg/mL and pKa=7.3.

pH	Solubility (µg/mL)
11.28	266.35
7.7	372.35
6.3	2929.63
6.1	4487.37
5.7	10869.11
4.9	67165.4

4.1.3.3.6 Microbiology studies

After having significantly improved both the solubility as well as the dissolution characteristics using the salt forms of TMP, the next stage of the work was to evaluate microbiological properties to study if the therapeutic effect of the drug was still retained upon preparation of the different salts.

Interestingly, zone of inhibition studies showed that use of amino acid salts not only retained the anti bacterial activity against TMP sensitive species; *Escherichia coli* but also had a significant increase in the total area of inhibition (Table 4.1.3). To rule out the possible effects of amino acids alone on bacterial growth inhibition, control experiments with the amino acids were performed which resulted in no inhibition of bacterial growth on the plates. Therefore, the higher zone of inhibition can be attributed to the significant improvement in solubility which potentially results in higher permeability across the agar plates resulting in larger zone of inhibition. This could possibly translate into a faster therapeutic effect along with reduced therapeutic dose in a clinical setting.

On the other hand, neither the drug nor the salts showed any activity against TMP resistance species *Pseudomonas aeruginosa.* This is probably due to the complex structure of *Pseudomonas aeruginosa* membrane as it is intrinsically resistant to TMP and prevents the entry of both the drug and amino acid salts.

Table 4.1.33:- Zone of inhibition studies of TMP and its prepared salts against *Escherichia coli* and *Pseudomonas aeruginosa.*

	Escherichia coli		*Pseudomonas aeruginosa*
	Area (cm^2)	*% compare to the total plate area*	
TMP	4.03±0.2	18.7	****
TMP aspartate	4.6±0.2	21.4	****
TMP glutamate	4.65±0.2	21.6	****

Bacterial minimum inhibitory concentration was carried out as well in order to accurately determine the MIC of the TMP and its salts. Two species were used in this study; *Escherichia coli* and the intrinsically resistant organism, *Pseudomonas aeruginosa*. The MIC of TMP on *E. coli* was 0.00048 mM and TMP aspartate and glutamate salt had similar MIC values which confirm our previous finding that salt preparation did not impair the pharmacological function of TMP (Table 4.1.4).

Table 4.1.34:- MICs of TMP and its prepared salts against *Escherichia coli and Pseudomonas aeruginosa.*

	Escherichia coli	*Pseudomonas aeruginosa*
TMP	0.00048 mM.	> 0.5 mM
TMP aspartate	0.00048 mM	> 0.5 mM
TMP glutamate	0.00048 mM	> 0.5 mM

4.1.4. Conclusion

TMP is a basic synthetic antibacterial agent which is poorly water soluble. In order to improve its solubility, the ability of TMP to form new salts with L and D isomers of acidic amino acids was investigated in this study. The study has demonstrated that TMP solubility increased significantly upon coupling with aspartic and glutamic acid and this increase was attributed to the novel salt formation which has self buffering capacity yielding favourable pH for salt solubility during dissolution. Moreover, the antibacterial activity of these new salts was investigated and no change was seen in their MIC when compared against TMP free base. Using different isomers; L- and D- forms did not show any significant difference in the salt characteristics. Our future work will investigate the effect of amino acids salts on the absorption characteristics of TMP across intestinal membrane using Caco-2 cells.

A systematic and mechanistic evaluation of aspartic acid as filler for directly compressed tablets containing trimethoprim and trimethoprim aspartate

4.2.1. Introduction

Oral drug delivery is considered the most common and convenient route for drug administration. Solid dosage formulations, especially tablets, account for the large proportion of dosage forms delivered orally (Sam and Fokkens, 1997; Rasenack and Muller, 2002). In addition to the active pharmaceutical ingredient (API), tablets comprise of various pharmaceutical excipients which not only support the manufacturing process but also ensure high quality of the final product. Therefore, appropriate selection and precise concentration of excipients is critical in the tableting process.

Most commonly used excipients include fillers (diluents), binders, lubricants, glidants, disintegrants, colorants and flavouring modifiers (Gohel, 2005). Diluents/fillers are added to tablets to bulk up the formulation for processing and handling. Mannitol is a free-flowing powder which is widely used as diluent for tablet manufacture. It is characterised by its low elastic recovery, sweet taste and cooling sensation and has been reported as the best sugar for manufacturing directly compressed chewable tablets (Sangekar et al., 1972). Recent studies suggested that mannitol could reduce intestinal absorption of pharmaceutically active agents and in turn lower the overall bioavailability of the pharmaceutically active agents (Adkin. et al., 1995a; Adkin et al., 1995b). Studies conducted by Adkin et al on the formulation of cimetidine (H_2-receptor antagonist) found that the bioavailability of the drug was reduced when combined with mannitol even at small concentrations (Adkin. et al., 1995a). This was attributed to the cathartic effect of mannitol on the small intestine which results in reducing

the small intestine transit time (Adkin et al., 1995b). Moreover mannitol is known to be taken up by the cells paracellularly via the tight junctions between the transepithelial cells (Yee, 1997). Studies conducted by Baired *et al* (1997) and Iga and Ogawa (Iga and Ogawa., 1997) concluded that incorporating mannitol in pharmaceutical formulations would reduce drug absorption by competing with API for the paracellular pathways especially if the API is transported primarily through that route.

Another commonly used tablet filler is dicalcium phosphate dehydrate (DCPD) which is characterised by its low cost, low hygroscopicity and good flow characteristics (Carstensen and Ertell., 1990). Clarke and co-workers found that using DCPD as a filler had a negative impact on the dissolution profile of spiranolactone despite not affecting the overall bioavailability of the drug (Clarke. et al. 1977).

Other excipients such as talc and kaolin were found to adsorb charged molecules on their surface and as a result reduce the membrane permeability for drugs such as chlorpromazine (Nakano, 1971) and benzodiazepine (Naggar, 1981). The other majority of tablet fillers are believed to be inert and do not chemically interact or affect the pharmacokinetics of the active ingredient.

Among the new class of fillers for directly compressed tablets, amino acids have shown promising results. Amino acids have been used as diluents in previous studies (AlHusban et al., 2010; AlHusban et al., 2010; Sun and Grant, 2001). However, only few studies investigated the densification characteristics of these amino acids. Szabo-Revesz et al (2001) prepared new agglomerates of aspartic acid through salting out by controlled cooling. The prepared agglomerates were found to have higher tensile strength (0.75±0.03 MPa) and compressibility values when compared to a commercially available salt (0.13±0.1 MPa). Sun and Grant (2001) examined the effect of lysine salt forms on the tensile strength and compaction properties of tablets. It was concluded that the tensile strength increases exponentially with a resultant decrease in the porosity of the tablets.

Another aspect of directly compressed tablet manufacture is the bonding force/interactions between the different ingredients of the tablets including the active entity itself. During powder compaction, particles get closer to each other and densification does not take place until bond formations between particles occur. It is believed that the bonding mechanisms include formation of solid bridges, intermolecular forces and shape related bonding (mechanical interlocking) (Fuhrer, 1996). Intermolecular forces can be further divided into electrostatic, Van der waals forces and hydrogen bonds with electrostatic interactions operating between oppositely charged molecules through dipole-dipole interactions (Fuhrer C., 1996).

As mentioned above it is generally known that most of the pharmaceutical excipients used for oral drug delivery are inert. Therefore, inclusion of excipients which have multiple functions within the formulation will have a significant impact on the cost and quality of the formulations and possibly the bioavailability of the drug.

Our previous studies (ElShaer et al., 2012) investigated the use of aspartic acid and glutamic acid as salt forming agents with a model basic drug trimethoprim (TMP). The results from this study (substantial increase in drug dissolution due to ionisation in the presence of amino acid) provided the basis for investigating for the first time the potential multi functionality (dissolution enhancement and tablet diluent) inherent with in acidic amino acids. Investigations in the current study focus on mechanism of compaction of individual powders and binary mixtures of aspartic acid, TMP, TMP aspartate with an ultimate objective of determining the role of surface charge and morphology on the binding properties between the two entities.

4.2.2. Materials and methods

4.2.2.1. Materials

Trimethoprim (98% TLC), L-aspartic acid and magnesium stearate were purchased from Sigma Aldrich (Dorset, UK). Ethanol was purchased from Fisher Scientific (Loughborough, U.K.)

4.2.2.2. Methods

4.2.2.2. Physical mixtures (PMs) and salt preparations

PMs of TMP with various molar ratios of aspartic acid were prepared by weighing accurate amount of TMP and mixed by KitchenAid (Michigan, USA) at mixing speed of 3 for 5 minutes with the various ratios of aspartic acid. TMP aspartate salt was prepared using the method developed by ElShaer et al (2011). Equimolar amount of TMP and the free amino acid were solubilised in water. The solutions were mixed and stirred until equilibration and then filtered using 125 mm filter papers (Whatman®, Maidstone, UK). The filtrate was transferred into vials and freeze dried for 48h using a Modulyo freeze dryer (West Sussex, UK) at -40^{o}C shelf temperature and under vacuum (E2M5 Edwards pump, West Sussex, UK). The samples were collected and kept at 40^{o}C for 4h using a Gallenkamp vacuum oven. The physical mixtures of TMP aspartate and aspartic acid (SMs) were prepared in a similar manner to PMs.

Powder characterization

4.2.2.2. Powder flowability (Angle of repose method)

Powder flowability of the drug, salt, individual amino acid and physical mixtures of them was evaluated using angle of repose method. 25 gm of powders were poured through a funnel onto a glass plate. The funnel was positioned 10 cm from the glass plate and the powders were allowed to flow freely until the formation of a symmetrical cone. Both the base and height of the cone were measured and recorded. Equation (4.2.1) was used to calculate the angle of repose and the flow properties were interpreted as outlined in Table 4.2.1.

$$\tan(\alpha) = \frac{h}{0.5b}$$ **Equation 4.2.29**

Where h is the cone height and b is the cone base.

Table 4.2.1:- Flow properties of pharmaceutical powders according to the measured angle of repose.

Angle of repose (degree)	Flow property
25- 30	Excellent
31-35	Good
36-40	Fair (aid not needed)
41-45	Passable (may hang up)
46-55	Poor (must agitate, vibrate)
56-65	Very poor
> 66	Very, very poor.

4.2.2.2. Particle size analysis (laser diffractometry)

Powder particle size analysis was performed using a laser diffractometer (SympaTC, RODOS T4.1, Clausthal-Zellerfeld, Germany). An R3 lens with a working range between 0- 178 µm was used for this study. The instrument allows the powder to circulate constantly through the system during the measurements. The volume of distribution was used to calculate the median (50% volume percentile) and the span of distribution was calculated using equation (4.2.2). All the measurements were done in triplicate.

$$\textbf{Span of distribution} = \frac{X_{90} - X_{10}}{X_{50}} \quad \textbf{Equation 4.2.30}$$

4.2.2.2. Apparent, bulk particle density and porosity measurements

Bulk density was determined by using 10 ml cylinder to measure the volume (V) of a pre-weighed sample. Apparent particle density was measured using helium pycnometer (Multipycnometer Quantachrome Instruments, Hampshire, UK). Both bulk and true density values were used to determine the powder porosity according to equation (4.2.3).

$$\varepsilon = 100(1 - \rho_d / \rho_t) \quad \textbf{Equation 4.2.31}$$

Where ε is the porosity and ρ_d is the bulk density and ρ_t is the true density. All the measurements were done in triplicates.

4.2.2.2. Powder wettability (Contact angle)

The Wihelmy method was used to measure the wettability profile of the free powders by measuring the contact angle between the powders and distilled water (Hayes et al., 1994). A small glass slide (24x24 mm) was first covered with double sided tape (Scotch 12*1 mm) and then the free powders were uniformly coated on the tapped slides. The slides were attached to balance loop of the tensiometer microbalance (QCT-100 Interfacial Tensiometer, Camtel Ltd, Herts, UK) and the samples were lowered at a speed of 0.2 mm/s to a distance of 10 mm after contact with the liquid medium. 75 mL of double distilled water at 25 ºC was used as the liquid medium.

The Wilhelmy equation was used to calculate the contact angle at regular intervals and CAMTEL CDCA-100 software (version 2.01.015, Herts, UK) was used to draw a correlation between contact angle and the immersion depth.

4.2.2.2. Scanning electron microscopy (SEM)

Scanning electron microscopy (SEM, STEREOSCAN 90, Cambridge Instrument) was used to study the surface morphology of TMP and TMP aspartate. Samples were prepared by sprinkling the salts onto specimen stubs which were loaded onto a universal specimen holder. In order to enable electricity conduction, samples were coated with a fine layer of gold using a sputter coater (Polaron SC500, Polaron Equipment, Watford, UK) at 20 mA for three minutes at low vacuum and in the presence of argon gas (Polaron Equipment, Watford, UK).

4.2.2.2. Tablet preparation

Tablets of TMP, its aspartate salt and physical mixtures with excess of the amino acid counterions at (1:1), (1:2), (1:4) and (1:8) molar ratios were prepared to study tableting properties. The powders were compacted using uniaxial hydraulic press (Specac tablet presser, Slough, UK) and split die which prevents mechanical failure by allowing triaxial decompression.

Magnesium stearate in ethanol (0.5% w/v) was used to lubricate the die walls and punch surfaces. Powders were compressed at 10, 20, 30, 40 and 60 kN and at dwell time of 30 sec at ambient conditions (room temperature 20 ^{o}C and 70% relative humidity).

The prepared tablets were cylindrical with a diameter of 13 mm and weight of around 500 mg. Tablets were left in desiccators for 24 h prior to performing any mechanical testing.

Tablet characterization

4.2.2.2. Tensile strength measurements

The force required to crush the prepared tablets was measured using tablet hardness apparatus (Schleungier 4M, Thun, Switzerland). The measured force was used to determine the tablet tensile strength using equation (4.2.4).

$$\sigma = \frac{2F_c}{\pi dt} \quad \textbf{Equation 4.2.32}$$

Where σ is the tablet tensile strength, *Fc* is the crushing force required to break the tablet, *d* is the tablet diameter and *t* is the tablet thickness. All measurements were done in triplicate.

4.2.2.2. Disintegration time studies

Disintegration time is the time required for tablets to disintegrate completely without leaving any solid residue. *In vitro* disintegration time was evaluated using US pharmacopoeia monograph (<701> disintegration). Erweka ZT3, Appartebau, GMBH (Husenstamm, Germany) was used in this study as a disintegration apparatus and distilled water (800 ml) as disintegration medium; the disintegration medium temperature was maintained at 37 °C by thermostat. Six tablets were placed in the basket rack assembly and covered by transparent plastic disks. The disintegration time was taken as the time required for tablets to disintegrate completely without leaving any solid residue. All the measurements were carried out six times and presented as mean ± standard deviation.

4.2.2.2. Heckel analysis

The Heckel equation (4.2.5) was used to analyze tablets' compression data using out-of-die method (Heckel R. 1961a; Heckel R. 1961b).

$$\ln(1/(1-D)) = KP + A$$ **Equation 4.2.33**

Where D is the tablet relative density at pressure P, K is a material constant (slope of the straight line portion of Heckel plot) and is 1/3 of the yield strength. 1/K value is used to express the mean yield pressure. A is a function of the initial bulk volume and is calculated from the intercept of the straight line of The Heckel plot.

4.2.2.2. Statistical analysis

Graph Pad Instat® software (Version 3.01, CA, USA) was used for statistical analysis. Data groups were compared using one way analysis of variance (ANOVA) and pair-wise multiple comparisons method (Tukey test) by using the mean values, standard deviation (SD) and number of experiment (N). Standard deviation (SD) was used to report the error in the figures and texts. Probability values of 95% ($P < 0.05$) were used to determine the significant difference.

4.2.3. Results and discussion

4.2.3.1. Powder characterization

Prior to studying the compaction properties of binary mixtures, powder characterisation and densification properties of the individual powders were studied to understand the compaction mechanism of materials and determine the impact of inclusion of each excipient in binary combinations (Table 4.2.2).

4.2.3.1.1. Characterisation of powder flow properties using angle of repose (^{o})

The flow properties of TMP, aspartic acid and TMP aspartate salt were measured using angle of repose. Results (Table 4.2.2) show that aspartic acid has excellent flowability as the measured angle of repose was 26.6±2.3^o while TMP (angle of repose 32.41±0.32^o) had good flow properties. On the other hand, the flow characteristics of the prepared TMP aspartate salt were poor and the powder is considered passable as its angle of repose was 42.7±5.4^o.

The flowability for all PMs, prepared at various ratios of aspartic acid was good and no significant difference (P>0.05) was observed for the measured angle of repose for all the different ratios studied.

Table 4.2.2:- Powder characterisation of TMP, aspartic acid, TMP aspartate salt, their physical and salt mixtures.

Formulations	Angle of repose (^{o})	Bulk density (gm/cm^3)	True density (gm/cm^3)	Porosity
TMP aspartate salt	42.7±5.4	0.10±0.00	2.90±0.69	0.96±0.01
TMP	32.4±0.3	0.65±0.05	1.45±0.03	0.54±0.02
L-aspartic acid	26.6±2.3	0.67±0.04	1.92±0.05	0.64±0.03
PM 1:1	34.2±1.4	0.53±0.02	1.63±0.03	0.67±0.02
PM 1:2	35.2±0.8	0.57±0.01	1.86±0.17	0.69±0.03
PM 1:4	33.7±2.8	0.61±0.02	1.80±0.03	0.66±0.02
PM 1:8	32.1±2.8	0.60±0.02	1.97±0.12	0.69±0.03
SM 1:1	36.3±2.2	0.17±0.01	2.10±0.01	0.91±0.00
SM 1:2	45.6±2.3	0.21±0.02	2.57±0.87	0.91±0.03
SM 1:4	40.2±2.9	0.18±0.00	2.39±0.21	0.92±0.01
SM 1:8	34.02±6.6	0.28±0.01	1.98±0.08	0.85±0.01

4.2.3.1.2. Apparent, bulk particle density and porosity measurements

Interestingly, the true density of both the physical mixtures (PMs) and salt mixtures (SMs) were concentration dependent i.e. increasing the ratio of the oppositely charged aspartic acid resulted in an increase in the true density (Table 4.2.2). The bulk densities for the physical mixtures (PMs) were lower than that of the individual powders possibly due to the reduction of the surface charge upon using binary mixtures of the drug and aspartic acid which carry opposite charges. Such a reduction on the surface charge results in reducing the repulsive forces between similarly charged ions and lowers bulk density which was evident with increase in aspartic acid ratio in the powder blend (Fuhrer, 1996). However, the opposite effect was observed for the SMs and the bulk density increased from 0.1±0.0 for TMP aspartate salt to 0.28±0.01 (Table 4.2.2) upon adding excess of aspartic acid. This could possibly be attributed to the net surface charge of zero within the salt which becomes more negative upon increasing the concentration of aspartic acid resulting in greater repulsive forces and higher bulk density. Porosity measurement for the three powders revealed that preparation of the salt yields powder which has low bulk density and high porosity (Table 4.2.2) which is possibly due to the sublimation of ice during freeze drying which leaves behind porous channels between powder particles (Deville et al., 2007; AlHusban et al., 2010).

4.2.3.1.3. Particle size analysis

Previous research has shown that various factors including salt form, polymorphic transition, crystallinity, crystal and particle size influence inter-particulate bonding in the tablets (Alderborn, 2002). In the current investigation, particle size analysis of the powder samples (Table 4.2.3) and the crystalline structure were studied (Fig. 4.2.1). Particle size analysis was studied using laser diffractometer and has shown that TMP aspartate salt has small particle

size of 28.44±1.14 µm while TMP free base and L-aspartic acid had a mean particle size of 69.9±0.13 and 94.4±0.8 respectively.

Table 4.2.3:- Heckel parameters of TMP, aspartic acid and TMP aspartate salt.

	Yield strength (Y) MPa	Yield pressure (P_Y)	σ_0	d50%(µm)	Span value
TMP	107.52	322.58	273.85	69.9±0.13	1.98±0.02
L-aspartic acid	46.9	140.84	N/A	94.4±0.80	1.26±0.02
TMP aspartate	144.92	434.78	179.74	28.44±1.14	3.44±0.02

4.2.3.1.4. Surface morphology

Morpholgical analysis of powder crystals was carried out using SEM. L-aspartic acid had thin rectangular plates with smooth surface (Fig. 4.2.1B) while TMP crystals were found to be hexagonal in shape with irregular edges, rough surface and more than one crystal attached to each other (Fig. 4.2.1A &D). Interestingly, TMP aspartate salt showed small crystals which formed aggregates (Fig. 4.2.1C). The agglomerates salt form was previously reported and studied extensively by Szabó-Révész et al., (2001).

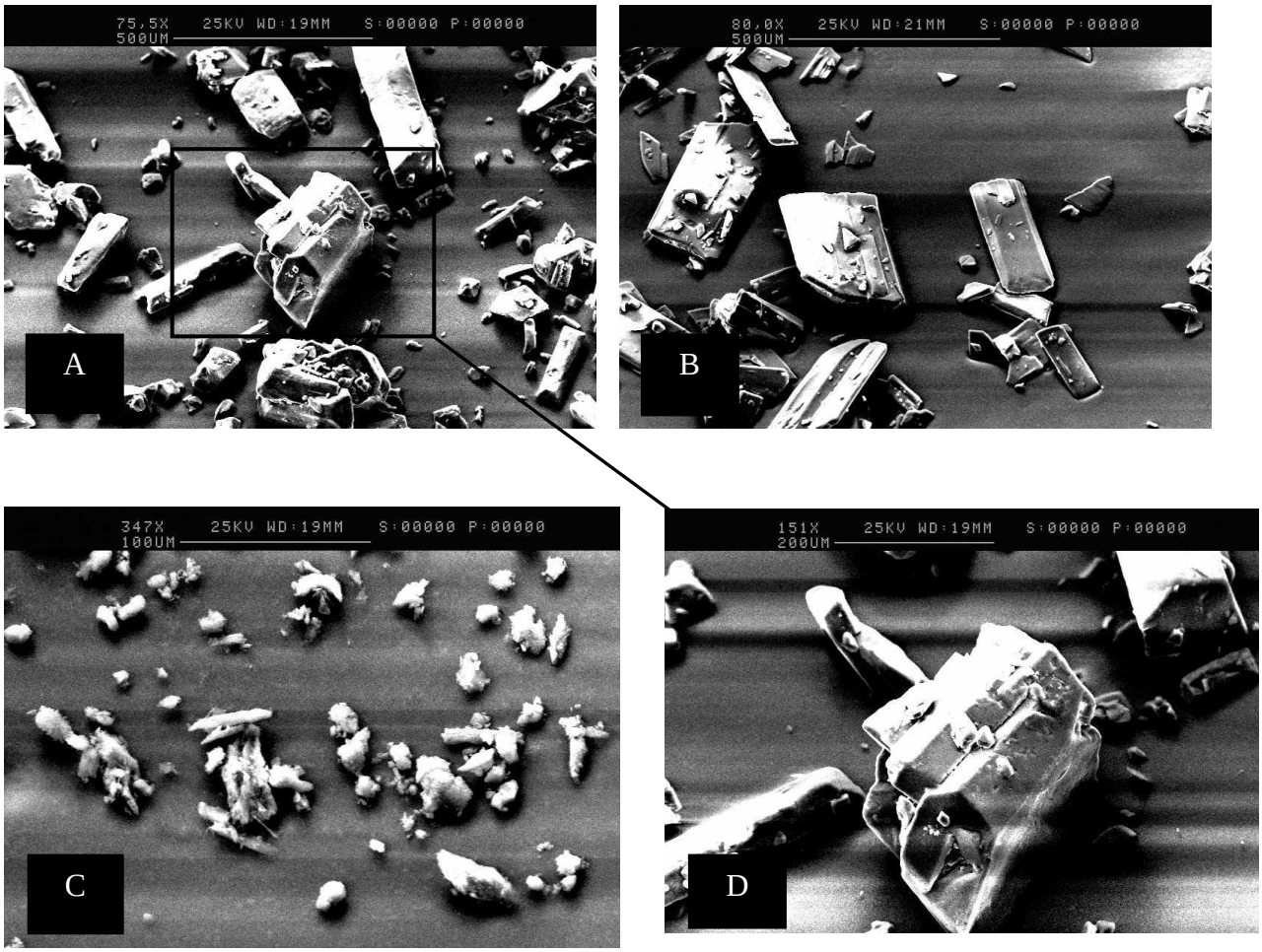

Figure 4.2.49:- SEM for TMP at low magnification 500 µM (A), at high magnification µM200 (D), aspartic acid (B) and TMP aspartate salt (C).

4.2.3.2. Tablets characterization

4.2.3.2.1. Compressibility

Having investigated powder properties, the next stage of evaluation was the preparation of compacts for the three different powders. The strength of the tablets is believed to be affected by the compressibility behaviour of the powders (Sun and Grant, 2001). Highly compressible powder (smaller porosity) enables the particles to get closer to each other which enhance interparticulate bonding resulting in the formation of stronger compacts (Alderborn and Nystrom, 2005).

Upon compressing TMP and aspartic acid, TMP showed the highest compressibility which was found to be less dependant on the compression force and remained unaffected ($p > 0.05$) when the compression force was increased (Fig. 4.2.2). On the other hand, aspartic acid porosity decreased by 32% upon increasing the compression force from 10 kN to 30 kN. Beyond 30 kN, the porosity remained constant ($p > 0.05$). The compressibility behaviour of TMP aspartate salt was similar to that of aspartic acid. Powder plasticity plays an important role during the densification of the powder and in order to understand the mechanism of densification of these powders, Heckel analysis was performed and the yield strength of the three powders was measured (Fig. 4.2.3).

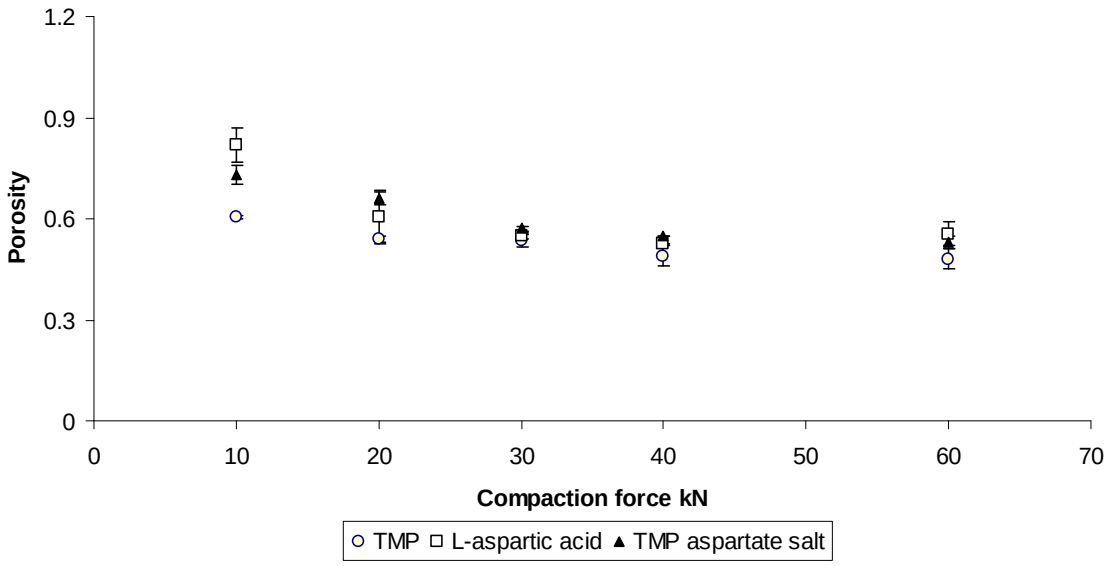

Figure 4.2.50:- Plots of tablet porosity against compaction pressure, showing the compressibility of TMP, aspartic acid and TMP aspartate salt (n= 3).

Heckel graph was established for each powder using out-of-die method and the linear part of the graph with R^2 values of 0.9, 0.96 and 0.96 for TMP, aspartic acid and TMP aspartate salt respectively was used to carry out Heckel analysis (Fig. 4.2.3). The data showed that none of the materials studied are brittle and that they densify via plastic deformation because of their high yield strength values (Table 4.2.3) as suggested by Kuny et al. (2003). In order to differentiate between plastic and elastic behaviour of these materials, the yield strength was

calculated using the Heckel equation (Equation 4.2.3) (Table 4.2.3). L-aspartic acid had the lowest yield strength which reflects high plasticity and low elasticity of the powder. Although, the lowest plasticity properties were exhibited by TMP aspartate salt (Table 4.2.3) the tablets survived the decompression phase and no capping was observed possibly because of the agglomerate form of the salt as discussed in detail below.

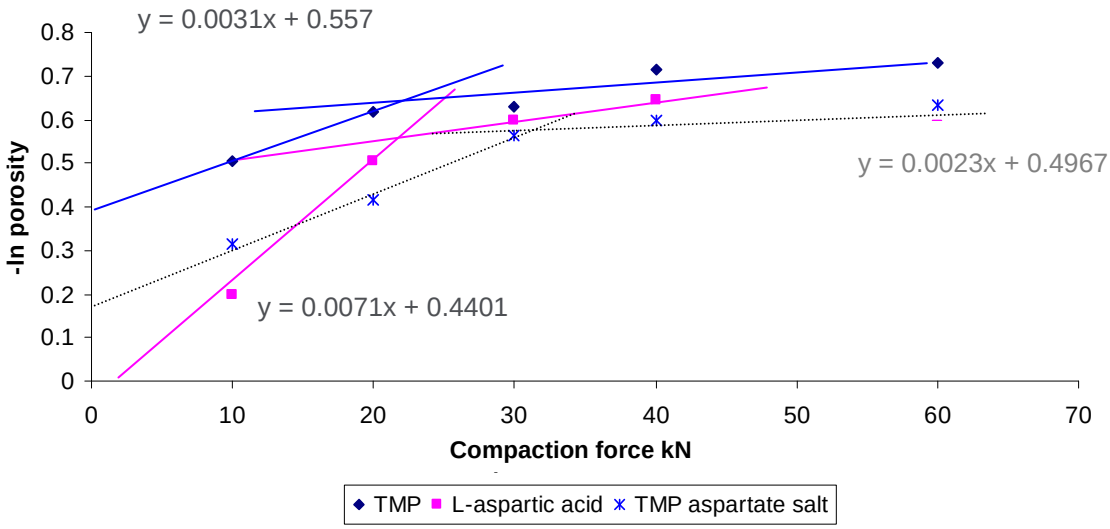

Figure 4.2.51:- Heckel plots for TMP, aspartic acid and TMP aspartate salt using out-of-die method (n=3).

Compressibility behaviour of TMP PMs and TMP aspartate SMs with various molar ratios of L-aspartic acid was also evaluated in this study (Fig. 4.2.4).

At low compression forces (10 kN), PMs with high amount of TMP showed better compressibility characteristics when compared to L-aspartic acid tablets (Fig. 4.2.4A). Yet, at higher compression forces, no significant difference ($p > 0.05$) was observed for the majority of the formulations. Interestingly, the compressibility behaviour of TMP:L-aspartic PM at 1:2 ratio was significantly higher for the all formulations ($p<0.001$). This behaviour might be related to the percloration threshold of the binary mixture (Leuenberger H., 1982). If a binary mixture consisting of two materials A and B (TMP and L-aspartic acid in this study) undergoes

compression, a lattice is formed by particles of type A or type B. At high concentration of substance A, many particles of A become direct neighbours and build a cluster in the lattice. Therefore, substance A dominates the behaviour of the system. Upon increasing the amount of B, substance B starts to replace A in the lattice resulting in phase inversion, when the system dominated by A is replaced by substance B (Leuenberger, 1982) at critical concentration called percolation threshold (1:2 ratio might be the percolation threshold for TMP/ aspartic acid binary mixture).

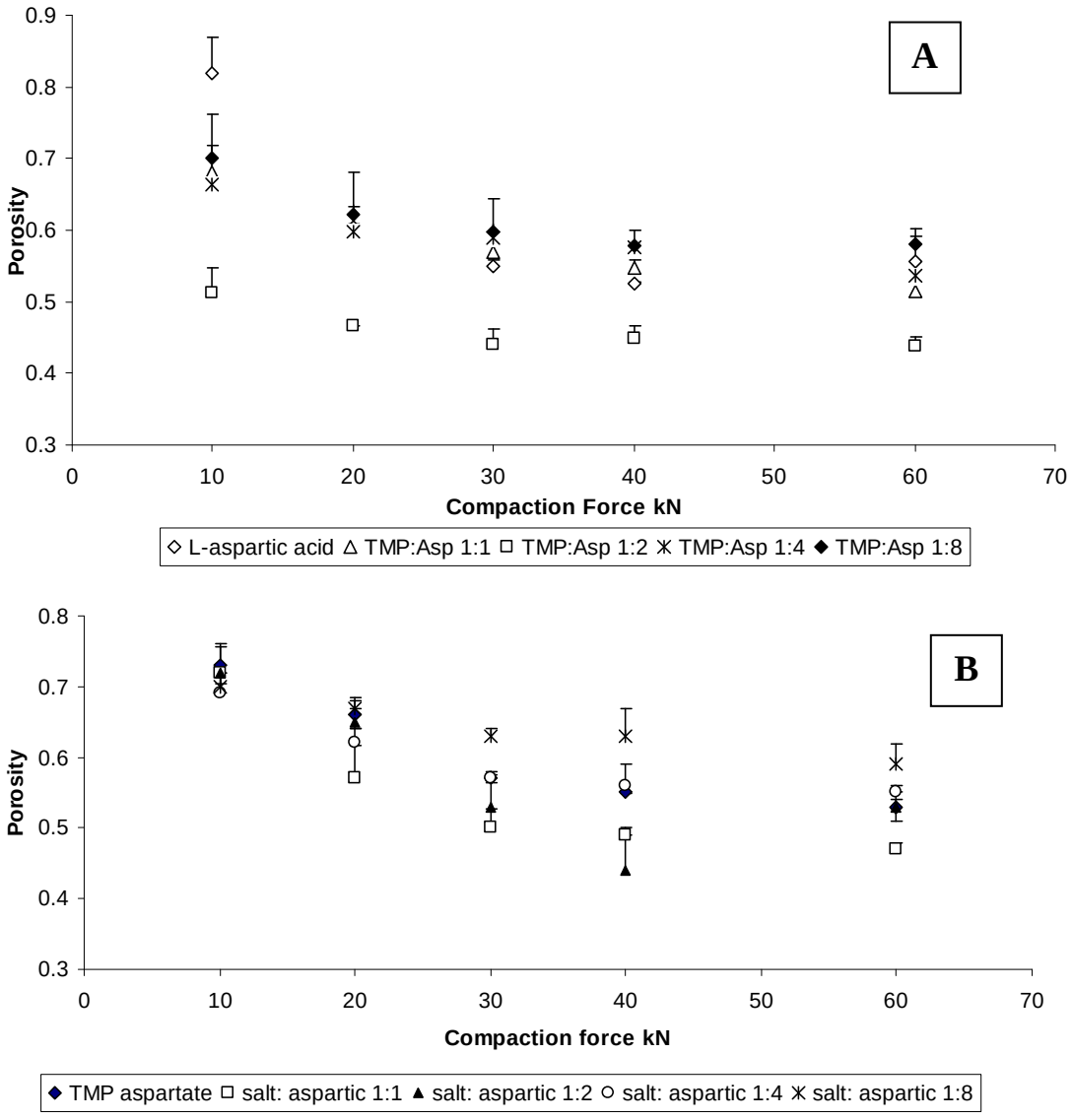

Figure 4.2.52:- Plots of tablet porosity against compaction force, showing (A) the compressibility of TMP and aspartic acid PMs(n= 3), (B) the compressibility of TMP aspartate and aspartic acid SMs (n= 3).

Compressibility profile for the salt/acid binary mixtures was also studied (Fig. 4.2.4B). The data showed that there was no significant difference between majority of the formulations at low compaction forces. Increasing the ratio of aspartic acid deteriorated the compressibility profile of the SMs. The highest compressibility was exhibited by 1:1 and 1:2 ratios of salt: aspartic acid (Fig. 4.2.4B) and was found to be higher than that of the individual components. These results support the findings previously suggested by Wu *et al* (2005) which showed that the behaviour of a binary mixture is not usually linear between the two bulk components used in the system (Wu *et al.,* 2005). The compressibility profile of the PMs and SMs were comparable and no siginificant improvement was observed upon using the salt form instead of the free drug, probably because of the high content of aspartic acid which in turn dominates compressibility characteristics of the binary mixtures.

4.2.3.2.2. Compactability

The ability of the pharmaceutical powder to form a tablet with sufficient strength under the effect of densification is known as compactability (Joiris et al., 1998). Although compression enables particles to come into close contact during the applied force, bond formation between particles is necessary to form strong tablets (Fuhrer, 1996).

The relationship between tablet porosity and tensile strength is shown in Fig. (4.2.5). An exponential relationship between tensile strength and porosity was observed for both TMP and TMP aspartate salt with correlation of 0.96 and 0.95 respectively. This correlation was previously discussed by Ryshkewitch and was used to assess the tensile strength at zero porosity (σ_o) using equation 6 (Ryshkewitch, 1953) and summarized in table 4.2.3.

$$\sigma = \sigma_0 e^{-b\varepsilon}$$ **Equation 4.2.34**

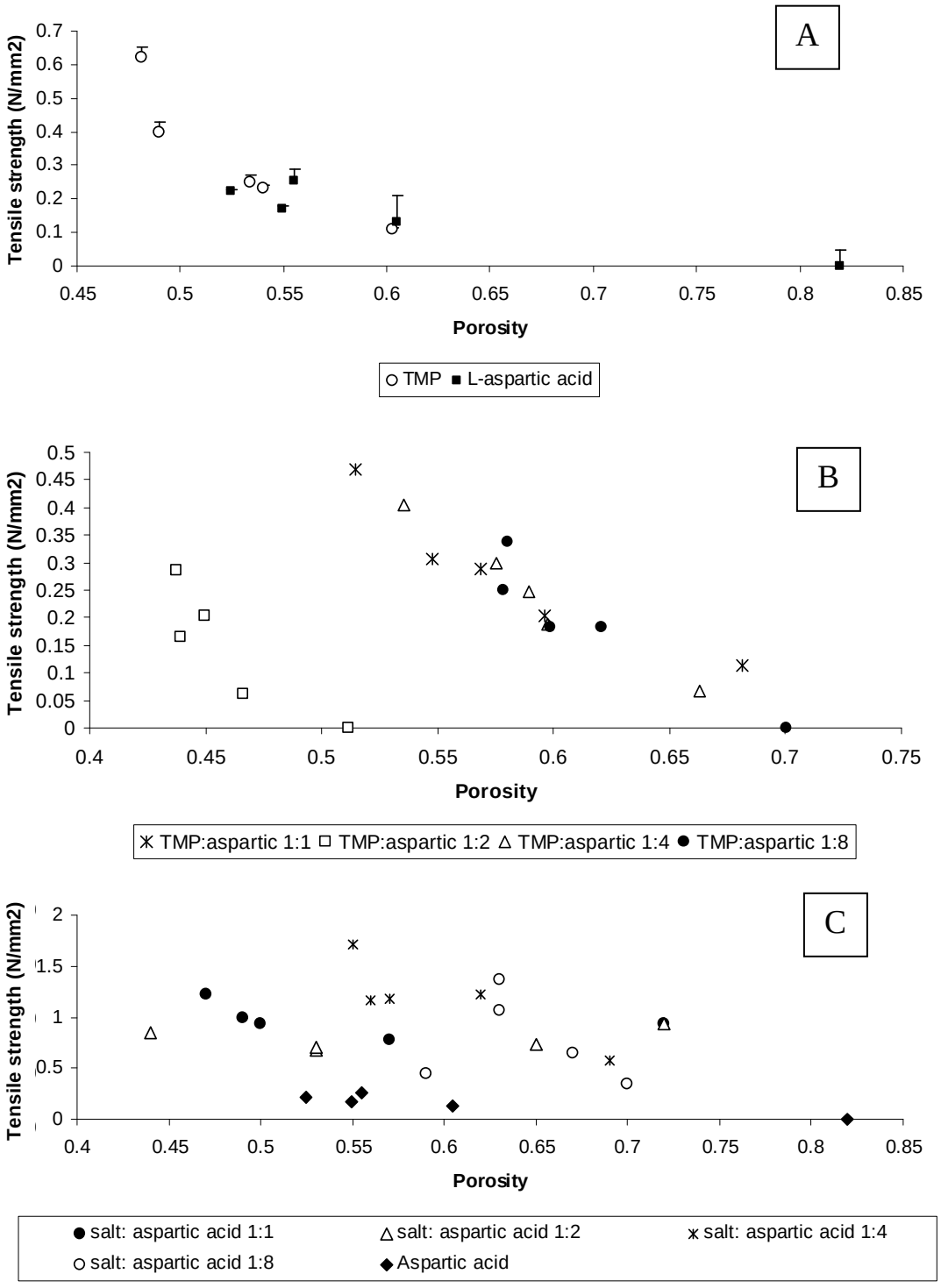

Figure 4.2.53:- Plots of tablet tensile strength against porosity, showing (A) the compactability of TMP, aspartic acid and TMP aspartate salt, (B) TMP and aspartic acid PMs, (C) TMP aspartate salt and aspartic acid SMs (n= 3).

Although the three powders showed similar compressibility beyond 30 kN, compactability results were significantly different. The highest compactability was exhibited by TMP aspartate salt which had tensile strength of 7.24±0.09 with a tablet porosity of 0.53±0.02 (data not shown). However, the highest tensile strength demonstrated by L-aspartic acid and TMP was 0.25±0.094 and 0.62±0.41 at porosity of 0.55±0.03 and 0.48±0.035 respectively (Fig. 4.2.5A). These results suggest that the TMP aspartate salt form has 10 fold higher tensile strength than aspartic acid despite the latter having higher plasticity.

As discussed above, various factors affect inter-particulate bonding within the tablets including salt form, polymorphic transition, crystallinity, crystal habit and particle size (Alderborn G., 2002). Particle size analysis showed that TMP aspartate salt had a mean particle size of 28.44±1.14 μm while SEM showed small crystals of the salt which formed aggregates. The agglomerate salt form was previously studied by (Szabó-Révész et al., 2001) and it was found to have higher tensile strength when compared to commercial salt with no agglomerates. This suggests that both agglomerate formation during salt preparation and the small particle size of these agglomerates play a major role during the densification of the salt form.

However, TMP free base and L-aspartic acid had particle size of 69.9±0.13 and 94.4±0.8 μm respectively. Besides, morphological analysis of the powders crystals showed that L-aspartic acid had thin rectangular plates with smooth surfaces (Fig. 4.2.1B) which would slide over each other and the smooth surface would prevent any mechanical bonding.

On the other hand, the rough surface of the hexagonal crystals of TMP (Fig. 4.2.1A) could have played a role in mechanical interlocking during densification as it could allow enhanced contact and retention between different crystals.

Intermolecular bonding is one of the major forces involved during bond formation in pharmaceutical compacts (Fuhrer, 1996). Therefore, the effect of surface charge on bond formation was evaluated in this study by incorporating anionic amino acid (aspartic acid) with the cationic TMP and neutral salt form.

PMs compactability profile was studied and summarized in Fig. 4.2.5B. Generally, decreasing the porosity increases the tensile strength. It was clear that increasing the ratio of aspartic acid results in decreasing the compactability profile of the PMs as aspartic acid replaces TMP and dominates in the system and therefore results in higher compactability. Interestingly, TMP:L-aspartic 1:2 showed the lowest porosity, yet the tensile strength for this binary mixture was lower when compare with other binary mixtures. Although low porosity should allow higher interparticulate bonding area in the tablets, the tensile strength of 1:2 tablets was not the highest among the binary mixtures used. The highest tensile strength was exhibited by 1:1 tablets. This is probably because of the high content of TMP, which has better compaction characteristics than aspartic acid as discussed before. This suggests that TMP dominates in the system and nullifies the effect of lower bonding area exhibited by 1:2 tablets. It was hypothesised that at 1:1 ratio electrostatic interaction is highest and would result in the formation of stronger compacts. However, upon comparing the compactability of 1:1 PM against TMP alone, the results showed that the free drug has higher compactability. This result suggests that the electrostatic interaction has lower effect during densification of TMP aspartic acid PM. Upon increasing the amount of L-aspartic acid, the tensile strength began to decline and for reasons unknown the compactability characteristics of 1:2 ratio was the lowest.

On the other hand, all the SMs formulations showed higher compactability than that of the free aspartic acid (Fig. 4.2.5C). The highest compactability was shown by 1:4> 1:1 ratios> 1:8 > 1:2. This order was not the same as that of TMP/aspartic acid physical mixtures profiles, possibly because the compactability characteristics of a binary mixture are not often predictable from individual material characteristics (Vromans and Lerk., 1988; Veen et al., 2000).

Interestingly, all of the SM formulations exhibited higher compactability than the PMs, although the former is a mixture between neutral and anionic moieties and no electrostatic

interaction is expected to take place. This confirms the early finding that the surface charge has minimal effect during bond formation of both PMs and SMs.

4.2.3.2.3. Tabletability

The ability of the powder to form a tablet with sufficient mechanical properties under the effect of compaction pressure is known as tabletability (Joiris et al., 1998). Generally, the tabletability characteristics of all the three powders improved with an increase in compaction pressure possibly due to the reduction in tablet porosity upon increasing the compaction pressure (reduction in tablet porosity increases contact area between the particles and therefore results in higher bonding and harder tablets) (Nystrom and. Karehill., 1995). L-aspartic acid had poor tabletability among the three powders. The highest tensile strength of L-aspartic acid was 0.25±0.094 at 60 kN. The tensile strength of TMP tablets was almost twice (0.62±0.41) that of L-aspartic acid. Interestingly, TMP aspartate salt showed a very high tensile strength (2.48±0.38) even at very low compaction pressures. The tensile strength of the salt increased to 3.9±0.68 when the compression force was doubled to 20 kN. At 30 kN the tensile strength rose to 7.78±0.37 and remained constant beyond 30 kN.

Despite the similar compressibility profile of TMP and TMP aspartate salt (as they showed constant compressibility beyond 30 kN), the tabletability profile was significantly different ($p<0.001$). The tensile strength of TMP tablets increased even when the porosity was constant ($p>0.05$) beyond the compression force of 30 kN (Fig. 4.2.6A) which suggests that crystal interlocking takes place during tablet densification as mechanical interlocking is not dependent on the distance between the particles (Nystrom and Karehill, 1995). However, the tensile strength of TMP aspartate tablets did not change when the tablet porosity remained constant which suggests that alternative bonding mechanism is involved during the densification of TMP aspartate powders. Increasing the compaction force beyond 30 kN did not result in further decrease in tablet porosity (as discussed above) hence, particle surfaces cannot get into closer

proximity any more and the tensile strength remained constant. Intermolecular bonding which is also known as distance attraction forces is affected mainly by the surface area available for bonding suggesting that intermolecular bonding could be the main bonding mechanism for the salt forms. Hydrogen bonds play a vital role in intermolecular bonding and structure analysis of TMP aspartate salt shows that the salt form has a total of nine hydrogen bond donors and acceptors atoms which further confirm the assumption that intermolecular bonding is the major binding force (Nystrom and Karehill, 1995).

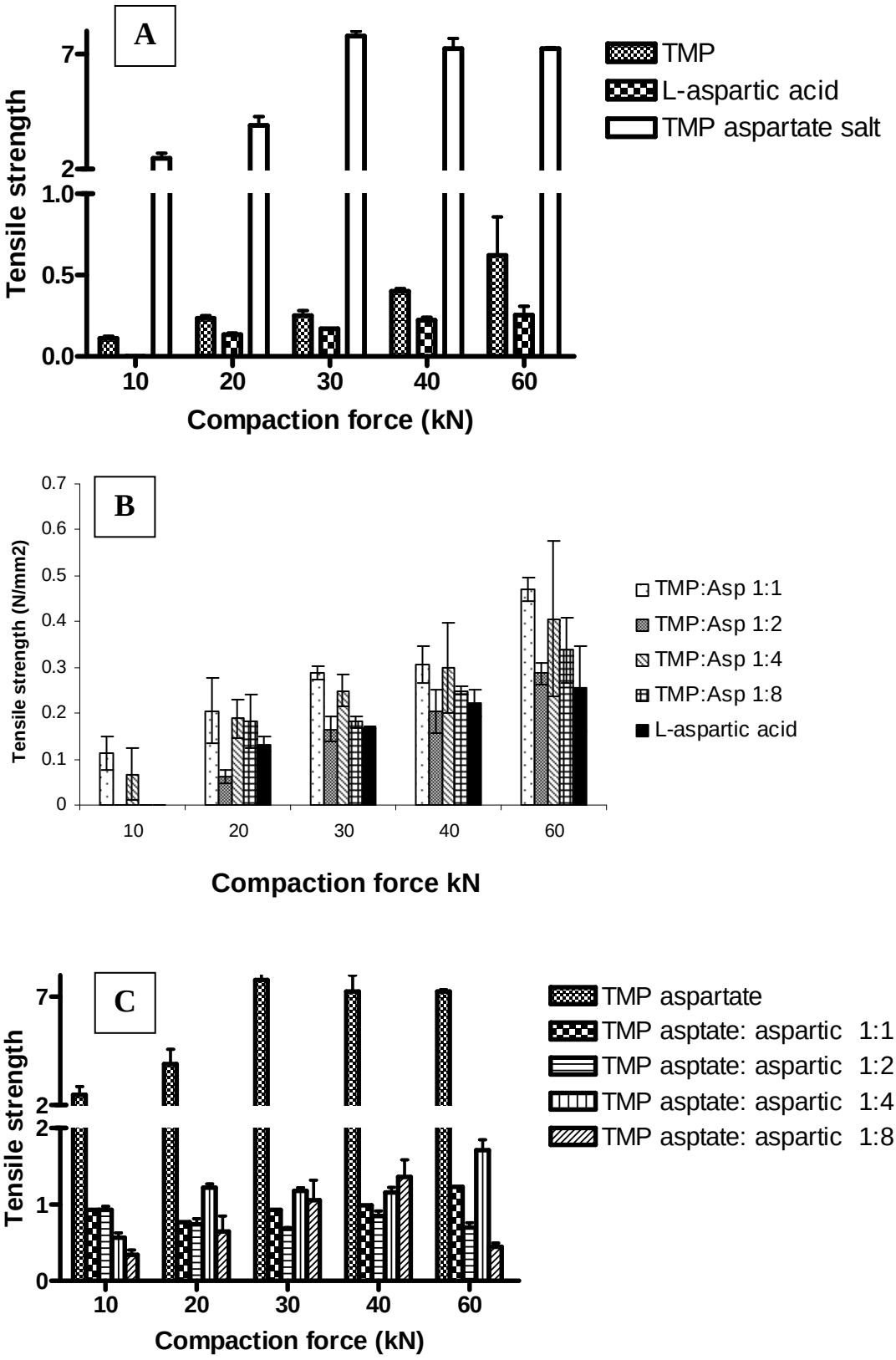

Figure 4.2.54:- Plots of tablet tensile strength against compaction force, showing the tabletability of (A) TMP, aspartic acid and TMP aspartate salt, (B) TMP and aspartic acid PMs, (C)TMP aspartate salt and aspartic acid SMs (n= 3).

The tabletability plots for PMs are shown in (Fig. 4.2.6B). The crushing force was very low for some of the mixtures compressed at 10 kN. Upon plotting the tensile strength against the compaction force, a linear relationship was observed for all the PMs over the range of compression forces used. The tensile strength of the PMs was between that of the individuals components. As tabletability is determined by both bonding area (compressibility) and bonding strength (compactability) and as the bonding area is comparable for most of the PM formulations at each compression force (Fig. 4.2.4A), compactability was the main determinant for the tabletability characteristics of the binary mixtures. Again the highest tabletability was observed for 1:1 ratio mixture followed by 1:4> L-aspartic acid ≈ 1:2 (Fig. 4.2.6B).

Upon studying the tabletability profile of salt/aspartic acid binary mixture (Fig. 4.2.6C) it was found that all the SMs were significantly lower than that of the individual salt but higher than the individual aspartic acid and physical mixtures at all the compression forces. 1:4 salt mixture showed the highest tabletability followed by 1:1.

4.2.3.2.4. Disintegration time

After ingestion of a solid dosage form, the delivery system starts to disintegrate into small particles prior to dissolution in the gastrointestinal tract. Previous studies have suggested that tablet disintegration time increases as the compression forces rises (Riippi et al., 1998). The effect of compression force on the disintegration time of the prepared tablets was evaluated (Fig. 7A, B & C). Both TMP and L-aspartic acid showed an increase in the disintegration time upon increasing the compaction force (Fig. 4.2.7A). Moreover, TMP tablets failed to disintegrate with in 30 minutes at compression forces as low as 20 kN. Nevertheless, L-aspartic acid showed a linear relationship between the disintegration time and the applied compaction force. L-aspartic acid disintegrated very rapidly (6.6±3.7 s) when low compression forces were used (Fig. 4.2.7A).

TMP aspartate salt showed an interesting disintegration profile. The tablets disintegrated at 304±13 s when compressed at 10 kN. The disintegration time increased upon increase of compression force. However, beyond 30 kN the tablets' disintegration time started to decrease to 128±34 s at 60 kN.

Tablet disintegration takes place by various mechanisms such as swelling, porosity and capillary action. Prior to disintegration, the tablet surface should be wetted by the disintegration media (Fukami et al., 2006) which results in tablet disintegration via one of the above mechanisms.

In order to understand the mechanism of disintegration of the prepared tablets, wettability studies of the dry powder were performed using the protocol described in the methods section. Interestingly, all the three powders showed good wettability profile with zero contact angle. Contact angle depends on the hydrophilicity/hydrophobicity of the surface. The low contact angles exhibited by the three powders could be attributed to the high hydrophilicity for all powders.

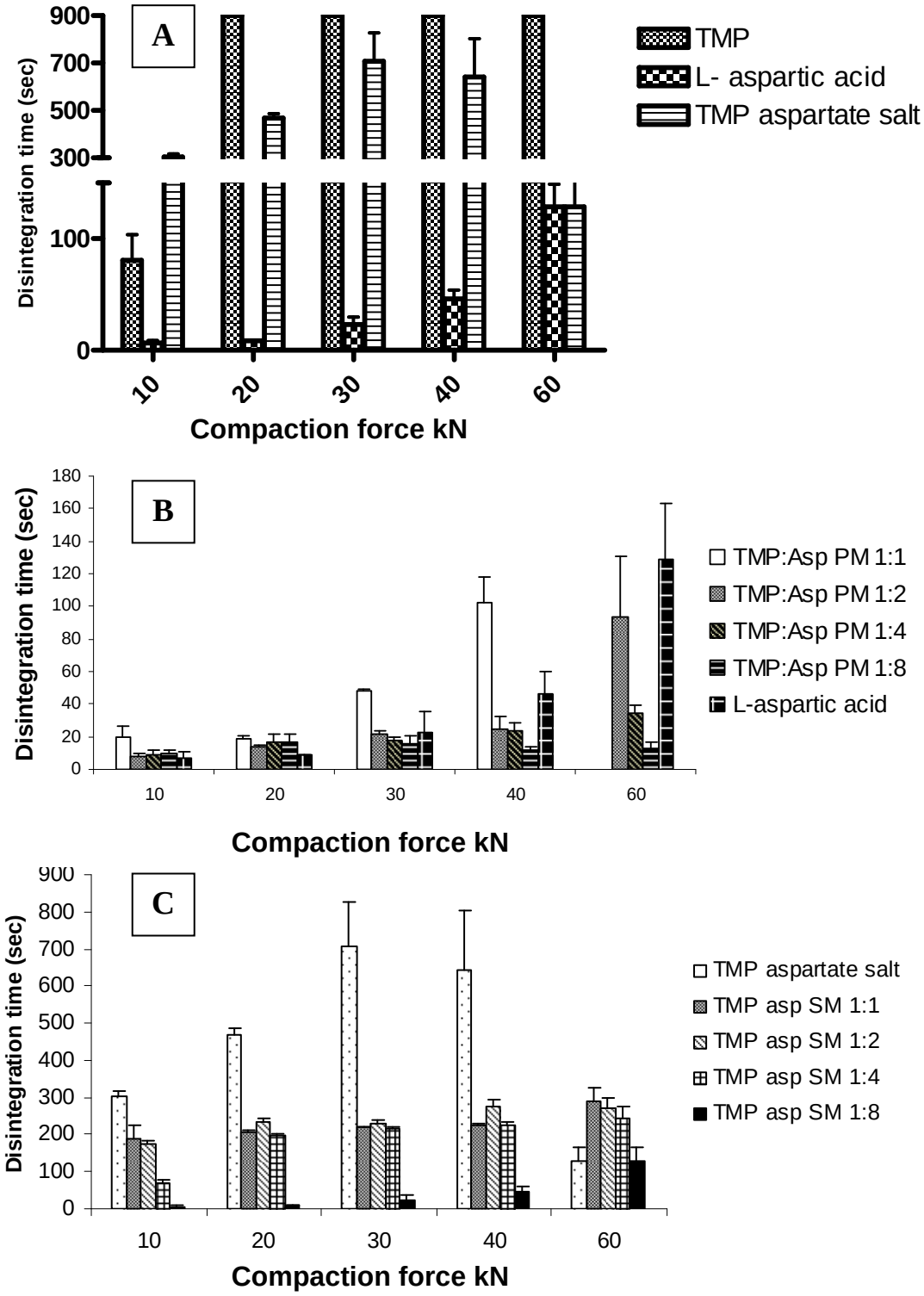

Figure 4.2.55:- Disintegration time of (A) TMP, aspartic acid and TMP aspartate salt, (B) TMP and aspartic PMs, (C) TMP aspartate salt and aspartic acid SMs at various compression forces (n=3).

For all the powders, increasing the compaction force resulted in increasing the disintegration time possibly because of the decrease in tablet porosity at higher compaction forces. 1:1 PM showed the highest disintegration time at all the compression forces (Fig. 4.2.7B). At low compression forces of 10 kN, 1:1 tablets disintegrated at 20±7 s and the disintegration time increased steadily until 287±40 s at 60 kN. Interestingly, increasing the amount of L-aspartic acid in the PMs formulations was found to decrease the disintegration time of the tablets significantly and the disintegration time was even lower than that of L-aspartic acid alone.

For instance, at 40 kN, 1:1 tablets disintegrated at 102±15.6 s and the disintegration time dropped significantly to around 25 s upon increasing the L-aspartic acid amount in 1:2 and 1:4 mixtures and to 12 s for 1:8 ratio. It is known that the porous structure of the tablets has a large effect on the disintegration time. Nevertheless, the porosity for all the tablets was comparable and it could not explain the rapid disintegration for the physical mixtures at 1:2, 1:4 and 1:8. It could be hypothesised that the use of water as disintegration media would have enhanced the ionisation of TMP and aspartic acid and facilitated tablet disintegration in line with the results reported by Ferrari et al., (1996).

Disintegration time profiles for the SMs were similar to that of the PMs. Disintegration time was found to decrease as the aspartic acid ratio increases. Nevertheless, the PMs disintegration times were faster than that of the salt mixtures.

4.2.4. Conclusion

The current study evaluated the compaction properties of aspartic acid, TMP and TMP aspartate salt. Both particle size analysis and surface morphology studies revealed that TMP has rough hexagonal crystals that interlock mechanically during densification, while the thin rectangular plates of aspartic acid slide over each other instead of mechanical intercalation. The very high tensile strength exhibited by TMP aspartate salt was attributed to its small particle size and formation of agglomerates during salt preparation. Although Heckel analysis

revealed that aspartic acid has high plasticity, inclusion of the acid as a tablet filler did not enhance the compaction properties of TMP and TMP aspartate salt possibly due to the large particle size of its crystals. It can be concluded that aspartic acid demonstrate multifunctionality as a filler (with no binder property), disintegration promoting agent thereby ultimately enhancing bioavailability and pharmacokinetics of BCS IV drug candidates.

TMP permeability studies and transcriptomic changes occurring during its uptake across Caco-2 cells

4.3.1. Introduction

One of the major obstacles in oral drug delivery is the poor permeability of drugs across the intestinal membrane. The majority of drugs are absorbed via passive diffusion through paracellular and transcellular routes. Nevertheless, the physico-chemical properties of the drug molecules limit their uptake via passive diffusion (Martinez et al., 2002). Active drug uptake mediated by carrier transporters enables some molecules to circumvent the issues associated with poor intestinal absorption (Lipka et al., 1996; Walter et al., 1996; Amidon et al., 1998). The complicated process of permeation across the intestinal membrane results in large numbers of new drugs which fail to exhibit therapeutic effectiveness *in-vivo;* even though they may have exhibited *in vitro* potency , as they cannot cross the cell membrane in the gastrointestinal tract due to their intrinsic molecular properties. Many approaches have been developed including prodrug formation and ion-pairing to improve the inherent physico-chemical properties of the drug candidates to enhance permeability.

The prodrug approach is based on formation of a covalent bond between the drug molecule and a lipophilic moiety in order to improve passive diffusion of the drug (Ettmayer et al., 2004). Although this approach has achieved success in improving drug uptake, covalently linking the drug with another moiety could potentially result in a new chemical entity with low or poor efficacy and/or increased toxicity.

Schankier 1960, discussed a similar approach to prodrugs which exploits electrostatic interactions between two moieties instead of covalent bond formation; this is referred to as ion-pairing. After being absorbed, the ion-pairs dissociate in the blood stream via dilution. This approach has many advantages over prodrug synthesis as it does not need activation by enzymes and does not rely on disrupting the integrity of the membrane to facilitate drug

uptake. The majority of the investigations carried out on ion-pairing focused on improving drug uptake via passive diffusion (Miller et al., 2010). In the current study we investigate whether ion-pairing of TMP with actively transported counter ions (aspartic and glutamic acids) would improve the overall absorption of the drug candidate via active transporter carriers.

Trimethoprim is a synthetic antibacterial agent belonging to a group of compounds known as diaminopyrimidines. It was first synthesized as a dihydrofolate reductase inhibitor (DHFR) and used mainly in combination with sulfonamides to treat pneumonia and urinary tract infections. TMP has cationic nature with a pka of 7.3. This basic drug is very slightly soluble in water (0.2 mg/mL) and has poor intestinal absorption and hence classified as BCS IV according to the Biopharmaceutical Classification System (ElShaer et al., 2012).

In order to improve TMP solubility, Li et al. (2005) utilized β-cyclodextrin as a complex forming agent. The increased surface area of contact between TMP and the cyclodextrin along with the reduction in drug crystalinity were shown to be responsible for improvement of TMP solubility. Previous work carried out by ElShaer et al., 2012 showed that coupling TMP with glutamic acid and aspartic acid improved the drug solubility by 280 fold. Despite a Log P value of 1.4, TMP has low oral permeability (Kasim et al., 2003). The low absorption profile is attributed to high efflux through P-gp (Victoria E., 2009). A study by Joseph et al., (2001) suggested that basal to apical flux for TMP was 3.61 times higher than its apical to basal absorption. Moreover, the study demonstrated that TMP activates ATPase which provides the energy required for P-gp activity. Conversely, the studies carried out by Romiti et al., (2002) on human kidney-2 (HK-2) cells suggested that TMP does not interfere with P-gp activity nor modulate human multidrug resistance gene (MDR-1). Wendy et al (2002) and Jung et al (2008) studies reported that TMP is a substrate for human organic cation transporters (hOCT) suggesting that TMP could be transported actively via OCT1 and OCT2 transporters. The degree of TMP ionisation was also found to determine its capacity to interact with hOCT2. Jung et al., 2008 studies demonstrated that decreasing TMP ionisation by increasing the pH of the transport media from 7 to 8

resulted in lowering the binding with hOCT transporter. Nevertheless, the kinetic calculations based on the proportion of molecules charged at each pH value showed higher inhibitor effect than predicted. These results were attributed to the difference between the pH values of the membrane and that of the bulk of the media or the difference of TMP pKa values at the transport receptor region and that in the free solution (Jung et al., 2008). OCT1 and OCT2 are expressed predominantly in liver, kidney (Jung et al., 2008) ileum, duodenum and colon (Englund et al., 2006). Moreover, OCT1 transporters were also found to be expressed in Caco-2 monolayers, 3 times higher than in ileum and duodenum (Englund et al., 2006). The major focus of this study is to ion-pair the poorly absorbed TMP to a highly permeable counter ion which has a full transporter system across the intestinal membrane. Interestingly, most of the living cells express a combination of common and specific transporter systems for amino acids as they play a vital role in cellular activities of the living cells. Because the cationic nature of the drug used in this study (TMP), anionic amino acids (aspartic acid and glutamic acid) were selected as potential counter ions. Cellular uptake of anionic amino acids is mediated by solute carrier transporters known as high affinity glutamate transporters (SLC1 or X^-_{AG}). SLC1 was first identified in 1992 by (Kanai and Hediger) and were further characterised into five sub-families: SLC1A1, SLC1A2, SLC1A3, SLC1A6, and SLC1A7. X^-_{AG} is Na^+ and K^+ dependent transporters which mediates the uptake of glutamic acid and aspartic acid accompanied by co-transport of $3Na^+$, $1H^+$ and counter-transport of $1K^+$. X^-_c is another carrier transporter which is Na^+ independent antiport system that transports glutamate and cystine in order to protect the cells against oxidation (Robert et al., 1998). X^-_{AG} and X^-_c were reported to be fully expressed in Caco-2 monolayers and mediate the transport of glutamic acid, aspartic acid (Mordelle et al., 2000) and cysteine (Andy et al., 2006) during the differentiation of caco-2 cells.

The aim of the current work is to investigate whether anionic amino acids (glutamic acid and aspartic acid) would ion-pair strongly with the cationic model drug, TMP and if the new ion -

pairs would have better uptake across the Caco-2 monolayers. Both aspartic and glutamic acids are similar in their structure apart from an extra alkyl group in the glutamic acid side chain.

4.3.2. Materials and methods

4.3.2.1. Materials

Trimethoprim, L-Glutamic acid (Reagent plus ≥ 99%), L-aspartic acid (≥ 98%) and ninhydrin reagent (2% solution) were purchased from Sigma Aldrich, UK.

Sodium hydroxide and sodium chloride were purchased from Fisher Scientific UK.

Dulbecco's modified Eagle's medium (DMEM), fetal bovine serum (FBS), Nonessential amino acids (NEAA), 1% pencillin-streptomycin, 2mM glutamine and Hank's balanced salt solution (HBSS) were purchased from Bio Sera, UK. 1% Trypsin–EDTA was obtained from Gibco Lab. UK.

RNeasy kit (RNA free water, buffer RLT, buffer RW1 and buffer RPE) was purchased from Qiagen (Hiden, Germany). Gene expression hybridization kit, low input Quick Amp labelling kit, RNA spike-in kit (one color) all were purchased from Agilent (Cedar Creek, Texas, USA). Agilent gene expression washing buffer 1 and 2 were ordered from Agilent (Wilmington, DE, USA) and Ethanol which was purchased from Fisher scientific (Leicestershire, UK).

4.3.2.2. Methods

4.3.2.2.1. Preparation of pre-saturated solution of 1-octanol and de-ionised water.

1000 ml of de-ionised water was added to 4 mL of 1-octanol. The mixture was shaken for few minutes and left overnight. The de-ionised water was separated from 1-octanol using 1000 mL separation funnel.

4.3.2.2.2. Octanol- water partitioning experiment

500 µg of TMP was added to 100 mL octanol-saturated deionised water with molar excess of aspartic acid/glutamic acid (in ratios 1:1, 1:2, 1:4 and 1:8). 5 mL of the aqueous phase was allowed to equilibrate with 5mL of octanol at room temperature and stirred for 24 hours using magnetic stirrer. The two phases were then separated by centrifugation and TMP

concentration $[TMP_t]_{Aq}$ in the aqueous phase was measured using HPLC. Mass balance was used to calculated TMP concentration in octanol phase $[TMP_t]_{Oct}$ using equation (4.3.1).

$[TMP_t]_{Oct}$ = total drug put into the system- $[TMP_t]_{Aq}$ Equation 4.3.35

The apparent distribution coefficient D_B could be calculated using equation (4.3.2)

$D_B = [TMP_t]_{Oct}/[TMP_t]_{Aq}$ Equation 4.3.36

4.3.2.2.3. HPLC method to study the concentration of trimethoprim

The amount of Trimethoprim (TMP) dissolved in the solution samples was quantified using the HPLC (Dionex 1100 system) method reported by Gallego and Arroyo (2002). HPLC was operated at 25^{o}C on RP-C18, (Phenomenex 110A, 150x4.6 mm, 5µm) column using acetonitrile-NaH_2PO_4 buffer (10 mM) (70:30, v/v) (pH 3) as mobile phase which was pumped at 1.0 mL/min flow rate using gradient pump (GP50). UV detector (UVD 170U) was used and the analysis was monitored at 230 nm. The retention time was 1.74±0.037 min and a rectilinear calibration curve was established at concentrations ranging between 10- 500µg/mL (R^2 of 0.99). LOD and LOQ were calculated using standard deviation of response and slope and were found to be 0.109 and 0.364 respectively.

4.3.2.2.4. Ninhydrin analysis

The concentrations of aspartic acid and glutamic acid in octanol/water partitioning studies were quantified using the ninhydrin method. In order to construct a calibration curve, serial dilutions of the amino acids were prepared and 1 mL of the prepared samples was mixed with 0.5 mL of ninhydrin reagent and vortexed for 20 seconds. The samples were heated in a pre-warmed water bath at 80 ^{o}C for 20 minutes. The samples were removed from the water bath and left to cool. The intensity of the coloured Ruhemann purple was analysed using a UV spectrophotometry at a wavelength of 560 nm.

Calibration curves were constructed with regression coefficients of 0.994 and 0.999 for aspartic and glutamic acid respectively. After constructing the calibration curves, the concentration of the amino acids in the aqueous layer were determined using the linear curve equations (4.3.3) and (4.3.4) for aspartic acid and glutamic acid respectively.

Y=0.0695x **Equation 4.3.37**

Y=0.0895x **Equation 4.3.38**

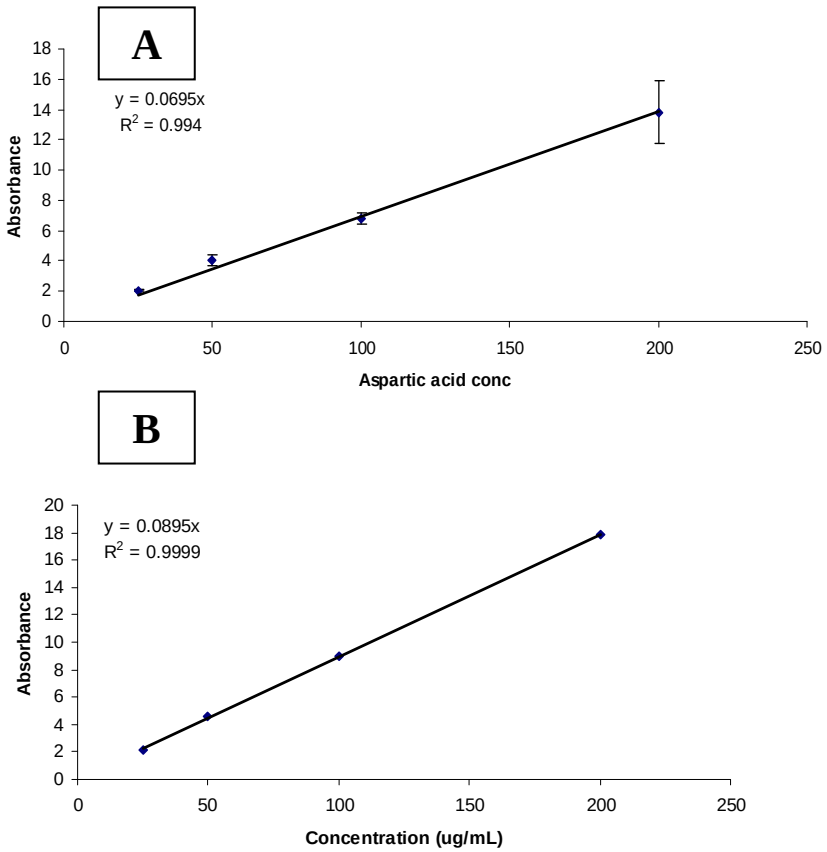

Figure 4.3.56:- Ninhydrin calibration curve for aspartic acid (A), glutamic acid (B) n=3.

4.3.2.2.5. Procedure for Caco-2 cell culture

Caco-2 cells at passage 48 were gifted from Huddersfield University and used at passages 50-80. Cells were allowed to grow in 75cm² T-flasks and maintained using Dublecco's modified Eagle's medium (DMEM) with 10% fetal bovine serum (FBS), 0.5% pencillin-streptomycin, 2mM glutamine and 1% nonessential amino acids (NEAA). Culture medium was changed every 2 to 3

days and cells were grown at a temperature of 37°C and 5% CO_2. The cells were passaged using 5 mL trypsin-EDTA when they reached 90% confluence. A transepithelial transport assay was carried out using Khan et al., (2011) methods. 2 x 10^5cells/cm² were seeded on polycarbonated-coated membranes (6-well transwell plates, 24mm, 4.7cm²) and were allowed to grow for 21 days and the media in both apical and basal compartments was changed every 2-3 days. The transepithelial electrical resistance (TEER) was measured at the start and end of every study.

4.3.2.2.6. Trimethoprim permeability studies

Caco-2 monolayers were used 19-21 days after seeding. The apical to basolateral permeability of TMP and its formulations was assessed. The transwells were rinsed and incubated for 15 minutes with drug-free transport medium (Hanks balanced salt solution; HBSS). Following incubation, HBSS was removed and 1.5 mL of the medium containing TMP alone (500 µg/mL) and TMP with various molar ratios of the anionic amino acids (1:1, 1:2, 1:4 and 1:8) were introduced to the apical side. Sample aliquots (300µL) were taken from the basolateral side at given time intervals (0, 5, 10, 15, 20, 30, 60 and 90 minutes). After each sampling, an equal volume of fresh transport buffer (pre-warmed at 37°C) was added to the receiver compartment (basal side) and kept the cells at a temperature of 37°C and 5% CO_2 during experiment. Samples were subsequently analyzed by HPLC. In order to confirm the mass balance, samples were taken from both apical and basolateral compartments at the last time point (90 mins). All experiments were performed at 37°C (n = 5). Apparent permeability coefficient P_{app} (cm/s) was calculated using (equation 4.3.5)

$$P_{app} = dQ / dt \times 1 / AC_0 \quad \textbf{Equation 4.3.39}$$

Where *dQ/dt* is the rate of appearance of the drugs on the basolateral side (nmol s^{-1}), C_o is the initial concentration on the apical side and *A* is the surface area of the monolayer (4.7 cm^2).

The data presented were validated using HPLC measurement of drug transfer during the process of permeability. This included repetition of drug permeability studies in the preparations used for microarray analysis.

4.3.2.2.8. Recovery

The amounts of TMP recovered from both apical and basolateral compartments at the end of the experiment were calculated using equation (4.3.6).

$$\text{Recovery}(\%) = \frac{C_{R90\,\text{min}} \times V_R + C_{D90\,\text{min}} \times V_D}{C_{D0\,\text{min}} \times V_D} \times 100 \qquad \textbf{Equation 4.3.40}$$

Low recovery data is attributed to entrapment of the compounds into the cell monolayers or adsorption to the device surface which in turn results in error calculating the transport rate (Aungst et al., 2000)

4.3.2.2.9. RNA extraction for microarray studies

Samples for microarrays studies was collected at 5, 30, 60 minutes for TMP, TMP:glutamic acid at 1:1 (PM 1:1) and 1:8 (PM 1:8) molar ratios. Caco-2 monolayers were treated with ethanol: phenol mixture (95:5) for 24 hours. Cell pellets were obtained by centrifugation of the scrubbed cells at 2000 rpm and 4 ^{o}C for 10 minutes. All pellets were stored at -80 ^{o}C until the RNA extraction step.

Total RNA was extracted by using RNeasy kit (Qiagen) and quantified using the Nanodrop 1000 spectrophotometer (Themoscientific, Wilmington, DE) and data are summarised in Table (4.3.1).

Table 4.3.35:- Quantification of total RNA using nanodrop spectrophotometer.

Sample	Conc (ng/µl)	Total RNA 260/280 ratio	260/230 ratio
Control 5	983.1	2.02	1.57
Control 60	842.5	2.01	1.94
TMP, 5 min	631.3	2.04	2.05
TMP: Glu 1:1, 5 min	952.1	1.99	1.92
TMP :Glu 1:8 , 5 min	851.8	1.96	1.63
TMP, 30 min	507.7	1.99	1.69
TMP : Glu 1:1, 30 min	362.2	1.98	1.68
TMP :Glu 1:8, 30 min	318	2.03	1.97
TMP 60 min	889.8	2	1.78
TMP: Glu 1:1, 60 min	614.3	1.99	1.29
TMP : Glu 1:8, 60 min	1286.3	1.99	1.82

4.3.2.2.10. Microarray study

In order to investigate the systemic changes of the gene expression upon exposing Caco-2 cells to TMP and its various formulations, approximately 45,000 cDNA were hybridized with the microarray probe using Agilant one-color-spike procedure. Briefly, 1.5µl of 25 ng of total RNA was mixed with 2 µl of diluted one-color-spike mix. cDNA master mix (Agilent Technologies, Santa Clara, CA) was used to prepare cDNA for all the samples which were labelled using cy3-dUTP. The yield and specific activity (Table 4.3.2) for fluroscent cDNA probes were determined by using equations 4.3.7 and 4.3.8 respectively, after quantifying cDNA (ng/µl) and cyanine 3 (pmol/ µl) using the Nanodrop 1000 spectrophotometer (Themoscientific, Wilmington, DE). All samples were hybridized to Agilent 4x44 K whole genome array for 16 hours at 65 ^{o}C in hybridization oven (Sheldon manufacturer, Corneilus, OR). After hybridization, samples were scanned at 50n resolution and at 20 bit scan using an Agilent scanner (Agilent Technologies, Santa Clara, CA). 16-bit TIFF images were obtained and used as input for the feature extraction software (V10.7, Santa Clara, CA).

$$\textbf{Yield} = \frac{Conc.of.cRNA \times elution.volume}{1000} \qquad \textbf{Equation 4.3.41}$$

$$\textbf{Specific activity} = \frac{Conc.of.Cy3}{Conc.of.cRNA} \times 1000 \qquad \textbf{Equation 4.3.42}$$

Table 4.3.36:- Yield and specific activity of the complementary DNA used for hybridization in TMP studies.

Sample	Conc (ng/µl)	260/280 ratio	cDNA probe cystine dye pmol/ µl	Yield	specific activity
Control 5	131.3	2.2	2.5	3.939	19.04
Control 60	165.2	2.2	3.1	4.956	18.7
TMP, 5 min	160.7	2.15	2.4	4.821	14.9
TMP: Glu 1:1, 5 min	226.4	1.97	1.7	6.792	7.5
TMP :Glu 1:8 , 5 min	148.5	2.15	2.6	4.4	17.5
TMP, 30 min	348.3	2.18	2.7	10.4	7.75
TMP : Glu 1:1, 30 min	214.1	2.29	1.7	6.42	7.94
TMP :Glu 1:8, 30 min	144.8	2.35	1	4.34	6.9
TMP 60 min	72.5	2.29	0.6	2.17	8.27
TMP: Glu 1:1, 60 min	257.1	2.16	1.6	7.71	6.22
TMP : Glu 1:8, 60 min	257.1	2.19	1.6	7.71	6.223259

4.3.2.2.11. Data Processing (Image analysis and data normalization)

The feature extraction software (V10.7, Santa Clara, CA) was used to study the quality of the obtained images. The image was analysed in terms of grid alignment, signal quantification and overall slide quality.

Background intensities in the DNA microarray data such as optical background and non-specific binding (NSB) were adjusted using the R library gcrma (Boes and Neuhäuser, 2005). The gcrma converted the background adjusted probe intensities into expression measures (Fig. 4.3.2) while, the probe sequence information were used to estimate probe affinity to non-specific binding (NSB). The levels of probe intensities between the arrays before and after normalization were compared using box-plots. The middle line of the box-plot represents the median while the two ends of the box represent the upper and lower quartiles. Values which are more than 1.5 the interquartile range are outliners (small circles), while the horizontal lines connected to the box-plots are not considered outliners. Figure (4.3.2A) shows that the intensities levels for most of the arrays differ and were corrected upon normalization (Fig. 4.3.2B).

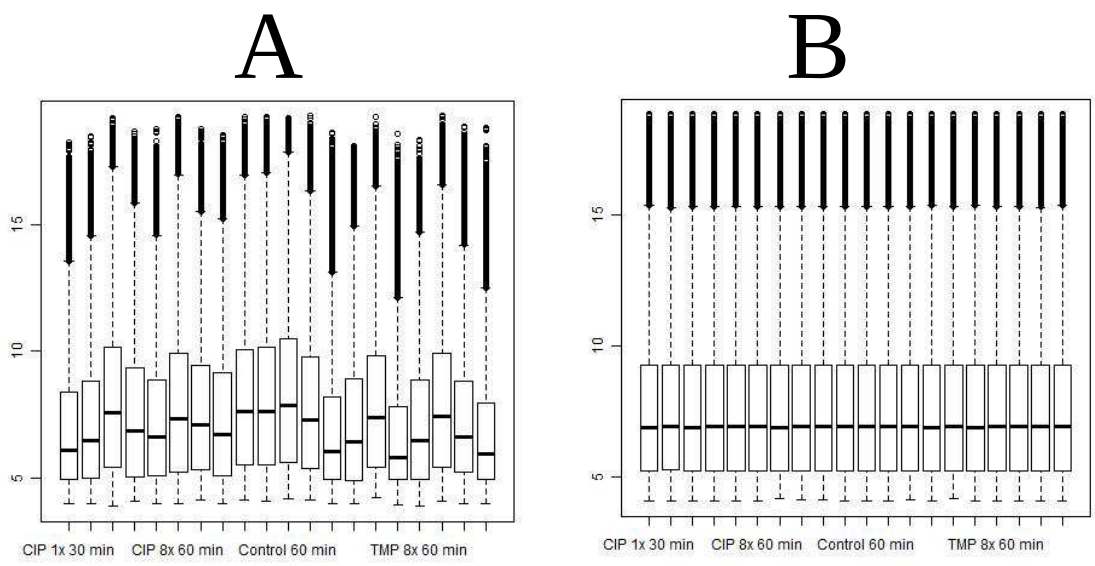

Figure 4.3.57:- Box-plots showing raw data before normalization (A), and centred distributed normalized microarray data (B).

4.3.2.2.12. Data clustering and filtering

Data clustering was carried out on the normalized data using TMEV software (version TM4, WA, USA). The genetic changes were clustered according to their similarities in the pattern of their expression using hierarchical clustering algorithm. The mean values were used to compare between the various data sets used in this study. In order to highlight the main variability in the multidimensional data set principle component analysis was carried out using TMEV software. Microsoft excel (version 2003, Toulouse, France) was used to filter out the non-expressed genes or the genes which do not show variation across sample types. Genes which were up or down regulated by two fold were selected for further analysis. Equations (4.3.9 and 4.3.10) were used to calculate the folds of up or down-regulation of the expressed genes when compared against the control (Caco-2 cells).

In order to investigate the changes occurring in various pathways during the absorption process, up and down-regulated genes were uploaded online onto Kyoto Encyclopaedia of

Genes and Genomes (KEGG) *http://www.genome.jp/kegg/* and the expression changes were high- lighted in red.

$$IF_{(E>C)} = 2^{(E-C)} \quad \textbf{Equation 4.3.43}$$

$$IF_{(E<C)} = -2^{(C-E)} \quad \textbf{Equation 4.3.44}$$

4.3.3. Results and discussion

4.3.3.1. Octanol-Water partitioning.

In order to investigate the partitioning behaviour and hence the passive diffusion capacities of the cationic drug upon pairing with the anionic amino acids, octanol/water partitioning (log P) was carried out. For this study both the free drug and salt form were paired with the anionic counter ions to investigate whether the salt form has any advantage over the free TMP during the partitioning and absorption studies.

During partitioning, it is assumed that an ion-pair is formed between TMP (basic drug) and the acidic amino acids (aspartic/glutamic acid) in octanol-water mixture. The formation and destruction of ion-pairing and partitioning process between octanol-water will take place at equilibrium conditions. The association constant for ion-pair formation in the aqueous phase (K_{11aq}) is calculated using equation (4.3.11).

$$K_{11aq} = \frac{[AB]_{aq}}{[A]_{aq}[B]_{aq}} \quad \textbf{Equation 4.3.45}$$

Where $[A]_{aq}$, $[B]_{aq}$ and $[AB]_{aq}$ are the concentrations of the acidic counter ion, TMP and the ion-pair in the aqueous phase respectively.

The total amount of TMP in octanol would exist only as an ion-pair which means that $[B_t]_{oct}$ will equal $[AB]_{oct}$ and the apparent octanol aqueous distribution coefficient of TMP can be calculated using equation (4.3.12).

$$D_B = \frac{[AB]_{oct}}{[B]_{aq} + [AB]_{aq}}$$ **Equation 4.3.46**

Where $[B]_{aq}$ represents the concentration of TMP free drug in the aqueous phase and $[B_t]_{aq}$ is the total concentration of TMP in the aqueous phase $[B_t]_{aq} = [B]_{aq} + [AB]_{aq}$.

The intrinsic partition coefficient of the ion-pair in octanol-water, P_{AB} is defined as the ratio between the ion-pair concentration in octanol to its concentration in water equation (4.3.13)

$$P_{AB} = \frac{[AB]_{oct}}{[AB]_{aq}}$$ **Equation 4.3.47**

Upon combining equations (4.3.11) (4.3.12) and (4.3.13), a common equation is obtained.

$$\frac{1}{D_B} = \frac{1}{K_{11aq} P_{AB} [A]_{aq}} + \frac{1}{P_{AB}}$$ **Equation 4.3.48**

Upon plotting the double reciprocal of the apparent octanol-water distribution coefficient of TMP as a function of the acidic amino acid concentration (i.e plotting $1/D_B$ Vs $1/[A]_{aq}$) an exponential curve is obtained and is used to calculate K_{11aq} and P_{AB}. The concentration of TMP in the aqueous layer was determined using HPLC method , while the concentrations of the anionic amino acids were calculated using ninhydrin test.

In this study the partitioning behaviour of TMP and TMP aspartate salt at various molar ratios of aspartic acid were studied and summarised in figures (4.3.3 & 4.3.4). Log P value for TMP was calculated using the octanol/water partitioning method and was found to be 1.07 (Fig. 4.3.3) which comes in line with the previous findings by Kasim et al., 2003. On the other hand, the log P value for the salt form was significantly lower than that of the free drug (log P= -1.13) which reflects the very high polar nature of the salt form.

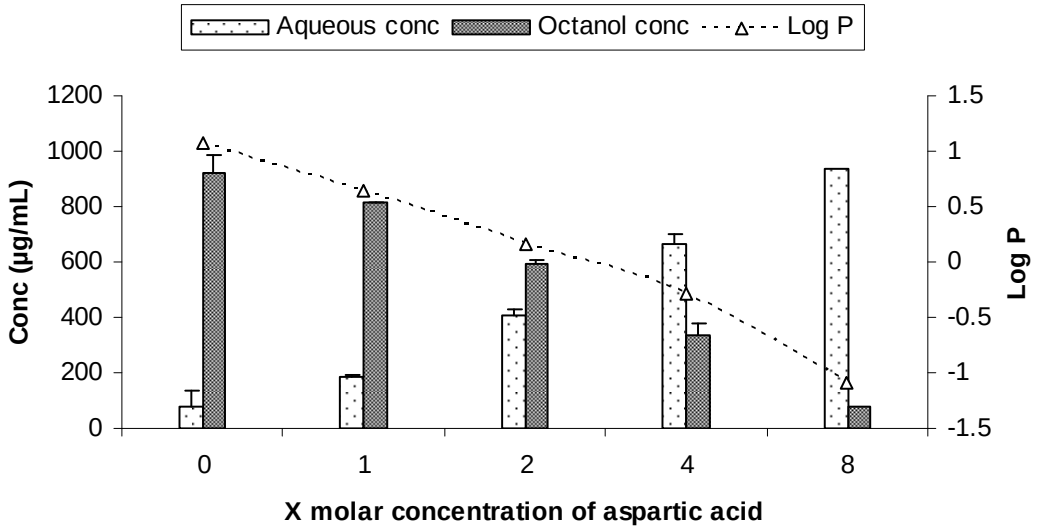

Figure 4.3.58:- TMP partitioning in the aqueous and octanol layers and its corresponding Log P values at various concentrations of aspartic acid (n=3).

Increasing the molar ratios of aspartic acid was found to decrease the partitioning capacity of TMP in the octanol layer and increase the migration of the cationic drug into the aqueous phase and hence the Log P values was found to decrease steadily as the molar ratio of the anionic amino acid increases (Fig. 4.3.3). TMP Log P value was halved upon incorporating aspartic acid at 1: 1 ratio and became 0.157 and -1.08 when aspartic acid was increased to PM 1:2 and PM 1:8 ratios.

For the salt form, increasing the concentration of aspartic acid resulted in very poor partitioning into the octanol layer as all the TMP molecules were detected in the aqueous phase. Although dissociation of TMP aspartate salt was expected to take place in water yielding the ionised form of the cationic drug and the anionic amino acid at 1:1 ratio, the partitioning behaviour of the salt form was different from the TMP: aspartic acid physical mixture at 1:1 molar ratio, probably because of the self-buffering capacity of the salt forms which yield different pH at the diffusion bilayer between the aqueous and oily phase as suggested by Forbes et al., 1995; ElShaer et al., 2011.

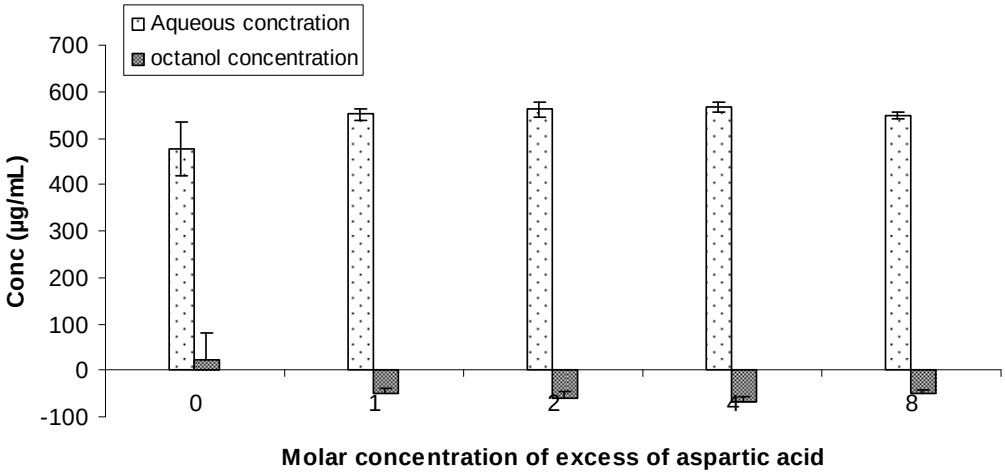

Figure 4.3.59:- TMP aspartate partitioning in the aqueous and octanol layers at various concentrations of aspartic acid (n=3).

The difference in the buffering capacities between the salt form and the physical mixtures resulted in significant difference in the partitioning behaviours as suggested by Sangster, (1989).

In order to calculate the K_{11aq} and P_{AB}, the double reciprocal plots of apparent octanol/water distribution coefficient of TMP at various molar concentrations of aspartic acid was evaluated (Fig. 4.3.5). Similar to IND studies, a strong negative exponential relationship (R^2=0.94) was observed. Increasing the molar concentration of aspartic acid resulted in an exponential decrease in the partition coefficient of TMP due to the low inherent lipophilicity of aspartic acid (Log P= -3.89).

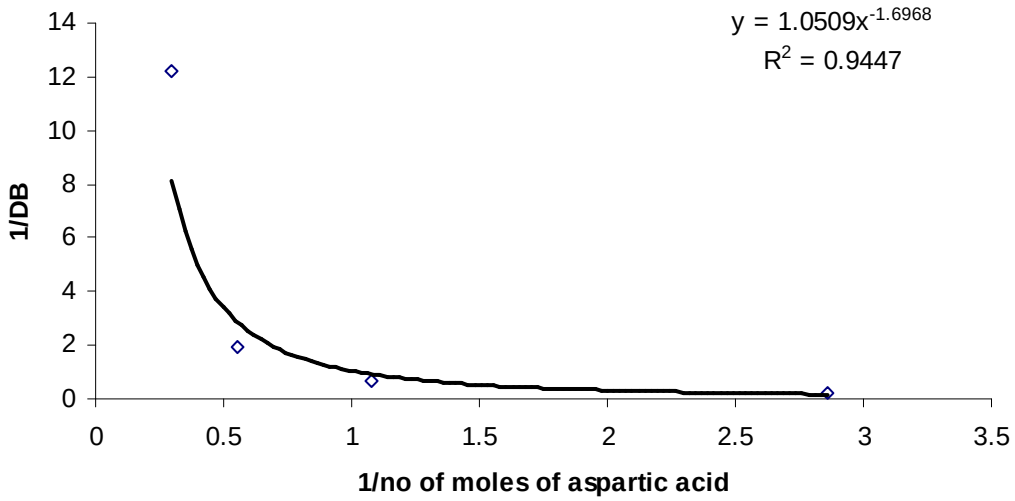

Figure 4.3.60:- Double reciprocal plot of the apparent octanol-water distribution coefficient of TMP as function of aspartic acid molar concentration.

The equation (equation 4.3.15) obtained from figure (4.3.5) was used to calculate the intrinsic octanol water partitioning (P_{AB}) and the aqueous binding constant (K_{11aq})

The intercept of the curve = -1.69x Log 1.05 and equals 1/intrinsic octanol/water partitioning ($1/P_{AB}$). Hence P_{AB} was found to be 27.9 while K_{11aq} equals 0.021 mM^{-1} (21 M^{-1}).

$$Y = 1.059\,x^{-1.698}$$ **Equation 4.3.49**

4.3.3.2. Permeability studies of TMP aspartic acid ion-pairs

The absorption profiles of TMP and TMP aspartate salt at various ratios of aspartic acid were studied and summarised in (Fig. 4.3.6). The concentration of TMP (500 µg/mL) was kept constant for all the experiments while the concentration of aspartic acid was changed. TEER values were measured before and after the run of the experiments and recorded in Table (4.3.3.) TEER values demonstrate the full integrity of the Caco-2 monolayers as all the values were higher than 300 Ω/cm^2 (Miller et al., 2010).

Table 4.3.37:- TEER measurements for TMP aspartate formulations before and after the permeability assay (n=5)

Formulations	TEER (Ω/cm^2)	
	Before	After
TMP free base	502±33	504±44
TMP: aspartic 1:1	532±87	462±46
TMP: aspartic 1:2	563±56	503±90
TMP: aspartic 1:4	547±16	544±81
TMP: aspartic 1:8	486±45	515±25
TMP aspartate salt	552±42	556±41
TMP asp salt: aspartic 1:1	552±67	515±30
TMP asp salt: aspartic 1:2	627±19	561±13
TMP asp salt: aspartic 1:4	611±8	568±10
TMP asp salt: aspartic 1:8	572±30	552±3

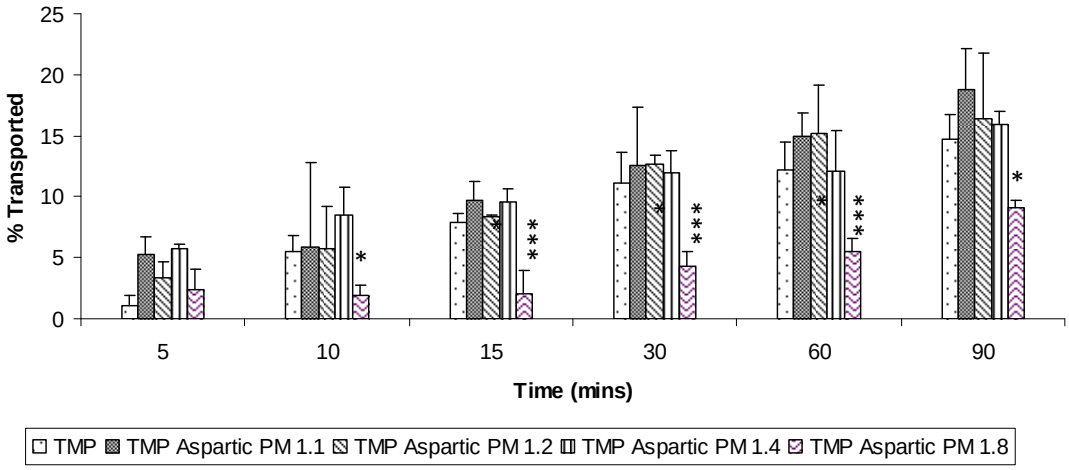

Figure 4.3.61:- Percentage of TMP transported across Caco-2 monolayers from TMP alone formulations and its physical mixtures (PM) with various molar ratios of aspartic acid (n=5). One way analysis of variance (ANOVA) and pair-wise multiple comparisons method (Tukey test) against drug alone at each time point were used for statistical analysis and probability values of (P< 0.05, * and P<0.001,*) were used to determine the significant difference.**

The percentage of TMP transported across Caco-2 cells was found to increase with time. For instance, the percentage absorbed of TMP aspartic acid physical mixture at 1:1 ratio (PM 1:1) was 5.2±1.5 after 5 minutes and increased to 18.75±3.38 after 60 minutes.

Interestingly, no significant difference ($p>0.05$) was observed between the percentages of TMP transported at various ratios of aspartic acid, apart from PM 1:8 ratio. It could be argued that the lack of difference in the permeability profile for the prepared ion-pairs is due to the weak aqueous binding constant (K_{11aq} = 21 M^{-1}) between TMP and aspartic acid. Interestingly, the percentage of TMP transported dropped significantly ($p<0.001$) when aspartic acid was used at

8x molar concentrations of TMP and the P_{app} decreased from (8.78±1.16)x10^{-6} for TMP to (5.39±0.3)x10^{-6} at PM 1:8 ratio (Fig. 4.3.8) probably because of the very high increase in the polarity of the cationic drug brought by the significant drop of the pH of the media by aspartic acid. It was suggested in chapter (3.3) that the high content of amino acid might saturate the amino acid or the dipeptidyl transporters which are involved in uptake of the ion-paired formulation but this is unlikely to occur in the current study because of the very low K_{11aq} for TMP aspartic acid ion-pairing as the ion-pairs cannot be transported as one moiety through the membrane transport carriers.

On studying the permeability profile of TMP aspartate salt alone and with excess of aspartic acid (Fig. 4.3.7), the data showed no significant difference ($p>0.05$) between the absorption profiles of the various formulations during the first 30 minutes (Fig. 4.3.7). At 60 minutes of the permeability assay, it was observed that the percentage permeated from the salt form (18.2±0.12) is significantly higher than that from TMP alone (12.18±2.3), and this percentage increased more at TMP aspartate: aspartic acid salt mixture (SM 1:2) to (25.35±3.95). Similar to the previous studies carried out on IND, at molar ratios greater than SM 1:2 and especially at SM 1:8, the percentage of TMP transported across the Caco-2 membrane started to decrease again to reach (11.13±1.6%) at 60 minutes.

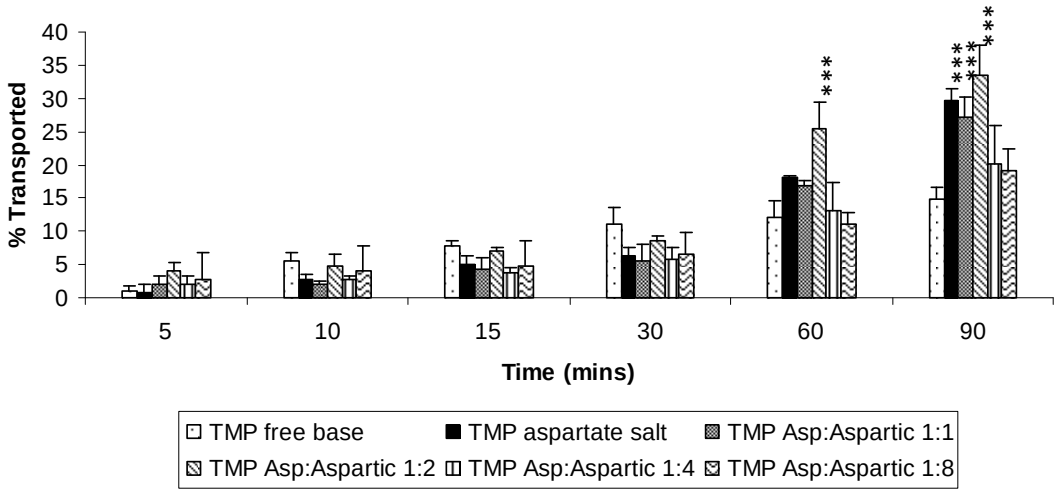

Figure 4.3.62:- Percentage of TMP transported across Caco-2 monolayers from TMP aspartate salt and salt mixtures (SM) with various molar ratios of aspartic acid (n=5). One way analysis of variance (ANOVA) and pair-wise multiple comparisons method (Tukey test) against drug alone at each time point were used for statistical analysis and probability values of (P< 0.05, * and P<0.001,*) were used to determine the significant difference.**

The apparent permeability coefficient (P_{app}) for TMP, TMP aspartic acid physical mixtures, TMP aspartate salt and TMP salt mixtures with aspartic acid were calculated using equation (4.3.5). P_{app} for TMP alone was found to be (8.78±1.16) $x10^{-6}$ cm/sec; studies carried out by (Sun et al., 2011) suggested a higher value for TMP P_{app} ($22x10^{-6}$ cm/sec) probably because of the low TEER values for the transwells used in their experiment. According to Artursson et al compounds are classified as highly permeable and low permeable if they have P_{app} >$1x10^{-6}$ and P_{app}<$1x10^{-7}$ cm/sec respectively. This means that TMP is highly permeable according to Artursson et al classification and not poorly absorbed as suggested by Joseph et al (2001). P_{app} permeability studies for the physical mixtures and the salt mixtures showed a similar trend; the apparent permeability increases as the molar ratio increases up to 2x and raising the molar ratio beyond 1:2 the apparent permeability starts to decrease again and drops to the lowest at 1:8 ratios for the physical and salt mixtures (Fig. 4.3.8).

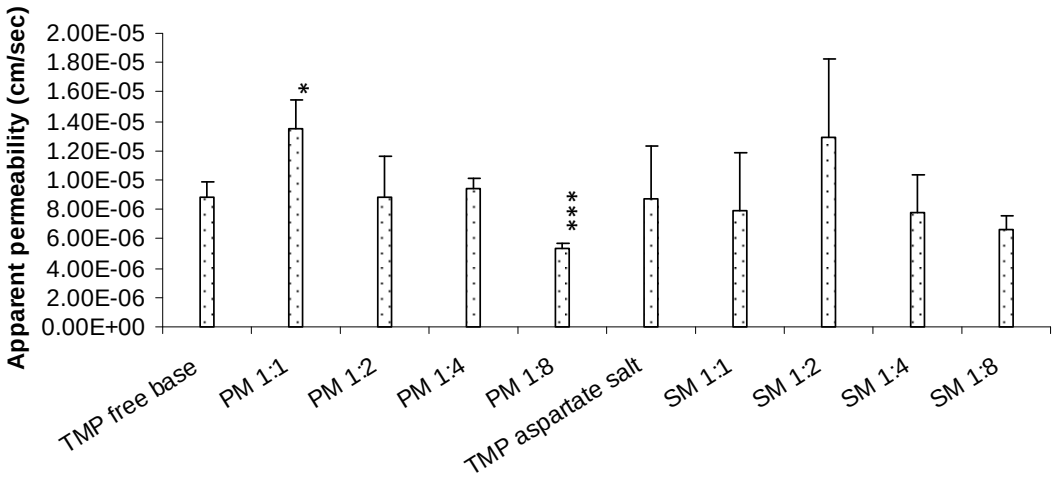

Figure 4.3.63:- P_{app} permeability values at 60 minutes for TMP, TMP aspartate and their mixtures with various molar ratios of aspartic acid. One way analysis of variance (ANOVA) and pair-wise multiple comparisons method (Tukey test) against drug alone at each time point were used for statistical analysis and probability values of (P< 0.05, * and P<0.001,*) were used to determine the significant difference.**

4.3.3.3. Partitioning studies for TMP glutamate formulations

In order to investigate the effect of the side chain of the amino acid counter ion on the binding capacity occurring during the ion-pair formation, glutamic acid was used. Glutamic acid has a similar structure to aspartic acid apart from an additional alkyl side chain ($-CH_2-$).

Octanol/water partitioning for TMP glutamic acid physical and salt mixtures was studied and summarised in (Fig. 4.3.9&4.3.11). Similar to TMP aspartic acid partitioning studies discussed above, the ability of TMP to partition into the organic phase was found to decrease gradually as the molar concentration of glutamic acid increases. TMP Log P value was 1.07 and decreased to 0.33 at PM 1:2 with glutamic acid and -0.27 at 1:8 molar ratio of TMP to glutamic acid respectively. Increasing the concentration of glutamic acid results in lowering of the pH of the media and in turn enables the domination of cationic charge on TMP thereby influencing its solubility.

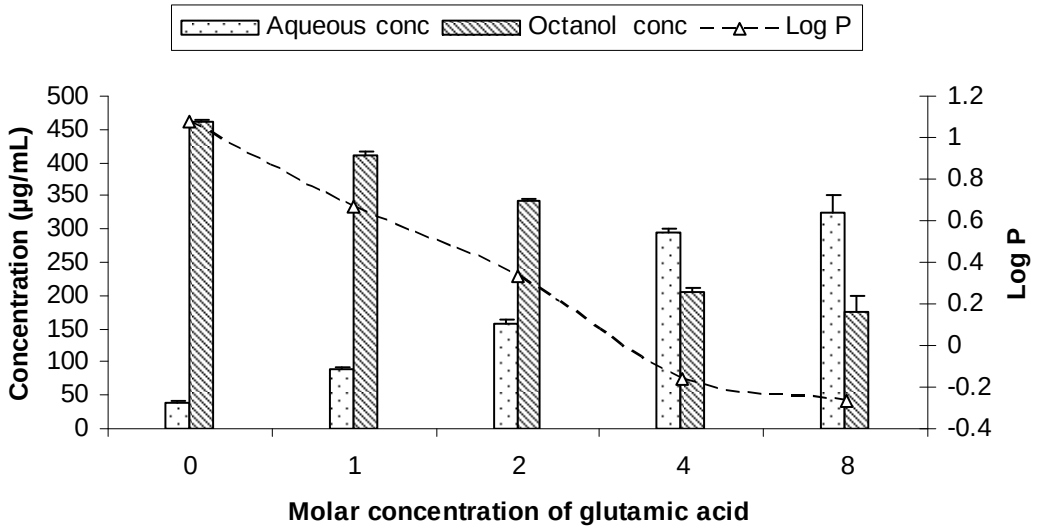

Figure 4.3.64:- TMP partitioning in the aqueous and octanol layers and its corresponding Log P values at various concentrations of glutamic acid (n=3).

Upon studying the double reciprocal plot of the apparent octanol/water distribution coefficient of TMP as a function of molar concentration of glutamic acid, a strong (R^2=0.95) negative exponential correlation was observed (Fig. 4.3.10), i.e. increasing the molar concentration of glutamic acid resulted in an exponential decrease in TMP partitioning coefficient. The exponential curve equation (equation 4.3.16) was used to calculate the K_{11aq} and P_{AB} as discussed before. Interestingly, the aqueous phase binding constant (K_{11aq}= 66 M^{-1}) was found to be three times higher than the K_{11aq} of TMP aspartic acid ion-pairs (K_{11aq}= 21 M^{-1}) despite the high similarity of the bond formed between the two ion-pairs. The ionic bonding between TMP and aspartic acid is similar to that between TMP and glutamic acid as ΔpKa value is very comparable; ΔpKa is 5.42 between TMP and aspartic acid and 5.11 between TMP and glutamic acid. Moreover, aspartic acid and glutamic acid have similar number of H-donors and H-acceptors hence similar H-bonding is also expected. Nevertheless, glutamic acid has an extra alkly chain (-CH_2-) in its structure which might have played a role during the secondary interactions (non-covalent interactions) taking place during ion-pair formation. This phenomenon is known as odd-even effect which was extensively studied in solution phases

(Pistolis et al., 2005) and is believed to affect the packing of the molecules, morphology and physical properties (Khan et al., 2011).

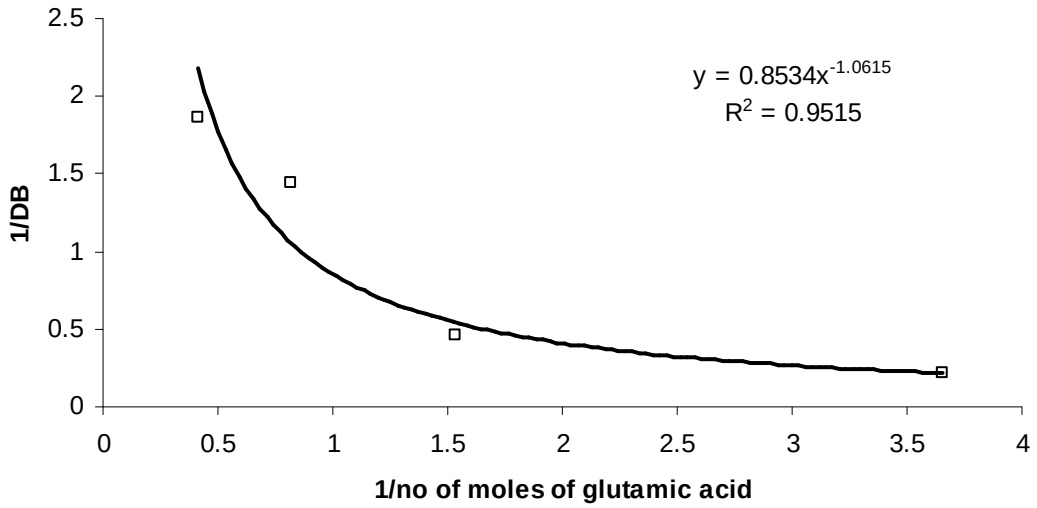

Figure 4.3.65:- Double reciprocal plot of the apparent octanol-water distribution coefficient of TMP as function of glutamic acid molar concentration.

$$Y = 0.85x^{-1.06}$$ **Equation 4.3.50**

Conversely, studying the partitioning behaviour of TMP glutamate salt showed that the partitioning of the TMP glutamate salt in the aqueous layer was very high even at the low concentrations of glutamic acid (Fig. 4.3.11). The log P value for the salt form was -0.738 reflecting the high hydrophilicity of the salt. Log P value was found to decrease upon increasing the molar ratio of glutamic acid until it reached -1.55 at 1:8 ratio of the salt to aspartic acid (Fig 4.3.11).

Such a difference in the partitioning behaviour of the salt form from the physical mixture could be explained by the self-buffering capacity of the salt form as discussed above.

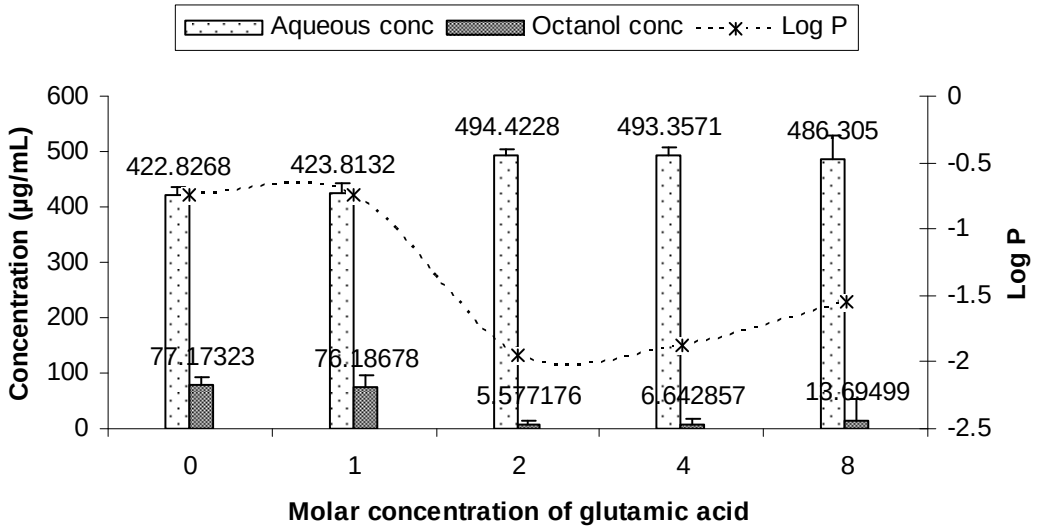

Figure 4.3.66:- TMP glutamate partitioning in the aqueous and octanol layers at various concentrations of glutamic acid (n=3).

The double reciprocal plot of the apparent octanol/water distribution coefficient of TMP glutamate salt as function of the molar concentration of glutamic acid is summarised in Fig (4.3.12).

From the curve equation (equation 4.3.17) the intercept was found to be (-4.8x Log 1.16) and equals 1/intrinsic octanol water partitioning ($1/P_{AB}$), hence P_{AB} equals 3.2. While, the slope was -4.8 and equals $1/K_{11aq}P_{AB}$. Therefore K_{11aq} will equal 64 M^{-1}.

$$Y = 1.163\,x^{-4.8} \quad \textbf{Equation 4.3.51}$$

Although the partitioning behaviour of the salt form was different from that of the physical mixtures, the aqeous phase binding constant was the same when the salt form and the free drug was used in the double reciprocal studies.

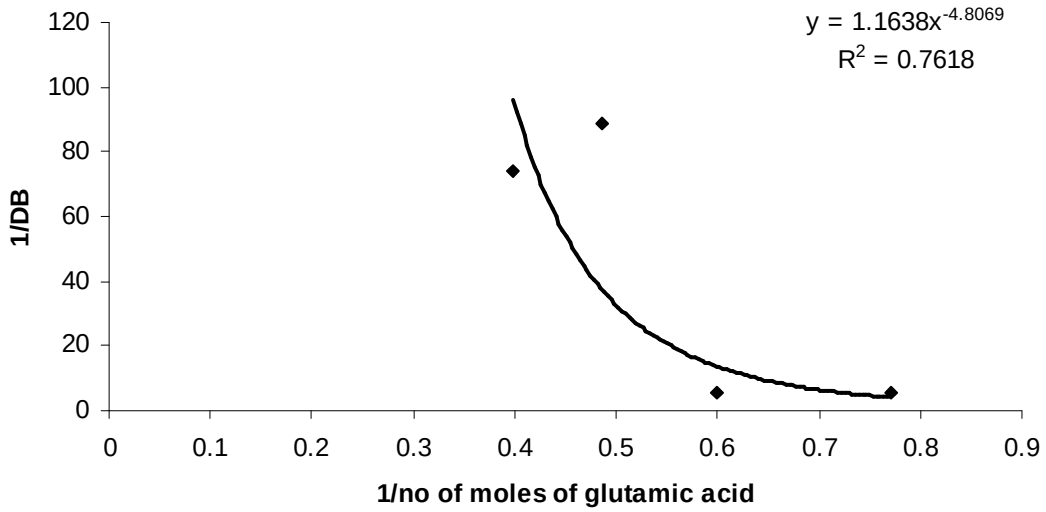

Figure 4.3.67:- Double reciprocal plot of the apparent octanol-water distribution coefficient of TMP glutamate salt as function of glutamic acid molar concentration.

4.3.3.4. Permeability studies for TMP glutamic formulations

The effect of various molar concentrations of glutamic acid on the absorption profile of TMP and TMP glutamate salt was studied (Fig. 4.3.13 & 4.3.14). All the transwells used for this study showed TEER values higher than 300 Ω/cm^2. For all the formulations, the percentage of TMP transported across the Caco-2 monolayers increased with time. The percentage of TMP absorbed after 5 minutes of the permeability assay was 1.02±0.84 % and increased gradually to 14.7±1.94 % after 90 minutes. Incorporating glutamic acid with TMP at 1:1 molar ratio resulted in a significant increase in TMP absorption at all the time points. For instance, the percentage of TMP absorbed from TMP alone formulations was 12.18±2.3% after 60 minutes and increased to 40.3±1.71% when glutamic acid was added at 1:1 molar ratio to TMP. Further increase was observed at PM 1:2 which remained constant at PM 1:4 and started to decrease again at PM 1:8 of TMP to glutamic acid (Fig. 4.3.13).

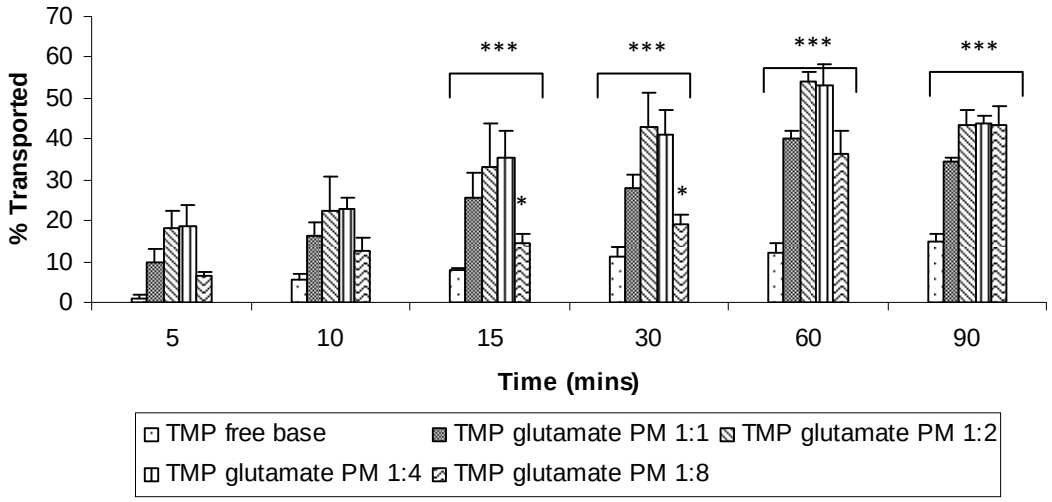

Figure 4.3.68:- Percentage of TMP transported across Caco-2 monolayers from TMP alone formulations and its physical mixtures (PM) with various molar ratios of glutamic acid (n=5). One way analysis of variance (ANOVA) and pair-wise multiple comparisons method (Tukey test) against drug alone at each time point were used for statistical analysis and probability values of (P< 0.05, * and P<0.001,*) were used to determine the significant difference.**

Although octanol/water partitioning studies showed a decrease in the partitioning ability of TMP into the organic layer upon pairing with glutamic acid, permeability studies showed better absorption at PM 1:1, PM 1:2 and PM 1:4. The partitioning data suggest that passive absorption is reduced upon pairing the cationic drug with the anionic amino acid. However, the increase in the overall uptake suggests the involvement of active transporter carriers during the permeation process.

TMP permeability from the salt form and the salt mixtures are shown in Fig. (4.3.14). The use of TMP glutamate salt resulted in a significant increase in the absorption profile of TMP despite having lower Log P value and partitioning capacities. The percentage of TMP absorbed was increased by around 6% upon using the salt form after 5 minutes of running the permeability experiment. The total percentage of TMP absorbed from the salt form at the end of the experiment was 22.99±5.74% compared to 14.7±1.94 %from the free drug. Similar to the physical mixture, increasing the molar ratio of the counter ion significantly ($p<0.001$) increased

the permeability profile of TMP especially at SM 1:1 and SM 1:4 which again started to drop at SM 1:8.

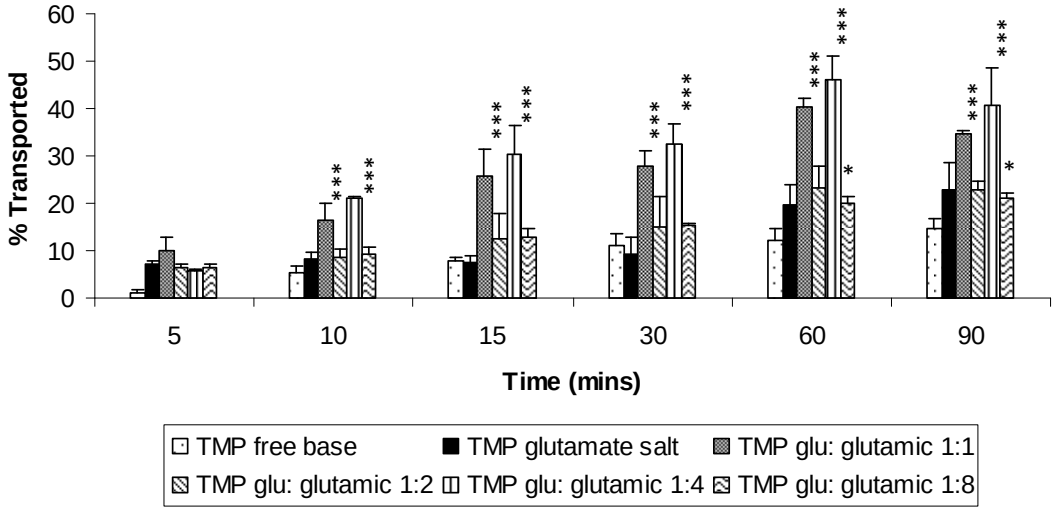

Figure 4.3.69:- Percentage of TMP transported across Caco-2 monolayers from TMP glutamate salt and salt mixtures (SM) with various molar ratios of glutamic acid (n=5). One way analysis of variance (ANOVA) and pair-wise multiple comparisons method (Tukey test) against drug alone at each time point were used for statistical analysis and probability values of (P< 0.05, * and P<0.001,*) were used to determine the significant difference.**

The P_{app} permeability for all TMP formulations is shown in figure (4.3.15).The data shows that glutamate PMs and SMs have higher P_{app} when compared to that of the free base and aspartate formulations. This may be attributed to the high aqueous binding constant between the glutamate counter ion and TMP base (K_{11aq}= 64 M^{-1}) compared to that between aspartate and TMP (K_{11aq}= 21 M^{-1}) i.e three times higher.

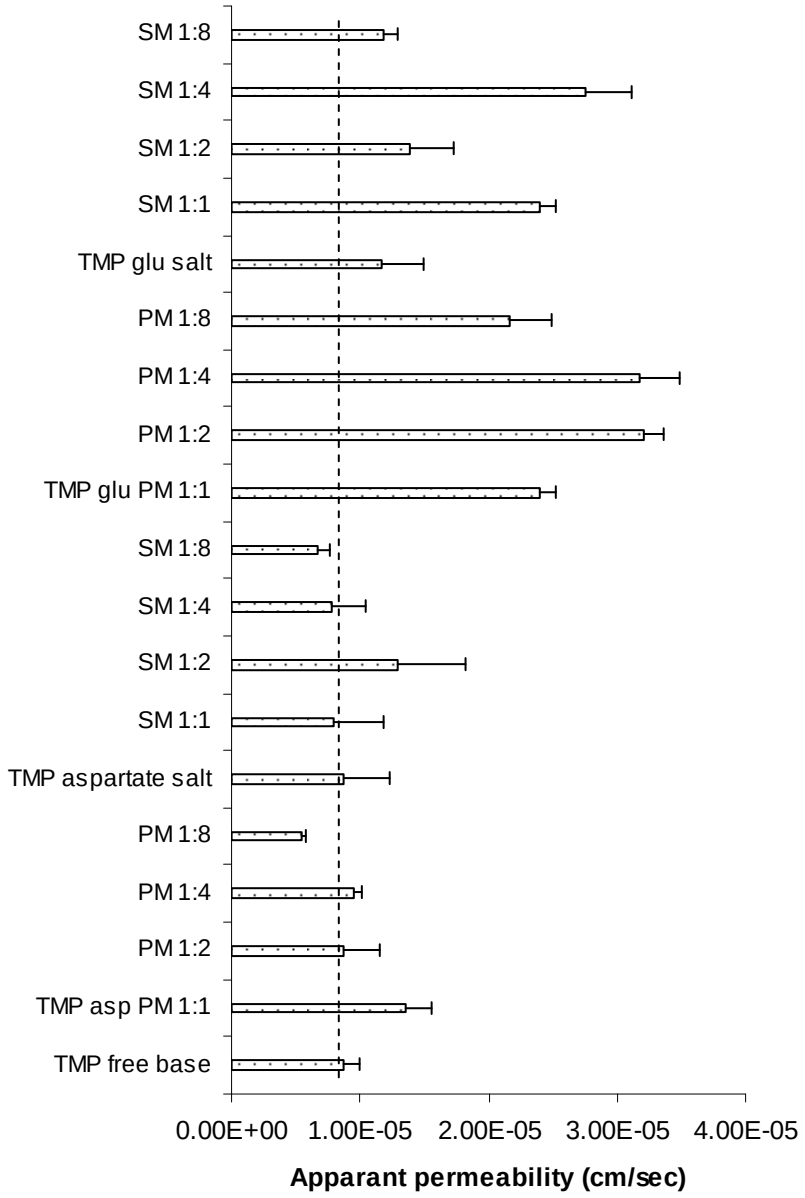

Figure 4.3.70:- P_{app} permeability values at 60 minutes for TMP, TMP aspartate, TMP glutamate and their PM and SM with aspartic acid and glutamic acid.

Microarray studies

Permeability data discussed earlier in this chapter showed a significant increase of the amount of TMP absorbed across Caco-2 monolayers upon ion-pairing the drug with glutamic acid. Therefore, three formulations were selected for the microarray study; namely TMP alone, TMP 1:1 PM and TMP 1:8 PM and time course analysis at 5, 30 and 60 minutes was studied as

cellular changes are affected by the time course of exposure to therapeutic agent. The expression patterns for the cells at the basal state (without exposure to TMP or any other formulations) were used as control. After RNA extraction and quantification, around 45,000 cDNA were hybridized with the microarray probe using Agilent one-color-spike procedure and microarrays slides were scanned and quality of the obtained TIFF images was analyzed prior to carrying out data normalization and clustering.

4.3.3.5. Image analysis

Finding spot centroids is a critical feature to ensure the quality of the microarray image. If the location of one or more of the spot centroids is off-centre, hybridization has to be carried out again using new grid. The four spot centroids in the current experiment were mapped accurately (Fig. 4.3.16A) for all slides which reflects the high quality of the used slides and successful hybridization of the probes.

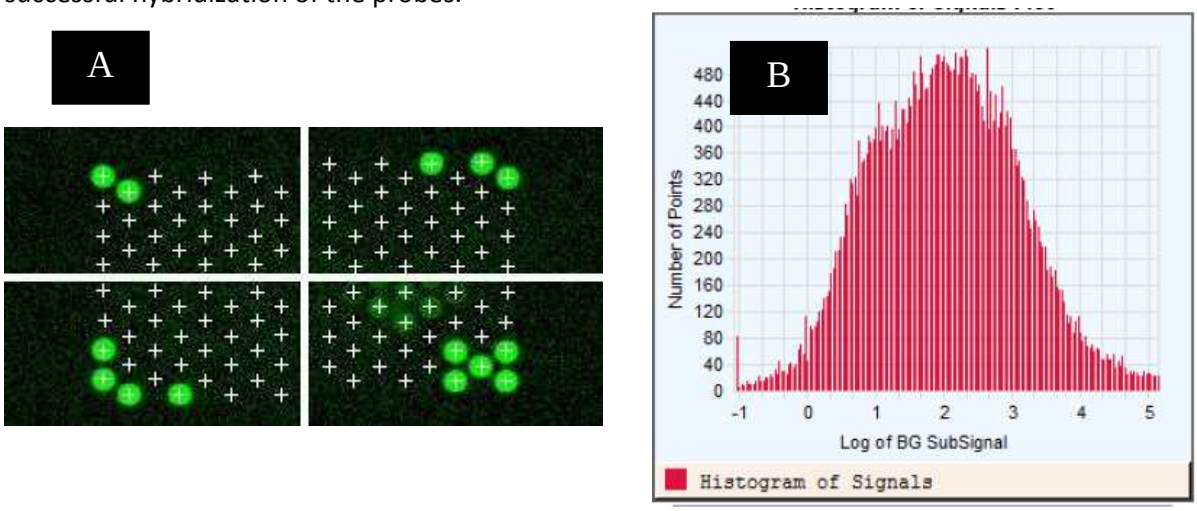

Figure 4.3.71:- Microarrays image analysis showing Spot Finding of the Four Corners of the Array (A), Histogram of Signals Plot (B) data were generated by feature extraction software.

The level of signal and shape of signal distribution were also evaluated using feature extraction software. A histogram of the line plot of number points in the intensity bins against the logarithm of the processed signal was obtained (Fig 4.3.16B). The obtained histogram showed that the intensity bins were normally distributed with a good bell shape (symmetric) reflecting

the high quality of the signals. A good correlation between the logarithmic values of the processed signal and the logarithmic values of the corresponding concentrations was obtained for most of the slides with R^2 values ranging between 0.99 and 1 (Fig. 4.3.17A).

In order to evaluate multiplicative detrending, the median of the processed signal and the median of the background subtracted signal (mean signal- BG used) for each column and over all the rows on the arrays were plotted which yielded a flat line (Fig 4.3.17B) indicating low multiplicative detrending (i.e. similar intensities from various replicate probes on the microarray slide). One-color-spike chips have number of probe replicates across the microarray and these replicates were used to evaluate the reproducibility of the signals. A low median coefficient of variation (%CV) of 3.9 was obtained reflecting the high signal reproducibility across the arrays. Image quality analysis was satisfactory for all the used arrays and the obtained data was used for normalization and further analysis.

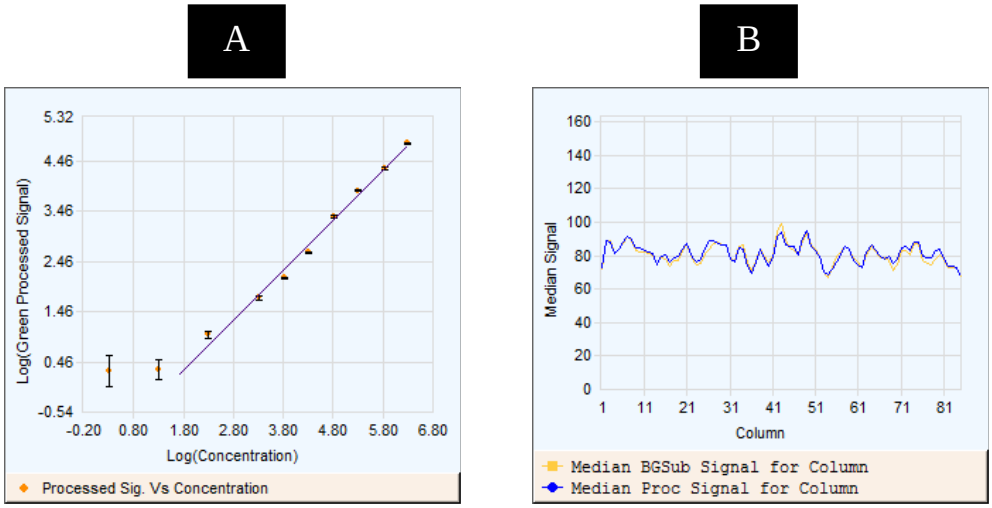

Figure 4.3.72:- Correlation between log signal against log Relative concentration (A) and spatial distribution of median signals for each column (B).

4.3.3.6. Data Clustering and Principle component analysis (PCA)

The data obtained from each microarray experiment is highly complex in terms of quantity and dimensions. Many statistical and computational approaches (i.e. supervised learning) are employed in order to interpret the biological meaning of the data (Fisher, 1936). Data clustering or unsupervised learning is another analysis method which is used to reduce data by adding the observations into a cluster which can be represented by an average value. Various clustering computational approaches are available including; K-means clustering (Hartigan and Wong., 1979), hierarchical clustering (Everitt and Rabe-Hesketh, 1997; Eisen et al., 1998), self-organizing maps (Kohonen, 1990) and artificial network (Bishop, 1996). As none of these methods offer any specific advantage over each other, hierarchical clustering was used in this study as it measures the distance between rows of various data to cluster them. After measuring the distance between every couple of genes, the algorithm then merges the genes which are close to each other (i.e. has shorter distance between them) into one cluster. The midpoint of the two merged genes is used to merge the distance between them and other genes. This iteration takes place for the all data set and final cluster is obtained showing the up-regulated genes in red and the down regulated genes in green (Fig. 4.3.18).

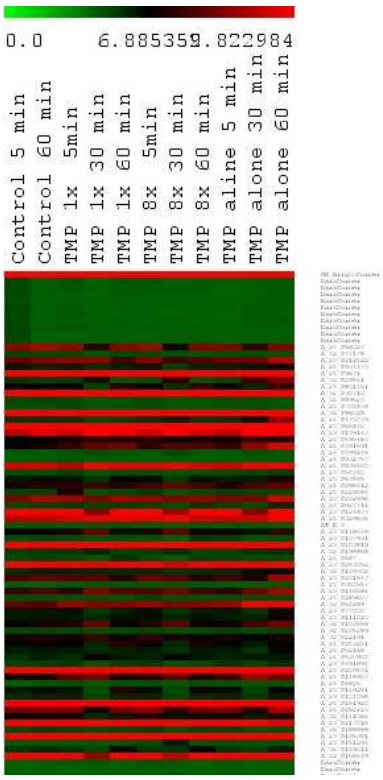

Figure 4.3.73:- Data clustering for TMP formulations at various time points; green clusters show down-regulations while red clusters show up-regulations.

As the experimental conditions for all the arrays are controlled, any variation in the expression pattern will be introduced by the conditions under investigation i.e. as a result of exposure to various formulations. Nevertheless, this study measured 45,000 genes at 11 different conditions. Therefore the obtained data could form a matrix of 11x45,000 measurements. If a scatter plot of 11 axes (one axis for each experimental condition) was used to plot these 45,000 genes in muti-dimensional space, the resultant graph will be a cloud of values in the space. Therefore, principle component analysis (PCA) was used to identify the dimension where the data (cloud) is more extended.

TMEV software was used to calculate the Eigen values for the 11 principle components and the highest Eigen values were shown by the first three principle components. In total 69.5% of the genetic changes were extended along the first, second and third principle components. Hence,

the first three components were selected for analysis of gene expression changes occurring during the uptake of TMP, TMP 1:1 PM and TMP 1:8 PM.

First and second PCA showed that the time course had a great effect on the expression pattern of the genes. At the beginning of the experiment (i.e. 5 minutes) most of the genetic expressions were centered around the origin, suggesting minimal variations at the first five minutes of permeability study. Leaving the formulations for another 25 minutes (i.e. after 30 minutes of the beginning of the permeability assay) resulted in significant changes in the cellular behavior of Caco-2 monolayers (Fig. 4.3.19) where the majority of the genetic changes occurred along the first component (40.85% as suggested by Eigen values). These changes returned back to the origin after 60 minutes of exposing the cells to TMP, TMP 1x and TMP 8x.

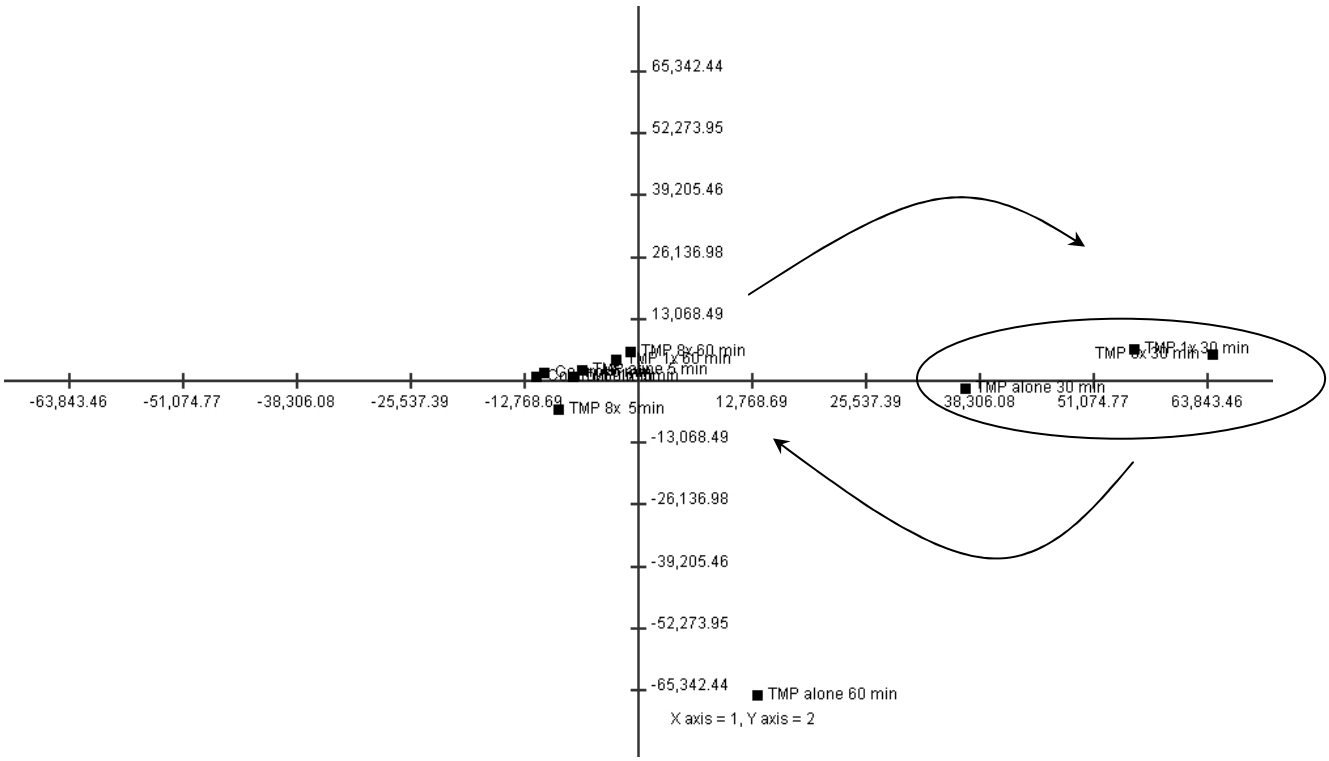

Figure 4.3.74:- First and second principal component analysis on the transcriptional time course for TMP and its various ion-paired formulations at 0, 30 and 60 minutes. The number represents the time points. The plot represents the data for the mean values at each time point.

9.2% of the genetic changes occurred at the third principle component and were attributed to the genetic changes that took place after 60 minutes of exposing the cells to ion-paired formulations (Fig. 4.3.20).

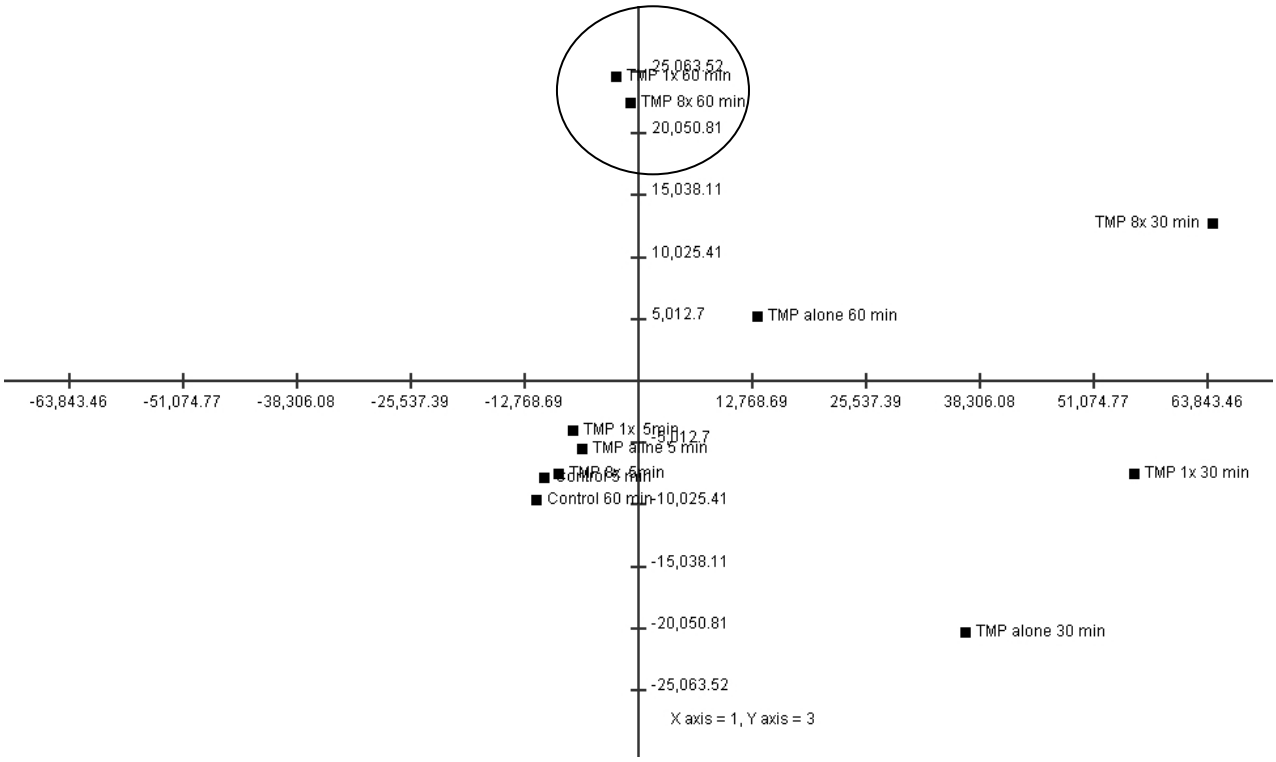

Figure 4.3.75:- First and third principal component analysis on the transcriptional time course for TMP and its various ion-paired formulations at 0, 30 and 60 minutes. The number represents the time points. The plot represents the data for the mean values at each time point.

4.3.3.7. Genetic changes of transporters pathways

Cellular behavior including physiological changes in disease condition or in response to toxic agents or drug treatment is reflective of the pattern of gene expression. Monitoring such changes enables better understanding of disease progression or toxic and therapeutic effects of drugs which results in better targeting of disease conditions at cellular level thereby promoting higher therapeutic efficacy. The aim of the current study was to understand and study differences in gene expression profile upon exposure to different formulation types of

the drug candidate during permeability across Caco2 monolayers. Results obtained from permeability studies showed significant increase in drug uptake of some of the ion-paired formulations when compared to the free form of the drug and other formulations at various ratios of the counter ions. Drug absorption across the gastrointestinal tract is affected by many variables such as drug solubility, partitioning abilities, pH of the surrounding environment and genetic changes along the intestinal membrane. The majority of the physicochemical properties of TMP and CIP that could affect their uptake were evaluated prior to studying the genetic changes taking place across the cells. Microarray studies were carried out to visualize how different genes of various pathways vary in expression upon exposure to therapeutic agent and various formulations with a particular emphasis on transporter carrier genes. In order to carry out the microarrays experiment cDNA were hybridized with approximately 45,000 gene probes attached to the microarrays chips. After normalization and clustering analysis, the obtained data were filtered and only genes which were over-expressed or down-regulated by two fold or more when compared against the control were selected for further investigations.

Genetic changes that occurred after exposing Caco-2 cells to TMP alone formulations for 5, 30 and 60 minutes were monitored (Fig. 4.3.21). One ABC transporter was over-expressed after 5 minutes of exposure to TMP. The number of up-regulated ABC transporters increased to 5 after 30 and 60 minutes of the permeability assay. The numbers of ABC genes down-regulated were 1, 10 and 7 after 5, 30 and 60 minutes respectively.

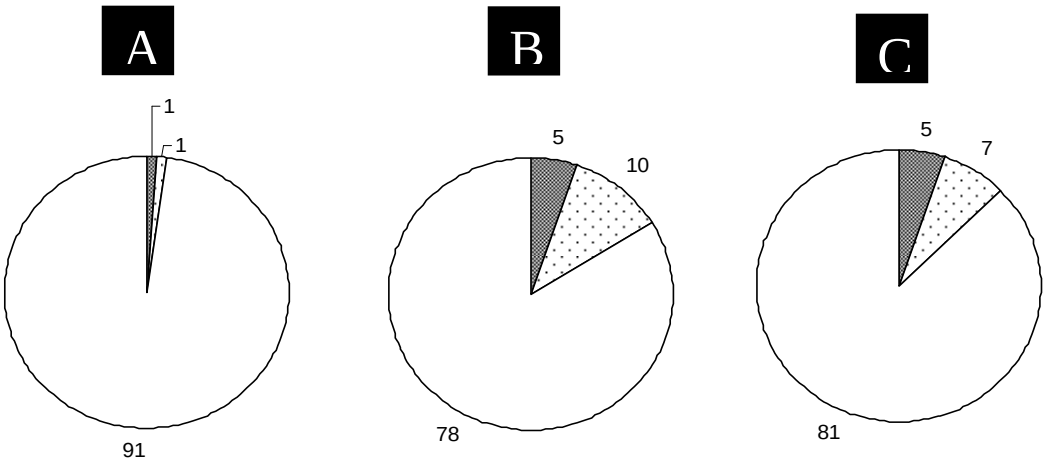

Figure 4.3.76:- Total number of ABC genes over-expressed ( ), suppressed ( ) and unchanged ( ) after 5 minutes (A), 30 minutes (B) and 60 minutes (C) of exposure to TMP.

Table (4.3.4) summarises all the ABC transporters over-expressed during TMP permeability across Caco-2 monolayers. MRP7 was among the over-expressed genes after 5 minutes and 30 minutes of TMP uptake across the cells. The transporter gene was over-expressed in more than one of the replicate probes which reflects the high involvement of MRP7 in mediating the efflux of TMP. MRP7 is member 7 of multiple resistance protein and is also known as ABCC10. MRP7 has similar topology to other ABCC members such as MRP 1, 2, 3 and 6 as it has three membrane binding domains and two nucleotide binding domains (Kuang et al., 2010). Various studies suggested that MRP7 is expressed in cancer cells and confers resistance to a range of chemotherapeutic agents (Naramoto et al., 2007). Drugs such as 17-β-estradiol, paclitaxel, vincristine, vinblastine (Chen et al., 2003; Hopper-Borge et al., 2004) and vinorelbine (Bessho et al., 2009) were reported to be effluxed by MRP7. Microarray results suggest that MRP7 plays a key role in the efflux of TMP and hence decreases the overall uptake of the drug across the epithelial membranes. The role of MRP7 in TMP efflux was not reported before in the literature where majority of the previous studies reported the involvement of P-gp (Joseph et al., 2001; Murakami and Takano, 2008) in TMP efflux. In the current study, P-gp was not filtered as up or down-regulated gene and having investigated the expression changes of P-gp it was found to be less than 2 fold up-regulated (1.83 fold) which suggests the relatively lower

role of P-gp in mediating TMP efflux. These results are in consensus with Romiti et al's (2002) suggestion that TMP efflux is not supported by P-gp activity in HK-2 cells even at high concentrations of the drug (50 μM) (Romiti et al., 2002).

Table 4.3.38:- Summary of the over-expressed ABC transporters during TMP permeability across Caco-2 monolayers.

Time point	probes	Gene symbol	Expression level
5 minutes	A_23_P215720	MRP7	2.02
30 minutes	A_23_P215720	MRP7	2.85
	A_32_P29703	ABCA17P	2.22
	A_24_P235429	ABCA1	2.04
	A_23_P78018	ABCA5	2.47
	A_23_P92602	ABCA11P	2.53
60 minutes	A_32_P29703	ABCA17P	2.57
	A_23_P43504	ABCA2	2.15
	A_24_P235429	ABCA1	2.02
	A_23_P78018	ABCA5	2.40
	A_23_P201918	ABCB10	2.42

Another interesting finding is that many members of ABCA family -including ABCA1, ABCA5 and ABCA17- were over-expressed upon treating the cells with TMP. The three transporter genes were up-regulated at 30 and 60 minutes of TMP permeability study (Table 4.3.4). The prototype of this family is ABCA1 which was first identified in 1994 (Luciani et al., 1994) and more members were identified and sequenced later on (Connors et al., 1997; Allikmets et al., 1997). The structure of ABCA1 was studied by Santamarina-Fojo et al (2000) and the transporter is composed of 50 exons that encode 2261 amino acids. ABCA1 was found to be associated with the removal of cellular cholesterol in to plasma utilizing ATP hydrolysis as an energy source (Morales et al., 2008). As a result, ABCA1 mutation was reported to cause Tangier disease (Bodzioch et al., 1999) due to the accumulation of cholesterol esters and cholesterol in spleen, liver and other tissues (Francis et al., 1995). Similar functions were reported for both ABCA17 (Morales et al., 2012) and ABCA5 (Ye et al., 2010). From the current investigation, the results suggest that TMP efflux is co ordinate via multiple members of ABCA family. To further analyze our findings, the structure of TMP and cholesterol were compared in order to determine similarities between the two molecules (Fig. 4.3.22). However, no

similarities were observed between the two molecules. Moreover cholesterol has higher lipophilicity (log P= 7.17) possibly because of the long aliphatic side chain (Stanculescu et al., 2006).

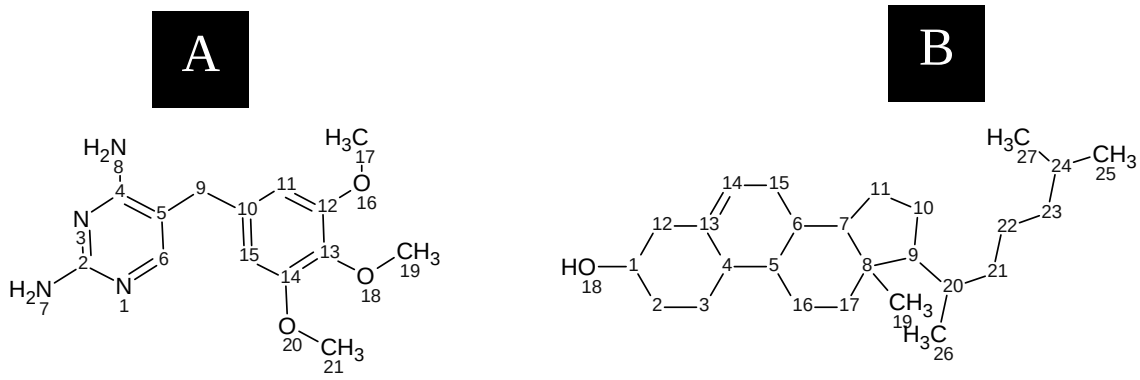

Figure4.3. 77:- Comparison between the molecular structure of TMP (A) and cholesterol (B).

Solute carrier transporters (SLCs) were also investigated to determine their role in TMP transport (Fig. 4.3.23). The data shows that the number of solute carrier transporters up-regulated after 30 minutes was 26 and increased to 35 at the end of the experiment (Fig. 4.3.23C).

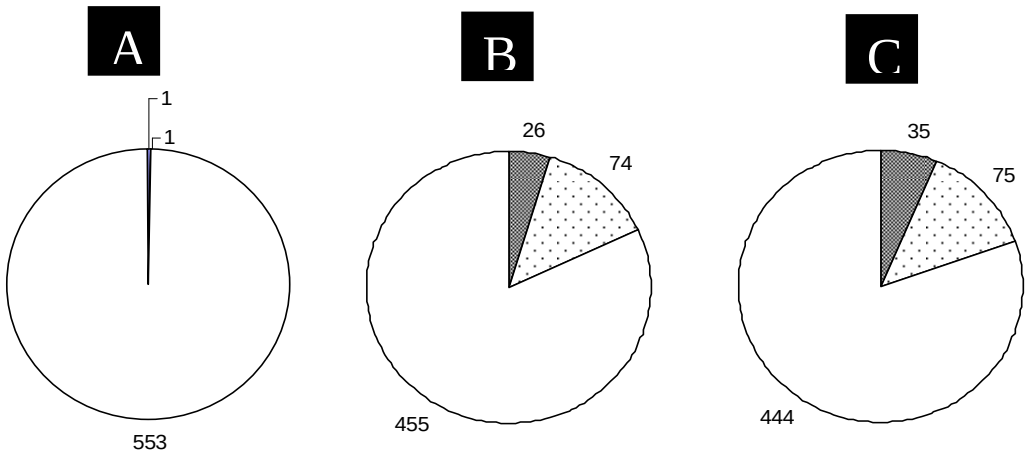

Figure 4.3.78:- Total number of SLC genes over-expressed ( ), suppressed ( ) and unchanged ( ) after 5 minutes (A), 30 minutes (B) and 60 minutes (C) of exposure to TMP.

SLC22A4 (OCTN1) is among the over-expressed genes as its expression increased by 2.36 fold after 60 minutes. OCTN1 is an organic cation transporter which mediates the transport of

pyrilamine, quinidine and tetraethylammonium (Wu et al., 2000). Various studies demonstrated that OCTN1 is pH-dependent which suggests that changes in pH will change the level of expression of the transporter (Wu et al., 2000; Tamai et al., 1997) possibly because of the cationic nature of its substrates. Majority of OCTN1 substrates carry cationic nitrogen which also exists in TMP pyrimidine ring possibly explaining the permeation of TMP across the Caco-2 monolayers by active transport. It was reported in the literature that SLC22A1 (OCT1) and SLC22A2 (OCT2) mediate the uptake of TMP, however in this study the expression of OCT1 and OCT2 was not affected by TMP treatment.

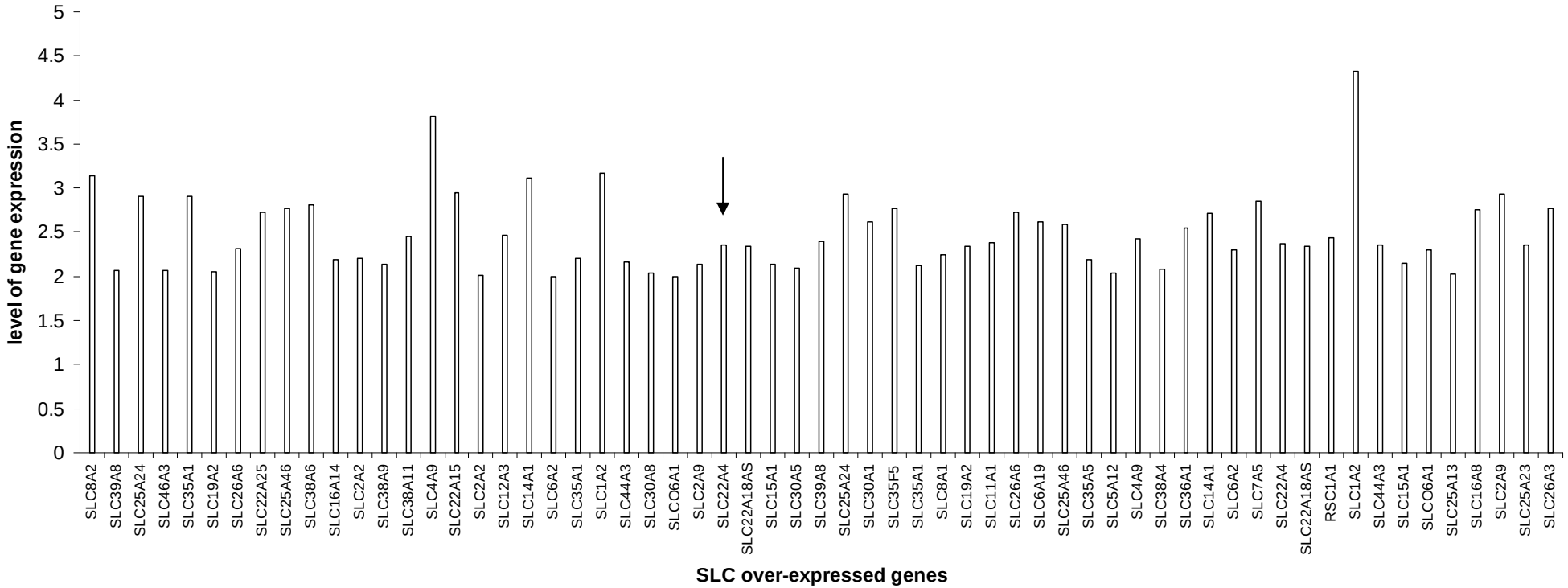

Figure 4.3.79:- Gene expression of SLC transporters of Caco-2 cells after 30 minutes of exposure to TMP.

The effect of ion-paired formulations at 1:1 and 1:8 molar ratios were also evaluated at the same time points; 5, 30 and 60 minutes. Incorporating glutamic acid into the formulations resulted in activation of various members of SLC1 across Caco-2 monolayers as summarised in Table (4.3.5).

SLC1 is glutamate/neutral amino acid transporter which has 5 high affinity glutamate transporters previously described as X^{-AG} (EAAT4/5, GLAST, EAAC1 and GLT1) and two Na^+ dependent neutral amino acid transporters (ASC; ASCT1 and ASCT2). Glutamate transporters mediate the uptake of L-Asp, D-Asp and L-Glu by co-transporting $1H^+/3Na^+$ and counter transport of $1K^+$ (Kanai and Hediger., 2003). On the other hand, ASC mainly transport alanine, serine and cysteine and protect the cells against glutamate excitatoxicity. SLC1 has a unique structure which comprises of 8-transmembrane domains and a highly conserved long hydrophilic chain attached to its C-terminus. Both glutamate and ASC transporters share similar structure and recognize common substrates (Zerangue and Kavanaugh., 1996).

EAAT4 (SLC1A6) was over-expressed by 3.36 fold after 5 minutes of exposing the cells to TMP 1x formulation while SLC1A1 was up-regulated at 30 minutes. At higher concentrations of glutamic acid (i.e. TMP 8x formulations) the two Na^+ dependent ASC transporters were over-expressed. Both ASCT1 (SLC1A4) and ASCT2 (SLC1A5) were up-regulated by 2.27 and 2.97 respectively. It can be hypothesized that the low concentration of glutamic acid in TMP 1x formulations activated high affinity glutamic acid transporter SLC1A6 and SLC1A1 whereas increase of concentration to 8x results in the expression of ASCT1 transporters. Moreover, it is believed that as the pH of the media decreases (in the current study due to increase in glutamate concentration), glutamate uptake shifts towards ASC transporter (Utsunomiya-Tate et al., 1997).

Table 4.3.39:- Summary of SLC1 transporters up-regulated during the uptake of TMP glutamic acid ion-paired formulations across Caco-2 monolayers.

Formulation	Probes	Gene symbol	Expression difference
TMP 1x 5 minute	A_24_P179467	SLC1A6	3.364774
TMP 1x 30 minute	A_24_P232252	SLC1A1	2.362158
TMP 8x 30 minute	A_24_P232252	SLC1A1	2.240894
TMP 8x 60 minute	A_23_P55998	SLC1A5	2.973543
	A_23_P91151	SLC1A4	2.276961

The expression of OCTN1 is also affected by the ion-paired formulations and an interesting pattern was observed. OCTN1 was over-expressed by 2.2 fold during the absorption of TMP:glutamic acid at 1:1 molar ratio. On the other hand, the expression of this gene dropped to reach the basal state when the cells were treated by TMP:glutamic acid 1:8 ratio. A similar trend was explained by Wu et al (2000) when human retinal pigment epithelial (HRPE) cells were used to evaluate the uptake of tetraethylammonium at various pH. It is possible that increasing the ratio of glutamic acid in the ion-paired formulations resulted in increasing the drug uptake as discussed above in the permeability study. Such increase could be attributed to the activation of OCTN1 transporters by 1:1, 1:2 and 1:4 molar ratios but increasing this ratio further to 1:8 resulted in a drop in drug uptake. Hence it can be concluded that glutamic acid would have affected the pH during the uptake of TMP which in turn has affected the expression levels of OCTN1 as early suggested by (Wu et al., 2000).

MRP7 was found to mediate the efflux of TMP in this study; hence it was interesting to track the expression changes for this upon inclusion of the ion-paired formulations. MRP7 remained at the basal state; as it was expressed 1.6 fold during the uptake of TMP 1x formulations. It was over-expressed to 2.9 and 3.02 after 30 and 60 minutes respectively. Similar trend was observed when TMP 8x formulations were used. Nevertheless, the expression level was significantly higher at 30 minutes for TMP 8x formulations as MRP7 was over-expressed by 6.4 fold. This could possibly explain the low uptake of TMP from TMP 8x formulations.

It can be concluded that the ratio of glutamic acid in the ion-paired formulations has a significant effect on the flux of TMP as it increased OCTN1 expression in a parabolic manner

and shifted the uptake of glutamic acid from high affinity transporters to the low affinity carriers. Nevertheless, no evidence exists that the ion-paired formulations are transported as one entity as none of the dipeptidyl carriers were over-expressed.

4.3.3.8. Genetic changes of metabolic pathways and other pathways

As mentioned before, cellular function varies in both disease state and upon exposure to toxins. Cells identify therapeutic agents as toxins and modify/activate functions/pathway to protect them as seen in transporter network changes. Those genes which were either up-regulated or down-regulated were uploaded onto KEGG database to visualize the cellular changes occurring upon treating the cells with TMP and its ion-paired formulations. Multiple pathways were found to be affected including metabolic pathways, oxidative phosphorylation, cytokine-cytokine interactions and xenobiotic metabolism.

TMP exhibits several adverse reactions since it is used in combination with sulfamethoxazole (Lai et al., 1999). Moreover, the use of TMP alone resulted in many idiosyncratic reactions, neutropenia (Hawkins et al., 1993) and hypersensitivity reactions (Carr et al., 1993) and the mechanism by which TMP causes these adverse effects is still not clear. Only few studies (Meshi and Sato, 1972; Van et al., 1992; Schwartz et al., 1970; Brooks et al., 1973) proposed some metabolic mechanisms for TMP and are summarised in Fig. (4.3.25).

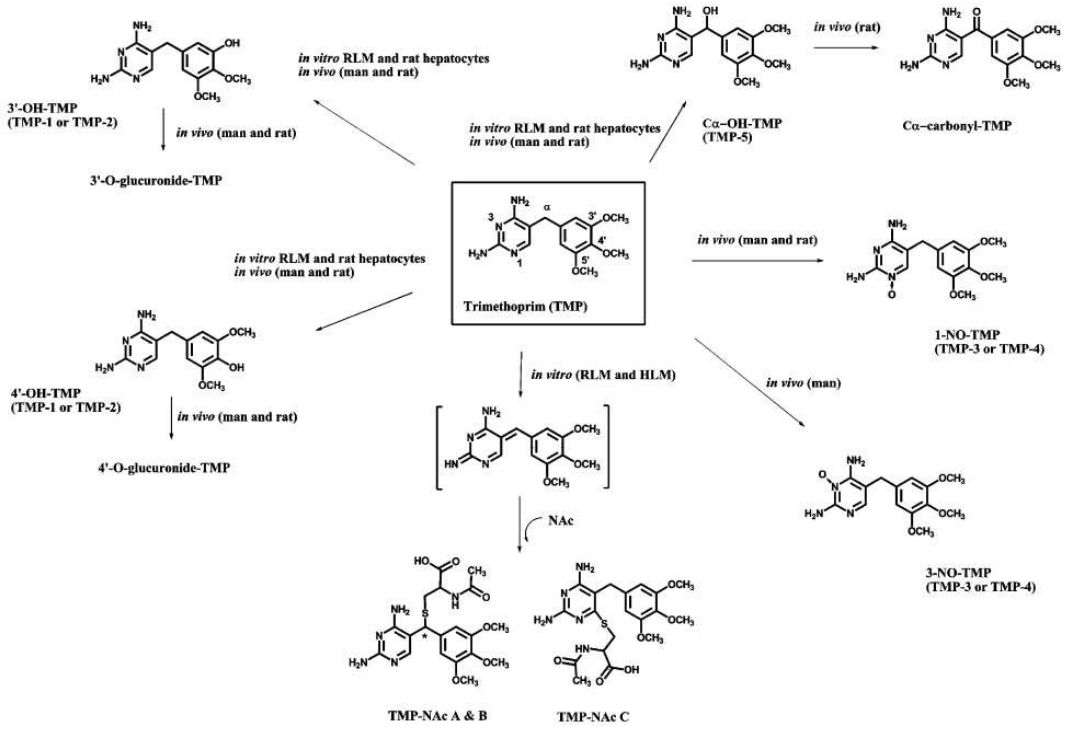

Figure 4.3.80:- A scheme of the known metabolites and reactive intermediates (in brackets) of TMP obtained from *in vitro* and *in vivo* experiments. The figure is adapted from Damsten et al., 2008.

Frisch studies suggested that TMP hepatic and cutaneous reactions are caused by immunologic mechanisms rather than direct toxicity (Frisch, 1973). The studies carried out by Lai et al. (1999) demonstrated that TMP is oxidized by both hepatic macrosomes and human neutrophils into reactive metabolites. In a similar way to oxidation of phenolic compounds by cytochrome P-450 enzymes and peroxidase, TMP was found to be oxidized into iminoquinone methide and pyrimidine iminoquinone (Lai et al., 1999). Microarray data shows the high involvement of oxidative phosphorylation reactions upon treatment with TMP as 30 reactions were activated (Fig. 4.3.26). Both cytochrome C oxidase (COX5B, COX6B, COX7A and COX7B) and NADH dehydrogenase were activated possibly to oxidise the nitrogen atom to yield TMP-1-N-oxide and TMP-3-N-oxide as suggested by (Damsten et al., 2008).

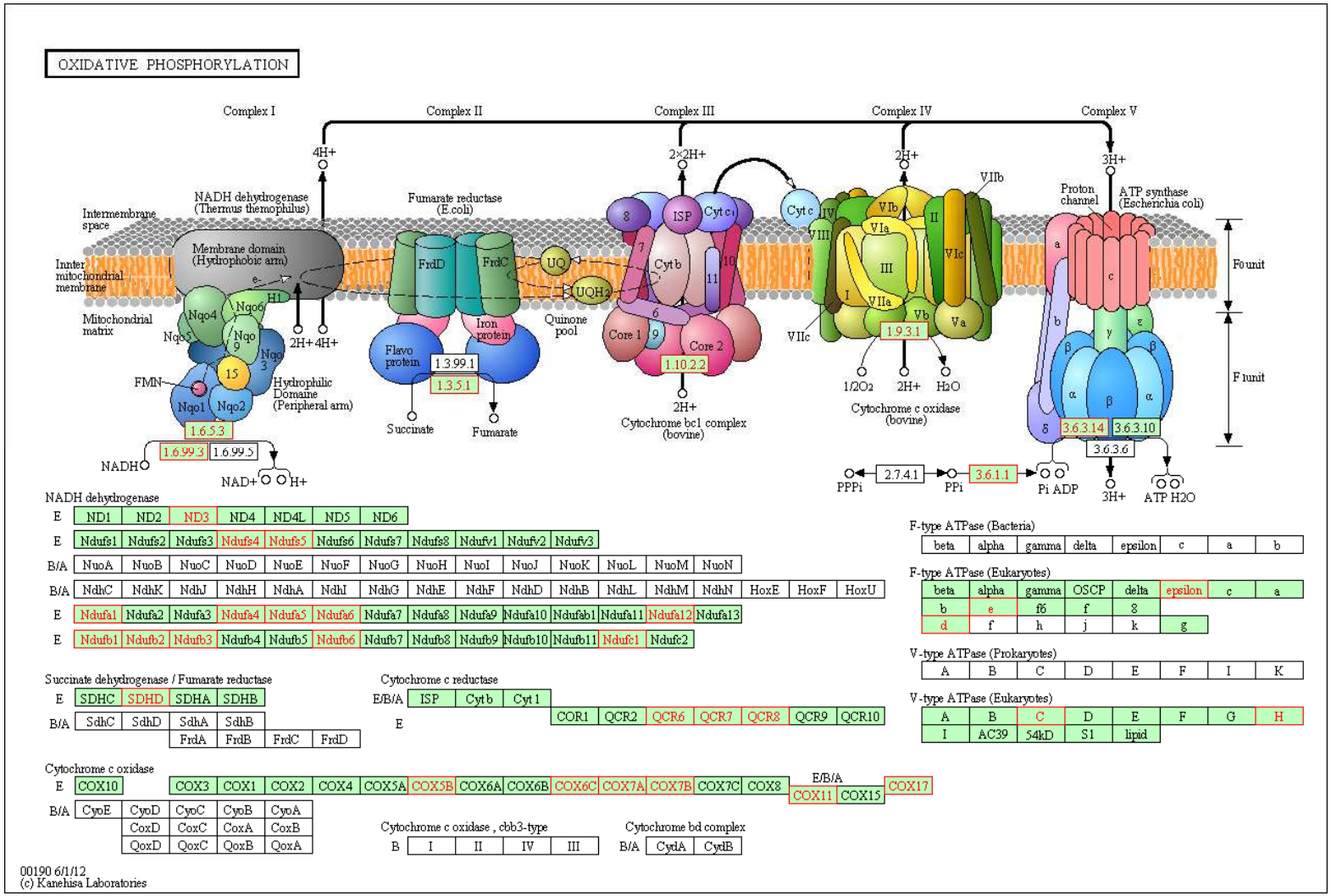

Figure 4.3.81:- Various oxidative phosphorylation reactions activated upon exposing Caco-2 monolayers to TMP alone formulations for 30 minutes (over-expressed genes are highlighted in red). The graph was created by KEGG online database.

No information was available on the role of cytochrome P450 enzymes (CYP450) on the oxidative metabolism of TMP until 2008 when Damsten et al investigated the role of human CYP450 enzymes on TMP metabolism. Our microarray data proposed that at least five CYP450 enzymes are involved in TMP metabolism as these enzymes were activated upon exposing the cells to TMP especially for 30 and 60 minutes (among the activated enzymes include CYP1A2, CYP2C9, CYP2C19 and CYP3A4). Our findings come in line with Damsten et al studies who reported that both CYP1A2 and CYP3A4 oxidize TMP by dehydrogenation of the terminal -NH_2 group to form an intermediate that interacts with glutathione (GSH) to form TMPG-1 and TMPG-2 metabolites (Damsten et al., 2008). Damsten and co-workers also suggest that CYP1A2 oxidizes TMP to TMP-N-oxide probably by using nonspecific monooxygenase (1.14.14.1) as shown in Fig. (4.3.28) and as suggested by (Kranendonk et al., 2008). TMP-N-oxide converts into intermediates that are dehydrogenated by CYP2A3 and get conjugated to GSH (which was also activated; 2.5.1.18) to form TMPG-5 and TMPG-6 (Damsten et al., 2008). On the other hand, CYP2C19 plays a role in demethylation of two of the three methoxy groups (-OCH_3) attached to TMP benzene ring to yield TMP-6 metabolite (Damsten et al., 2008).

Non specific monooxygenase (1.14.14.1), glutathione (2.5.1.18) and glucuronosyltransferase (2.4.1.17) were found to be over-expressed during the absorption of TMP (Fig. 4.3.28 & 4.3.29). The role of glucuronosyltransferase in trimethoprim metabolism is still unknown and therefore warrants further investigation.

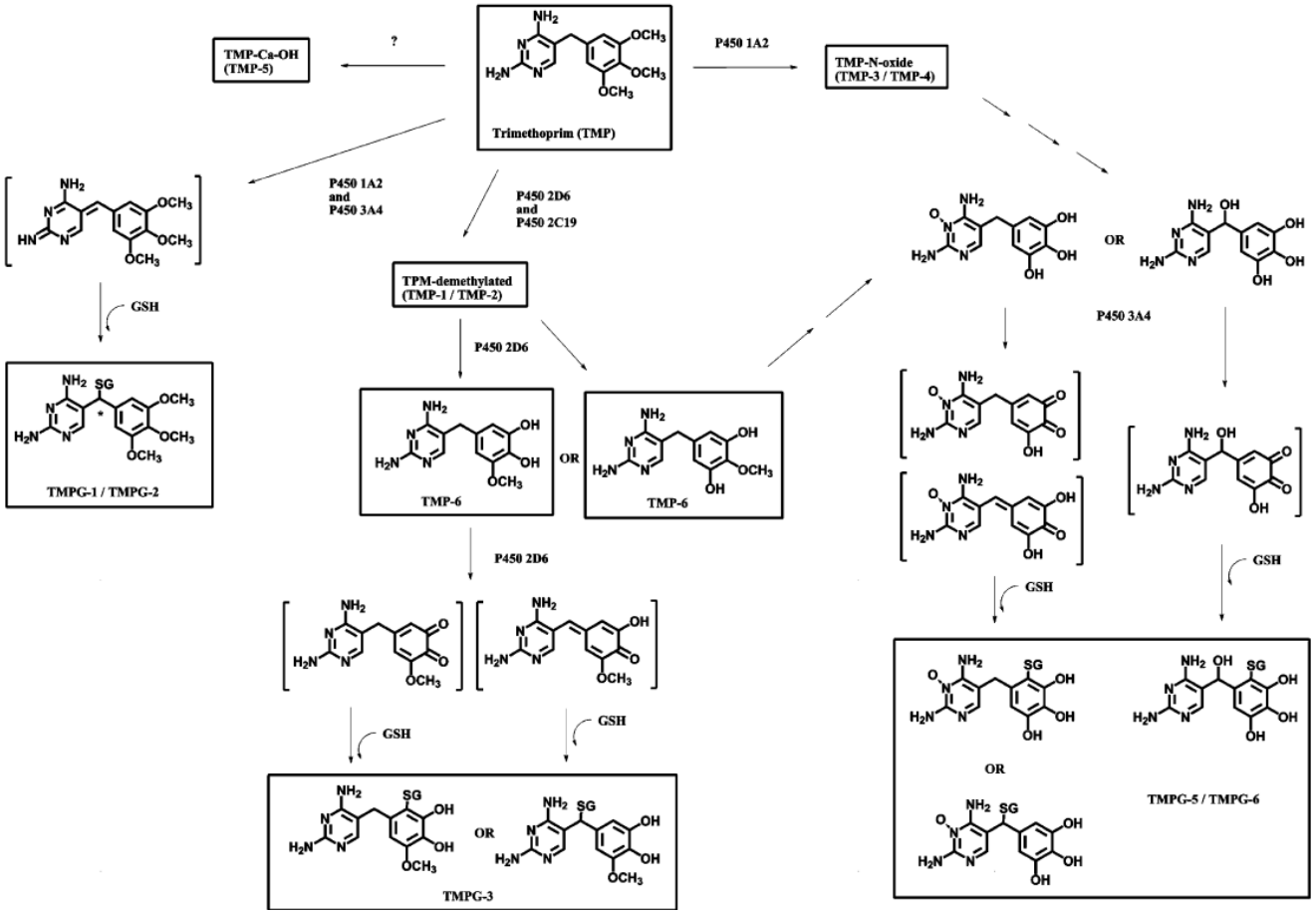

Figure 4.3.82:- Scheme showing all in vitro human metabolites and reactive intermediates (in brackets) of TMP. The role of CTYP450 isoforms involved in the metabolites formation is also shown in this figure. The figure is adapted from Damsten et al., 2008.

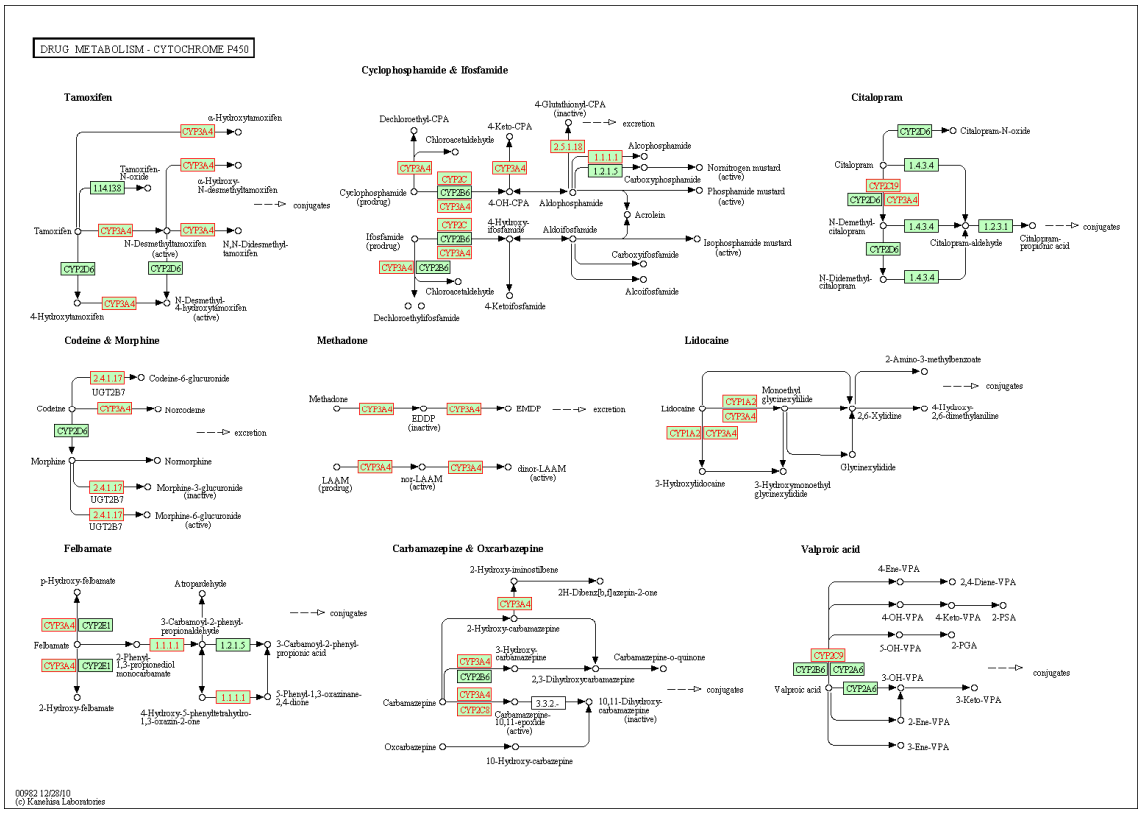

Figure 4.3.83:- Various metabolic pathways activated upon exposing Caco-2 monolayers to TMP alone formulations for 30 minutes (over-expressed CYP450 isomers and enzymes are highlighted in red). The graph was created by KEGG online database.

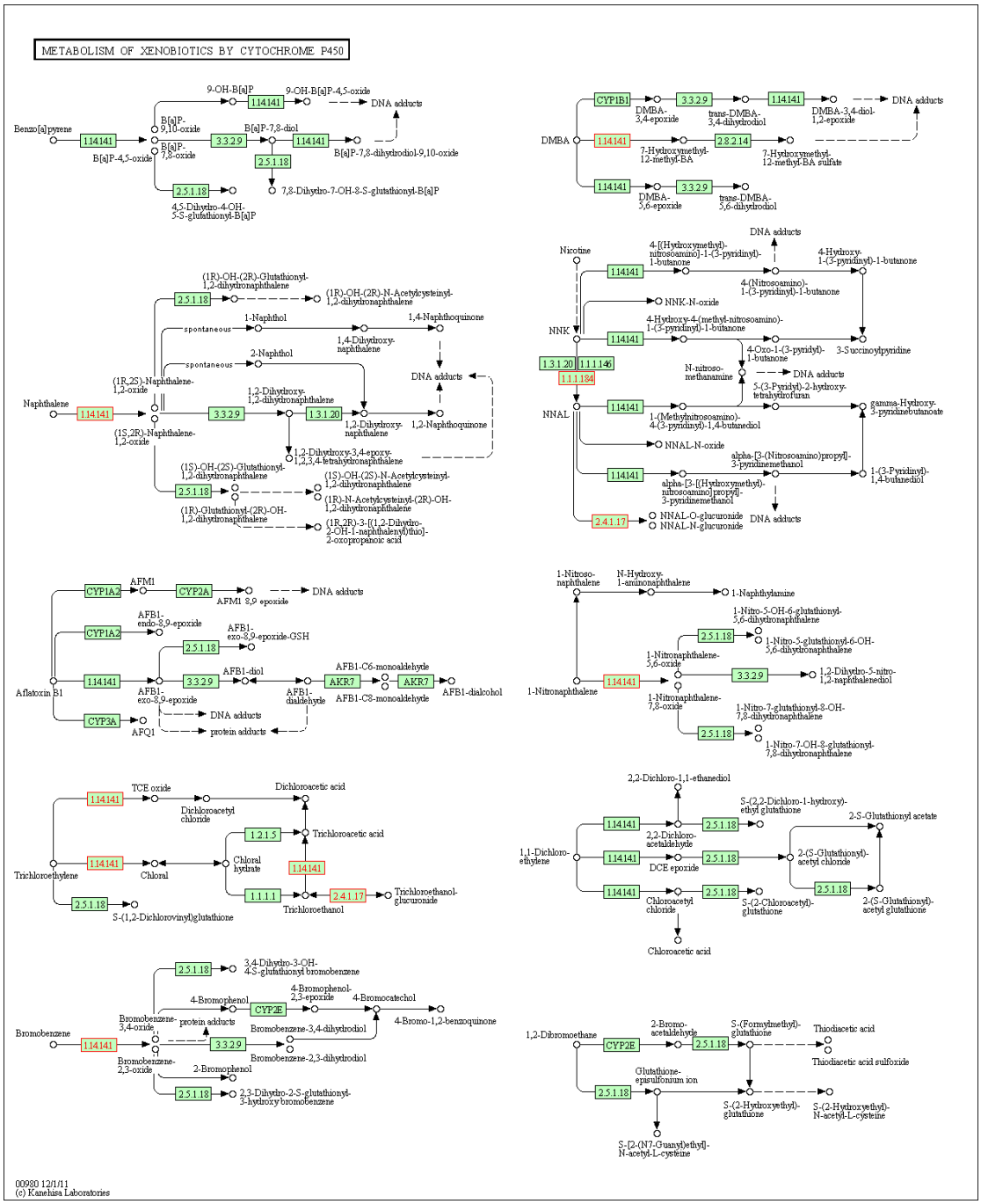

Figure 4.3.84:- Various enzymes activated upon exposing Caco-2 monolayers to TMP alone formulations for 30 minutes (over-produced enzymes are highlighted in red). The graph was created by KEGG online database.

Investigating the metabolic profile of the ion-paired formulations, the results showed the involvement of oxidative phosphorylation reactions and CYP450 enzymes in the metabolism of TMP in addition to the activation of glutamate metabolic enzymes such as glutamate

dehydrogenase (1.4.1.3) which converts L-glutamate into 2-oxoglutamate and ammonia (Di Prisco and Garofano, 1974) and glutaminase A (3.5.1.2).

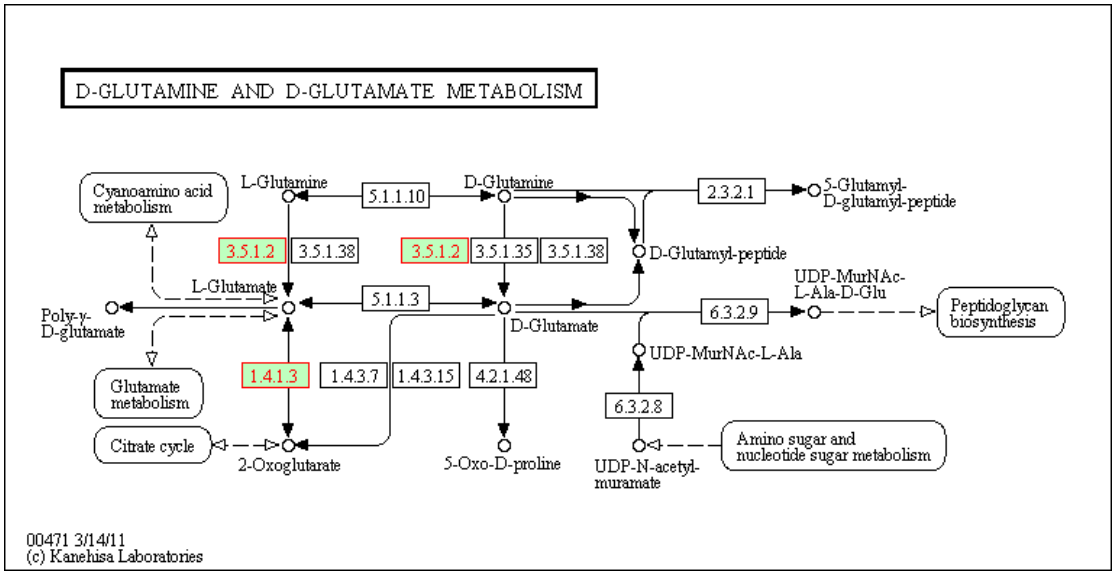

Figure 4.3.85:- Various enzymes involved in glutamic acid metabolism upon exposing Caco-2 monolayers to TMP: glutamic acid 1:8 ratio formulations for 30 minutes. glutamate dehydrogenase and glutaminase A (both highlighted in red) were over-produced. The graph was created by KEGG online database.

4.3.4. Conclusion

The ion-pairs formed between aspartic acid and TMP showed low aqueous binding constant, which was tripled when an amino acid with an extra alkyl side chain was used. The improvement of K_{11aq} upon using glutamic acid resulted in a 3 fold increase in the permeability profile of TMP. Probably the ion-paired formulation is transported as one moiety across the Caco-2 monolayers. Although ion-pairing TMP with glutamic acid had a negative effect on the partitioning capacities of the drug, the increased overall uptake suggest the involvement of active transporters rather than just passive diffusion. Genetic changes across Caco-2 showed that MRP7 is the major efflux protein that extrudes TMP from the cells while P-gp seems to have a minimal role in its efflux. Our results strongly agree with the literature, that TMP is actively uptaken by organic cation transporters as OCTN1 was over-expressed by 2.36 fold. The molar ratio of glutamic acid is believed to affect the expression of OCTN1 as its expression

reached 2.2 fold for 1:1 formulations and dropped to the basal state for 1:8 ion-paired formulations. Interestingly, the microarray data revealed the involvement of many cytochrome P450 isomers in the metabolism of TMP.

Chapter 5

Ciprofloxacin

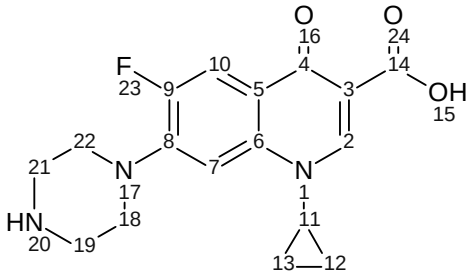

Papers relating to chapter 5

Amr ElShaer, Defang Ouyang, Peter Hanson and Afzal R Mohammed., Preparation and evaluation of amino acid based salt forms of model zwitterionic drug ciprofloxacin (submitted)

Preparation and characterization Ciprofloxacin salts with anionic and cationic counter ions

5.1.1. Introduction

Ciprofloxacin (CIP) (1-cyclopropyl-6-fluoro-4-oxo-7-piperazin-1-yl-quinoline-3-carboxylic acid) is a member of quinolone antibiotics which are widely used due to broad spectrum of activity, low resistance and high tolerance (Appelbaum & Hunter, 2000). CIP is characterised by the presence of two types of rings in its structure (Fig. 5.1.1); napthyridine ring which contains nitrogen atom at position 17 and 20, the second nucleus known as quinolone nucleus containing one nitrogen at position 1 (Park et al., 2002). Ciprofloxacin contains keto oxygen at C-4 and carboxylic acid side chains at C-3 which are essential for ciprofloxacin activity. It acts by inhibiting bacterial DNA gyrase enzyme; this process depends greatly on the pH and concentration of the acid (Neuman, 1988). Moreover, CIP is classified according to the biopharmaceutical classification system as a class IV drug (BCS IV). Its solubility is pH dependent and ranges between 0.15 mg/mL to 6.19 mg/mL at pH 7 and 5 respectively (Li et al., 2007).

As shown in Fig. 5.1.1 CIP is a zwitterionic molecule with pKa's of 6.09 and 8.74 and p*I* of 7.42 and is an ideal candidate for salt formation with both acidic and basic counter ions. Complexation of CIP with multivalent cations such as Ca^{+2}, Al^{+3}, Fe^{+3} and Mg^{+2} was approved by FDA as alternative for the parent active (Susana et al., 2009). Therefore these complexes were commonly used with CIP and other fluroquinolones in order to improve the solubility of these drugs with the aim of increasing their bioavailability (Susana et al., 2009). Nevertheless, fluroquinolone metal complexes were found to have a negative impact on bioavailability (Sahai et al., 1993; Kozjek et al., 1996) as the resultant complexes were too large to be effectively transported across the cell membranes. As a consequence, the efficacy of fluroquinolones was lower (Hart et al., 1991) and the risk of developing bacterial resistance was greater. Although

salt formation is a commonly used approach in order to improve drug solubility, fluroquinolones hydrochloride (HCl) salts (most commonly and widely used for CIP) failed to dissolve completely at intestinal pH of 6.8 (Breda et al., 2009). Another study conducted by Ramanuk et al showed an improvement in CIP solubility together with taste masking for a new salt with saccharin (Romanuk et al., 2009).

Hence, improving the solubility of fluroquinolones without impairing their permeability behaviour would be a challenging task which if achieved would provide CIP within a BCS biowaiver.

The aim of this study was to improve the solubility and dissolution properties of CIP via salt formation. In addition, we investigated the role of inter- and intra molecular interaction between the drug and amino acids by integrating experimental and theoretical approaches.

Investigation of published literature has shown that limited work has been done on theoretical studies on CIP complexes as listed in Table 5.1.1 (Aristilde et al., 2010; Turel et al., 2008; Aristilde et al., 2008; Sadeek et al., 2011). These studies utilised the simple force field (COMPASS force field) and short simulation time (up to 40 ps) resulting in low precision. The current paper utilises all-atomic molecular dynamics simulation with general AMBER force field (gaff) to study the molecular interaction between CIP molecules and amino acids.

Table 5.1.1 Computer simulation about ciprofloxacin complexes

Complexes	Simulation details	References
Ciprofloxacin/humic substance complexes	InsightII version 2000.1 software package with COMPASS force field, 5-A° layer of water box; up to 40 ps	(Aristilde et al., 2010)
Mg/ciprofloxacin complexes	HyperChem and the MM+ force field Langevin dynamics with a simulated annealing method	(Turel et al., 2008)
Ciprofloxacin/metal complexes	Cerius package with COMPASS force field, 35 ps simulation, water box	(Aristilde et al., 2008)
Solid complexes [Y(CIP)2(H2O)2]Cl3·10H2O and [ZrO(CIP)2Cl]Cl·15H2O	Gaussian98W package by density functional theory (DFT) at the B3LYP/CEP-31G level of theory	(Sadeek et al., 2011)

5.1.2. Materials and methods

5.1.2.1. Materials

Ciprofloxacin, L-Arginine (non-animal source), L-Histidine (Reagent plus ™), L-Lysine, L-Glutamic acid (Reagent plus ≥ 99%), L-aspartic acid (≥ 98%) and Potassium bromide (99% FT-IR grade) all were purchased from Sigma Aldrich, UK. Methanol and acetic acid were purchased from Fischer scientific.

D_2O (99.9% min) was purchased from Coss Scientific Instrument Ltd.

5.1.2.2. Methods

5.1.2.2.1. Salt preparation

Equimolar amounts of CIP and the free amino acid were solubilised in water, and the solutions were mixed and stirred until equilibration was achieved and filtered. The filtrate was transferred into a stainless steel pan and freeze dried for 42 h using Virtis Advantage (wizard 2.0) freeze dryer. Salts were primary dried at -40^{o}C shelf temperature and under -55 mTorr vacuum for 36 h and secondary dried at 20 ^{o}C for 6 h.

5.1.2.2.2. HPLC analysis

The amount of ciprofloxacin (CIP) dissolved in the samples was quantified by HPLC using a Dionex 1100 system fitted with autosampler (AS50), gradient pump (GP50), UV detector (UVD 170U) and RP-C18 analytical column (Phenomenex 110A, 150x4.6 mm, 5µm). Mobile phase consisting of methanol: water: acetic acid (840:158:2) and pumped at 1.0 mL/min was used to elute CIP. *λmax* was determined using Unicam UV-Visible Spectrophotometer and the HPLC UV detector was set at *λmax* of 280 nm. CIP was eluted with a retention time of 1.5±0.1 min and a rectilinear calibration curve was established at concentration range between 10-200µg/mL.

5.1.2.2.3. Phase solubility diagram.

Phase solubility diagram was established by measuring the saturated solubility of CIP free drug with various concentrations of cationic amino acids (L-arginine, L-lysine and L-histidine) and anionic amino acids (L-aspartic acid and L-glutamic acid) as previously discussed by (Elshaer et al., 2011). Excess CIP was added into screw-capped tubes containing serial dilutions of the amino acids solutions and agitated at room temperature (Stuart SB 162 stirrer) for 24 h. After equilibrium the supernatant was filtered through 0.45 µm filters and analysed by HPLC to determine CIP concentration. The pH of amino acid solutions was monitored using a Xisherbrand Hydrus 500 pH meter.

5.1.2.2.4. Differential scanning calorimetry and Thermogravimetric analysis

Thermal events such as melting point and crystallization exotherms of CIP and its prepared salts were measured using Differential Scanning Calorimeter (Pyris Diamond DSC). Approximately, 2-5 mg of the salts were weighed and transferred to an aluminium sample pan (50 µL capacity) then sealed with aluminium top. Intra cooler 2P system was used to initially cool the samples to 50 ^{o}C and then sample heated to 300 ^{o}C at rate of 10 ^{o}C/min. Nitrogen was used as a purge gas at a flow rate of 20 mL/min, Indium and Zinc were used to calibrate the heat flow and melting point onset (156.6 ^{o}C for Indium and 419.47 ^{o}C for Zinc). The obtained thermograms were analysed using Pyris Manager Software (version 5.00.02). The experiment was performed in triplicate and an empty aluminium pan, sealed in the same way of the samples, was used as a reference cell for all the measurements.

Moisture content and decomposition temperature of CIP and its prepared salts were determined using thermogravimetric analyser (Pyris 1 TGA, Perkin Elmer). 5- 10 mg of samples were added to an open pan and analysed at temperature range 30- 300 ^{o}C at 10 ^{o}C/min scanning rate and under nitrogen stream. The resultant thermograms were analysed using Pyris Manager Software (version 5.00.02)

5.1.2.2.5. FT-infrared (IR) spectroscopy

Nicolet IR 200 spectrometer (Thermo electron corporation) was used to measure FTIR absorbance spectra of CIP and its salts using the KBr disc technique. Crystalline KBr was dried at 65^{o}C over night before use. Samples were prepared by mixing CIP or its salts with dry KBr at 1:100 (w/w) ratio and pressed at 8 tones for 5 min (using Specac tablet presser) to form KBr discs. 64 scans were performed over wavelength 4000- 400 cm^{-1} for each sample. FTIR spectra were interpreted using EZ OMNNIC 7.0 software.

5.1.2.2.6. ^{1}HNMR

Samples were analysed with Bruker Avance DPX-250 NMR (at 250.1 MHz) and Bruker Topspin software was used to analyse the data. Approximately, 1-2 mg of the salts were dissolved in 1 mL of deuterated water (D_2O) and placed in a sample capillary vial up to 5-10 cm height.

5.1.2.2.7. Solubility and dissolution studies.

The method of Hugchi and Connor (Higuchi & Connors, 1965) was used to measure the solubility of CIP salts. An excess amount of CIP or its salts was added to capped test tubes with 5 mL of deionised water and stirred for 24 hours at room temperature until equilibrium was reached. Subsequently, the suspension was filtered through 0.45µm syringe filters and suitably diluted and the concentration was measured by HPLC.

Conventional tablets weighing 500 mg and containing 50 mg of CIP or equivalent amounts of the prepared salts were prepared for dissolution studies. Starch was used as a tablet binder and anhydrous lactose was used as a diluent in 1: 8 ratio respectively. All the excipients were geometrically mixed with the active ingredients and compressed using (Specac tablet presser) at 8 tones pressure for 10 minutes.

USP II paddle method (ERWEKA DT-600) was used to perform the in-vitro dissolution studies. The prepared tablets were placed into dissolution vessels containing 900 mL of phosphate

buffer (pH 7.2) and the dissolution media was maintained at 37^{o}C±0.5^{o}C and stirred at 50 rpm. 5mL of samples were collected at predetermined time intervals (1, 5, 10, 15, 20, 25, 30 and 40 min) then filtered through 0.45 μm Millipore filters. The dissolution media was replaced by 5mL of fresh dissolution fluid in order to maintain a constant volume. The samples were analysed by HPLC as mentioned above.

5.1.2.2.8. Simulation studies

MD simulations were carried out using the AMBER11 software package (Case et al., 2005) with the general AMBER force field (gaff) for all molecules (Wang et al., 2005). All molecules were built by Discovery Studio Visualizer 3.1 (http://accelrys.com/products/discovery-studio/index.html). At neutral pH (pH ~ 7), all the primary amines of amino acids were protonated and carboxyl groups of amino acids were negatively-charged. Using the LEAP module in AmberTools 1.5, the amino acids were positioned near the ciprofloxacin molecules (at least 3 Å for enough sampling). The electrostatic interactions were calculated using the particle mesh Ewald method (Darden et al., 1993; Essmann et al., 1995; Crowley et al., 1997; Sagui et al., 1999; Toukmaji et al., 2000; Sagui et al., 2004) and the cutoff was 10 Å. Using the LEAP module in AmberTools 1.5, the complex structure was immersed in a truncated octahedral water box with a solvation shell of 10 Å thickness using TIP3P model for water (Jorgensen et al., 1983). This procedure resulted in solvated water structures containing approximately 10 000 atoms which included 164 ciprofloxacin atoms and different numbers of amino acid atoms, with the remainder being water molecules.

The minimization procedure for solvated complex consisted of two steps. In the first stage, the complex was fixed and positions of water and ions were minimized. The solvated structures were then subjected to 500 steps of steepest descent minimization followed by 500 steps of conjugate gradient minimization (Leach, 2001; Hans-Dieter et al., 2008). During this minimization process the complex was fixed in its starting conformation using harmonic

constraints with a force constant of 500 kcal/mol/Å^2. In the second stage, the entire system was minimized by 1000 steps of steepest descent minimization followed by 1500 steps of conjugate gradient minimization without the restraints.

The minimized structure was then subjected to 20 ps of MD, using a 2 fs time step for integration. During the MD simulation the system was gradually heated from 0 to 300 K using 10 kcal/mol/Å^2 weak positional restraints on the complex. The SHAKE algorithm was used in which all bonds involving hydrogen are constrained (Ryckaert et al., 1977). After the system was heated at constant volume with weak restraints on the complex, MD was performed for 1 ns with a time step of 2 fs under constant pressure/constant temperature (NPT ensemble) at 300 K with an average pressure of 1 atm without positional restraints. The random number seed of every restart was changed (Cerutti, 2008). Isotropic position scaling (Berendsen, 1984) was used to maintain the pressure and a relaxation time of 2 ps was employed. SHAKE was used to constrain bonds involving hydrogen and the temperature was kept at 300 K with Langevin dynamics (Wu & Brooks, 2003) using a collision frequency of 1.0 ps^{-1}.

5.1.3. Results and discussion

5.1.3.1. Ciprofloxacin phase solubility profile.

CIP is a zwitter ionic molecule as it has a positively charged nitrogen atom (N^{20}) and negatively charged carboxylic group (Fig. 5.1.1). Therefore, the ability of CIP to form new salts with cationic and anionic amino acids was investigated in this study.

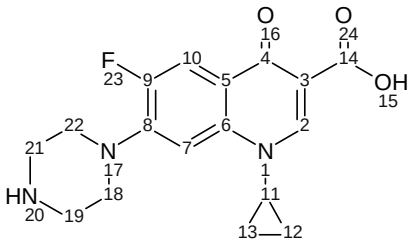

Figure 5.1.86. Structure of ciprofloxacin. The central structural unit is a quinolone ring with a fluorine atom at the 9-position, a piperazine moiety at the 8-position, a cyclopropyl ring at position 1 and a carboxyl group at position 3. There are two pK values, pKa;COOH = 6.09 and pKa;N20 = 8.7.

Fig. 5.1.2 shows the phase solubility diagram of CIP with three basic amino acids namely; L-arginine, L-lysine and L-histidine and two acidic amino acids; L-aspartic acid and L-glutamic acid. Phase solubility diagram show that both aspartic acid and glutamic acid ionised CIP to a greater extent while the extent of ionisation for CIP was lower with basic amino acids such as arginine and lysine. No ionisation was observed upon inclusion of histidine. Therefore, four salts were prepared in this study and further investigated by FT-IR, ^{1}HNMR, DSC and TGA to confirm salt formation.

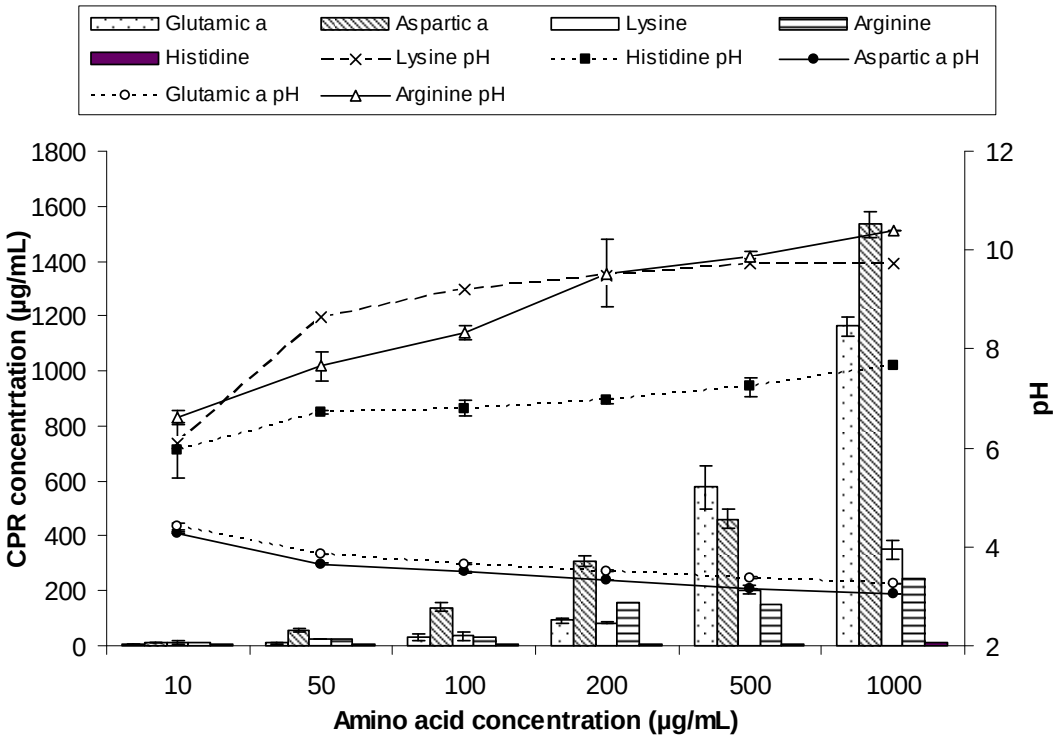

Figure 5.1.87:- Phase solubility diagram of CIP in the presence of different concentrations of arginine, lysine, histidine, glutamic acid and aspartic acid at different pH (n=3)

CIP solubility in water was found to be 7.22±1.02 µg/mL at 25 ^{o}C. The use of acidic amino acids considerably improved the solubility of CIP. CIP solubility increased significantly upon solubilising in L-glutamic acid solution especially at high concentrations of the counter ion. Around 1.2 mg of CIP was solubilised in 1 mL of 1000 µg/mL of glutamic acid. These results suggest that CIP acts as a strong base in glutamic acid solution possibly due to the big difference between the pKa values of CIP and glutamic acid (8.74 and 2.19 respectively). Therefore, the basic amino group is completely ionised in glutamic acid solution favouring salt formation between the basic group of CIP and the acidic group of the amino acid. Similarly, the solubility of CIP increased in L-aspartic acid solution and could be potentially due to salt formation between the two ionised species (these data were further confirmed using FT-IR and ^{1}HNMR as discussed below).

On the other hand, solubilizing CIP in various concentrations of L-histidine solutions showed no improvement in solubility with a maximum solubility of 9.65±0.28 µg/mL at 1000 µg/mL of histidine solution. Poor solubilisation of CIP can potentially be due to similar pKa of basic group on histidine (pKa 6) and the carboxylic group of CIP resulting in no ionisation of the parent drug.

Interestingly, increasing the concentration of L-arginine solution was found to improve the solubility of CIP. At a concentration of 10 µg/mL arginine, CIP solubility was 10.7±2.8 µg/mL and the solubility increased linearly upon increasing the concentration of arginine solution where CIP solubility was 247.8±4.2 µg/mL at 1000 µg/mL of arginine solution (Fig. 2).

Although the pKa of the –NH2 side chain of L-arginine (12.48) is much higher than the pKa of CIP acidic side chain, CIP was ionised to a lower degree. A similar trend was observed when L-lysine was used as CIP solubility increased from 11.62±5.8 µg/mL to 350.7±34 µg/mL when lysine concentration increased from 10 µg/mL to 1000 µg/mL.

Characterization of CIP salts

5.1.3.2. Fourier Transform Infrared Spectroscopy (FT-IR)

The phase solubility diagram has shown that CIP possibly dissociates in acidic amino acids solution and some of the basic amino acids. The next stage of the work was to prepare five salts of CIP amino acids and to investigate and characterise the salt formation using physico-chemical methods such as FT-IR, ^{1}HNMR and DSC.

Fig. 5.1.3 shows the FT-IR spectra of CIP, CIP aspartate and CIP glutamate. CIP had characteristic absorption peaks at 3044 cm^{-1} which can be assigned to C-H olefinic and aromatic chains, 1617.8 corresponding to C4O16 keto group. Since CIP is in the zwitterionic form, the carboxylic group C14=OOH does not appear in CIP FT-IR spectrum (Romanuk et al., 2009).

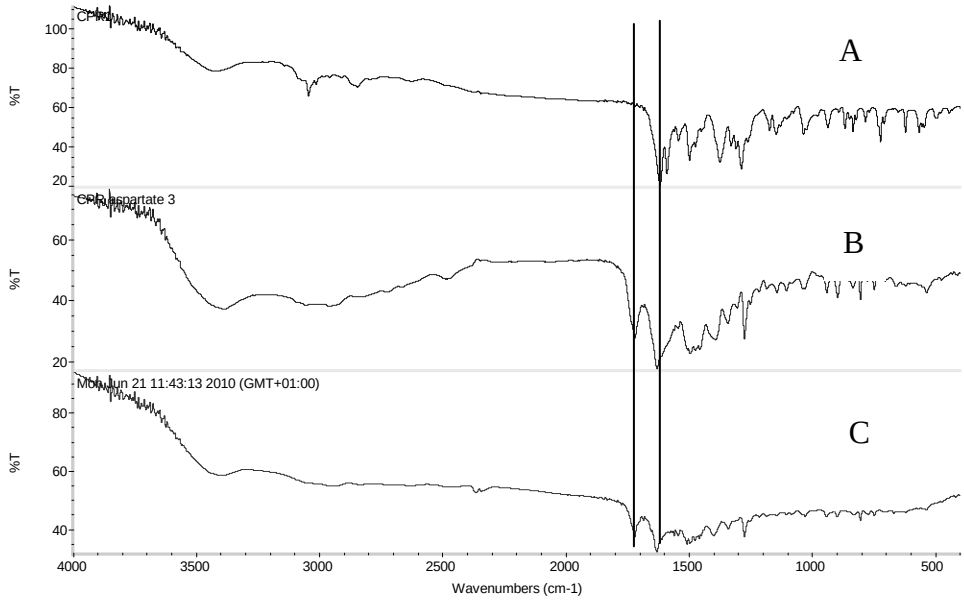

Figure 5.1.3:- FTIR spectra of (A)Ciprofloxacin, (B) CIP L-aspartate and (C) CIP L-glutamate

Interestingly, this carboxylic group was present in CIP glutamate and aspartate salts at 1720 and 1719 respectively suggesting that the zwitterionic nature of CIP was reverted by proton transference from L-aspartic acid and L-glutamic acid. These results are in line with results obtained by (Romanuk et al., 2010) On the other hand, FT-IR data for basic amino acids with

CIP does not show the C4O16 keto group at 1617.8 but had an absorption band at 1579.55 and 1646.4 corresponding to carboxylic group C=O of lysine (Ogura et al., 1998) and arginine (Petrosyan, 2007) respectively. Upon comparing CIP lysine and lysine free amino acid, similar spectrum was observed which support our findings (Fig. 5.1.4 C& D). Our results were further confirmed using ^{1}HNMR as discussed below.

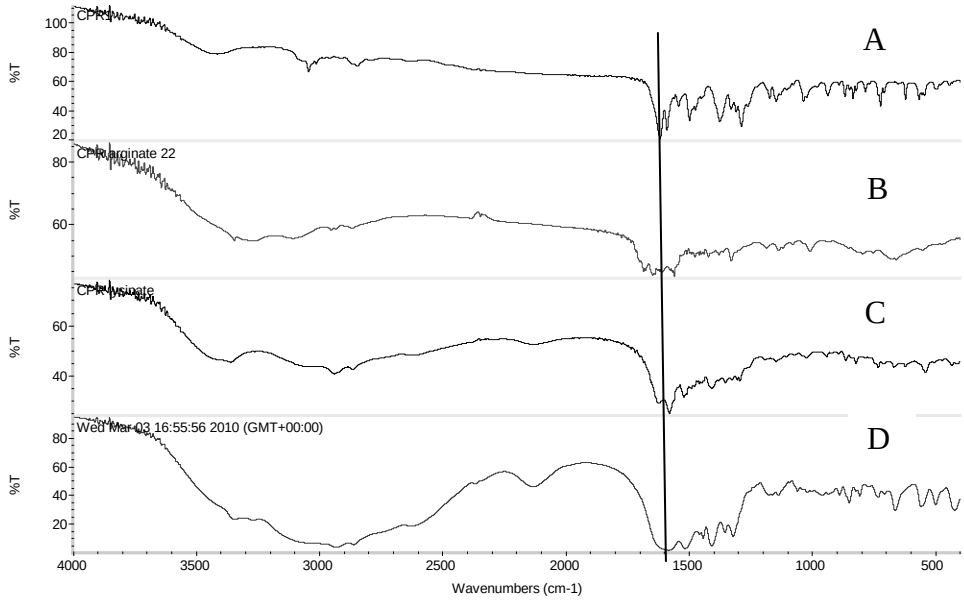

Figure 5.1.4:- FTIR spectra of (A)Ciprofloxacin, (B) CIP arginine, (C) CIP lysine, (D) lysine

5.1.3.3. ^{1}HNMR

To further confirm the salt formation and investigate the molar ratio of interaction between CIP and the counter ions, the total number of protons in the prepared salts was studied using ^{1}HNMR.

Fig. 5.1.5 shows the ^{1}HNMR data for CIP aspartate. Both C12H2 and C13H2 of the cyclopropyl group of CIP appeared at 1.08 and 1.3 ppm, while the C11H group was deshielded at higher (δ) due to the deshielding effect exerted by N1. Piperazine ring 8 protons C22H2, C21H2, C18H2 and C19H2 appeared as multiplet at around 3.79 ppm. C2H, C7H, C10H appeared deshielded at

8.5, 7.4 and 7.33 respectively. The total integration of CIP was found to be 16 similar to what was previously reported by Wetzsein et al (1999).

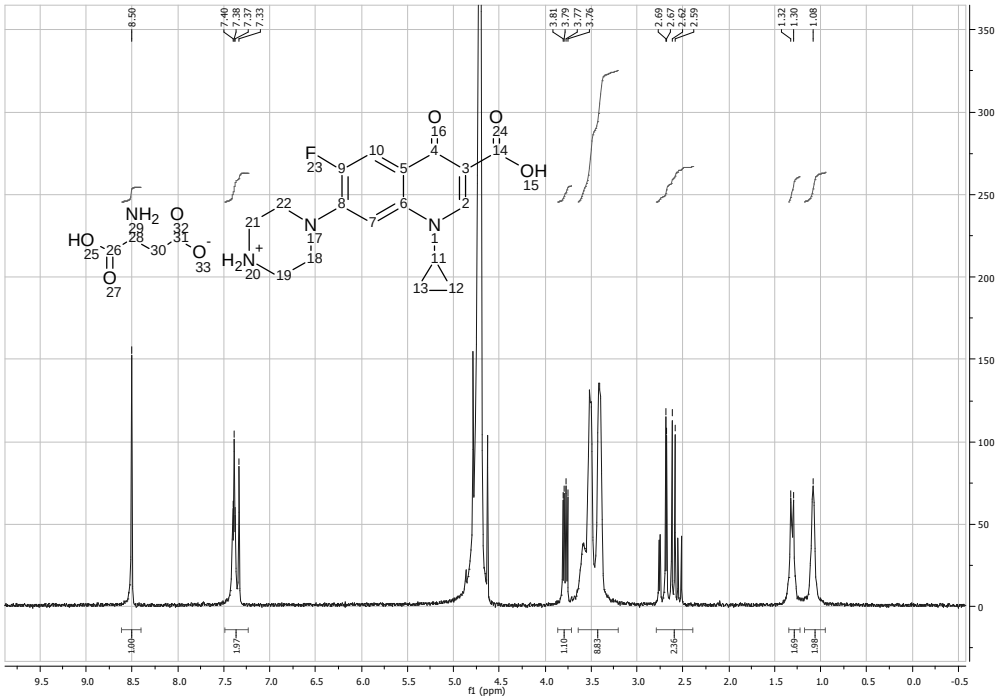

Figure 5.1.5:- ^{1}HNMR spectra for Ciprofloxacin Aspartate dissolved in D2O

Two new bands appeared at 2.67 and 3.81 ppm corresponding to three protons of one molecule of aspartic acid (C28H and C30H2). This data shows that one molecule of CIP has formed a salt with one molecule of aspartic acid in 1:1 ratio.

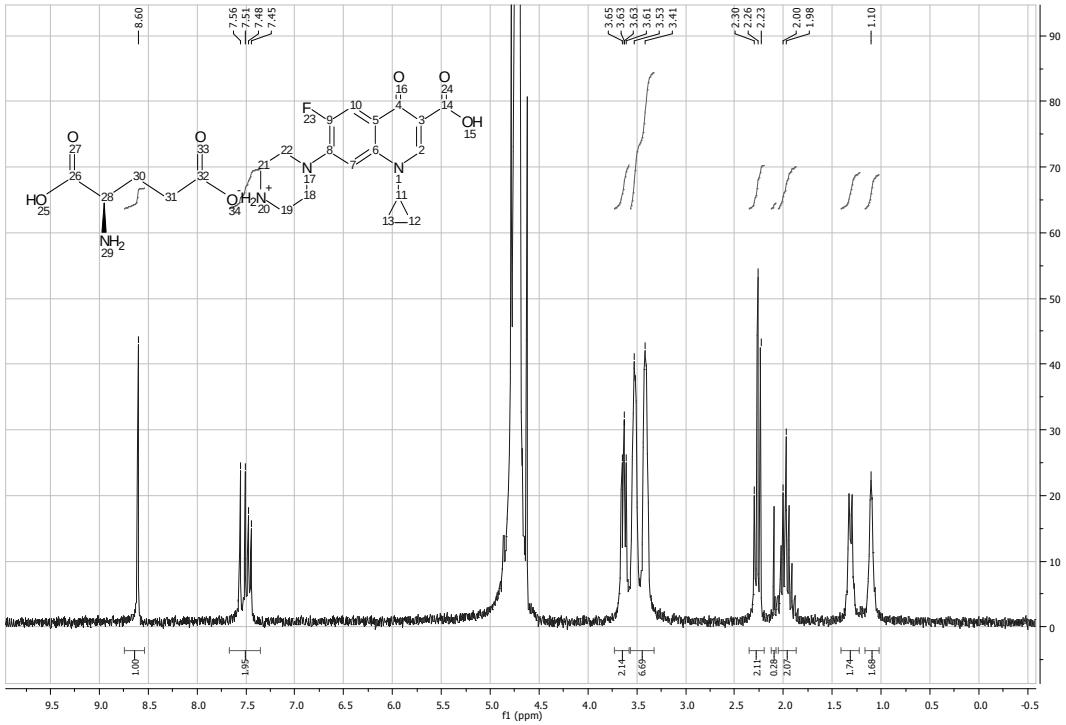

Figure 5.1.6:- ^{1}HNMR spectra for Ciprofloxacin glutamate dissolved in D2O

Similarly, the ^{1}HNMR spectrum of CIP glutamate (Fig. 5.1.6) showed 5 new proton assignments between 1.98 and 2.3 ppm which correspond to the 5 alphatic protons of L-glutamic acid. However, the ^{1}HNMR data for CIP basic amino acid preparations show no salt formation and only protons of the free basic amino acids were detected by the ^{1}HNMR (see figures 5.1.7 & 5.1.8).

These data suggest that only acidic amino acids were capable of forming salts with CIP, while the basic amino acids failed to form salts as suggested by the FT-IR studies above.

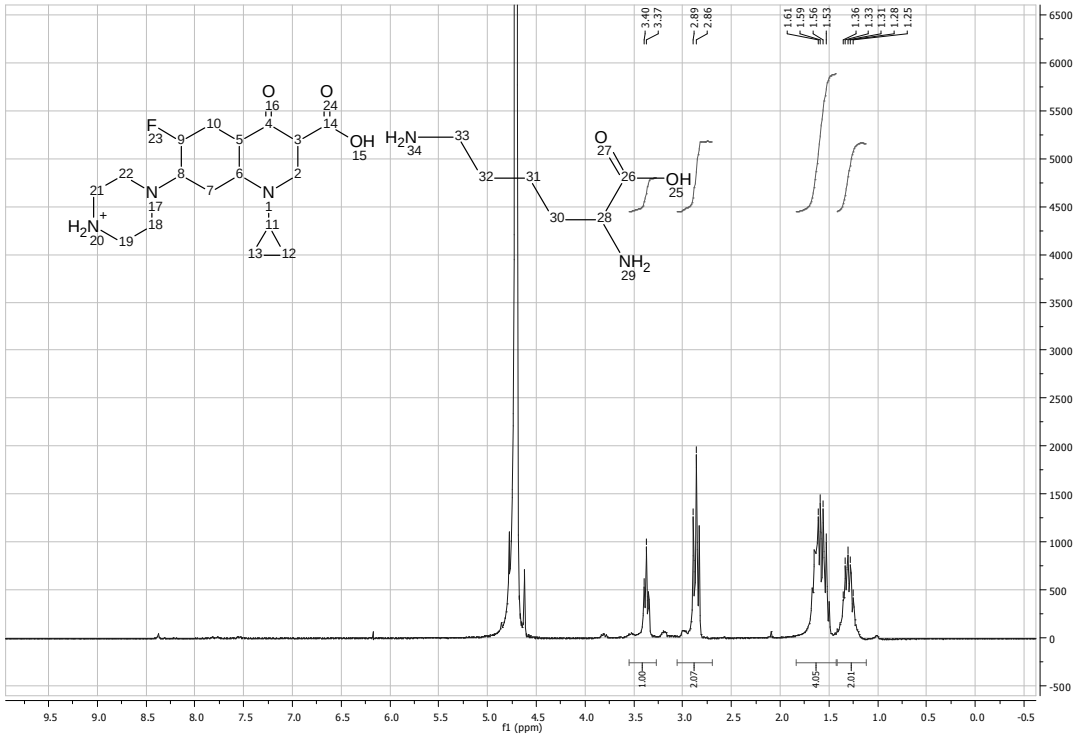

Figure 5.1.7:- ^{1}HNMR spectra for Ciprofloxacin lysine dissolved in D2O

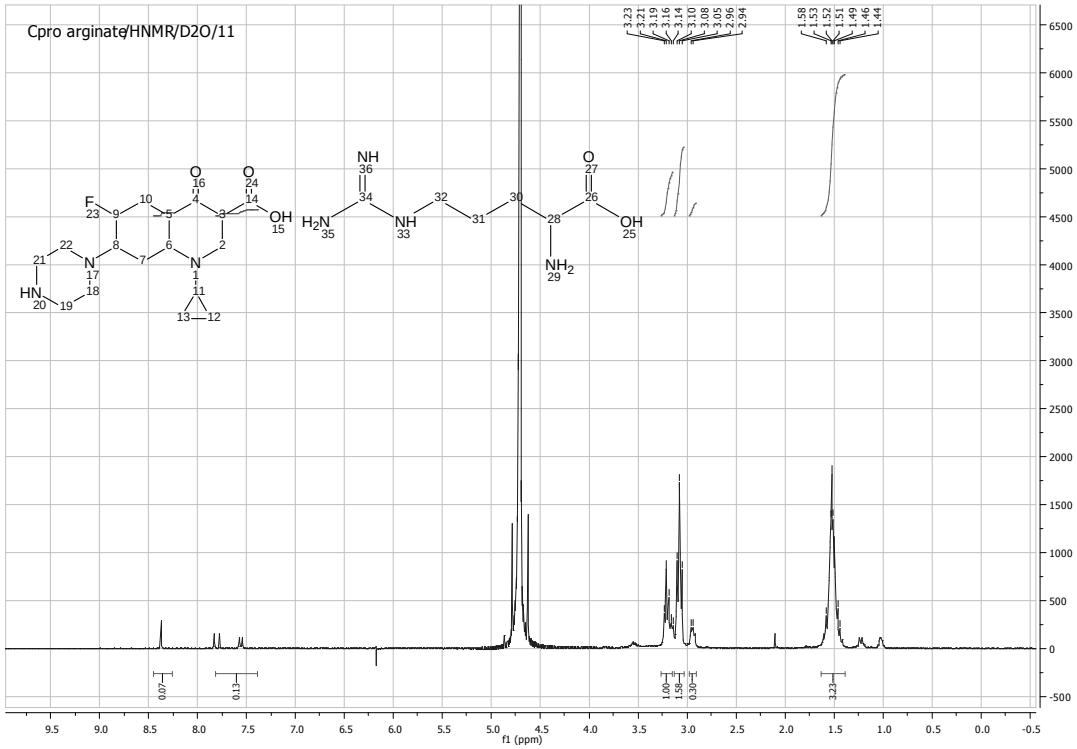

Figure 5.1.8:- ^{1}HNMR spectra for Ciprofloxacin arginine dissolved in D2O

5.1.3.4. Differential scanning calorimetry and thermogravimetric analysis.

New salts have different physical behaviour from their parent components. Therefore, the melting point and degradation temperature of CIP and its salts were investigated using DSC and TGA.

CIP free drug was in the crystalline form and showed an endothermic peak at 272.15 ^{o}C (ΔH= 173.19 J/g) corresponding to its melting endotherm. TGA data showed start of drug degradation upon completion of its melt. On the other hand, the CIP aspartate salt had two endothermic peaks at 224.63 and 237.8 ^{o}C suggesting that the CIP aspartate salt has two forms. On the other hand, the CIP glutamate salt showed a single melting endotherm at 203.35^{o}C. Arginine CIP formulations melted at 227.31 ^{o}C which was found to be similar to that of arginine free base and the absence of CIP melting endotherm or any other new melts confirms the failure of salt formation between CIP and basic amino acids as discussed previously.

5.1.3.5. Simulation studies

Characterisation studies showed that anionic amino acids form new salts with CIP while the cationic amino acids failed to form any salts with the drug. This was contrary to the generally accepted hypothesis that a 3 unit difference in pKa between the parent compound and the counter ion results in salt formation. Therefore, the role of inter and intra molecular interaction between CIP and the amino acid was investigated using molecular dynamic simulation studies in order to gain further understanding of CIP in different solutions of amino acids. Two amino acid models were used in this study; aspartic acid and histidine as aspartic acid resulted in CIP salt formation while histidine failed.

Figure 5.1.9 shows the interaction between CIP molecules; two CIP molecules in water aggregate together after 400 ps due to the hydrophobic interaction thereby further confirming the role of hydrophobic forces in the low solubility of CIP. The lab based experiments showed

that CIP solubility in aspartic acid increased significantly especially at high concentrations of aspartic acid solution. Thus the interaction of two CIP molecules with one aspartic acid molecule in water (low concentration), and the interaction of two CIP molecules with four aspartic acid molecules in water (high concentration) was studied using molecular simulations. As shown in Figure 5.1.10, the aggregation of CIP molecules is delayed until 800 ps in the presence of one amino acid (aspartic acid) molecule. On the other hand, aggregation of CIP molecules was hindered in the solution with high concentration of amino acid (four aspartic acid molecules) as shown in Figure 5.1.11. Data obtained from the simulation studies were in agreement with the results of experiments where high concentrations of amino acid solutions (e.g. 500 and 1000 μg/mL) resulted in significant increases in solubilisation capability, while the low concentration of amino acid solutions have less effect. However, it was interesting to see that inclusion of histidine did not prevent aggregation of CIP molecules even at high concentrations (with four histidine molecules), as shown in Figure 5.1.12. It further confirms experimental results of the solubilisation incapability of histidine. These results indicated that two factors influence the inter- and intra-action between CIP molecules and amino acids. On one hand, CIP is an amphoteric electrolyte and acts as the base in aspartic acid solution due to the difference between the pKa values of -NH group of CIP (8.74) and -COOH group of aspartic acid (3.86). The positively-charged -NH group of CIP and negatively-charged -COOH group of aspartic acid form the electrostatic interaction. The pKa of the basic amino group of L-histidine (6) is almost the same as that of the CIP carboxylic group (6.09) possibly resulting in no enhancement in solubility. Besides, hydrophobic interaction is also an important factor in CIP aggregation. When ionic interactions and/or hydrophobic interactions between CIP molecules and amino acid molecules are stronger than hydrophobic interaction between CIP molecules, the solubilisation process is accelerated.

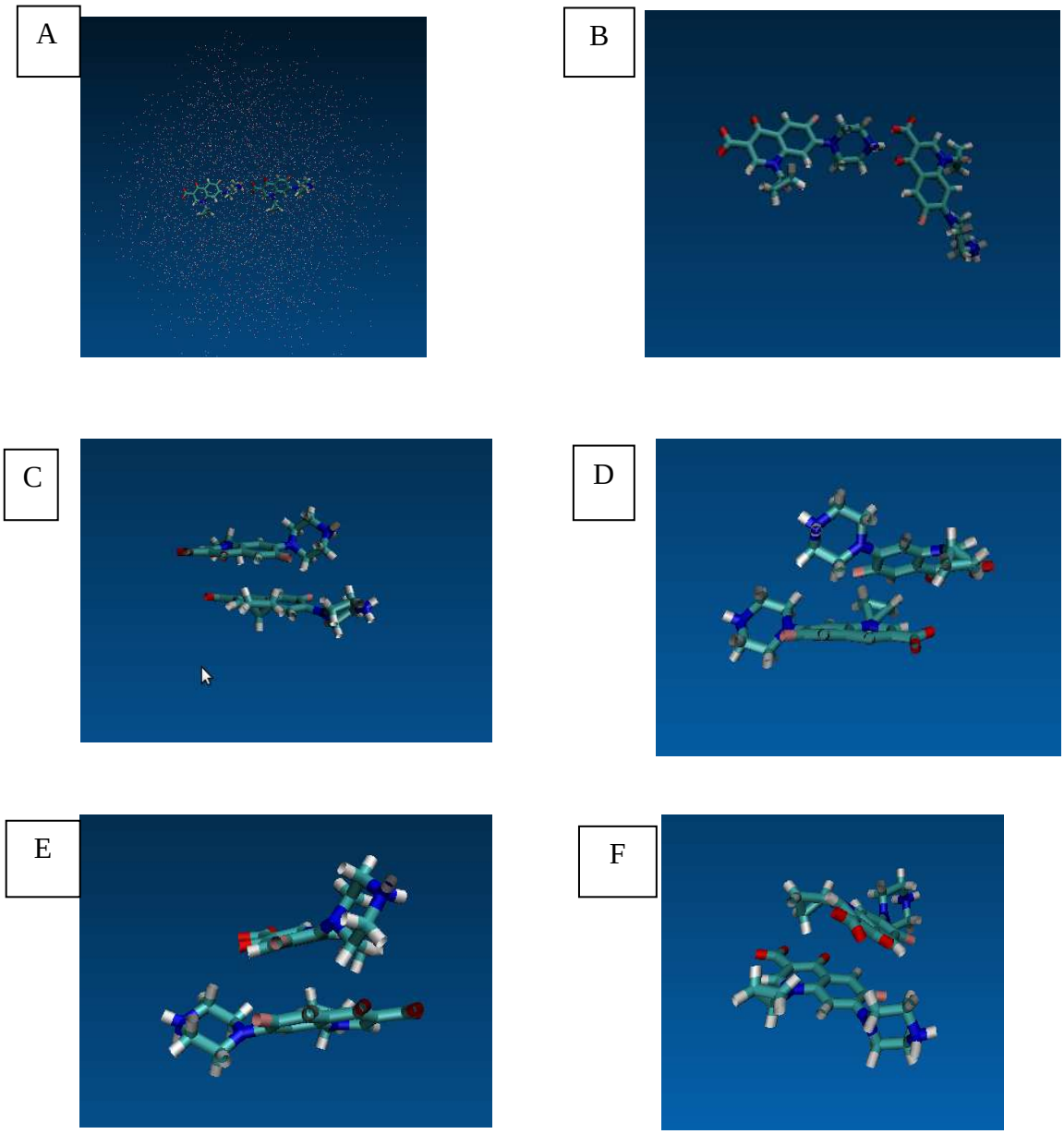

Figure 5.1.9. Snapshots of two ciprofloxacin molecules in water: (A) at 0 ns, (B) after 200 ps, (C) after 400 ps, (D) after 600 ps, (E) after 800 ps and (F) after 1 ns. (Water is only shown in A) and is ignored from B) to F) for clarity)

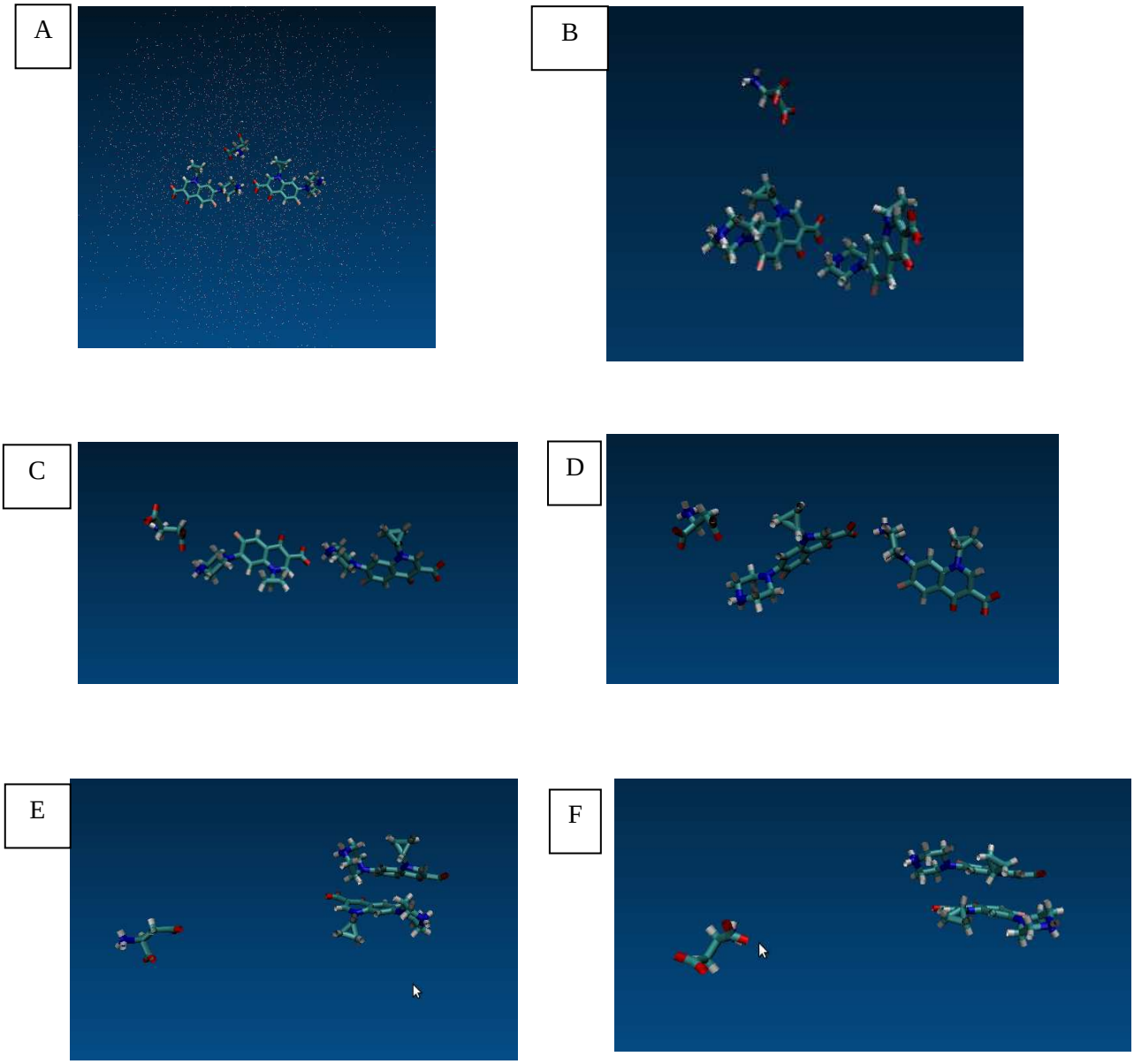

Figure 5.1.10. Snapshots of two ciprofloxacin molecules with one aspartic acid molecule in water: (A) at 0 ns, (B) after 200 ps, (C) after 400 ps, (D) after 600 ps, (E) after 800 ps and (F) after 1 ns. (Water is only shown in A) and is ignored from B) to F) for clarity)

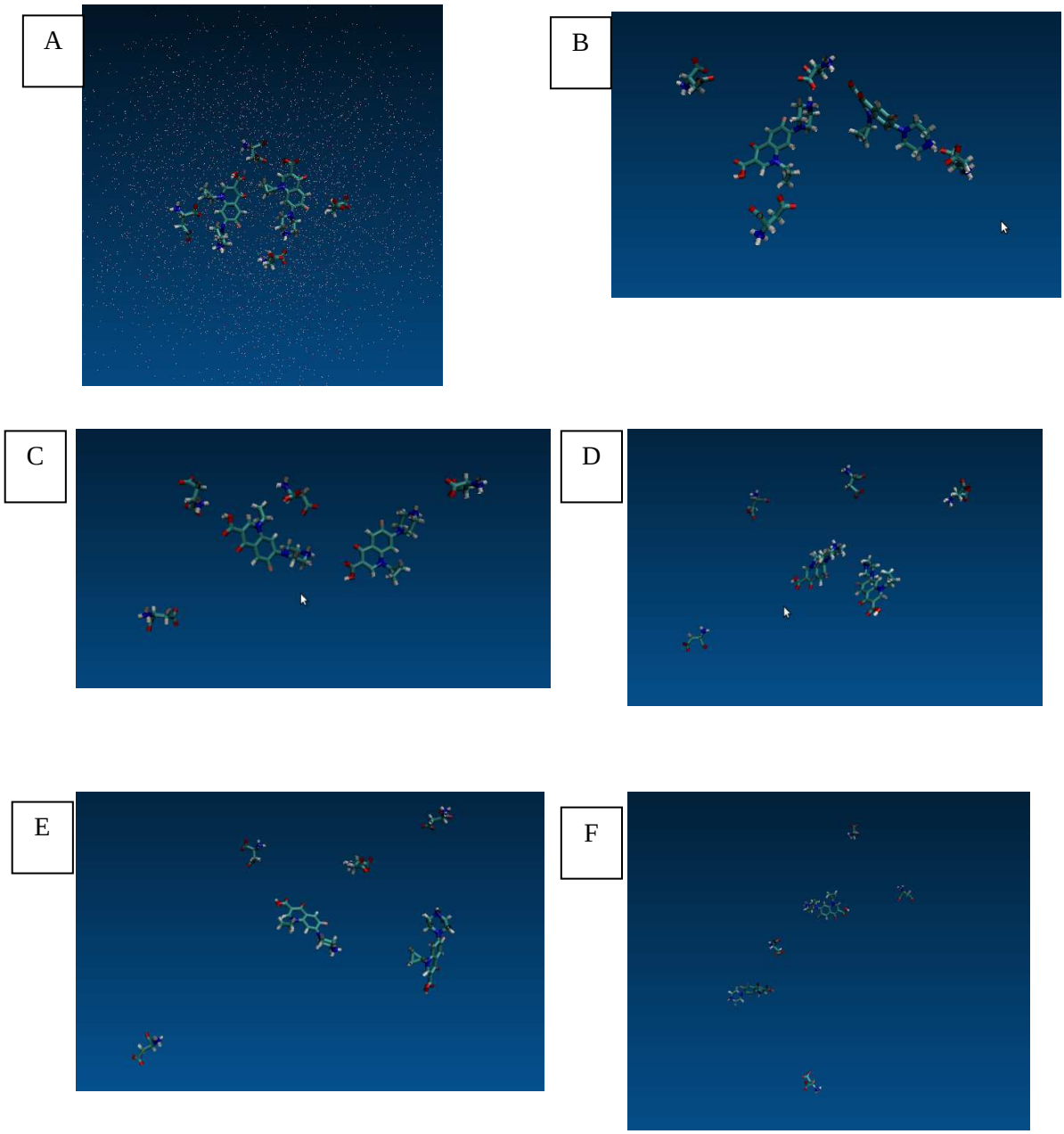

Figure 5.1.11. Snapshots of two ciprofloxacin molecules with four aspartic acid molecules in water: (A) at 0 ns, (B) after 200 ps, (C) after 400 ps, (D) after 600 ps, (E) after 800 ps and (f) after 1 ns. (Water is only shown in A) and is ignored from B) to F) for clarity)

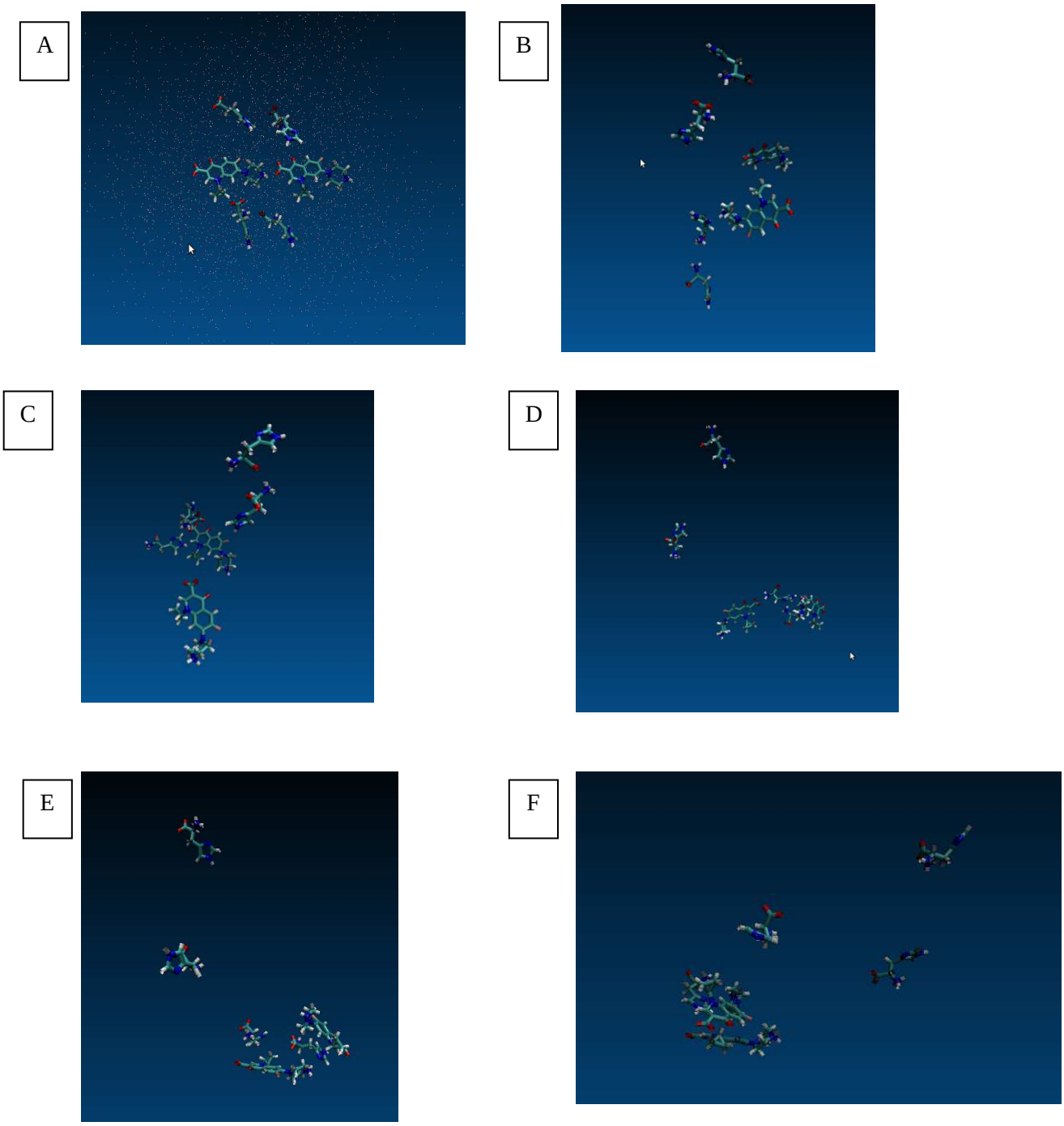

Figure 5.1.12. Snapshots of two ciprofloxacin molecules with four histidine molecules in water: (A) at 0 ns, (B) after 200 ps, (C) after 400 ps, (D) after 600 ps, (E) after 800 ps and (f) after 1 ns. (Water is only shown in A) and is ignored from B) to F) for clarity).

5.1.3.6. Solubility & dissolution studies

In order to assess the saturated solubility of CIP and its prepared salts, excess amount of the drug and its prepared salts were stirred in 2 mL of deionised water and stirred for 12 hours until equilibrium was achieved. Drugs were adequately diluted and their solubility was measured using HPLC. The highest solubility was exhibited by the CIP glutamate salt which was found to be 215±13.3 mg/mL while the solubility of CIP aspartate was 185.4±8.6 mg/mL. As demonstrated by DSC study the melting point of CIP aspartate salt was lower than that of the parent drug which requires less energy to break the crystalline structure of the salt and hence solvate the drug. Other factors such as gravitation index, charge on the most negative atom, and number of hydrogen bonding acceptors might also have played a role in favour of higher water solubility of the salt form (Mitchell & Jurs, 1998).

In vitro dissolution studies of CIP free drug were compared against it salts and amino acids physical mixtures (Fig. 5.1.13). After 10 minutes of dissolution test, only 16.09±1.15 % of CIP was released from CIP containing tablets while 58.3±10.37 of CIP was released from CIP aspartate salt tablets. More than 75% of CIP was dissolved from CIP salt tablets after 40 minutes of the dissolution study while only 54.3±10 and 61.8±5.02 were released from CIP and CIP aspartic acid physical mixture respectively (Fig. 5.1.13A).

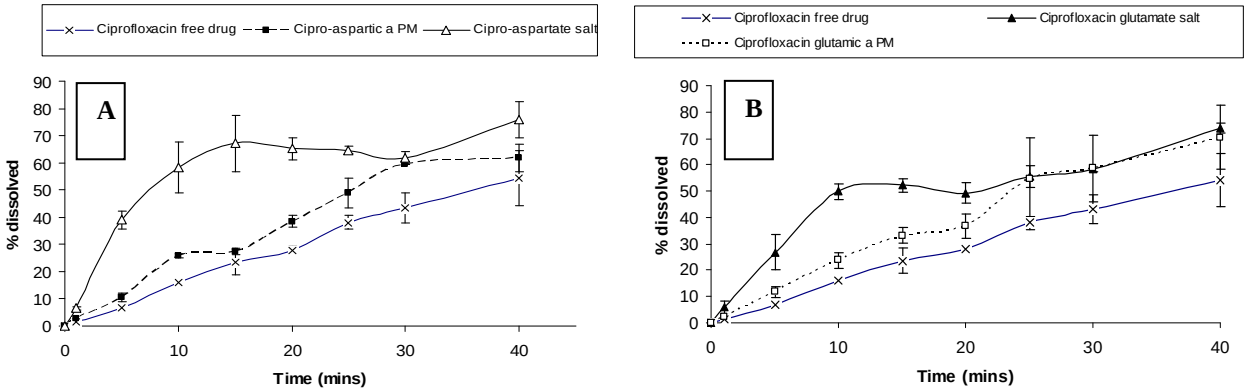

Figure 5.1.88:- (A)Dissolution profile for CIP free drug, CIP aspartic acid physical mixture and CIP aspartate, (B) Dissolution profile for CIP glutamic acid physical mixture and CIP glutamate, data are represented as mean±SD (n=3).

Figure 5.1.13B shows the dissolution profiles of CIP glutamate, CIP and CIP glutamic acid physical mixture. The highest dissolution profile was exhibited by CIP glutamate salt as 26.7±6.7 % of CIP was released from this formulation during the first 5 minutes of dissolution studies. These results suggest that CIP aspartate and glutamate salts have relatively high buffering capacity which in turn improves the dissolution profile by increasing the pH of the surrounding diffusion layer.

5.1.4. Conclusion

CIP is a BCS IV drug with low solubility and permeability. Due to its zwitterionic nature the use of basic and acidic amino acids to formulate new CIP salts was investigated. Acidic amino acids formed two novel salts with high solubility when compared to CIP alone. Phase solubility diagrams have shown a high degree of ionisation of CIP in presence of L-aspartic and L-glutamic acid. Characterization studies confirmed the formation of salt which was supported by FTIR, NMR and DSC studies. ^{1}HNMR demonstrated that the molecular interaction between CIP and the acidic counter ions was a 1:1 ratio. Moreover, the molecular dynamic simulations have shown for the first time that the hydrophobic interactions between CIP molecules decrease in the presence of the acidic amino acids and in turn form a stable salt.

Ciprofloxacin permeability studies and the transcriptomic changes occurring during its uptake across Caco-2 cells

5.2.1. Introduction

Ciprofloxacin (CIP) is a flurinated-4-quinolone derivative which belongs to the fluoroquinolone antibiotic group and is structurally related to nalidixic acid. The broad spectrum synthetic antibiotic is used for systemic therapy against acid-alcohol resistant bacteria (Eliopoulos et al., 1984) and is classified as a BCS IV drug with both low solubility and permeability (Wu et al., 2005). CIP is zwitter ionic in nature with a "U" shaped pH solubility profile exhibiting lowest solubility values near its isoelectric point and the highest value below pH 5 and above 10 (Olivera, 2011). Studies reported by Bergan et al., (1987) and Neuman (1988) suggest that 55-85% of CIP becomes bioavailable after oral administration. This percentage was found to be slightly lower than other fluoroquinolone compounds. The low dissolution profile from oral dosage forms and the first pass metabolism were believed to be the reasons behind the incomplete absorption of CIP. It was believed that CIP was eliminated entirely by the kidney until Sorgel et al (1989) found that the intestine eliminates around 10% of CIP and this percentage increases in patients with renal failure (Rohwedder et al., 1990). The importance of the intestine in the elimination of CIP was further studied by Rubinstein et al., (1994) and Metz & Soergel, (1990) using an *ex vivo* rat intestinal perfusion model. The intestinal secretion for most of the fluoroquinolones is mediated by efflux proteins P-glycoprotein (P-gp) and multidrug resistance associated protein 2 (MRP2). In 2002 Lowes and Simmons suggested that CIP is not a substrate for MRP2 and P-gp but secreted by an alternative pathway which was termed as CIP sensitive pathway. Lowes and Simmons believed that two efflux proteins located on the apical and basal sides of the epithelial cells control efflux of CIP. A similar phenomenon of active efflux of CIP was also reported in bacteria such as *Streptococcus pneumoniae* (Valerie et al., 1997) and *Salmonella enterica* (Etienne et al., 2000).

Pharmacokinetics and pharmacodynamics of CIP are also affected by the concomitant intake of food which has clinical implications for the bioavailability of CIP (Singh, 1999; Harris et al., 2003). Food also affects the pharmacokinetics of the drug by altering the GI pH, gastric emptying rate, bile flow and physical/chemical characteristics of the drug molecule. Various proposed mechanisms for reduction in bioavailability by food include chelation of the drug and reducing solubility of basic drug upon reaching the small intestine (Leyden, 1985; Carver et al., 1999).

CIP bioavailability is known to decrease upon co-administration with food containing metal ions (Hoffken et al., 1985; Lomaestro and Bailie, 1995) which was attributed to complex formation with the metal ions (Wallis et al., 1996). The formed complexes have different geometry, size and charge from the non complexed drug and therefore have a reduced passive diffusion across the cell membranes and the tight junctions of intestinal epithelial cells. Another study conducted by Ledergerber et al., (1985) demonstrated that concomitant administration of CIP oral tablets with food prolongs the time required to reach peak serum levels without affecting the overall bioavailability.

The aim of the current study was to study the ion-pair formation between the anionic amino acids; aspartic acid and glutamic acid and the zwitter ionic model drug (CIP) and the impact of ion-pairing on the permeability profile of CIP and to visualize the molecular genetic changes happening during the uptake of CIP and its ion-paired formulations. This study also investigated the effect of pH and the media composition (fed and fast state) on the absorption patterns of CIP.

5.2.2. Materials and methods

5.2.2.1. Materials

Ciprofloxacin, L-Glutamic acid (Reagent plus ≥ 99%), L-aspartic acid (≥ 98%), ninhydrin reagent (2% solution), sodium taurocholate, lecithin, glycerylmonooleate, sodium oleate and maleic acid were purchased from Sigma Aldrich, UK.

Sodium hydroxide and sodium chloride were purchased from Fisher Scientific, UK.

Dulbecco's modified Eagle's medium (DMEM), fetal bovine serum (FBS), Nonessential amino acids (NEAA), 1% pencillin-streptomycin, 2mM glutamine and Hank's balanced salt solution (HBSS) were purchased from Bio Sera, UK. 1% Trypsin–EDTA was obtained from Gibco Lab. UK.

RNeasy kit (RNA free water, buffer RLT, buffer RW1 and buffer RPE) was purchased from Qiagen (Hiden, Germany). Gene expression hybridization kit, low input Quick Amp labelling kit, RNA spike-in kit (one color) all were purchased from Agilent (Cedar Creek, Texas, USA). Agilent gene expression washing buffer 1 and 2 were ordered from Agilent (Wilmington, DE, USA) and Ethanol which was purchased from Fisher scientific (Leicestershire, UK).

5.2.2.2. Methods

5.2.2.2.1. Preparation of pre-saturated solution of 1-octanol and de-ionised water.

1000 ml of de-ionised water was added to 4 mL of 1-octanol. The mixture was shaken for few minutes and left overnight. The de-ionised water was separated from 1-octanol using a 1000 mL separating funnel.

5.2.2.2.2. Octanol- water partitioning experiment

500 µg of CIP was added to 100 mL octanol-saturated deionised water with molar excess of aspartic acid/glutamic acid (in ratios 1:1, 1:2, 1:4 and 1:8). 5 mL of the aqueous phase was allowed to equilibrate with 5mL of octanol at room temperature and stirred for 24 hours using a magnetic stirrer. The two phases were then separated by centrifugation and CIP

concentration $[CIP_t]_{Aq}$ in the aqueous phase was measured using HPLC. Mass balance was used to calculated CIP concentration in octanol phase $[CIP_t]_{Oct}$ using equation (5.2.1).

$[CIP_t]_{Oct}$ = total drug put into the system- $[CIP_t]_{Aq}$ Equation 5.2.52

The apparent distribution coefficient D_B may be calculated using equation (5.2.2)

$D_B = [CIP_t]_{Oct}/[CIP_t]_{Aq}$ Equation 5.2.53

5.2.2.2.3. HPLC method to study the concentration of ciprofloxacin

The amount of ciprofloxacin (CIP) dissolved in the samples was quantified by HPLC using a Dionex 1100 system fitted with an autosampler (AS50), gradient pump (GP50), UV detector (UVD 170U) and RP-C18 analytical column (Phenomenex 110A, 150x4.6 mm, 5µm). Mobile phase consisting of methanol and 1.25% acetic acid was mixed in the pump and analysis of CIP was done using gradient elution at 1.0 mL/min. *λmax* was determined using a Unicam UV-Visible Spectrophotometer and the HPLC UV detector was set at *λmax* of 280 nm. CIP was eluted with a retention time of 1.5±0.1 min and a rectilinear calibration curve was established in the concentration range between 10- 200µg/mL.

5.2.2.2.4. Ninhydrin analysis

The concentrations of aspartic acid and glutamic acid in octanol/water partitioning studies were quantified using the ninhydrin method. In order to construct a calibration curve, serial dilutions of the amino acids were prepared and 1 mL of the prepared samples was mixed with 0.5 mL of ninhydrin reagent and vortexed for 20 seconds. The samples were heated in a pre-warmed water bath at 80 ^{o}C for 20 minutes. The samples were removed from the water bath and left to cool. The intensity of the coloured Ruhemann purple was analysed using a UV spectrophotometer at a wavelength of 560 nm.

Calibration curves were constructed with a regression coefficient of 0.99 and 0.99 for aspartic and glutamic acid respectively. Subsequent to the construction of the calibration curves, the concentration of the amino acids in the aqueous

layer was determined using the linear curve equations (5.2.3) and (5.2.4) for aspartic acid and glutamic acid respectively.

Y=0.0695x **Equation 5.2.54**

Y=0.0755x **Equation 5.2.55**

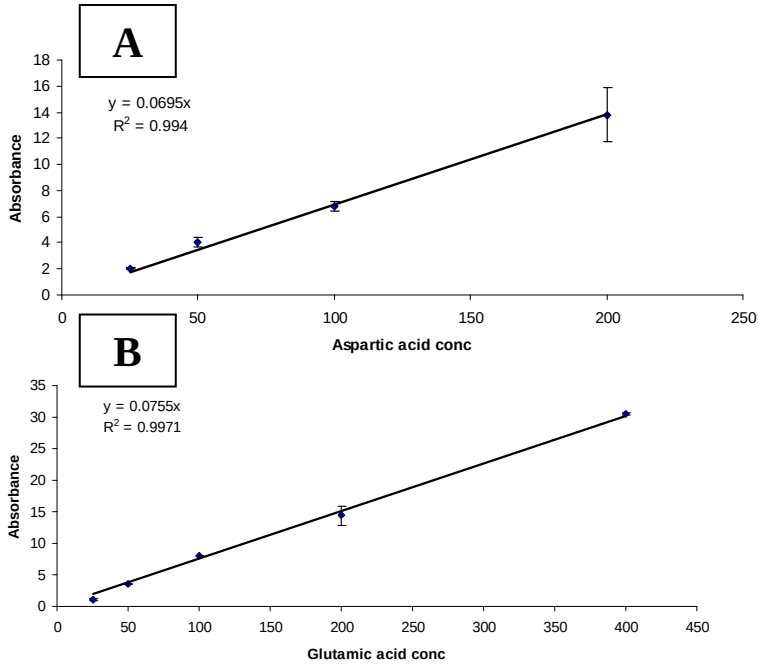

Figure 5.2.89:- Ninhydrin calibration curve for aspartic acid (A), glutamic acid (B) n=3.

5.2.2.2.5. Procedure for Caco-2 cell culture

Caco-2 cells at passage 48 were gifted from Huddersfield University and used at passages 50-80. Cells were allowed to grow in 75cm² T-flasks and maintained using Dublecco's modified Eagle's medium (DMEM) with 10% fetal bovine serum (FBS), 0.5% pencillin-streptomycin, 2mM glutamine and 1% nonessential amino acids (NEAA). Culture medium was changed every 2 to 3 days and cells were grown at a temperature of 37°C and 5% CO_2. The cells were passaged using 5 mL trypsin-EDTA when they reached 90% confluence. Transepithelial transport assay was carried out using Khan et al., (2011) methods. 2 x 10^5cells/cm² were seeded on polycarbonated-coated membranes (6-well transwell plates, 24mm, 4.7cm²) and were allowed to grow for 21 days and the media in both apical and basal compartments were changed every

2-3 days. Transepithelial electrical resistance (TEER) was measured at the start and end of every study.

5.2.2.2.6. Ciprofloxacin permeability studies

Caco-2 monolayers were used 19-21 days after seeding. Apical to basolateral permeability of CIP and its formulations was assessed. The transwells were rinsed and incubated for 15 minutes with drug-free transport medium (Hanks balanced salt solution; HBSS). Following incubation, HBSS was removed and 1.5 mL of the medium containing CIP alone (500 µg/mL) and CIP with various molar ratios of the anionic amino acids (1:1, 1:2, 1:4 and 1:8) were introduced to the apical side. Sample aliquots (300µL) were taken from the basolateral side at given time intervals (0, 5, 10, 15, 20, 30, 60 and 90 minutes). After each sampling, an equal volume of fresh transport buffer (pre-warmed at 37°C) was added to the receiver compartment (basal side) and the cells maintained at a temperature of 37°C and 5% CO_2 throughout the experiment. Samples were subsequently analyzed by HPLC. In order to confirm the mass balance, samples were taken from both apical and basolateral compartments at the last time point (90 mins). All experiments were performed at 37°C (n = 5). In order to investigate the effect of pH on the permeability profile of CIP, the pH of HBSS was adjusted using 0.1N HCl solution until it reached a pH of 4.5, 5.5 and 6.8. CIP was added to HBSS and 1.5 mL of the solutions were introduced to the apical side and the permeability profile was assayed as discussed above.

Apparent permeability coefficient P_{app} (cm/s) was calculated using (equation 5.2.5)

$$P_{app} = dQ / dt \times 1 / AC_0 \quad \textbf{Equation 5.2.56}$$

Where *dQ/dt* is the rate of appearance of the drugs on the basolateral side (nmol s^{-1}), C_o is the initial concentration on the apical side and *A* is the surface area of the monolayer (4.7 cm^2).

The data presented was validated using HPLC measurement of drug transfer during the process of permeability. This included repetition of drug permeability studies in the preparations used for microarray analysis.

5.2.2.2.7. Fed and fasted state media preparation

Fed (FeSSIF) and fasted state (FaSSIF) media was prepared using a method reported by Jantratid et al., (2008) and the composition and the properties of the media used in the permeability study are summarised in table (5.2.1). 50 mg of CIP was added to 100 mL of the simulated media and 1.5 mL of the solution was transferred to the apical side of the Caco-2 monolayers' transwells and permeability across the monolayers was assessed using the method discussed above.

Table 5.2.40:- Composition of the media to simulate the fasted state simulated intestinal fluid (FaSSIF) and the fed state simulated intestinal fluid (FeSSIF).

Composition (mM)	FaSSIF	FeSSIF
Sodium taurocholate	3	10
Lecithin	0.2	2
Glyceryl monooleate	-	5
Sodium oleate	-	0.8
Maleic acid	19.12	55.02
Sodium hydroxide	34.8	81.65
Sodium chloride	68.62	125.5
Properties		
pH	6.5	5.8
Osmolality	180±10	390±10
Buffer capacity (mmol/L/pH)	10	25
Surface tension (mN/m)	54.3	40.5±0.2

5.2.2.2.8. Recovery

The amount of CIP recovered from both apical and basolateral compartments at the end of the experiment was calculated using equation 5.2.6.

$$\text{Recovery}(\%) = \frac{C_{R90\,\text{min}} \times V_R + C_{D90\,\text{min}} \times V_D}{C_{D0\,\text{min}} \times V_D} \times 100 \qquad \textbf{Equation 5.2.57}$$

Low recovery data is attributed to entrapment of the compounds into the cell monolayers or adsorption to the device surface which in turn results in error calculating the transport rate (Aungst et al., 2000).

5.2.2.2.9. RNA extraction for microarray studies

Samples for microarrays studies were collected at 5, 30, 60 minutes for CIP, CIP:glutamic acid at 1:1 (1x) and 1:8 (8x) molar ratios. Caco-2 monolayers were treated with ethanol: phenol mixture (95:5) for 24 hours. After scrubbing the cells, pellets were obtained by centrifugation at 2000 rpm at 4 ^{o}C for 10 minutes. All pellets were stored at -80 ^{o}C until the total RNA was extracted. Total RNA was extracted using RNeasy kit (Qiagen) and quantified using a Nanodrop 1000 spectrophotometer (Themoscientific, Wilmington, DE).

5.2.2.2.10. Microarray study

Systemic changes of the gene expression upon exposing Caco-2 cells to CIP and its various formulations were evaluated using the Agilent one-color-spike procedure discussed before. Briefly, 1.5µl of 25 ng of total RNA was mixed with 2 µl of diluted one-color-spike mix. cDNA master mix (Agilent) was used to prepare cDNA for all the samples which were labelled using cy3-dUTP. The yield and specific activity for fluroscent cDNA probes were determined using equations 5.2.7 and 5.2.8 respectively; the data obtained is summarised in (Table 5.2.2), after quantifying cDNA (ng/µl)and cyanine 3 (pmol/ µl). All samples were hybridized to Agilent 4x44 K whole genome array for 16 hours at 65 ^{o}C in hybridization oven (Sheldon manufacturer, Corneilus, OR). After hybridization, samples were scanned at 50nm resolution and at 20 bit scan using Agilent scanner (Agilent Technologies, Santa Clara, CA). 16-bit TIFF images were obtained and used as input for the feature extraction software (V10.7, Santa Clara, CA).

$$\textbf{Yield} = \frac{Conc.of.cRNA \times elution.volume}{1000} \qquad \textbf{Equation 5.2.58}$$

$$\textbf{Specific activity} = \frac{Conc.of.Cy3}{Conc.of.cRNA} \times 1000 \qquad \textbf{Equation 5.2.59}$$

Table 5.2.41:- Summary of Quantifying of total RNA, yield and specific activity of the complementary DNA used for hybridization in CIP studies.

Sample	Total RNA			cDNA probe				
	conc (ng/µl)	260/280 ratio	260/230 ratio	conc (ng/µl)	260/280 ratio	cystine dye pmol/ µl	Yield	specific activity
Control 5	983.1	2.02	1.57	131.3	2.2	2.5	3.939	19.04
Control 60	842.5	2.01	1.94	165.2	2.2	3.1	4.956	18.76
CIP 5 min	631.3	2.04	2.05	241.8	2.21	2.4	7.254	9.92
CIP:Glu 1:1, 5 min	952.1	1.99	1.92	155.1	2.1	0.9	4.653	5.80
CIP:Glu 1:8, 5 min	851.8	1.96	1.63	210.8	2.1	1.6	6.324	7.593
CIP, 30 min	507.7	1.99	1.69	190.2	2.23	2.6	5.706	13.66
CIP:Glu 1: 1, 30 min	362.2	1.98	1.68	199.8	2.21	1.6	5.994	8.00
CIP :Glu 1:8, 30 min	318	2.03	1.97	132.2	2.1	1	3.966	7.56
CIP, 60 min	889.8	2	1.78	182.4	2.19	2.8	5.472	15.35
CIP:Glu 1: 1, 60 min	614.3	1.99	1.29	133.2	2.26	2.4	3.996	18.01
CIP:Glu 1: 8, 60 min	1286.3	1.99	1.82	135.9	2.14	1.7	4.077	12.50

5.2.2.2.11. Data Processing (Image analysis and data normalization)

The feature extraction software (V10.7, Santa Clara, CA) was used to study the quality of the obtained TIFF images. The image was analysed in terms of grid alignment, signal quantification and overall slide quality.

Background intensities in the DNA microarray data such as optical background and non-specific binding (NSB) were adjusted using the R library gcrma (Boes and Neuhäuser 2005). The gcrma converted the background adjusted probe intensities into expression measures while the probe sequence information were used to estimate probe affinity to non-specific binding (NSB). The levels of probe intensities between the arrays before and after normalization were compared using box-plots as discussed in TMP chapter. The middle line of the box-plot represents the median while the two ends of the box represent the upper and lower quartiles. Values which are more than 1.5 the interquartile range are outliners while the horizontal lines connected to the box-plots are not considered outliners.

5.2.2.2.12. Clustering analysis and filtering

Data clustering was carried out on the normalized data using TMEV software (version TM4, WA, USA). The genetic changes were clustered according to their similarities in the pattern of their expression using hierarchical clustering algorithm. The mean values were used to compare between various data set used in this study. In order to highlight the main variability in the multidimensional data set principle component analysis was carried out using TMEV software. Microsoft Excel (version 2003, Toulouse, France) was used to filter out the non-expressed genes or the genes which do not show variation across sample types. Genes which were up or down-regulated by two fold were selected for further analysis. In order to investigate the changes in various pathways during the absorption process, up and down-regulated genes were uploaded online onto the Kyoto Encyclopaedia of Genes and Genomes (KEGG) *http://www.genome.jp/kegg/* and the expression changes were high-lighted in red.

5.2.3. Results and discussion

5.2.3.1. Ciprofloxacin/aspartic acid octanol/water partitioning and permeability studies

Similar to the previous studies that were conducted for TMP and IND, partitioning studies of CIP and its ion-paired formulations were investigated using water and octanol system. Figure 5.2.2 shows the partitioning behaviour of CIP at various concentrations of aspartic acid. CIP alone was found to have high partitioning in the organic layer with a log P value of 1.63. This was fairly similar to the values reported by Olivera, (2011) (log P 1.32). The octanol/water partitioning slightly dropped upon pairing CIP with aspartic acid as the drug concentration in the aqueous layer increased upon increasing the concentration of aspartic acid. The highest aqueous concentration was exhibited at 1:8 ratio of CIP to aspartic acid respectively and the log P dropped by more than one unit to 0.28.

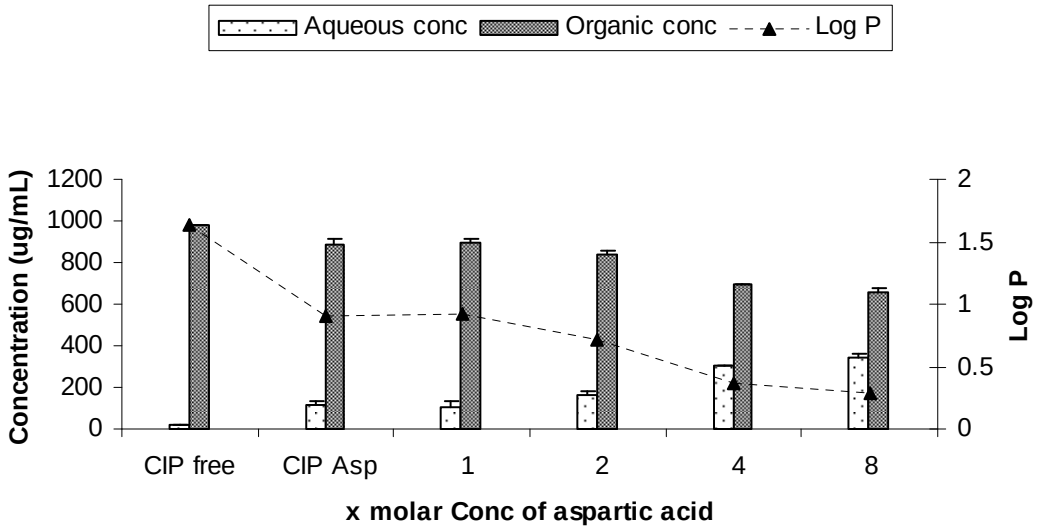

Figure 5.2.90:- CIP concentrations in aqueous and octanol layers and its corresponding Log P values at various concentrations of aspartic acid (n=3).

Ion-pairing theory assumes that pairing between the oppositely charged ions occurs during partitioning for basic or acidic drug with its counterpart (acidic or basic counter ion). CIP is zwitter ionic in nature characterised by both acidic and basic groups capable of forming ion-

pairs. In the current investigation, anionic amino acids were used as previous studies have shown that stable salt forms cannot be obtained with cationic amino acids due to the lack of formation of inter and intra molecular bonds which was studied using molecular simulations. We therefore assumed that CIP will behave as a cationic molecule upon pairing with acidic amino acids. Equation 5.2.9 was used to plot the double reciprocal of the apparent octanol/water distribution coefficient of CIP and the concentration of the acidic amino acid.

$$\frac{1}{D_B} = \frac{1}{K_{11aq} P_{AB} [A]_{aq}} + \frac{1}{P_{AB}}$$ **Equation 5.2.60**

Table 5.2.42:- pH measurements during the partitioning study for CIP aspartate (n=3).

Formulation	pH measurements
CIP	4.46±0.03
CIP aspartic acid PM 1:1	4.02±0.1
CIP aspartic acid PM 1:2	3.96±0.06
CIP aspartic acid PM 1:4	3.76±0.12
CIP aspartic acid PM 1:8	3.61±0.026

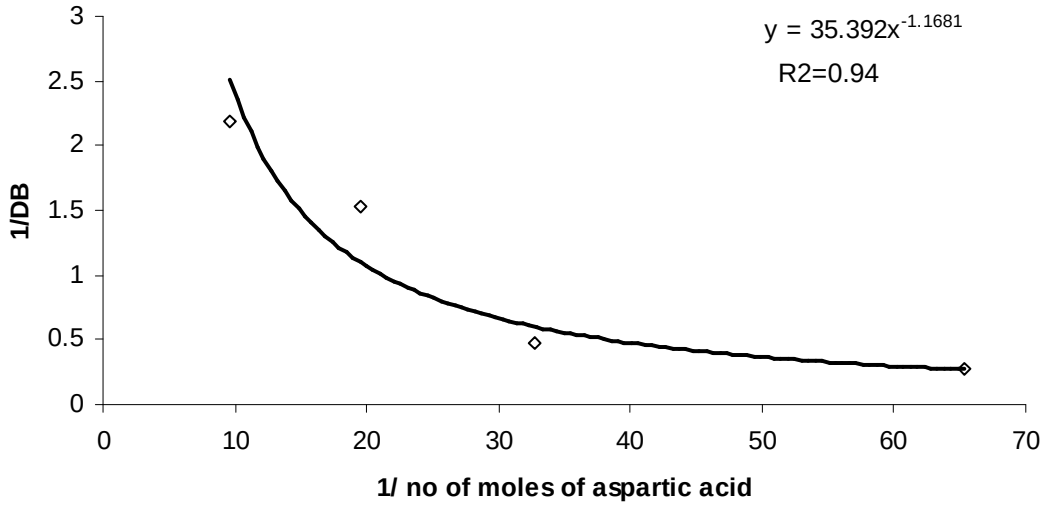

Figure 5.2.91:- Double reciprocal plot of the apparent octanol-water distribution coefficient of CIP as function of aspartic acid molar concentration.

A negative exponential relationship (R^2= 0.94) was observed between the double reciprocal of the apparent octanol/water distribution coefficient of CIP and the concentration

of the acidic amino acid suggesting that an increase in the molar concentration of aspartic acid would result in an exponential decrease in the partitioning coefficient of the zwitter ionic drug. Using equation (5.2.10), the intrinsic octanol water partitioning (P_{AB}) was calculated and found to be 0.56 while the aqueous binding constant (K_{11aq}) was 1.54 mM^{-1} (1540 M^{-1}). Although the number of H-donor and H-acceptors for both CIP and TMP was similar (i.e. similar degree of H-bond formation), the aqueous binding constant between CIP and aspartic acid was significantly higher than that between TMP and aspartic acid (21 M^{-1}). Nevertheless, the degree of ionic bonding between CIP and the amino acid is higher than that between TMP and aspartic acid possibly because of the higher ΔpKa (6.86 in case of CIP and 5.42 in TMP).

$Y = 35.39\,x^{-1.1681}$ **Equation 5.2.61**

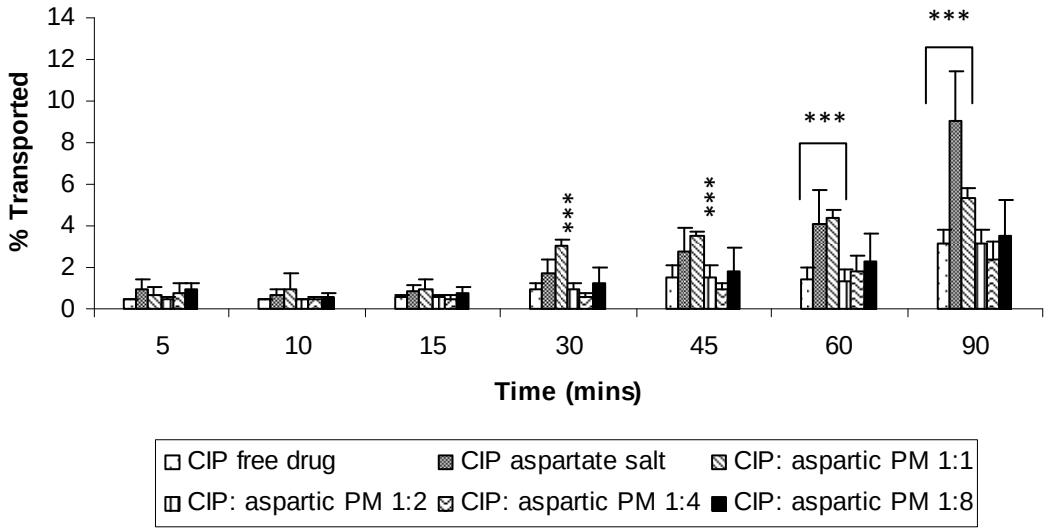

Figure 5.2.92:- Percentage of CIP transported across Caco-2 monolayers at various molar ratios of aspartic acid (n=5). One way analysis of variance (ANOVA) and pair-wise multiple comparisons method (Tukey test) against drug alone at each time point were used for statistical analysis and probability values of (P< 0.05, * and P<0.001,*) were used to determine the significant difference.**

Figure 5.2.4 summarises the permeability profile of various formulations of CIP across Caco-2 monolayers. 0.45±0.06% of CIP was absorbed across the monolayers after 5 minutes of start of the experiment. The percentage absorbed increased slightly with time to 3.1±0.67% after 90

minutes. The apparent permeability for CIP (P_{app}) was $0.81x10^{-06}$±$3.24x10^{-07}$ cm/sec which reflects the very low permeability of the drug. No significant difference (p> 0.05) was observed for most of the formulations for up to 15 minutes and the amount of CIP absorbed did not exceed 1%. After 30 minutes the percentage of CIP permeated began to increase for CIP aspartate salt (1.69±0.72%) and CIP aspartic acid PM 1:1 (3.02±0.34%) while the rest of the formulations showed no significant increase relative to 30 min control. Moreover, the apparent permeability for CIP increased in the PM 1:1 and the salt formulations to $1.28x10^{-06}$±$2.91x10^{-07}$ and $2.45x10^{-06}$±$1.15x10^{-06}$ cm/sec respectively.

Table 5.2.43:- Summary of the TEER measurements before and after the permeability assay (n=3), the percentage recovery and the apparent permeability calculations for CIP aspartic acid and glutamic acid formulations.

Formulation	TEER measurements (Ω/cm^2) Before	TEER measurements (Ω/cm^2) After	Recovery (%)	Apparent permeability at 60 min (cm/sec)
CIP free drug	452.24±11.7	420.3±26.5	86.5	8.12E-07±3.24E-07
CIP Asp PM 1:1	440.36±18.3.73	430.6±11.2	79.2	1.28E-06±2.91E-07
CIP Asp PM 1:2	446.5±32.3	438.5±20.5	97.1	8.80E-07±3.69E-07
CIP Asp PM 1:4	502±15.2	460.6±28.1	82.5	1.06E-06±5.45E-07
CIP Asp PM 1:8	420.6±10.5	412.6±12.8	96.2	1.38E-06±9.35E-07
CIP Asp salt	455.2±23.1	420.25±13.2	75.9	2.45E-06±1.15E-06
CIP Glu PM 1:1	390.7±12.2	387±30.45	85.2	1.15E-06±2.88E-07
CIP Glu PM 1:2	348±32.1	337.66±5.16	89.7	9.50E-06±1.54E-06
CIP Glu PM 1:4	412.3±20.5	352.6±38.6	95	43.2E-06±8.54E-06
CIP Glu PM 1:8	440.4±11.5	400.1±26.2	98.1	61.1E-06±9.49E-06
CIP Glu salt	401.2±10.2	392.66±12.6	92.3	2.19E-06±4.39E-07

5.2.3.2. Ciprofloxacin/glutamic acid octanol/water partitioning and permeability studies

The octanol/water partitioning of CIP and various concentrations of glutamic acid were studied and the results are summarised in Fig. 5.2.5. Similar to aspartic acid based formulations, the concentration of CIP in the aqueous phase increased upon increasing the concentration of glutamic acid which resulted in a steady decrease in the log P values until it finally reached 0.12 at 8 molar concentration of glutamic acid.

Table 5.2.44:- pH measurements during the partitioning study for CIP glutamate (n=3).

Formulation	pH measurements
CIP	4.46±0.03
CIP glutamic acid PM 1:1	4.29±0.015
CIP glutamic acid PM 1:2	4.21±0.012
CIP glutamic acid PM 1:4	4.05±0.03
CIP glutamic acid PM 1:8	3.85±0.028

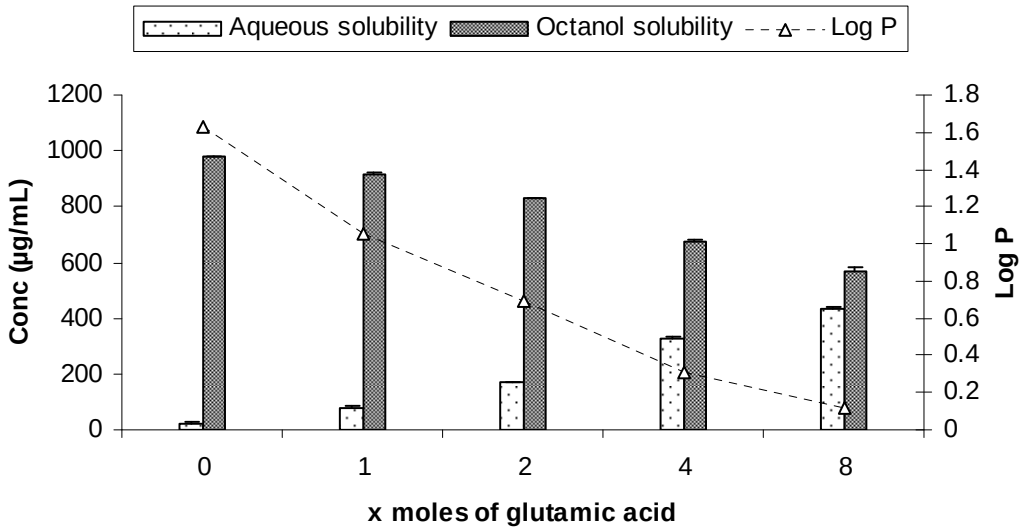

Figure 5.2.93:- CIP concentrations in aqueous and octanol layers and its corresponding Log P values at various concentrations of glutamic acid (n=3).

The double reciprocal plot of apparent octanol/water distribution coefficient of CIP and the concentration of glutamic acid showed similar trend as that of aspartic acid (Fig. 5.2.6). Upon using the equation (equation 5.2.11), the intrinsic octanol water partitioning (P_{AB}) was 2.17 while the aqueous binding constant (K_{11aq}) was found to be 0.48 mM^{-1} (480 M^{-1}).

$Y = 0.33x^{-0.96}$ **Equation 5.2.62**

As discussed before in chapter 5.1, ionic and H-bond formation are expected to be the same between aspartic acid and CIP ion-pairs and glutamic acid and CIP ion-pairs due to the high similarity between the two amino acids in terms of the pKa values and number of H- bond donors and H-acceptors. Nevertheless, the aqueous binding constant (K_{11aq}) between aspartic

acid and CIP was higher than the K_{11aq} of gluatmic acid and CIP. These findings are contradictory to our previous findings in chapter 5.1. This can be possibly due to the zwitter ionic nature of CIP which could result in lower kinetic energy upon ion-pairing with aspartic acid resulting in higher aqueous binding constant.

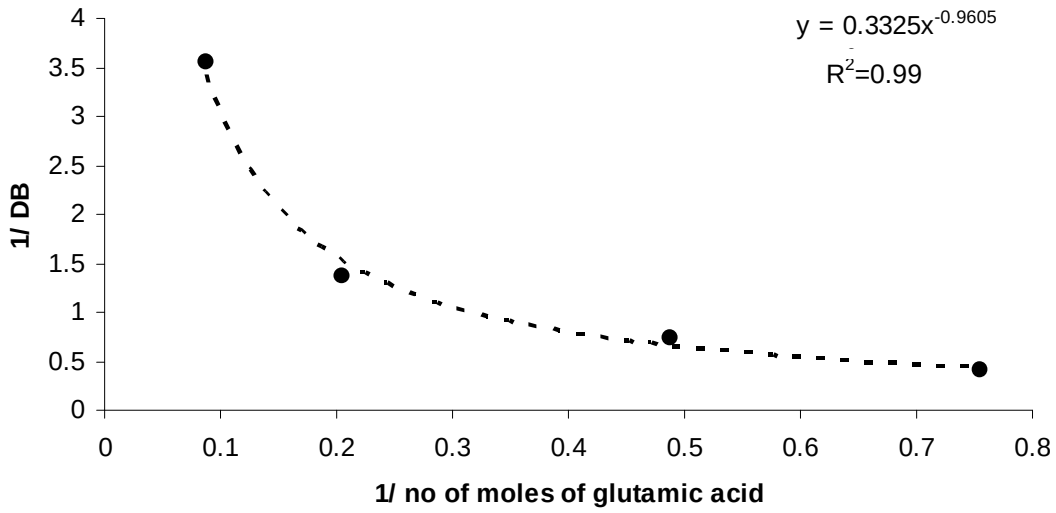

Figure 5.2.94:- Double reciprocal plot of the apparent octanol-water distribution coefficient of CIP as function of glutamic acid molar concentration.

The permeability profile of CIP at various molar concentrations of glutamic acid was studied (Fig. 5.2.7). CIP, CIP glutamate salt and CIP glutamic acid PM 1:1 showed low absorption profile with highest permeation from the salt form (6.99±0.48%) after 90 minutes. Interestingly, increasing the molar concentrations of glutamic acid beyond 1:1 for PM ratio was found to have a significant effect on the permeability profile of CIP. The percentage of CIP absorbed from PM 1:2 formulations reached 9.7±2.6% after 30 minutes and exceeded 30% and 65% for PM 1:4 and PM 1:8 respectively. At the end of the permeability experiment 92.57±3.29% was absorbed from PM 1:4 and 100% of CIP was absorbed from 1:8 formulations.

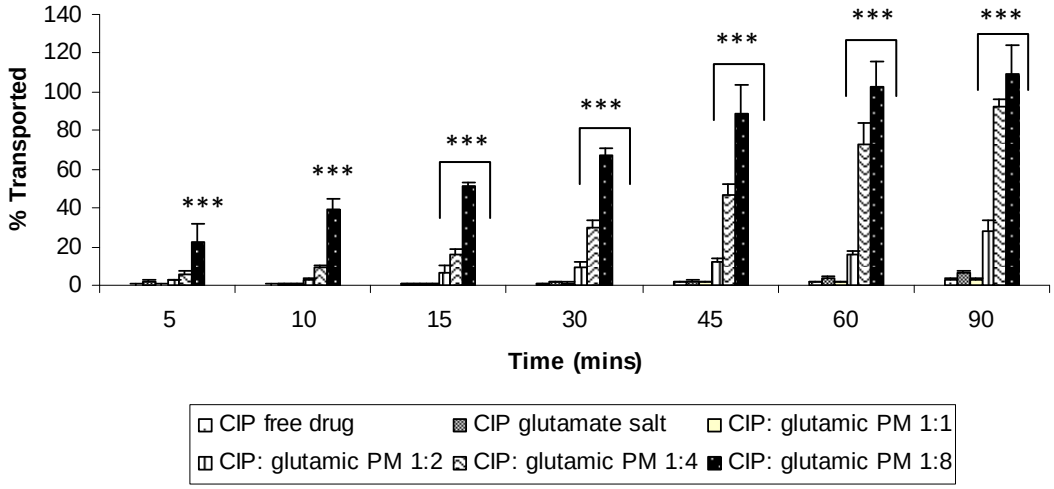

Figure 5.2.95:- Percentage of CIP transported across Caco-2 monolayers at various molar ratios of glutamic acid (n=5). One way analysis of variance (ANOVA) and pair-wise multiple comparisons method (Tukey test) against drug alone at each time point were used for statistical analysis and probability values of (P< 0.05, * and P<0.001,*) were used to determine the significant difference.**

The apparent permeability (P_{app}) increased by around 10, 50 and 75 fold for CIP glutamic acid formulation containing PM 1:2, PM 1:4 and PM 1:8 respectively (Fig. 5.2.8). Our previous studies conducted on IND and TMP demonstrated that increasing the molar concentrations of the amino acids -especially beyond 1:2 ratio has a negative effect on the permeability profile of the therapeutic agents. Partitioning studies showed that increasing the molar concentration of glutamic acid results in increasing the concentration of CIP in the aqueous layer; i.e. more fraction of the drug is in the ionized form and therefore lower log P values. According to the pH-partitioning theory only the unionized form of the drug can permeate across the cellular membranes, however Palm et al (1999) have demonstrated that the ionised forms of the drugs can also be transported across the Caco-2 cells. Moreover, it can be expected that ion-pairing CIP with glutamic acid supports the reversion of zwitter ionic nature of CIP by proton transfer (Romanuk et al., 2010) from glutamic acid resulting in an overall anionic charge on the ion-paired molecule (Fig. 5.2.9).

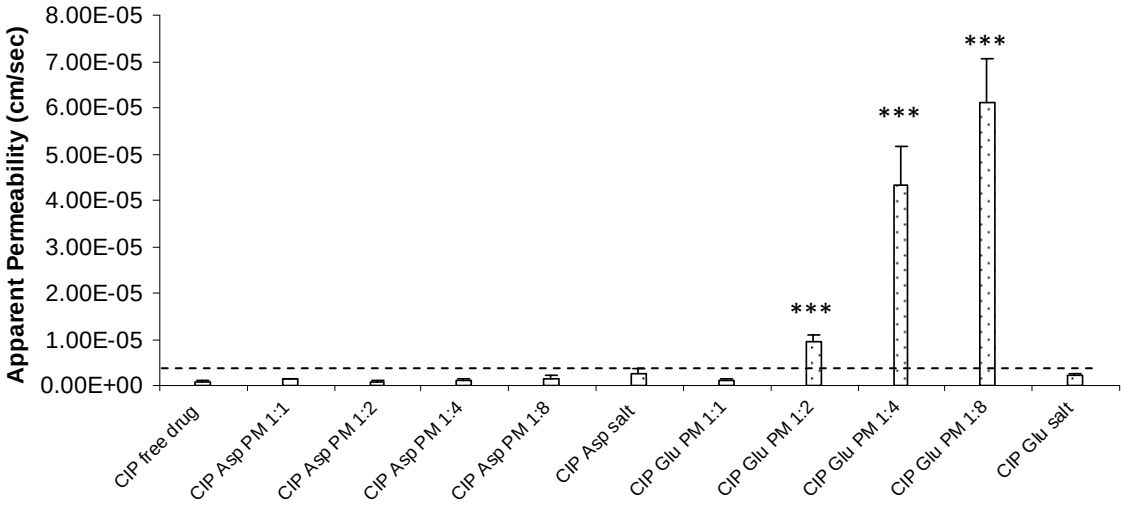

Figure 5.2.96:- P_{app} permeability values at 60 minutesfor CIP alone and CIP at various molar ratios of aspartic acid and glutamic acid. One way analysis of variance (ANOVA) and pair-wise multiple comparisons method (Tukey test) against drug alone at each time point were used for statistical analysis and probability values of (P< 0.05, * and P<0.001,*) were used to determine the significant difference.**

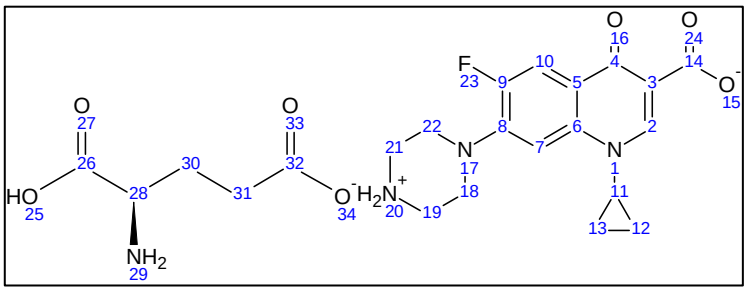

Figure 5.2.97:- structure representing the reversion of the zwitter ionic nature of CIP by the proton transference from the glutamic acid and hence an overall anionic charge on ion-paired molecule.

5.2.3.3. Effect of fed and fasted state on CIP permeability

As discussed above the environment in fed state in the gastrointestinal tract might affect solubilisation and the degree of ionisation of the drugs. Moreover, food content might interact with the counter ion and prevent the uptake of the ion-paired CIP amino acid for transport across the intestinal membrane as one unit. Therefore, this study will investigate the effect of fast and fed state media on the absorption profile of CIP glutamate salt. CIP glutamate salt was selected for this study to determine the effect of media on salt absorption as it has shown to

have a relatively low P_{app} value ($2.19x10^{-06}\pm4.39x10^{-07}$ cm/sec) and any improvement in permeability would be significant.

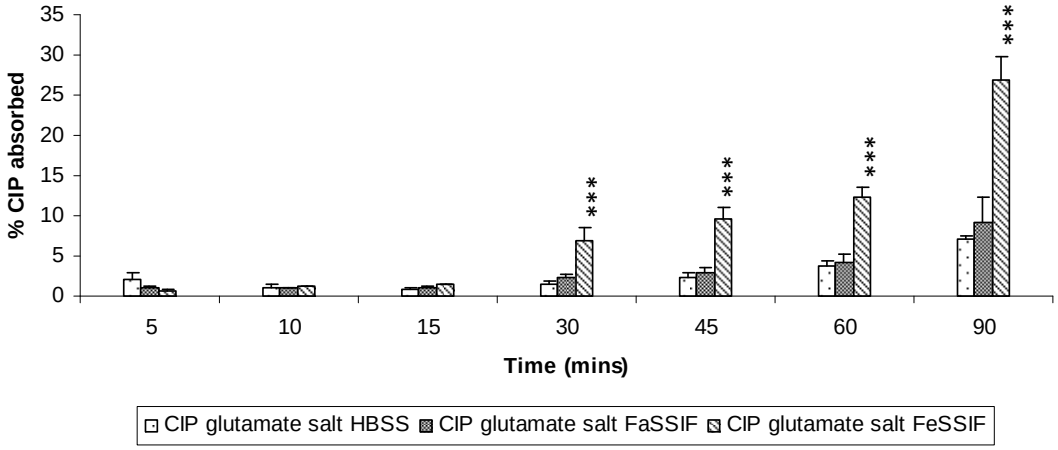

Figure 5.2.98:- Percentage of CIP glutamate salt transported across Caco-2 monolayers from HBSS, FaSSIF and FeSSIF media (n=5). One way analysis of variance (ANOVA) and pair-wise multiple comparisons method (Tukey test) against drug alone at each time point were used for statistical analysis and probability values of (P< 0.05, * and P<0.001,*) were used to determine the significant difference.**

Figure 5.2.10 shows the permeability profile for CIP glutamate salt in HBSS media, FaSSIF and FeSSIF. During the first 15 minutes of the permeability assay, the media did not have any effect on the absorption profile of CIP glutamate salt and no more than 2% of the salt was transported across the cell lines. After 30 minutes, the percentage of CIP absorbed from the salt form in the FeSSIF media increased significantly ($p<0.001$) when compared to the salt in HBSS and FaSSIF media and the total percentage permeated from FeSSIF increased to reach 26.84±2.9% after 90 minutes. On the other hand, the FaSSIF media did not have any significant effect ($p> 0.05$) on the percentage of CIP absorbed and the percentage absorbed after 90 minutes did not exceed 10%. Apparent permeability calculations showed a significant increase of CIP apparent permeability in FeSSIF media ($P_{app}= 7.35x10^{-6}\pm0.8x10^{-6}$cm/sec) and no significant effect in FaSSIF ($P_{app}= 2.49x10^{-6}\pm0.7x10^{-6}$cm/sec) when compared to P_{app} ($2.19x10^{-06}\pm4.39x10^{-07}$ cm/sec) of CIP glutamate salt in HBSS.

Table 5.2.45:- The percentage recovery and TEER measurements before and after the permeability assay of CIP glutamate salt from HBSS, FaSSIF and FeSSIF (n=5).

Media	TEER measurements (Ω/cm^2) Before	TEER measurements (Ω/cm^2) After	Recovery (%)
HBSS	401.2±10.2	392.66±12.6	92.3
FaSSIF	440.36±18.3	380.4±15.3	89.6
FeSSIF	446.5±32.3	172±20.5	84

Interestingly, the TEER values for Caco-2 cells in FeSSIF media dropped significantly at the end of the permeability assay (Table 5.2.6) possibly because of the high concentration of sodium taurocholate (10 mM) as well as the high osmolarity of the media (390±10). Similar results were obtained by Ingels et al., (2002) which demonstrated that FeSSIF with 15 mM of sodium taurocholate affects the morphology of the cells and disrupts the cellular nuclei and the stored glycogen. As a result the tight junctions between the epithelial cells become loose and more CIP molecules were able to be absorbed across Caco-2 cells. Moreover according to Meyerhoffer and McGown studies the concentration of sodium taurocholate in FeSSIF is in the critical micile concentration range (Meyerhoffer and McGown., 1989). However, further investigations is required to confirm CMC formation.

5.2.3.4. Effect of pH on CIP permeability

CIP has a zwitter ionic nature and the pH of the media affects the dissolution profile of the drug and might have an impact on its absorption across the intestinal membrane. pH ranging between 4.5 and 6.8 were selected for this study in order to mimic the gastrointestinal tract pH (Neuhoff et al., 2005).

Figure (5.2.11) shows the effect of three different pH (4.5, 5.5 and 6.8) environments on the permeability of CIP across Caco-2 monolayers. Lowering the apical pH from 6.8 to 4.5 shows a significant increase in the percentage of CIP absorbed across the cells.

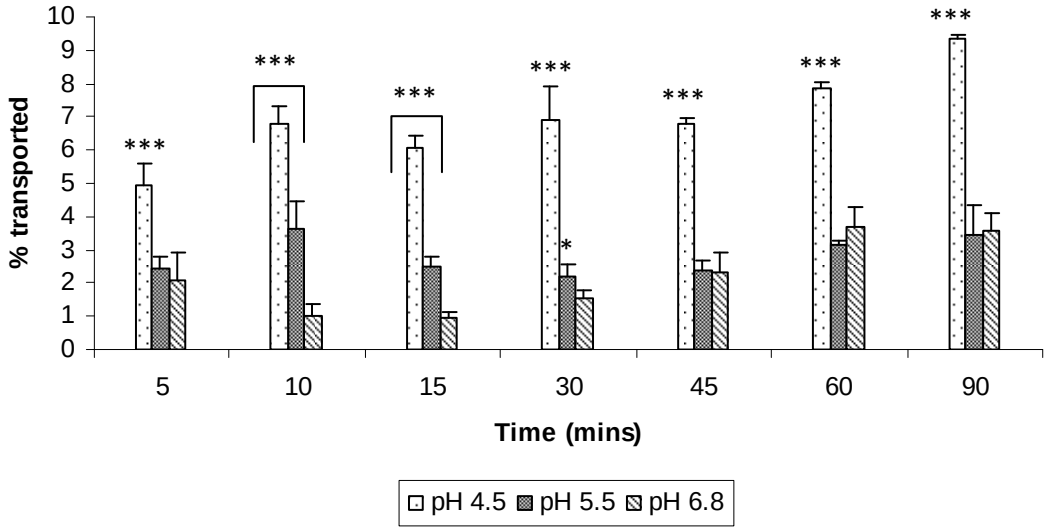

Figure 5.2.99:- Percentage of CIP transported across Caco-2 monolayers at various pHs (n=5). One way analysis of variance (ANOVA) and pair-wise multiple comparisons method (Tukey test) against drug alone at each time point were used for statistical analysis and probability values of (P< 0.05, * and P<0.001,*) were used to determine the significant difference.**

After 5 minutes 2.31±0.68% CIP was absorbed at pH 6.8 and the percentage slightly changed to 2.41±0.39% and significantly increased to 4.92±0.68% when the apical pH was dropped to 5.5 and 4.5 respectively. The percentage of CIP transported increased from the transwells with lower pH (4.5) until it reached 9.34±0.098% after 90 minutes, while at higher pH the percentage transported did not exceed 4%. The improvement in permeability at lower pH could be attributed to the increase of CIP solubility as suggested by Li et al., (2007); this would subsequently have a significant impact on dissolution profile making a higher concentration of CIP available for permeability. Similar findings were reported by Lee et al., (2005) who found that changing the apical pH of Caco-2 monolayers from 7.4 to 6.5 resulted in a five to 8 fold increase in the apparent permeability of acidic and basic drugs. In contrast, conducting similar experiments in rabbit jejunum has not shown any impact on the drug uptake at different pHs (Shiau et al., 1985). The study concluded that the presence of an adherent layer of mucus gel on the rabbit jejunum acts as a protective barrier for the epithelial cells and maintains the

acidic microclimate by hindering the movement of hydrogen within the surrounding matrix of the lumen (Shiau et al., 1985).

Table 5.2.46:- The percentage recovery and TEER measurements before and after the permeability assay of CIP at pHs of 4.5, 5.5 and 6.8 (n=5).

pH	TEER measurements (Ω/cm^2) Before	TEER measurements (Ω/cm^2) After	Recovery (%)
4.5	427.3±48.01	370±13.28	90
5.5	481.3±10.26	380.3±4.16	79.8
6.8	456.6±15.2	390±22.24	87.2

Microarrays studies

5.2.3.5. Image analysis, data clustering and principle component analysis (PCA)

According to our permeability studies, significant increase of the amount of CIP absorbed was observed. Hence, three formulations were selected for the microarray experiment namely CIP alone, CIP PM 1:1 and CIP PM 1:8 with glutamic acid. in order to visualise the genetic changes occurring during exposing the cells to the therapeutic agent and its ion-paired formulations with glutamic acid, three time points were selected 5, 30 and 60 minutes. Genetic changes that occur for Caco-2 cells without application of any therapeutic agents were selected as a control for this study (basal state). Prior to data normalization and clustering, the quality of the TIFF image obtained from the scanner was assessed for its quality. Spot centroids were located for each corner of the slides and only slides with correctly located spots were used in this study. A symmetric histogram of number of points against the logarithm of the processed signals was obtained for the used slides. Besides, all the slides used showed low multiplicative detrending and median coefficient of variation ranging between 3.6 and 7.01 which reflects the high reproducibility of the signals of the arrays.

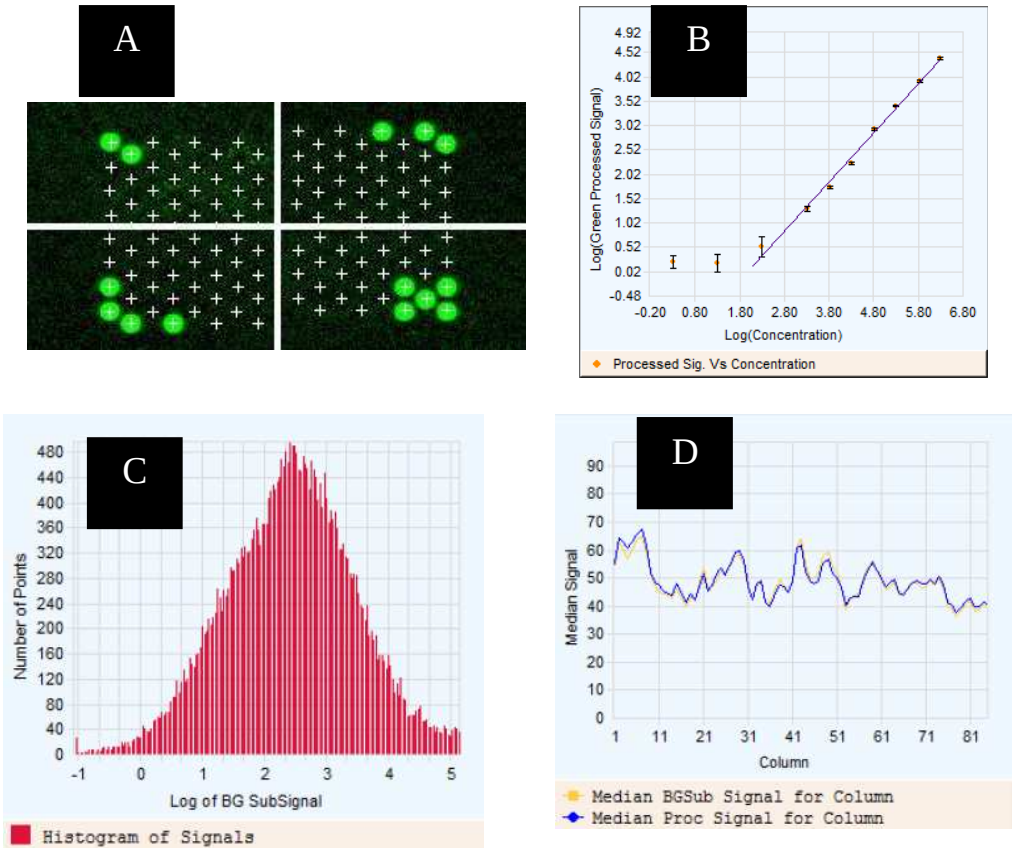

Figure 5.2.100:- Microarray image analysis; spot finding for four corners (A), correlation between log signal against log Relative concentration (B) histogram of signals plot (C), and spatial distribution of median signals for each column (D). Data were generated by feature extraction software.

The data obtained from each microarray experiment is highly complex in terms of quantity and dimensions. In order to interpret the biological meaning of the obtained data, clustering and principle component analysis were carried out. After clustering the data using hierarchal clustering, PCA was studied in to identify the dimension of extension of the data as discussed earlier in TMP chapter. Eigen values were calculated using TMEV software and the data showed that 24.12% of the changes occur along the first component and 56.27% occurs along the first three components. Therefore, the principle component 1, principle component 2 and principle component 3 were used to describe the changes of the molecular state of the cell and to determine the dynamic trends during the absorption of CIP and its ion-paired formulations with glutamic acid.

Figure 5.2.13 shows that some of the data are gathered around the origin and these samples show minimal variation in gene expression over the time course of the experiment. Interestingly, significant variations were observed at 30 minutes at principle component 1. And it seems that the formulations have played a significant role in such variation as CIP alone, CIP 1x (i.e. CIP: glutamic acid at 1:1 molar ratio) and CIP 8x (i.e. CIP: glutamic acid at 1:8 molar ratio) were separated from the rest of the samples (Fig. 5.2.13).

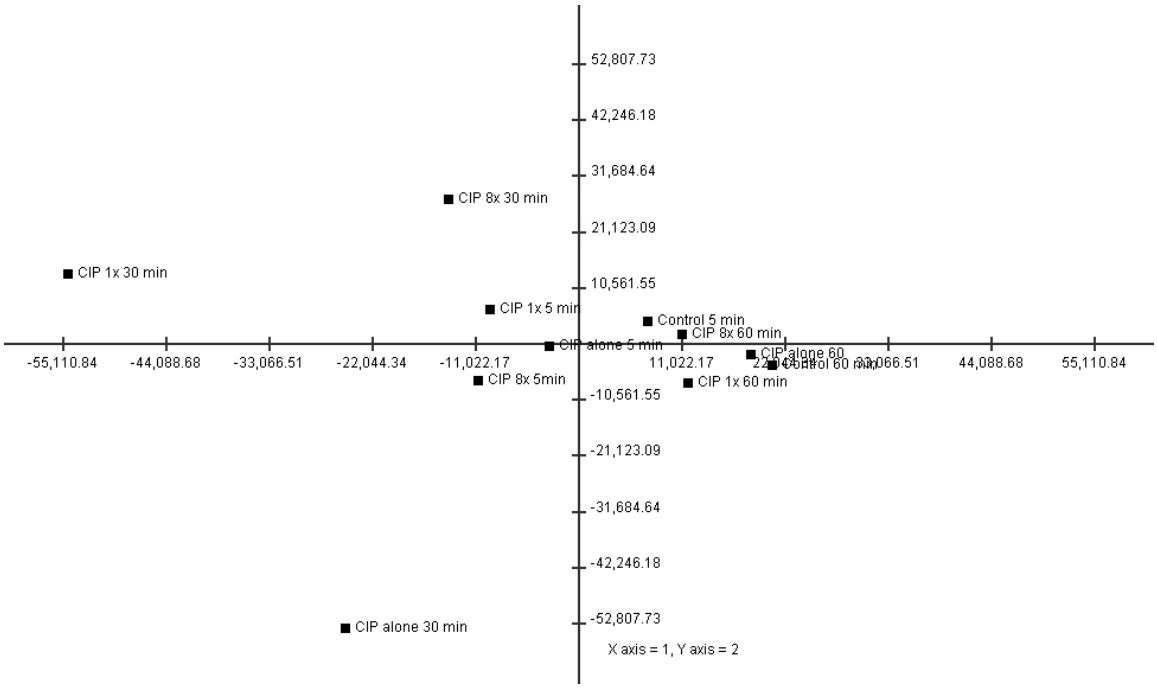

Figure 5.2.101:- First and second principal component analysis on the transcriptional time course (0, 30 and 60 minutes) for CIP and its various ion-paired formulations. The number represents the time points. The plot represents the data for the mean values at each time point.

On the other hand, principle component analysis for component 2 and 3 has showed a maximum variation based on the duration of the experiments. In another word, expression changes at 5 minutes varied from expression changes occurred at 30 minutes and both varied from the changes occurred at 60 minutes (Fig. 5.2.14).

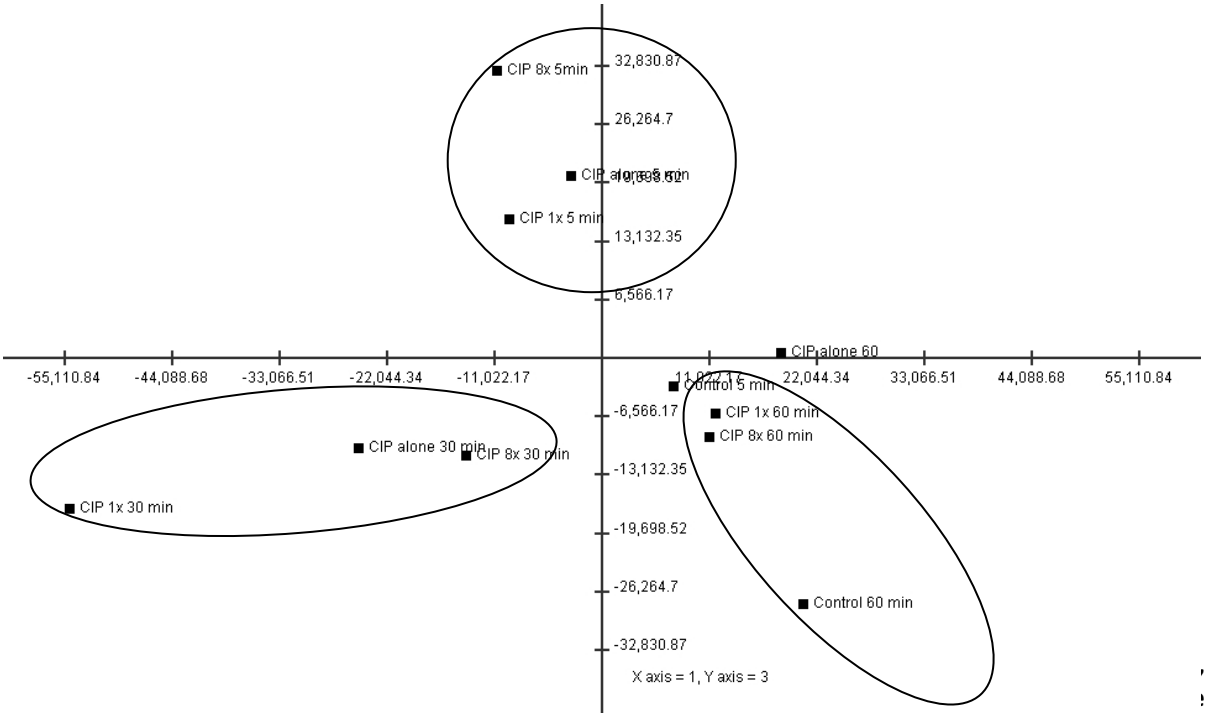

points. The plot represents the data for the mean values at each time point.

5.2.3.6. Genetic changes of transporters pathways

Approximately 45,000 cDNA were hybridized with the microarray chip probes in order to investigate the systemic changes of the gene expression occurring during CIP transportation study. Genes which were over-expressed or down-regulated by at least two fold when compared against the control were selected for this study. Equations 5.2.12 & 5.2.13 were used to calculate the level of up or down regulation of the expressed genes when compared against the control (Caco-2 cells).

$$IF_{(E>C)} = 2^{(E-C)} \quad \textbf{Equation 5.2.63}$$

$$IF_{(E<C)} = -2^{(C-E)} \quad \textbf{Equation 5.2.64}$$

The results showed that a total of 104 genes including 2 genes that code for drug transport were over-expressed after 5 minutes of exposing the cells to CIP alone when compared to control (Caco2 cells). On the other hand, 248 genes were down-regulated at the same time

point. Exposing the cells to CIP alone formulations for longer time (30 minutes) resulted in activation of 1790 genes (over-expressed by at least 2 fold), while 229 genes were down regulated suggesting that a turnaround time between 5 and 30 minutes is essential to determine any significant gene expression changes when studying drug transport. The total number of both over-expressed and down-regulated genes began to drop again after 60 minutes as shown in Fig. (5.2.15).

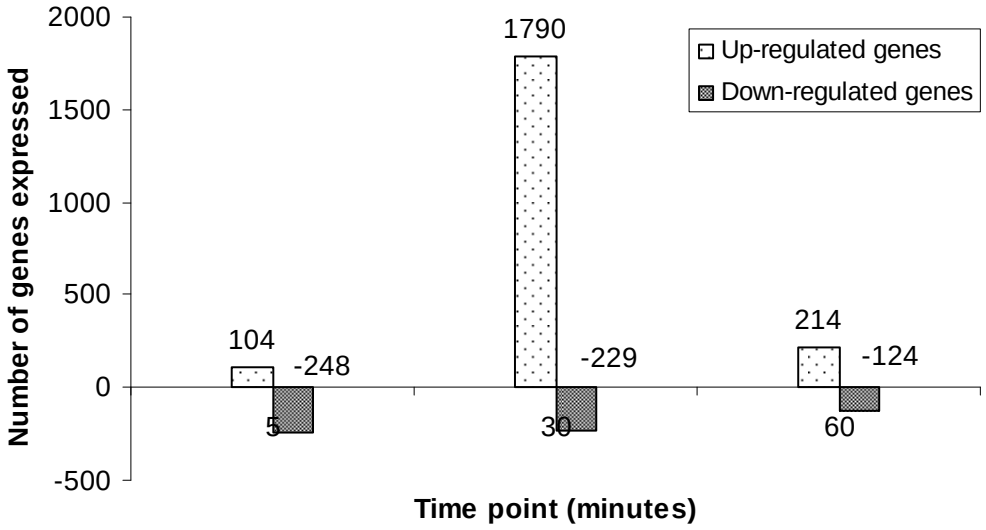

Figure 5.2.103:- Total number of genes up and down-regulated upon exposing the cells to CIP alone formulation at different time courses.

The next stage of data evaluation was focused on identifying various genes that are involved in drug transport from the total set of genetic changes (Fig. 5.2.15) and Table (5.2.8) summarises the genes over-expressed upon exposing Caco-2 cells to CIP alone formulations for 5, 30 and 60 minutes.

As data analysis using PCA indicated that major changes in expression profile occur after 30 minutes, genes exhibiting significant variations were uploaded onto KEGG to determine their role in various cellular pathways. Pathway analysis of significant genes showed that 15 different pathways including metabolic pathways, cytokine-cytokine interactions, pathways in

cancer, neuroactive ligand receptor interaction and regulation of actin cytoskeleton were affected.

Table 5.2.47:- Summary of the over-expressed transporter genes upon exposing Caco-2 cells to CIP alone formulations for 5, 30 and 60 minutes.

Time point	Probes	Gene symbol	Expression level
5 minutes	A_23_P307570	ABCC13	3.163352
	A_23_P159851	SLC7A3	4.083838
30 minutes	A_23_P215720	CFTR	2.01546
	A_24_P222291	ABCC4	2.32746
	A_23_P82523	ABCB1	3.996312
	A_23_P28246	SLC23A3	2.223539
	A_32_P130630	SLC16A7	5.549221
	A_24_P131880	SLC10A7	2.940933
	A_23_P355377	SLC12A5	2.028348
	A_24_P382467	SLC39A3	2.702885
	A_32_P381593	SLC26A7	15.35347
	A_24_P342829	SLC16A14	2.441215
	A_23_P137097	SLC16A2	3.813012
	A_23_P388900	SLC22A15	23.0606
	A_24_P910660	SLC6A2	4.799098
	A_32_P812442	SLC36A3	2.250099
	A_24_P270688	SLC38A7	2.482864
	A_23_P13725	SLC6A15	9.024523
	A_23_P77653	SLC12A3	2.828382
	A_23_P388170	SLC39A3	4.650775
	A_23_P159076	SLC17A8	2.137794
	A_23_P418562	SLC6A11	5.915653
	A_24_P191312	SLC1A4	4.691002
	A_23_P389799	SLC25A42	3.16615
	A_23_P431734	SLC25A37	4.422084
	A_24_P21829	SLC22A24	8.132694
	A_24_P913210	SLC11A2	2.042913
	A_24_P397435	SLC6A3	10.85624
	A_24_P101941	SLCO4C1	2.927174
60 minutes	A_23_P166297	ABCG1	-2.29228
	A_23_P143309	SLC4A11	-2.68538

By looking at ATP-binding cassette (ABC) transporter network (Fig. 5.2.16) it was observed that among the all ABC carriers only three (ABCB1, ABCC4 and CFTR) were over-expressed significantly after treating Caco-2 cells with CIP alone for 30 minutes as outlined in (Fig. 5.2.16).

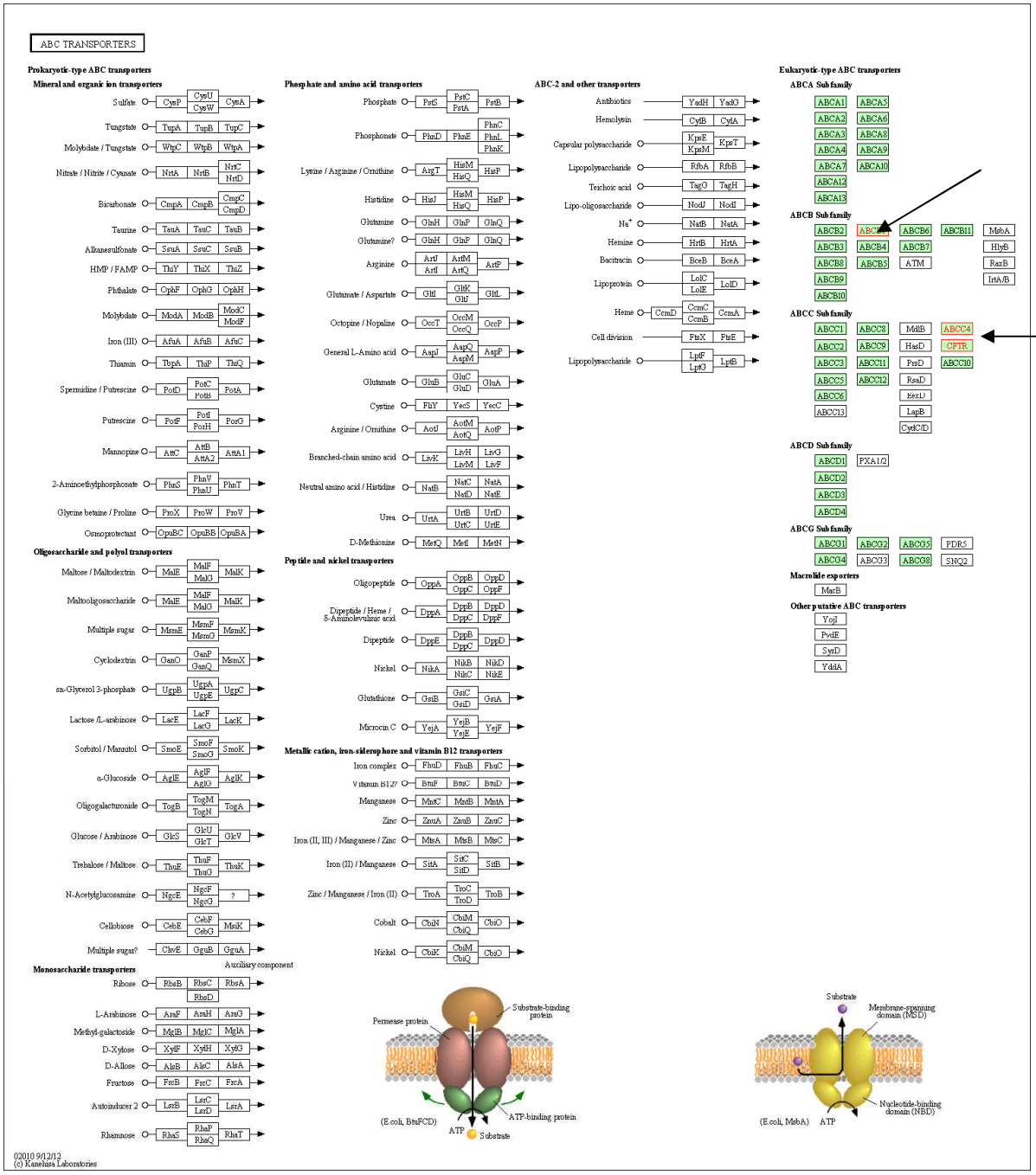

Figure 5.2.104:- Graph high-lightening the over-expressed ABC transporters during the absorption of CIP across Caco-2 cells. The graph was generated by KEGG online database.

ABCB1 which is also known as MDR1 or P-gp is an ATP-binding cassette transporter belonging to subfamily B (member 1) was 3.99 fold over-expressed when compared against the basal state of the cells (control; Caco-2 cells without drug treatment). These findings come in line with the results suggested by Park et al., (2011). Park and co-workers demonstrated that

MDCK1 and MDCK1-MDR1 cells over-express P-gp upon exposure to CIP and the basal/apical flux of CIP decreases if P-gp inhibitors such as ketoconazole, vinblastine and verapamil are used. The fourth member of the ATP-binding cassette subfamily 4 (ABCC4) is another over-expressed gene upon treating the cells with CIP alone for 30 minutes as it was up-regulated by 2.3 fold. ABCC4 is a multidrug resistance-associated protein and also known as MRP4 and plays a role in transporting organic anions. Marquez et al (2009) believed that the efflux of CIP is mediated by one of the multidrug resistance associated proteins. The study showed that MRP2 and MRP4 are up-regulated in CIP resistance cells with the expression of MRP4 overwhelmingly predominant than MRP2 (Marquez et al., 2009).

CFTR or cystic fibrosis transmembrane conductance regulator is another ABC transporter that was over-expressed by 2.01 fold in CIP alone formulations. CFTR is the 7th member of MRP family and functions as a chloride channel. The mutation of this gene was associated with an autosomal recessive disorder known as cystic fibrosis. No studies have evaluated the role of CFTR in the transport of CIP apart from Marquez et al (2009) who suggested that CFTR (MRP7) plays no role in the efflux of CIP.

Interestingly, treating Caco-2 cells with CIP alone formulations for 30 minutes resulted in triggering various signalling pathways which are involved in the tight junction (TJs) assembly. TJs define the boundaries between the apical and basolateral plasma membrane as they work as paracellular barriers that limit the uptake of solutes across the intercellular space (Salama et al., 2006). TJs are assembled by cascade of biochemical events in the cells which lead to the formation of various elements of the TJs which have only been partially characterized (Tsukita and Furuse, 1999). They are mainly composed of three proteins: occludin, claudin and immunoglobulin as adhesion protein (Matter and Balda, 2003). Assembly of TJ components is mediated by signalling pathways such as protein kinase A (PKA) and protein kinase C (PKC)

which regulates the junction pore size and cell polarity. Partition defective genes (PAR) are other signalling modulators that have two members; PAR3 and PAR6. PAR3 binds with PAR6 and PCKs to form PKC-PAR3-PAR6 complex that form TJ and build epithelial polarization (Matter and Balda, 2003).

Among the up-regulated PKC genes were protein kinase C beta (PRKCB) and protein kinase cGMP (PRKG1) which were over-expressed by 6.4 and 8.09 fold respectively (Fig. 5.2.17). From the partitioning defective genes, PAR6 was over-expressed by 13.9 fold (Fig. 5.2.17). Moreover, various genes associated with myosin light chain regulation such as MYO16, MYL7, MYL2 and MYO3B were over-expressed by 3.22, 2.4, 3.33 and 3.94 fold respectively. These genes activate myosin formation which serves as a link to the plasma membrane (Anderson et al., 1995). These results suggest that CIP would play a significant role in modulating the assembly of tight junctions across the epithelial cells and this could be another barrier that hinders CIP influx besides the efflux proteins.

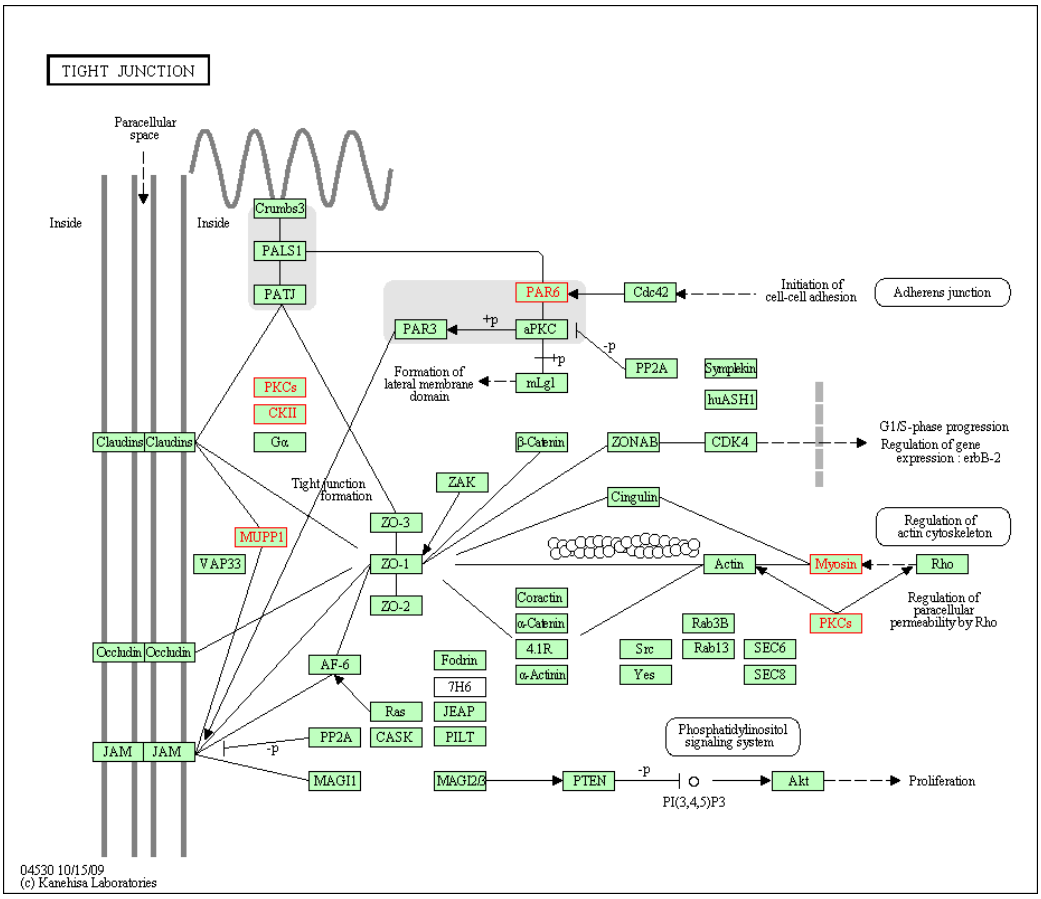

Figure 5.2.105:- The activated signalling pathways involved in tight junction formation. Activated mediators are highlighted in red. The graph was generated by KEGG online database.

The genetic changes that occur upon exposing the monolayers to the ion-paired formulations: CIP PM 1:1 and CIP PM 1:8 on Caco-2 cells were also investigated. Majority of the changes that took place for the transporter network were observed for solute carrier transporters and only few changes were recorded for ATP-binging cassettes (Fig. 5.2.18). CIP: glutamic acid PM at 1:1 molar ratio did not stimulate the over-expression of ABCB1 (P-gp) nor ABCC4 (MRP4) genes during the entire time course of the experiment. Moreover, the expression profile of P-gp and MRP4 were down regulated by 2.6 and 2.59 fold after 30 minutes of exposure to the 1:1 ion-paired formulations (Fig. 5.2.18). These results suggest that ion-paired formulations mask the triggering effects of CIP on the efflux protein and that both P-gp and MRP4 failed to identify CIP when it was formulated as an ion-pair with glutamic acid.

Besides, comparing the expression patterns of some of the genes as listed in Fig. 5.2.18 and (Table5.2.8) the results show that the genes up-regulated upon exposure to CIP were down-regulated to their basal state when the ion-paired formulations were used. For instance, ABCC13 and SLC7A3 were over-expressed by 3.16 and 4.08 fold respectively when the cells were exposed to CIP alone formulations but were down-regulated by 2.03 and 3.65 fold respectively when 1:1 molar ratio of ion-paired formulations were used which further confirms the inability of the transporters to identify CIP when it is ion-paired.

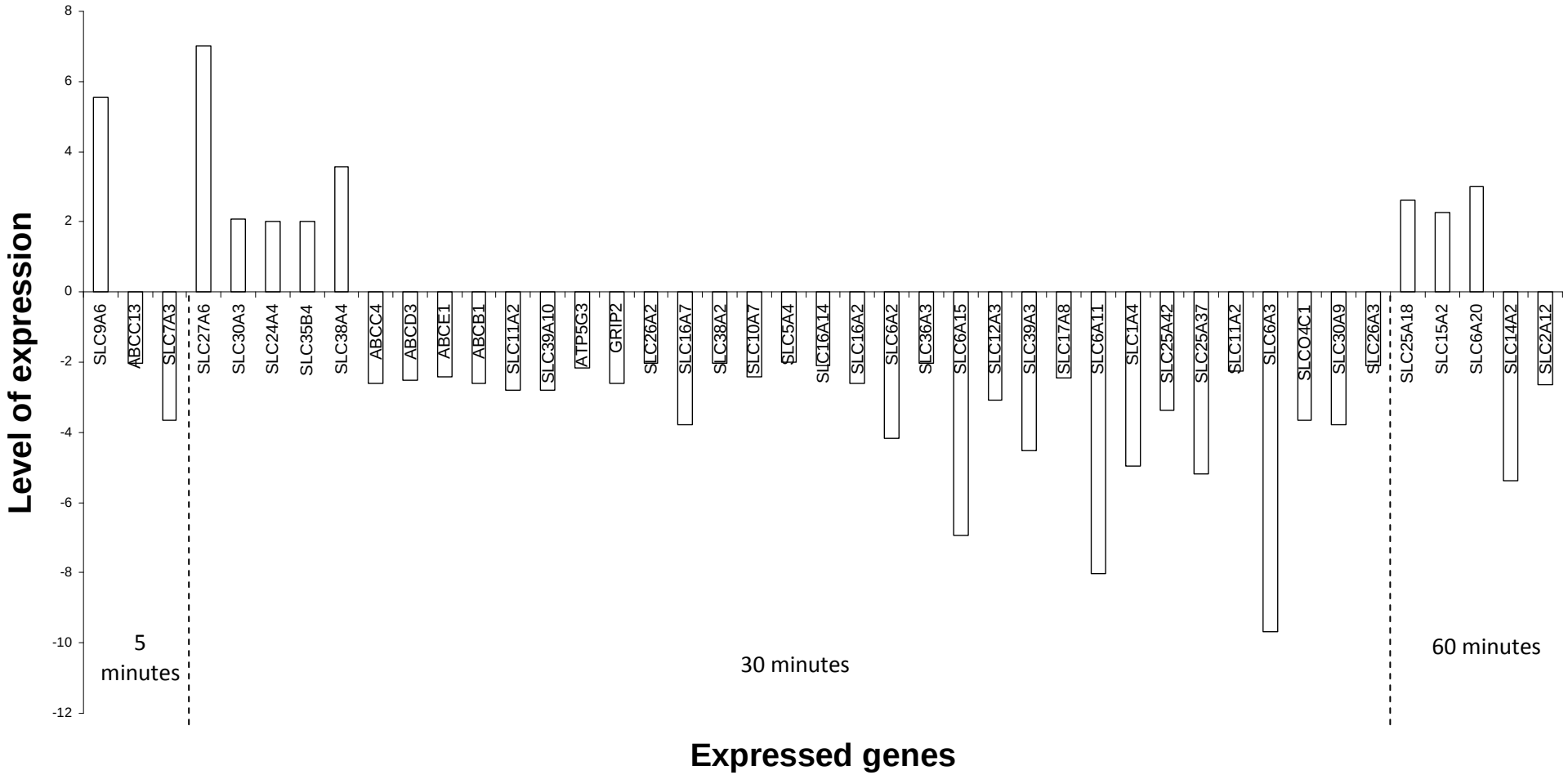
Level of expression
8
6
4
2
0
-2
-4
-6
-8
-10
-12
SLC9A6
ABCC13
SLC7A3
SLC27A6
SLC30A3
SLC24A4
SLC35B4
SLC38A4
ABCC4
ABCD3
ABCE1
ABCB1
SLC11A2
SLC39A10
ATP5G3
GRIP2
SLC26A2
SLC16A7
SLC38A2
SLC10A7
SLC5A4
SLC16A14
SLC16A2
SLC6A2
SLC36A3
SLC6A15
SLC12A3
SLC39A3
SLC17A8
SLC6A11
SLC1A4
SLC25A42
SLC25A37
SLC11A2
SLC6A3
SLCO4C1
SLC30A9
SLC26A3
SLC25A18
SLC15A2
SLC6A20
SLC14A2
SLC2A12
5 minutes
30 minutes
60 minutes
Expressed genes

Permeability data showed that increasing the molar concentration of glutamic acid in the formulations results in an increase in the overall uptake of CIP (Fig. 5.2.7). Nevertheless, partitioning studies have demonstrated that there is a steady decline of drug partition upon increasing the counter ion concentration (Fig. 5.2.5). Permeability data coupled with partitioning studies suggest that CIP fails to permeate across the lipid bilayers of Caco-2 cells and it is possible that there are cellular mechanisms responsible for the differences in permeability profile.

The genetic changes that occurs upon using CIP:glutamic acid 1:8 formulations were investigated and summarised in (Fig. 5.2.19) and table (5.2.9).

During the first 5 minutes 7 transporter genes were over-expressed; all of the over-expressed genes belong to solute transporter carriers (Fig. 5.2.19A).

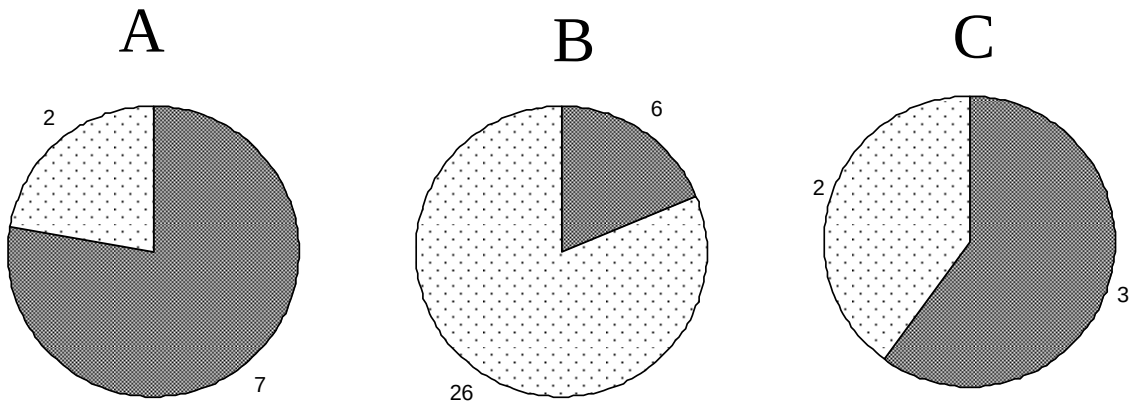

Figure 5.2.107:- Up-regulated( ) and down-regulated( ) genes after exposing Caco-2 cells to CIP: glutamic acid at 1:8 molar ratio after (A) 5 minutes, (B) 30 minutes and (C) 60 minutes.

Among the over-expressed solute carriers genes were amino acid transporters; SLC6A15 and SLC6A1. It can be hypothesised that the high content of glutamic acid in 1:8 formulations results in the over-expression of these transporters. Both the transporters belong to family 6 (Fig. 5.2.20) of the solute carrier transporters which play a significant role in transport of a broad range of amino acids across the epithelial cells and also remove any neurotransmitters

from brain cells (Broer et al., 2006; Takanaga et al., 2005). SLC6A15 was first isolated by Uhl and co-workers in 1992 and is a Na^+ dependent and Cl^- independent transporter. Later it was found that it has affinity to alanine, glutamine, proline, leucine isoleucine and methionine.

SLC6A1 on the other hand (also known as GAT1) is considered the predominant transporter for γ-amino butyric acid (Chen et al., 2004).

SLC6A15 and SLC6A1 were over-expressed by 2.12 and 2.56 respectively upon treating the cells with 1:8 molar ratio of CIP: glutamic acid.

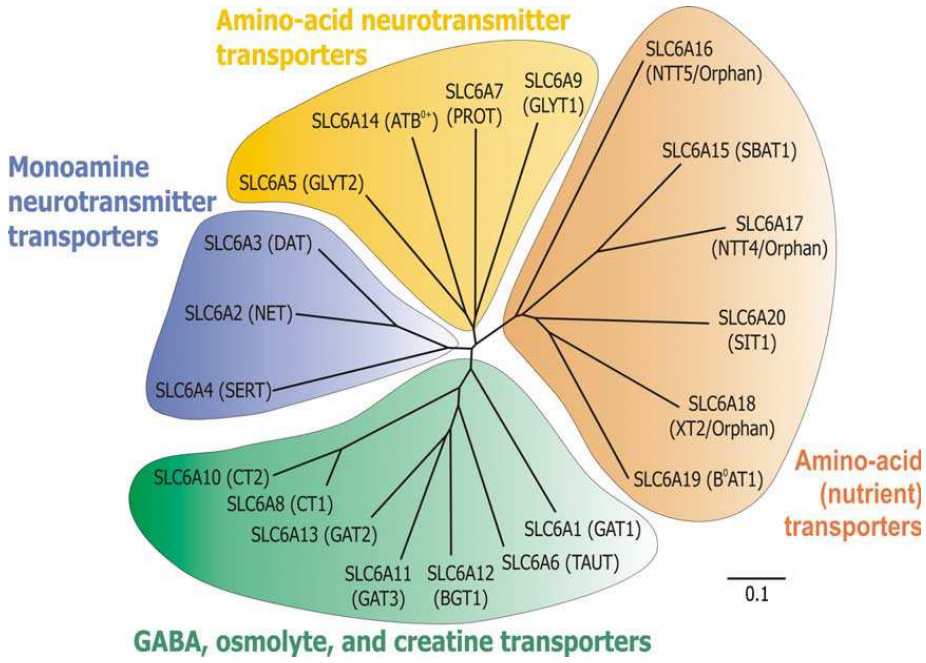

Figure 5.2.108:- Phylogenetic tree of various members of the human SLC6 transporter family adapted from Takanaga et al., 2005.

Interestingly, SLCO1A2 -an organic anion transporting polypeptide (OATPs)- was also over-expressed after 5 minutes (Table 5.2.9). The first member of OATPs was isolated in 1994 from rat liver and is believed to transport a variety of organic compounds in a sodium independent manner (Geyer et al., 2004). SLCO1A2 (also known as OATP1A2) was up-regulated 2.13 fold, and is possible that the loss of the zwitter ionic nature of CIP upon ion-pairing with glutamic

acid results in the up-regulation of SLCO1A2 as the ion-paired complex carries a net negative charge as discussed earlier.

Another up-regulated solute carrier transporter was SLC15A2 which belongs to a peptide transporter family and mediates the uptake of dipeptides and tripeptides (Rubio-Aliaga and Daniel., 2002). Two peptide transporters SLC15A1 (PEPT1) and SLC15A2 (PEPT2) have been identified in mammalian cells. Both PEPT1 and PEPT2 have similar function but differ in affinity and capacity. The two peptide transporters have been reported as potential targets for prodrug absorption. The uptake of L-DOPA L-Phe prodrug (Tamai, *et* al. 1998) and acyclovir L-valyl ester (Ganapathy, et al. 1998) was increased by several fold as their uptake was mediated by PEPT1 and PEPT2. It is possible that besides the organic anionic transporter, PEPT2 (SLC15A2) also mediates the uptake of the ion-paired formulations and hence results in the increase of CIP uptake across the Caco-2 monolayers.

Table 5.2.48:- Over-expressed genes upon exposure to CIP:glutamic acid at 1:8 molar ratio.

Time point	Probes	Gene symbol	Expression level
5 minutes	A_23_P131111	SLC27A1	2.037017
	A_24_P307653	SLC6A15	2.124151
	A_23_P13820	SLCO1A2	2.129753
	A_24_P268685	SLC6A1	2.564218
	A_23_P160159	SLC2A5	68.07858
	A_23_P22625	SLC9A6	6.909355
	A_24_P208345	SLC45A3	17.85949
30 minutes	A_23_P43504	ABCA2	2.777874
	A_23_P133694	SLC29A1	2.365923
	A_24_P79153	SCAMP4	2.263806
	A_23_P77049	SLC25A29	2.148496
	A_23_P316960	GRINA	2.094572
	A_23_P210521	SLC2A10	2.780049
60 minutes	A_24_P74508	SLC25A18	2.632616
	A_23_P92107	SLC15A2	2.270138
	A_23_P212379	SLC6A20	2.991979

Moreover, the efflux transporter genes; P-gp and MRP4 were down-regulated by 3.3 and 2.2 fold respectively upon using the ion-paired formulations at 1:8. The genetic profiling of the transporter genes demonstrated that the efflux transporters were down-regulated to their basal state upon the ion-pairing the formulations. The data also showed that ion-pairing has

resulted in new routes for uptake of CIP across the membrane which explains the increase in permeability profile despite the decrease in partitioning capacities of the drug upon pairing with the anionic counter ion.

5.2.3.7. Genetic changes of metabolic pathways and other pathways

Microarray data analysis has also revealed that other pathways in addition to transporter pathways were significantly affected during the time course of the experiment upon ion-pairing CIP formulations.

Cellular metabolism was among the most affected pathways during drug uptake. Four metabolic pathways were up-regulated when the Caco-2 cells were exposed to CIP for 5 minutes. The number of metabolic pathways increased to 36 when the drug was left to permeate for 30 minutes. The majority of the up-regulated pathways were involved in Glycan, carbohydrates and lipid metabolism (Fig. 5.2.21). Metabolism of glycan and carbohydrates is considered the major carbon and energy source for living cells. During glycan metabolism, oxidative processes are involved which utilize the produced electrons to form ATP which is considered as a fast energy source for the cells. It can be hypothesised that the high glycan metabolism was stimulated by the cells in order to produce more ATP which is required by the efflux transporters (MRP4 and P-gp). On the other hand, using the ion-paired formulations showed a significant drop in the pathways involved in glycan and carbohydrates metabolism (Fig. 5.2.22) again re iterating that the presence of oppositely charged ions masks the identification of CIP and that alternate pathways are used for drug permeation.

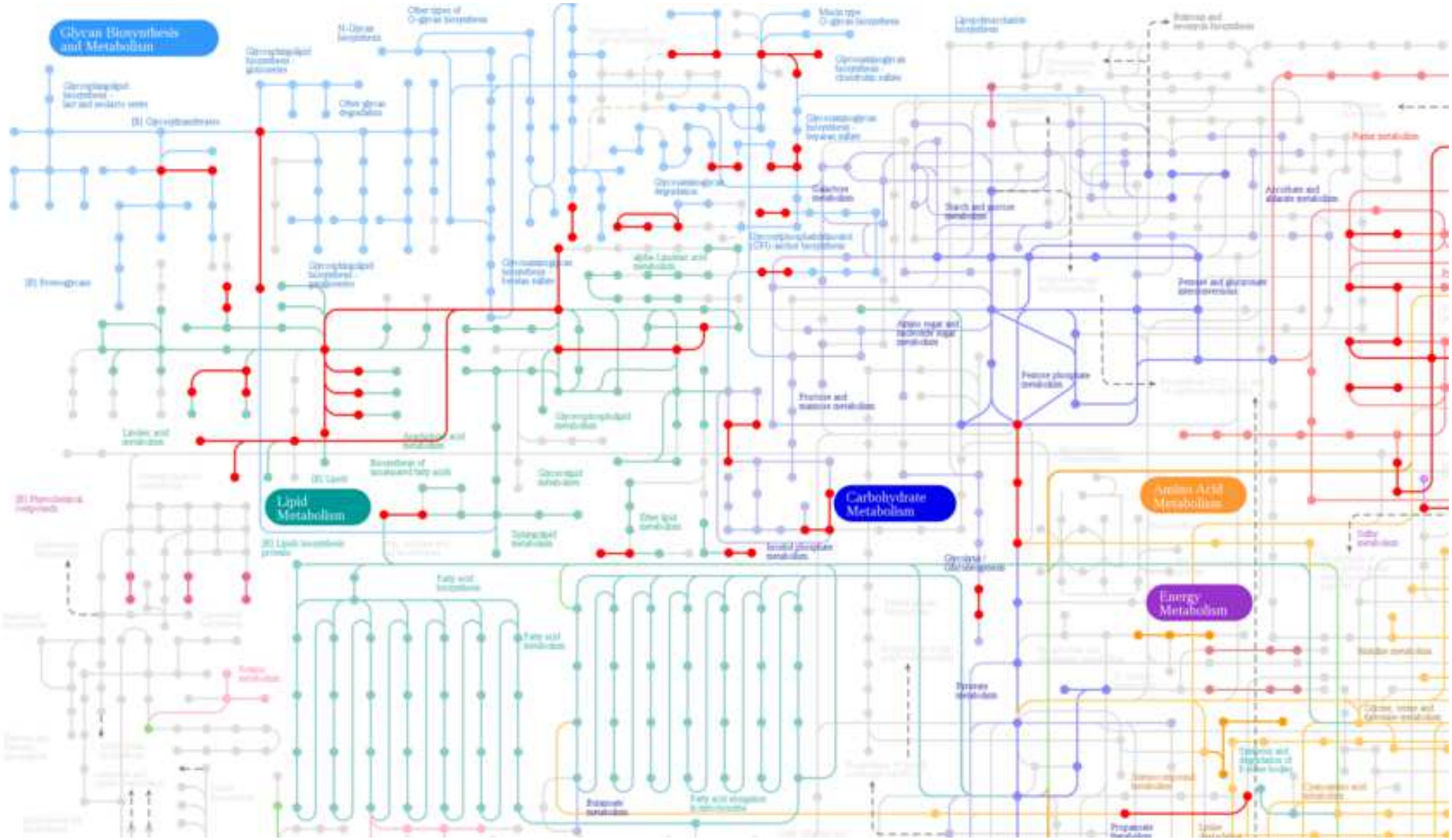

Figure 5.2.109:- Glycan synthesis and metabolism after 30 minutes of exposure to CIP alone formulations. The graph was generated by KEGG online database.

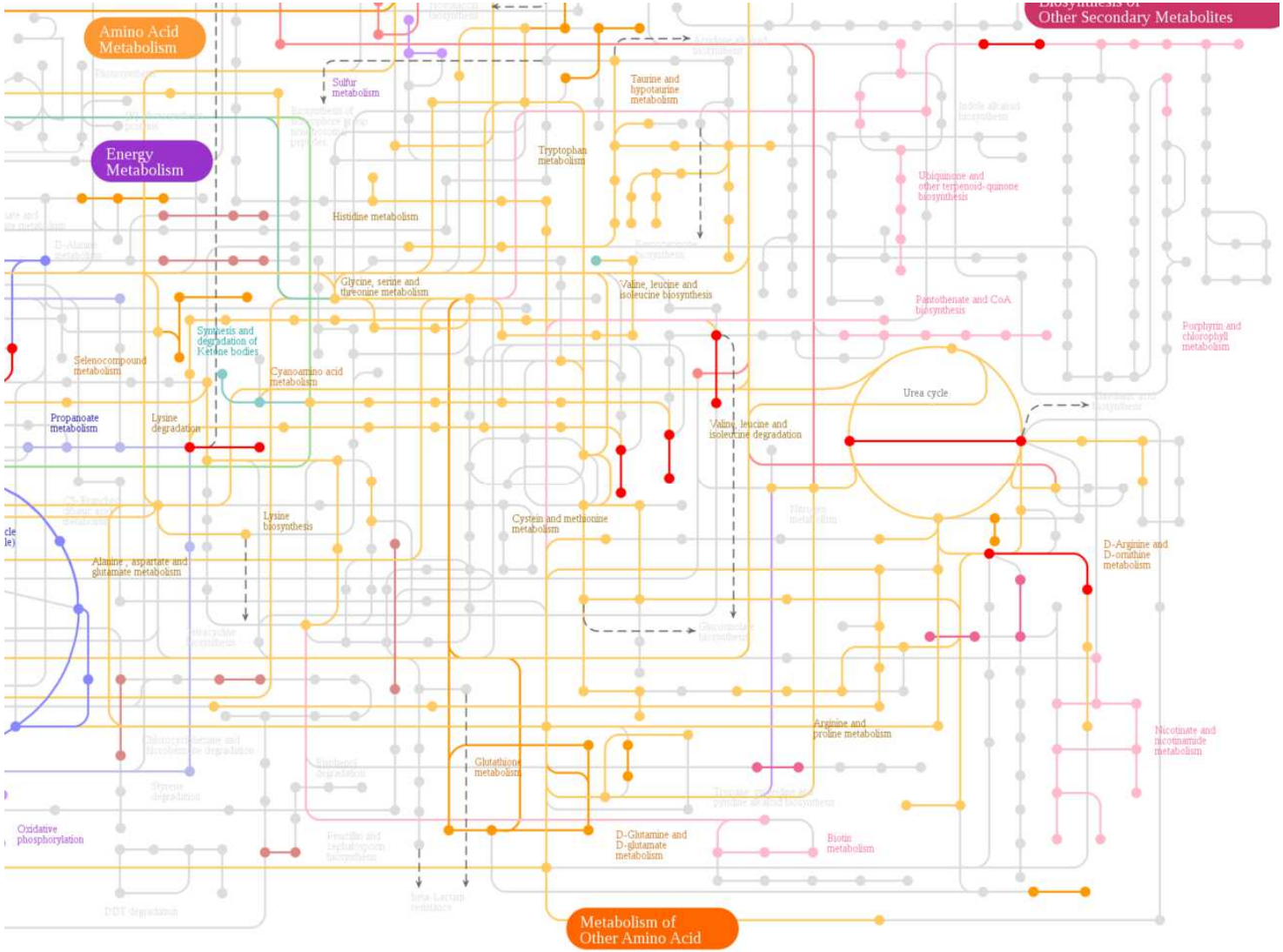

Figure 5.2.110:- Amino acid metabolic pathways activated after 30 minutes of exposure to CIP:glutamic acid at 1:1 molar ratio formulations. The graph was generated by KEGG online database.

Calcium signalling was another pathway that was found to be affected by exposing the cells to CIP. Calcium is essential to trigger the activity of nitric oxide synthase (NOS) in order to produce nitric oxide (NO). Nitric oxide is a universal intracellular messenger that modulates the normal activities, blood flow and also plays a role in protecting the cells against pathogens as it works as non-specific host defence (Pacher et al., 2007). Interestingly, CIP was found to deactivate NOS which could be because of the high ability of CIP to chelate with calcium (Susana et al., 2002) which in turn reduces Ca^{+2} concentration and NOS production. In order to decrease the Ca^{+2} flux into the mitochondria, voltage dependent anion channel (VDAC) was deactivated (Fig. 5.2.23) in a trial to decrease the calcium flux into the mitochondria as suggested by Tan and Colombini (2007).

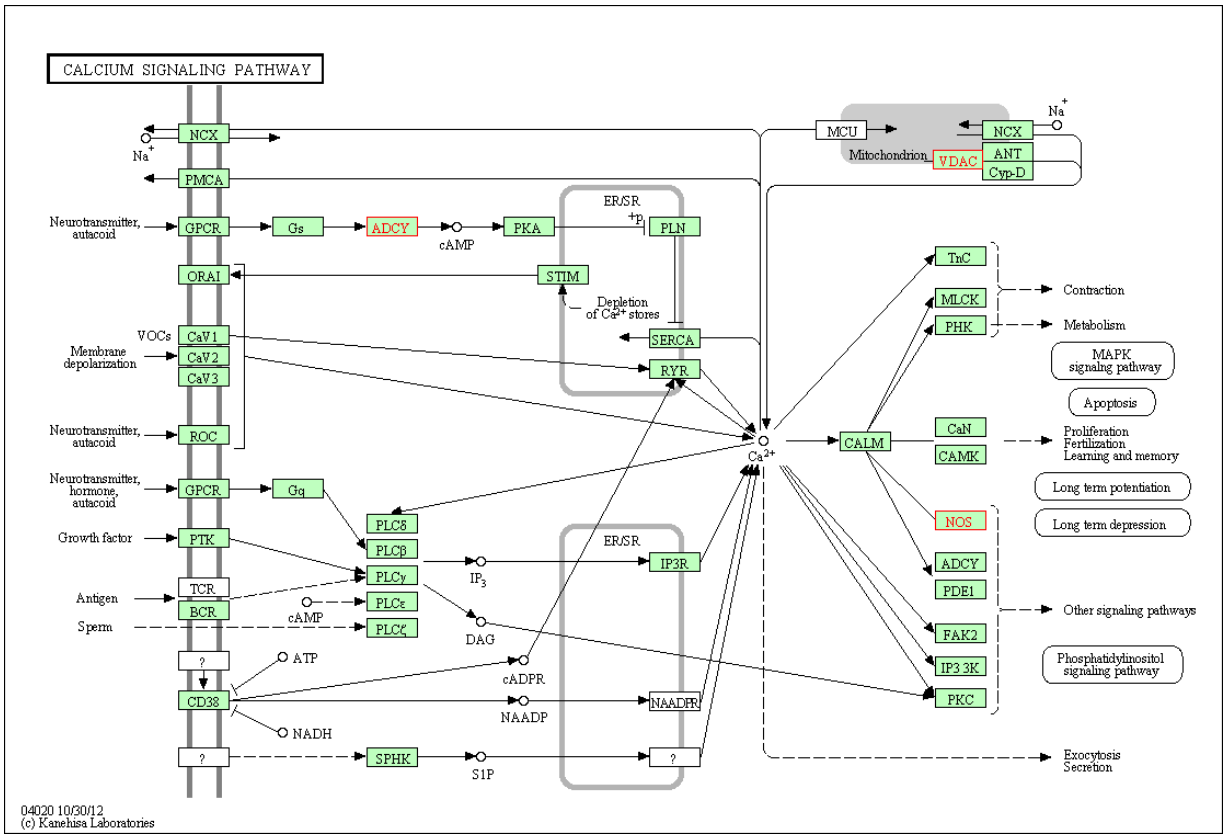

Figure 5.2.111:- Down-regulated mediators (highlighted in red) involved in calcium signalling pathways during CIP uptake across Caco-2 cells and after 30 minutes of the permeability assay. The graph was generated by KEGG online database

Calcium signalling pathway was reverted to the normal state upon coupling CIP with glutamic acid which reflects the stability of the formed ion-pair over complex formation with intracellular calcium.

5.2.4. Conclusion

CIP is a BCS IV drug that has low solubility and low permeability and it is believed that the small intestine plays a major role in its excretion. Despite showing high partitioning capacities in the organic phases, CIP permeability across Caco-2 monolayers was very low and did not exceed 10% after 90 minutes of the permeability assay. Microarray data showed that P-gp and MRP4 were over-expressed when the cells were exposed to CIP and they are believed to mediate the efflux of the drug. Moreover, tight junction formation was stimulated by CIP and this could be another barrier for CIP uptake. On the other hand, ion-pairing CIP with glutamic acid resulted in a significant improvement of CIP absorption as the apparent permeability increased by 10, 50 and 75 fold for PM 1:2, PM 1:4 and PM 1:8 respectively. Two solute carrier transporters (SLCO1A2 and SLC15A1) were up-regulated upon using the ion-paired formulations. It seems that these two carriers mediates the uptake of the ion-paired formulation especially SLCO1A2 because the ion-paired CIP carries anionic charge which might have stimulated the organic anion transporters. In conclusion, the improved uptake of CIP ion-paired formulations could be due to the reduced efflux by ABC transporters or increased entry and transport via new solute carrier transporters.

Conclusion

Biopharmaceutical properties of drug candidates have a great impact on their bioavailability as it was recognised that both the rate and extent of oral drug bioavailability is controlled by the aqueous solubility and gastro-intestinal permeability of the therapeutic agents (Amidon et al., 1995). Therefore a new biopharmaceutical classification system was introduced in 1995 and accepted by FDA in 2000. Various physical and chemical techniques were adapted in order to improve aqueous solubility and intestinal uptake. Solid dispersion, cyclodextrins and prodrugs were among the commonly used techniques for this purpose. The theory behind prodrug synthesis is binding additional functional groups onto the structure of the poorly water soluble drug molecule to enhance its solubility. This functional group splits from the drug molecule in vivo by enzymes. Interestingly scientists managed to use prodrugs to mask polar groups on therapeutic agents and hence improve the drugs ability to partition across membranes (Weller et al., 1993). Despite their great success, prodrugs have shown low solubilities which self limit their use as bioavailability enhancers (Majumdar et al., 2004). Moreover, prodrugs are new chemical entities and they may be inert and/or toxic. Therefore, looking for alternative methods that can improve drug bioavailability in a safe way became a must.

Counter ions were first introduced to improve solubility of low water soluble drugs until Irewin et al demonstrated that the rate and efficacy of isopropamide was improved upon ion-pairing with trichloroacetate. Since their introduction many studies tried to propose their mechanism of action as permeability enhancers. Quintanar-Gueerrero et al (1997) suggested that ion-pairs could lower the interfacial tension of the gut wall by binding to mucosal membrane.

In the current study, the use of amino acids as solubility and permeability enhancers for three model drugs was investigated. The first drug candidate is a weak acidic drug classified as BCS II as it solubility was found to be 0.244 µg/mL at pH of 4.95. This low solubility was found to

improve upon adding arginine and lysine at increasing concentrations as suggested by phase solubility diagram. Therefore, it was believed that both arginine and lysine could form highly soluble salts with IND. FT-IR confirmed salt formation as the spectrum of the carbonyl stretching of acidic group of IND disappeared due to the loss of proton and the involvement of the carboxylic group in the salt formation with the basic amino acids. Moreover, because salts have different physical properties from their components, IND arginine and IND lysine salts showed new melting endotherms at 209.73 ^{o}C and 223.26 ^{o}C respectively. Failure of histidine to bind strongly with IND was attributed to the low difference between their pk_a values. The aqueous solubility of IND improved by $2x10^3$ and 10^4 fold for IND arginine and IND lysine salts respectively.

Similarly, the solubility of TMP and CIP were enhanced by forming new salts with acidic amino acids. Although CIP is zwitter ionic in nature the drug only managed to form new salts with anionic amino acids; glutamic acid and aspartic acid resulting in increasing the solubility to 215±13.3 mg/mL and 185.4±8.6 mg/mL respectively. Simulation studies demonstrated that CIP hydrophobic interaction between its molecules decrease in the presence of acidic amino acids and in turn form stable salts, these interactions were not affected in the presence of arginine or lysine.

Results from chapters 3.1, 4.1 and 5.1 demonstrate high solubility and dissolution of IND, TMP and CIP salts reflecting the high ionisation of the salt form. Therefore, excess amounts of the counter ions were added in a trial to shift the salt ionisation equilibrium towards the non-ionised form of the salt. Octanol/water partitioning studies revealed that increasing the molar ratio of the counter ions results in a significant drop in the partitioning capacities for all the drugs in octanol organic layer. Nevertheless permeability data showed a significant increase in drug absorption especially for PMs of 1:2 molar ratios suggesting that active carrier might have

been involved in the absorption process of the ion-paired formulations as the drugs passive uptake is deteriorated by the presence of the counter ions.

Therefore, we believed that looking at the genetic changes occurring at the cellular levels of Caco-2 cells could enable better understanding about the involvement of any transporter carriers. DNA microarrays were used for this purpose as it enables visualising the systemic changes of 45,000 genes in one experiment. During TMP uptake across the monolayers, MRP7 were over-expressed significantly in more than one replicate probe across the array chip reflecting the high involvement of MRP7 in extruding TMP out of the cells. Although majorities of previous studies (Joseph et al., 2001; Murakami and Takano 2008) reported the involvement P-gp in TMP efflux, the current study showed a minimal role played by P-gp in mediating TMP efflux. Interestingly, TMP uptake was found to be mediated by organic cation transporters such as OCTN1 which was up-regulated by 2.36 fold during TMP absorption. The molar ratio of glutamic acid was found to affect the expression of OCTN1 as it expression reached 2.2 fold for 1:1 formulations and dropped to the basal state for 1:8 ion-paired formulations and hence the parabolic permeability profile was observed for TMP uptake.

Nevertheless, looking at the genetic changes that accompanied CIP uptake showed that P-gp and MRP4 were over-expressed when the cells were exposed to CIP and they are believed to mediate the efflux of the drug. Besides, tight junction formation was stimulated by CIP and this could be another barrier for CIP uptake. It seems that the anionic nature of the ion-paired CIP-glutamic acid stimulated the expression of SLCO1A2 transporters, while the high aqueous binding constant for their ion-pair (480 M^{-1}) allowed them to get absorbed as one entity through dipeptidyl transporters (SLC15A1).

Besides showing the high involvement of transporter carriers in the uptake of free drugs and their ion-paired formulations, microarrays showed the involvement of various metabolic

pathways on drug pharmacokinetics and the pharmacodynamic effects of the drug on the cellular signalling pathways.

In conclusion, amino acids could be used as a successful tool to improve the biopharmaceutical properties of drug candidates upon ion-pairing. Microarrays could be used as a powerful tool to screen new chemical entities' metabolic, toxic and absorption pathways.

List of References

Adkin, D., Davis SS., Sparrow R., Huckle P., Wilding IR. (1995a) The effect of mannitol on the oral bioavailability of cimetidine. *J. Pharm. Sci.* 84 1405–1409.

Adkin, D., Davis, SS., Sparrow, R.A, Huckle, P.D, Phillips, A.J, Wilding, IR. (1995b) The effects of pharmaceutical excipients on small intestinal transit. *Br. J. Clin. Pharmacol.* 39 381–387.

Aggarwal, S.K., Gogu, S.R., Rangan, S.R.S. and Agrawal, K.C., (1990) Synthesis and biological evaluation of prodrugs of zidovudine. *J. Med. Chem*., 33 1505-1510.

Alderborn, G., (2002) Tablets and compaction. In: Aulton, M.E. (Ed.), Pharmaceutics: The Science of Dosage Form Design. Churchill: Livingstone 397-440.

Alderborn, G., Nystrom, C., (2005) Pharmaceutical powder compaction technology., Porosity pressure functions. *Drugs and the pharm sci* . 71.

AlHusban, F.A., ElShaer, A., Kansara, J., Smith, A., Grover, L., Perrie, Y. Mohammed A., (2010a) Investigation of Formulation and Process of Lyophilised Orally Disintegrating Tablet (ODT) Using Novel Amino Acid Combination. *Pharmaceutics*; 2, 1-17.

AlHusban, F., Perrie, Y., Mohammed, A.R., (2010b) Formulation and characterisation of lyophilised rapid disintegrating tablets using amino acids as matrix forming agents. *EJPB*; 75 254-262.

Allikmets, R. (1997) A photoreceptor cell-speci¢c ATP-binding transporter gene (ABCR) is mutated in recessive Stargardt macular dystrophy, *Nature Genet*. 17, 122.

Alwine, J.C., Kemp, D.J., Stark, G.R., (1977). Method for detection of specific RNAs in agarose gels by transfer to diazobenzyloxymethyl-paper and hybridization with DNA probes. *Proc. Natl. Acad.* Sci. USA 74, 5350–5354.

Amidon, G.L., Leesman, G.D. and Elliott, R.L., (1980) Improving intestinal absorption of water-insoluble compounds: A membrane metabolism strategy. *J. Pharm. Sci.*, 69 1363 – 1368

Amidon, G. L. Lennernas, H. Shah, V. P and Crison. J. R. (1995) A theoretical basis for a biopharmaceutics drug classification: the correlation of in vitro drug product dissolution and in vivo bioavailability. *Pharm. Res*. 12:413–420

Amidon, G.L., Han, H., Oh, D.M., Walter, E., Hilfinger, J.M., (1998) Oral administration of peptide and protein drugs, *Alfred Benzon Symp*. 43, 146–156.

Amo, E.M., Urtti, A., Yliperttula, M., (2 0 0 8). Pharmacokinetic role of L-type amino acid transporters LAT1 and LAT2. *Eur. J. Pharm. Sci.* 35, 161–174

Anderson, B.D.; Conradi, R.A. (1985) Predictive relationships in the water solubility of salts of a nonsteroidal anti-inflammatory drug. *J. Pharm. Sci.* 74 (8), 815–820.

Aulton, M. E. (2002) Pharmaceutics: The Science of Dosage Form Design, 2nd Ed, ed. Ashford, M., Chapter 16 “The gastrointestinal tract – physiology and drug absorption. Churchill Livingstone: Edinburgh, UK. 217-233.

Augustijns, P., Mols, R., (2004). HPLC with programmed wavelength fluorescence detection for the simultaneous determination of marker compounds of integrity and P-gp functionality in the Caco-2 intestinal absorption model. *J. Pharm. Biomed. Anal*. 34: 971-978.

Anderle, P., P. Farmer, A. Berger, and M. Roberts. (2004). Nutrigenomic approach to understanding the mechanisms by which dietary long-chain fatty acids induce gene signals and control mechanisms involved in carcinogenesis. *Nutr.* 20,103-108.

Anderson, B.D., Conradi, R.A., (1985). Predictive relationships in the water solubility of salts of a nonsteroidal anti-inflammatory drug. *J. Pharm. Sci*. 74 (8), 815–820.

Anderson, J.M. Van Itallie, C.M. (1995). Tight junctions and the molecular basis for regulation of paracellular permeability, *Am. J. Physiol*. 269 (4 Pt 1) 467– 475.

Appelbaum, P. Hunter P. (2000). The fluoroquinolone antibacterials: past, present and future perspectives. *Int. J. Antimicrob. Agents*. 16, 5–15.

Aristilde, L., Sposito, G., (2010). Binding of ciprofloxacin by humic substances: a molecular dynamics study. *Environmental Toxicology and Chemistry* 29, 1, 90-98.

Aristilde, L., Sposito, G., (2008). Molecular modeling of metal complexation by a fluoroquinolone antibiotic. *Environmental Toxicology and Chemistry*. 27, 11, 2304-2310.

Artursson, P., Ungell, A-L., Löfroth, J-E., (1993). Selective paracellular permeability in two models for intestinal absorption: cultured monolayers of human intestinal epithelial cells and rat intestinal segments. *Pharm. Res*. 10: 1123-1129.

Artursson, P., K. Palm and K. Luthman, (2001). Caco-2 monolayers in experimental and theoretical predictions of drug transport. *Adv. Drug. Deliv. Rev*., 46, 27-43. DOI: 10.1016/S0169- 409X(00)00128-9

Artursson, P., Palm, K., Luthman, K., (1996). Caco-2 monolayers in experimental and theoretical predictions of drug transport. *Adv. Drug Deliv. Rev*. 22, 67-84.

Artursson, P.,(1990). Epithelial transport of drugs in cell culture. I: A model for studying the passive diffusion of drugs over intestinal absorptive (Caco-2) cells. *J. Pharm. Sci*. 79: 476-482.

Artursson, P., K. Palm and K. Luthman, (2001). Caco-2 monolayers in experimental and theoretical predictions of drug transport. *Adv. Drug. Deliv. Rev*. 46, 27-43. DOI: 10.1016/S0169- 409X(00)00128-9

Aungst, B.J. (1993). Novel formulation strategies for improving oral bioavailability of drugs with poor membrane permeation or presystemic metabolism. *J. Pharm. Sci*. 82, 979- 987.

Aungst, B.J., Nguyen, N.H., Bulgarelli, J.P., Oates-Lenz, K., (2000). The influence of donor and reservoir additives on Caco-2 permeability and secretory transport of HIV protease inhibitors and other lipophilic compounds. *Pharm. Res*. 17, 1175–1180.

Baird, A.W., Taylor, C.T., Brayden, D.J., (1997). Non-antibiotic anti-diarrhoeal drugs: factors affecting oral bioavailability of berberine and loperamide in intestinal tissue. *Adv. Drug Del. Rev.* 23111–120.

Baldwin, S.A., Beal, P.R., Yao, S.Y., King, A.E., Cass, C.E., Young, J.D., (2004). The equilibrative nucleoside transporter family, SLC29, *Pflugers Arch*. 447, 735–743.

Balimane, P.V., Chong, S., Morrison, R.M., (2000). Current methodologies used for evaluation of intestinal permeability and absorption., *Journal of Pharmacological and Toxicological Methods.* 44, 301-312

Barendt W. M. Wright., S. H. (2002). The Human Organic Cation Transporter (hOCT2) Recognizes the Degree of Substrate Ionization. *JBC*. 277, 25, 22491–22496,

Barlow, D. Satoh, T. (1994). The design of peptide analogues for improved absorption. *J. Control. Release* 29, 283–291.

Bastin, R.J., Bowker, M.J., Slater.B.J., (2000). Salt Selection and Optimisation Procedures for Pharmaceutical New Chemical Entities., *Organic Process Research & Development*, 4, 427-435

Behrens, I., Kamm, W., Dantzig, A., Kissel, T., (2004). Variation of peptide transporter (PepT1 and HPT1) expression in Caco-2 cells as a function of cell origin. *J. Pharm. Sci*. 93: 1743-1754.

Berendsen, H. J. C., Postma, J. P. M., Vangunsteren, W. F., Dinola, A., Haak, J. R., (1984). Molecular dynamics with coupling to an external bath. *J Chem Phys*. 81, 8, 3684-3690.

Bergan, T., Thorsteinsson, S. B., Solberg, R., Bjomskau, L., Kolstad, I.M., Johnsen, S. (1987). Pharmacokinetics of ciprofloxacin: intravenous and increasing oral doses. *Am. J. Med*. 82 (Suppl 4A): 97-102.

Berge, S.M., Bighley, L.D., Monkhouse, D.C., (1977). Pharmaceutical salts. *J. Pharm. Sci.* 66, 1, 1–19.

Bessho Y, Oguri T, Ozasa H, Uemura T, Sakamoto H, Miyazaki M, et al. (2009). ABCC10/ MRP7 is associated with vinorelbine resistance in non-small cell lung cancer. *Oncol Rep*. 21:263–8.

Bighley, L.D., Berge, S.M., Monkhouse, D.C. (1996). Salt forms of drugs and absorption. In: Swarbrick, J.; Boylan, J.C., Eds.; Encyclopedia of Pharmaceutical Technology, vol. 13. Marcel Dekker: New York. 453–499

Bishop C: (1996) Neural Networks for Pattern Recognition. Oxford University Press: Oxford. 225.

Breda, S.A., Jimenez Kairuz, A.F., Manzo, R.H., Olivera, M.E., (2009). Solubility behavior and biopharmaceutical classification of novel high-solubility ciprofloxacin and norfloxacin pharmaceutical derivatives. *Int J Pharm*. 371:106–113

Brewster, M.E., Loftsson, T., (2007). Cyclodextrins as pharmaceutical solubilizers., *Adv. Drug Deliv. Rev.* 59, 645–666

British Pharmacopoeia (2011). The leading global standards for UK pharmaceutical and medicinal products. Available at http://www.pharmacopoeia.co.uk/2011/access.htm . Accessed [20/03/2012]

Broer. S, (2008). Amino Acid Transport Across Mammalian Intestinal and Renal Epithelia., *Physiol Rev.* 88, 249–286.

Beoer, A. Tietze, N. Kowalczuk, S. Chubb, S. Munzinger, M., BAK L. K., Broer S, (2006). The orphan transporter v7-3 (slc6a15) is a Na+-dependent neutral amino acid transporter (B0AT2). *Biochem. J.* 393, 421–430

Benanti, G., (1989). Lysine salt of 4-diphenylacetic acid and its ophthalmic fomulations., US 4797423.

Brooke, D.N., Dobbs, A.J., Williams, N., (1986). Octanol:water partition coefficient (P). Measurement, estimation, and interpretation, particularly for chemicals with P > 105. *Ecotox. Environ. Safe*. 11, 251–260.

Brooks, M. A., De Silva, J. A., and D'aroconte, L. (1973). Determination of trimethoprim and its N-oxide metabolites in urine of man, dog, and rat by differential pulse polarography. *J. Pharm. Sci.* 62, 1395–1397.

Bodzioch, M. Orso, E. Klucken, J. Langmann , T. et al., (1999). The gene encoding ATP-binding cassette transporter 1 ismutated in Tangier disease, *Nat. Genet*. 22, 347–351.

Boes, T., Neuhäuser, M. (2005). Normalization for affymetrix genechips. *Methods Inf Med.* 44, 414–417

Boraldi, F., Quaglino, D., Croce, M.A., Garcia Fernandez, M.I., Tiozzo, R., Gheduzzi, D., Bacchelli, B., Ronchetti. I.P., (2003). Multidrug resistance protein-6 (MRP6) in human dermal fibroblasts. Comparison between cells from normal subjects and from Pseudoxanthoma elasticum patients. *Matrix Biology.* 22, 491-500.

Bolhuis G, Chowhan Z., (1995). Materials for direct compression, in pharmaceutical powder compaction technology edited by Alderborn G., Nystrom C., Marcel Dekker: New York.

Burstein, A.H., Cox, D., Mistry, B., Eddington, N., (1999). Phenytoin pharmacokinetics following oral administration of phenytoin suspension and fosphenytoin solution to rats, *Epilepsy Res*. 34 129–133.

Burton, P.S., Conradi, R.A., Hilgers, A.R., Ho, N.F.H. and Maggiora, L.L. (1992). The relationship between peptide structure and transport across epithelial cell monolayers. *J.Control. Release* 19, 87–98.

Carr A, Penny R. Cooper D.A. (1993). Efficacy and safety of rechallenge with low-dose trimethoprim-sulphamethoxazole in previously hypersensitive HIVinfected patients. *AIDS* 7:65–71.

Carstensen, J.T., Ertell, C., (1990). Physical and Chemical Properties of Calcium Phosphates for Solid State PharmaceuticalFormul ations. *Drug Dev. Ind. Pharm*. 16, 1121–1133.

Carver, P.L., Fleisher, D., Zhou, S.Y., Kaul, D., Kazanjian, P., Li, C., (1999). Meal composition effects on the oral bioavailability of indinavir in HIVinfected patients, *Pharm. Res*. 16., 718–724.

Case, D. A., Cheatham, T. E., Darden, T., Gohlke, H., Luo, R., Merz, K. M, Onufriev, A., Simmerling, C., Wang, B., Woods, R. J., (2005). The Amber biomolecular simulation programs. *Journal of Computational Chemistry*. 26 (16), 1668-1688.

Cerutti, D. S., Duke, R., Freddolino, P. L., Fan, H., Lybrand, T. P., (2008). A Vulnerability in Popular Molecular Dynamics Packages Concerning Langevin and Andersen Dynamics. Journal of Chemical Theory and Computation. 4, 10, 1669-1680.

Ciprofloxacin; Food and Drug Administration. (2007). http://www.fda.gov/medwatch/SAFETY/2007/Jun PI/Cipro Oral PI.pdf [accessed September 2011].

Chauhan, A.S.; Jain,N.K.; Diwan, P.V.; Khopade,J. (2004). Solubility Enhancement of Indomethacin with Poly(amidoamine) Dendrimers and Targeting to Inflammatory Regions of Arthritic Rats, *Journal of Drug Targeting*. 12 (9–10), 575–583

Chen J, Zhu Y, Hu M. (1994). Mechanisms and kinetics of uptake and efflux of l-methionine in an intestinal epithelial model (Caco-2). *J Nutr*, 124, 1907–1916

Chen ZS, Hopper-Borge E, Belinsky MG, Shchaveleva I, Kotova E, Kruh GD. (2003). Characterization of the transport properties of human multidrug resistance protein 7 (MRP7, ABCC10). *Mol Pharmacol*. 63, 351–8.

Chen N., Reith M., (2004). Quick Synaptic uptake and beyond: the sodium- and chloride-dependent neurotransmitter transporter family SLC6., *Eur J Physiol*, 447, 519–531

Chiou, W.L. and Riegelman, S. (1969). Preparation and dissolution characteristics of several fast-release solid dispersions of griseofulvin. *J. Pharm. Sci*. 58, 1505–1510

Choi, J-S., Jin, M.J., Han, H-K., (2005). Role of monocarboxylic acid transporters in the cellular uptake of NSAIDs. *J. Pharm. Pharmacol*. 57: 1185-1189.

Clarke. et al. (1977). Factors influencing comparative bioavailability of spironolactone tablets. *J. Pharm. Sci*. 66, 1429–1432.

Crowley, M. F., Darden, T. A., Cheatham, T. E., Deerfield, D. W., (1997). Adventures in improving the scaling and accuracy of a parallel molecular dynamics program. *Journal of Supercomputing.* 11 ,3, 255-278.

Collett, A., Tanianis-Hughes, J., Carlson, G.L., Harwood, M.D., Warhurst, G., (2005). Comparison of P-glycoprotein-mediated drug-digoxin interactions in Caco-2 with human and rodent intestine: Relevance to in vivo prediction. *Eur. J. Pharm. Sci.* 26, 386-393.

Colmenarejo, G., (2003). In silico prediction of drug-binding strengths to human serum albumin. *Med. Res. Rev*. 23, 275–301.

Conradi, R.A., Hilgers, A.R., Ho, N.F.H. and Burton, P.S. (1991). The influence of peptide structure on transport across Caco-2 cells. *Pharm. Res*. 8, 1453–1460.

Connors, K. A. Binding Constants. (1987). The Measurement of Molecular Complex Stability; John Wiley & Sons: New York.

Connors, T.D. Van Raay, T.J. Petry, L.R. Klinger, K.W. Landes, G.M. Burn, T.C. (1997). The cloning of a human ABC gene (ABC3) mapping to chromosome 16p13.3, *Genomics* 39, 231-234.

Cook, G.D., Summers, M.P., (1985). The tensile strength of aspirin-encompress tablets. *J. Pharm. Pharmacol*. 37

Daniel, H., Neugebauer, B., Kratz, A., Rehner, G., (1985). Localization of cid microclimate long intestinal villi of rat jejunum. *Am. J. Physiol*. 48, G293–G298

Dantzig AH, Bergin L. (1990). Uptake of the cephalosporin, cephalexin, by a dipeptide transport carrier in the human intestinal cell line, Caco-2. *Biochim Biophys Acta.* 1027, 211–217.

Darden, T., York, D., Pedersen, L., (1993). Particle mesh ewald - an n.log(n) method for ewald sums in large systems. *J Chem Phys*. 98 ,12, 10089-10092.

De Bruijn, J., Busser, F., Seinen, W., Hermens, J., (1989). Determination of octanol/ water partition coefficients for hydrophobic organic chemicals with the ‘‘slowstirring” method. *Environ. Toxicol. Chem*. 8, 499–512.

Del Valle,E.M., (2004). Cyclodextrins and their uses: a review, *Process Biochemistry,* 39, 1033–1046

Damsten, M.C., Vlieger, J.S., Niessen, W., Irth, H., Vermeulen, Commandeu. J.N. Trimethoprim: Novel Reactive Intermediates and Bioactivation Pathways by Cytochrome P450s., *Chem. Res. Toxico*l. 2008, 21, 2181–2187.

DeRisi J, Vishwanath RL, Brown PO. (1997). Exploring the metabolic and genetic control of gene expression on a gnomic scale. *Science*. 278, 680–686.

DeRisi, J., Penland, L., Brown, P.O., Bittner, M.L., Meltzer, P.S., Ray, M., Chen, Y., Su, Y.A., Trent J.M. (1996). Use of a cDNA microarray to analyse gene expression patterns in human cancer. *Nature Genetics*. 14, 457–60.

Deshpande, P.K., Desai, V.N., Yeole, R.D., Gupte, S.V., Patel, M.V., Sovza N.J. (2007). Benzoquinolizine-2-carboxylic acid arginine salt tetrahydrate US 0167627A1.

Deville, S., Saiz, E., Tomsia., A.P., (2007). Ice-templated porous alumina structures., *Acta Materialia*. 55, 1965–1974.

Dias, V.C., Yatscoff, R.W., (1994). Investigation of rapamycin transport and uptake across absorptive human intestinal cell monolayers. *Clin. Biochem*. 27: 31-36.

Di Prisco G, Garofano F. (1974). Purification and some properties of glutamate dehydrogenase from ox liver nuclei. *Biochem Biophys Res Commun*. 58, 3, 683-9.

Dressman, J. J., Lennernas, H. and Reppas, C. (2010). Oral Drug Absorption: Prediction and Assessment, 2nd Ed. Informa Healthcare: New York.

Donnenberg, VS., Donnenberg, AD., (2005). Multiple Drug Resistance in Cancer Revisited: The Cancer Stem Cell Hypothesis., *J Clin Pharmacol*., 45, 872-877

Doyle, L.A., Ross, D.D., (2003). Multidrug resistance mediated by the breast cancer resistance protein BCRP (ABCG2), *Oncogene* 22, 7340–7358.

Donovan, S.F., Pescatore, M.C., (2002). Method for measuring the logarithm of the octanol–water partition coefficient by using short octadecyl–poly(vinyl alcohol) high-performance liquid chromatography columns. *J. Chromatogr*. A 952, 47–61.

Duverne, C., Bouten, A., Deslandes, A., Westphal, J.F., Trouvin, J.H., Farinotti, R., Carbon, C., (1992). Modification of cefixime bioavailability by nifedipine in humans: involvement of the dipeptide carrier system. *Antimicrob. Agents Chemother*. 36: 2462-2467.

Egan, W., Lauri. G., (2002). Prediction of intestinal permeability., *Adv. Drug Deliv. Rev*. 54, 273–289

El-Badry, M.; Fetih, G.; Mohamed Fathy, M. (2009). Improvement of solubility and dissolution rate of indomethacin by solid dispersions in Gelucire 50/13 and PEG4000., *Saudi Pharmaceutical Journal.* 17, 217–225.

Eisen M, Spellman P, Brown PO et al. (1998). Cluster analysis and display of genome-wide expression patterns. *Proc. Natl. Acad. Sci*. 95, 14863-14868

Eliopoulos GM, Gardella A, Moellering RC Jr. (1984). In vitro activity of ciprofloxacin, a new carboxyquinoline antimicrobial agent. *Antimicrob Agents Chemother*. 25:331–5.

ElShaer, A., Khan, S., Perumal, D., Hanson, P., Mohammed, A.R, (2011). Use of amino acids as counter ions improves the solubility of the BCS II model drug, indomethacin. *Current Drug Delivery.* 8,4 , 363-72.

ElShaer, A., Hanson, P., Worthington, T., Lambert, P., Mohammed, A.R., (2012a). Preparation and Characterization of Amino Acids-Based Trimethoprim Salts. *Pharmaceutics* 4, 179-196

ElShaer, A., Peter Hanson, P., Mohammed A.M., (2012b) A systematic and mechanistic evaluation of aspartic acid as a filler for directly compressed tablets containing trimethoprim and trimethoprim aspartate., *European Journal of Pharmaceutics and Biopharmaceutics*. In press.

Englund, D.E., Johansson, E.D. (1981). Oral versus vaginal absorption in oestradiol in postmenopausal women. Effects of different particle size. Ups. *J. Med. Sci*. 86, 297-307.

Endres, C.J., Hsiao, P., Chung, F.S., Undkat, J.D., (2006). The role of transporters in drug interactions. *Eur. J. Pharm. Sci*. 27: 501-517.

Englund, G., Rorsman, F., R¨onnblom, A., Karlbom, U., Lazorova, L., Gra˚ sjo, J. ,Kindmark, A. , Artursson., P., (2 0 0 6). Regional levels of drug transporters along the human intestinal tract: Co-expression of ABC and SLC transporters and comparison with Caco-2 cells., *Eur. J. Pharm. Sci.* 2 9, 269–277

Eneroth, A., Åström, E., Hoogstraate, J., Schrenk, D., Conrad, S., Kauffmann, K-M., Gjellan, K., (2001). Evaluation of a vincristine resistant Caco-2 cell line for use in a calcein AM extrusion screening assay for P-glycoprotein interaction. *Eur. J. Pharm. Sci*. 12: 205-214.

Essmann, U., Perera, L., Berkowitz, M. L., Darden, T., Lee, H., Pedersen, L. G., 1995. A smooth particle mesh Ewald method. *J Chem Phys.* 103 ,19, 8577-8593.

Ettmayer, P., Amidon, G.L., Clement, B., Testa, B., (2004). Lessons learned from marketed and investigational prodrugs, *J. Med. Chem*. 47, 2393–2404.

Everitt, B., Rabe-Hesketh S., (1997). The Analysis of Proximity Data. John Wiley: New York.

Fabrizio, G.; Vetere S.M.C. (1973). erythromycin aspartate salt. US patent application

Fell, J.T., (1996). Compaction properties of binary mixtures; pharmaceutical powder compaction technology, *Drugs and the pharmaceutical Sciences*, 71, 501–515.

Feng, L.; Chen, X.; Sun, B.; Bian,X.; Chen. Z., (2011). Water-catalyzed racemisation of lactide Polymer Degradation and Stability. 96, 10, 1745-1750

Ferrari, F., Bertoni, M., Bonferoni, M.C., Rossi, S., Caramella, C., Nyström, C., (1996). Investigation on bonding and disintegration properties of pharmaceutical materials. *Int. J. Pharm.* 136, 71-79.

Finizio, A., Vighi, M., Sandroni, D., (1997). Determination of n-octanol/water partition coefficient (Kow) of pesticide critical review and comparison of methods. *Chemosphere*. 34, 131–161.

Fisher, R., (1936). The use of multiple measurements in taxonomic problems. Ann. Eugenics 7, 179-188

Francis, G.A. Knopp, R.H. Oram, J.F. (1995). Defective removal of cellular cholesterol and phospholipids by apolipoprotein A-I in Tangier Disease, *J. Clin. Invest.* 96, 78–87.

Frisch JM (1973). Clinical experience with adverse reactions to trimethoprimsulfamethoxazole. *J Infect Dis.* 128(Suppl):607–612.

Food and Drug Administration, (2002). Guidance for Industry: Food-Effect Bioavailability and Fed Bioequivalence Studies, Food and Drug Administration, Rockville, MD, Available at http://www.fda.gov/ cder/guidance/index.htm

Fogh, J., Fogh, J.M., Orfeo, T., (1977). One hundred and twenty seven cultured human tumor cell lines producing tumors in nude mice. *J. Natl. Cancer Inst*. 59: 221-226.

Forbes, R.T; York, P.; Davidson, J.R. (1995). Dissolution kinetics and solubilities of p-aminosalicylic acid and its salts. . *Int. J. Pharm*. 126, 199-208

Food and Drug Administration. (2000). Guidance for Industry: Waiver of In Vivo Bioavailability and Bioequivalence Studies for Immediate- Release Solid Oral Dosage Forms Based on a Biopharmaceutics Classification System. Food and Drug Administration, Rockville, MD. Available at http://www.fda.gov/cder/guidance/index.htm.

Fuhrer, C., (1996). interparticulate attraction mechanisms., pharmaceuticl powder compaction technology. Eds, Alderborn G., Nystrom C., Drugs and the pharmaceutical sciences., 71 Marcel Dekker: united states of America.

Fujisawa, H.; Okada, H., Miura, Y., Fujita, M., Shimamoto, T., (1976). Arginine & lysine salts of acid cephalosporin US 3984403.

Fukami, J., Ozawa, A., Yoshihashi, Y., Yonemochi, E., Terada., K., (2005) . Development of Fast Disintegrating Compressed Tablets Using Amino Acid as Disintegratation Accelerator: Evaluation of Wetting and Disintegration of Tablet on the Basis of Surface Free Energy., *Chem. Pharm. Bull*. 53,12, 1536-1539

Fukami, J., Yonemochi, E., Yoshihashi, Y., Terada, K., (2006). Evaluation of rapidly disintegrating tablets containing glycine and carboxymethylcellulose., *Int. J. Pharm.* 310, 1–2, 101–109.

Gallego, M., Arroyo, J., (2002). Simultaneous determination of dexamethasone and trimethoprim by liquid chromatography. *Journal of Pharmaceutical and Biomedical Analysis*, . 30, 1255-1261.

Ganapathy, M.E., Brandsch, M., Prasad, P.D., Ganapathy, V., Leibach, F.H., (1995). Differential recognition of beta-lactam antibiotics by intestinal and renal peptide transporters, EPT 1 and PEPT 2. *J. Biol. Chem*. 270, 25672–25677

Ganapathy, M.E. et al. (1998). Valacyclovir: a substrate for the intestinal and renal peptide transporters PEPT1 and PEPT2. *Biochem. Biophys. Res. Commun*. 246, 470–475

Garnero, C., Zoppi, A., Genovese, D., Longhi, M. (2010). Studies on trimethoprim:hydroxypropyl-[beta]-cyclodextrin: aggregate and complex formation. *Carbohydrate Research*. 345, 2550-2556.

Gavini, E., Rassu, G., Ferraro, L., Generosi, A., Rau, J. V., Brunetti, A., Giunchedi, P., Dalpiaz, A. (2010). Influence of Chitosan Glutamate on the In Vivo Intranasal Absorption of Rokitamycin from Microspheres *J. Pharm. Sci*.

Geyer, J. Do¨ring, B. Failing, Kl. Petzinger., E. (2004). Molecular cloning and functional characterization of the bovine (Bos taurus) organic anion transporting polypeptide Oatp1a2 (Slco1a2)., *Comparative Biochemistry and Physiology* Part B 137, 317–329

Giacomini, K.M., Mei Huang, S., Tweedie, D. et al., (2010). Membrane transporters in drug development. *Nat Rev Drug Discov*. 9, 3, 215-36

Gidal, B. E. (2006). Drug absorption in the elderly: Biopharmaceutical considerations for the antiepileptic drugs, *Epilepsy Res*. 68S, S65-S69.

Giraud, E., Cloeckaert, A., Kerboeuf, D., Chaslus-Dancla, E., (2000). Evidence for Active Efflux as the Primary Mechanism of Resistance to Ciprofloxacin in Salmonella enterica Serovar Typhimurium., *Antimicrobial agents and chemotherapy*. 44, 5.

Grant, D. J. W.; Higuchi, T. (1990). Ion Pairs and Solubility Behavior. In Solubility BehaVior of Organic Compounds; Weissberger, A., Ed.; John Wiley & Sons: New York, 399-433.

Greiner, B., Eichelbaum, M., Fritz, P., Kreichgauer, H.P., von Richter, O., Zundler, J., Kroemer, H., (1999). The role of intestinal P-glycoprotein in the interaction of digoxin and rifampicin. *J. Clin. Invest.* 104, 147-153.

Gohel, M.C., (2005). A review of co-processed directly compressible excipients. *J Pharm Pharmaceut Sci* (www.cspscanada.org) 8, 76-93.

Goldberg, A.H. et al. (1966). Increasing dissolution rates and gastrointestinal absorption of drugs via solid solutions and eutectic mixtures. IV. Chloramphenicol– urea system. *J. Pharm. Sci.* 55, 581–583

Gottesman, M.M., Fojo, T., Bates S.E., (2002). Multidrug resistance in cancer; role of ATP-dependent transporters, *Nature reviews*.

Gottlieb, H.E.; Kotlyar, V.; Nudelman. A., (1997). NMR Chemical Shifts of Common Laboratory Solvents as Trace Impurities., *J. Org. Chem*. 62, 7512-7515

Hal, N.L.W., Vorst, O., Houwelingen, A.M., Kok , E.J., Peijnenburg, A., Aharoni, A., Tunen , A.J., Keijer, J., (2000). The application of DNA microarrays in gene expression Analysis. *Journal of Biotechnology.* 78, 271–280

Hamalainen, M.D., Frostell-Karlsson.A., (2004). Predicting the intestinal absorption potential of hits and leads., *Drug Discovery Today:Technologies*. 1, 4.

Hancock, B.C. ; Zografi, G. (1997). Characteristics and significance of the amorphous state in pharmaceutical systems. *J. Pharm. Sci.* 86, 1–12.

Han, H., Vrueh, R.L., Rhie, J., Covitz, K.Y., Smith, P.L.,n Lee, C., Oh, D., Wolfgang Sadee, W., Amidon. G., (1998). 5'-Amino acid esters of antiviral nucleosides, acyclovir, and AZT are absorbed by the intestinal PEPT1 peptide transporter., *Pharm. Res*. 15, (8), 1154-1159

Hansch, C., Leo, A.J., (1979). Substituent constants for correlation analysis. In: Chemistry and Biology. Wiley:New York. 339-415

Hans-Dieter Höltje, Wolfgang Sippl, Didier Rognan, Folkers G. (2008). Molecular Modeling: Basic Principles and Applications 3rd ed.; Weinheim : Wiley-VCH. 413

Hargrove, J.T., Maxson, W.S., Wentz, A.C. (1989). Absorption of oral progesterone is influenced by vehicle and particle size. *Am. J. Obstet. Gynecol*., 161 948-951.

Harris,R.Z., Jang, G.R., Tsunoda, S., (2003). Dietary effects on drug metabolism and transport, *Clin. Pharmacokinet*. 42., 1071–1088

Hartigan J, Wong M., (1979). A k-means clustering algorithm. *Applied Statistics* 28, 100-108.

Hart, L., Middleton, R.K., Wanders, D.L., (1991). Significance of the ciprofloxacin-antacid interaction. *DICP Ann. Pharmacother*. 25, 473–475.

Hayes, R. A., Robinson, A. C., Ralston. J., (1994). Wilhelmy technique for the rapid assessment of solid wetting dynamics. *Langmuir.*, 10, 2850-2852.

Hawkins T, Carter JM, Romeril KR, Jackson SR and Green GJ (1993). Severe trimethoprim induced neutropenia and thrombocytopenia. *NZ Med J.* 106,251– 252.

Heckel, RW., (1961). Density-pressure relationships in powder compaction. Trans. *Metall. Soc. AIME*., 221, 671-675.

Heckel, RW., (1961). An analysis of powder compaction phenomena. *Trans. Metall. Soc. AIME*. 221, 1001-1008

Hemamalini, M., Muthiah, P.T., Bocelli. G. (2003). Cantoni A Hydrogen-bonded supramolecular motifs in trimethoprim-terephthalate-terephthalic acid (2/1/1): *Acta Crystallogr Sec E*. 59, 14-17.

Hemenway, J., Stella, V., (2007). Prodrugs and parenteral drug delivery, in: V. Stella, R.T. Borchardt, M. Hageman, R. Oliyai, H. Maag, J. Tilley (Eds.), Prodrugs: Challenges and Rewards, AAPS Press/ Springer.

Hilgers, A.R., Conradi, R.A., Burton, P.S. (1990). Caco-2 cell monolayers as a model for drug transport across the intestinal mucosa. Pharm Res, 7, 902–910.

Higuchi, T., Connors, K.A., (1965). Phase-solubility techniques, Adv. *Anal. Chem. Instr*. 4, 117–212.

Hodges, G.M., Carr, E.A., Hazzard, R.A., Carr, K.E., (1995). Uptake and translocation of microparticles in small intestine. Morphology and quantification of particle distribution, *Dig. Dis. Sci*. 40, 967– 975

Hopper-Borge E., Chen Z.S., Shchaveleva I., Belinsky MG, Kruh GD (2004). Analysis of the drug resistance profile of multidrug resistance protein 7 (ABCC10): resistance to docetaxel. *Cancer Res.* 64, 4927–30.

Hutchinson I, Jennings SA, Vishnuvajjala BR, Westwell AD, Stevens MFG (2002). Antitumour benzothiazoles. 16. Synthesis and pharmaceutical properties of antitumour 2-(4-aminophenyl)benzothiazole amino acid prodrugs. *J Med Chem*. 45, 744 – 747

Hunter, J., Hirst, B.H., (1997). Intestinal secretion of drugs. The role of P-glycoprotein and related drug efflux systems in limiting oral drug absorption., *Adv. Drug Deliv. Rev*. 25, I29-I57

Huang, Y., Anderle, P., Bussey, K.J., Barbacioru, C., Shankavaram, U., Dai, Z., et al., (2004). Membrane Transporters and Channels: Role of the Transportome in Cancer Chemosensitivity and Chemoresistance, *Cancer Res*. 64, 4294–4301

Huang Y., Sadee., W., (2006). Membrane transporters and channels in chemoresistance and -sensitivity of tumor cells., *Cancer Letters*. 239, 168–182

Huet, C., Sahuquillo-Merino, C., Coudrier, E., Louvard, D., (1987). Absorptive and mucus-secreting subclones isolated from a multipotent intestinal cell line (HT-29) provide new models for cell polarity and terminal differentiation. *J. Cell. Biol*. 105, 345-357

Hu, M., Borchardt, R.T., (1990). Mechanism of L-α-methyldopa transport through a monolayer of polarized human intestinal epithelial cells (Caco-2). *Pharm. Res*. 7, 1313-1319

Humber-Droz, P., Mordier, D., Doelker, E., (1983). Densification behaviour of powder mixtures, *Acta Pharm. Technol*. 29, 69–73.

Heller RA, Schena M, Chai A, Shalon D, Bedilion T, Gilmore J, Woolley DE, Davis RW. (1997) Discovery and analysis of inflammatory disease-related genes using cDNA microarray. *Proc Natl Acad Sci USA.* 94, 2150–5.

Iga, K., Ogawa, Y., (1997). Sustained-release buccal dosage forms for nitroglycerin and isosorbide dinitrate: increased bioavailability and extended time of absorption when administered to dogs. *J. Control. Release*. 49, 105–113.

Ilkka, J., Paronen, P., (1993). Prediction of the compression behaviour of powder mixtures by the Heckel equation, *Int. J. Pharm*. 94, 181–187.

Ingels, F., Deferme, S., Destexhe, E., Oth, M., Van den Mooter, G., Augustijns. P., (2002). Simulated intestinal fluid as transport medium in the Caco-2 cell culture model., *Int J. Pharm. Sci.* 232., 183–192

Irwin, G.M., Kostenbauder, H.B., Dittert, L.W., Staples, R., Misher A., Swintosky, J.V., (1969). Enhancement of gastrointestinal absorption of quaternary ammonium compound by trichloroacetate. *J. Pharm. Sci* .58, 313-315

Ito, K., Suzuki, H., Horie, T., Sugiyama, Y., (2005). Apical/basolateral surface expression of drug transporters and its role in vectorial drug transport. *Pharm. Res*. 22, 1559-1577.

Inui, K.-I., Okano, T., Maegawa, H., Kato, M., Takano, M., Hori, R., (1988). H+ coupled transport of p.o. cephalosporins via dipeptide carriers in rabbit intestinal brush-border membranes: difference of transport characteristics between cefixime and cephradine. *J. Pharmacol. Exp. Ther.* 247, 235-241.

Ivaturi, V., Kim, S., (2009). Enhanced Permeation of Methotrexate In Vitro by Ion Pair Formation With L-Arginine., *J. Pharm. Sci.* 98, 10.

Jantratid, E., Janssen, N., Reppas, C., DressmanJ.B., (2008). Dissolution Media Simulating Conditions in the Proximal Human Gastrointestinal Tract: An Update., *Pharm. Res*. 25, No. 7.

Jetzer, W., (1986). Compaction characteristics of binary mixtures, *Int. J. Pharm*. 31, 201–207.

Jonker, J.W., Smit, J.W., Brinkhuis, R.F., Maliepaard, M., Beijnen, J.H., Schellens, J.H.M., Schinkel, A.H., (2000). Role of breast cancer resistance protein in the bioavailability and fetal penetration of topotecan. *J. Natl. Canc. Inst*. 92, 1651-1656.

Joiris, E., Martino, P.D., Berneron, C., Guyot-Hermann, A. and Guyot. J.C., (1998). Compression behavior of orthorhombic paracetamol. *Pharm. Res*. 15, 1122–1130.

Jorgensen, W. L., Chandrasekhar, J., Madura, J. D., Impey, R. W., Klein, M. L., (1983). Comparison of simple potential functions for simulating liquid water. *J Chem Phys*. 79 ,2, 926-935.

Juliano R.L., Ling V., (1976). A surface glycoprotein modulating drug permeability in Chinese hamster ovary cell mutants, *Biochim. Biophys. Acta*. 455, 152- 162.

Jung, N., Lehmann, C., Rubbert, A., Knispel, M., Hartmann, P., Lunzen, J., Stellbrink, H., Faetkenheuer, G., and Taubert D. (2008). Relevance of the Organic Cation Transporters 1 and 2 for Antiretroviral Drug Therapy in Human Immunodeficiency Virus Infection., *Drug Metab Dispos.* 36, 8.

Kallioniemi A, Kallioniemi O P, Sudar D et al. (1992). Comparative genomic hybridisation for molecular cytogenetic analysis of solid tumours. *Science*. 258, 818--821.

Kanai Y, Hediger MA (1992). Primary structure and functional characterization of a high-affinity glutamate transporter. *Nature.* 360, 467–471

Kanai, Y. Hediger., M. A. (2003). The glutamate and neutral amino acid transporter family: physiological and pharmacological implications., *European Journal of Pharmacology*. 479, 237– 247

Kanai, Y., Segawa, H., Miyamoto, K., Uchino, H., Takeda, E., Endou, H., (1998). Expression cloning and characterization of a transporter for large neutral amino acids activated by the heavy chain of 4F2 antigen (CD98). *J. Biol. Chem*. 273, 23629–23632.

Kasim, N. A., Whitehouse, M., Ramachandran, C. , Bermejo, M.l., Lennerna, H., Hussain, A. S., Junginger, E., Stavchansky, S. A., Midha, K. K., Shah V. P., and Amidon, G. L., (2003). Molecular Properties of WHO Essential Drugs and Provisional Biopharmaceutical Classification., *Molecular Pharmaceutics*. 1, 1, 85-96

Kauffman, R.E., Thirumoorthi, M.C., Buckley, J.A., Aravind, M.K., Dajani, A.S., (1981). Relative bioavailability of intravenous chloramphenicol succinate and oral chloramphenicol palmitate in infants and children, *J. Pediatr*. 99, 6, 963–967

Kennedy, K.J., Lundquist, J.T., Simandan, T.L., Kokko, K.P., Beeson, C.C., Dix, T.A., (2000). Design rationale, synthesis, and characterization of non-natural analogs of the cationic amino acids arginine and lysine., *J. Peptide Res*. 55, 348-358.

Khan M. Sundararajan., P. R. (2011). Effects of Carbon Atom Parity and Alkyl Side Chain Length on the Crystallization and Morphology of Biscarbamates, A Set of Model Compounds for Polyurethanes., *J. Phys. Chem. B*. 115, 8696–8706

Kobayashi, D., Nozawa, T., Imai, K., Nezu, J., Tsuji, A., Tamai, I., (2003). nvolvement of human organic anion transporting polypeptide OATPB SLC21A9) in pH-dependent transport cross intestinal apical membrane. . *Pharmacol. Exp. Ther*. 306, 703–708.

Kohonen T., (1990). The self-organizing map. *Proc. IEEE* 78, 1464-1479.

Kotze, A.F., Luessen, H.L., Leeuw, B.J., Boer, A.G., Verhoef, J.C., Junginger, H.E., (1998). Comparison of the effect of different chitosan salts and N-trimethyl chitosan chloride on the permeability of intestinal epithelial cells (Caco-2), *J. Control. Release*. 51, 35– 46.

Kozjek, F., Palka, E., Krizman, I., Vodopivec, P., (1996). Pharmacokinetics of ciprofloxacin metal complexes. *Acta Pharm*. 46, 109–114.

Kramer, S.F., Flynn, G.L., (1972). Solubility of organic hydrochlorides. *J. Pharm. Sci*. 61, 1896–1904.

Kranendonk, M., Marohnic, C.C., Panda, S.P., Duarte, M.P., Oliveira, J.S., Masters, B.S., Rueff, J. (2008). Impairment of human CYP1A2-mediated xenobiotic metabolism by Antley-Bixler syndrome variants of cytochrome P450 oxidoreductase. *Arch Biochem Biophys.* 15, 475, 2, 93-99.

Kruh, G.D., Belinsky, M.G., (2003). The MRP family of drug efflux pumps, *Oncogene* 22 ,7537–7552

Kovach, I.M., Pitman, I.H. and Higuchi, T., (1975). Amino acid esters of phenolic drugs as potentially useful prodrugs. *J. Pharm. Sci*. 64, 1070-1071.

Kobayashi, D., Nozawa, T., Imai, K., Nezu, J.I., Tsuji, A., Tamai, I., (2003). Involvement of human organic anion transporting polypeptide OATP-B (SLC21A9) in pH dependent transport across intestinal apical membrane. *J. Pharmacol. Exp. Ther*. 306, 703-708.

Konishi, Y., Hagiwara, K., Shimizu, M., (2002). Transepithelial transport of fluorescein in Caco-2 cell monolayers and use of such transport in in vitro evaluation of phenolic acid availability. *Biosci. Biotechnol. Biochem*. 66, 2449-2457.

Kuang , Y. Shen , T. Chen , X. Sodani , K. Hopper-Borge, E. et al., (2010). Lapatinib and erlotinib are potent reversal agents for MRP7 (ABCC10)-mediated multidrug resistance. *Biochemical Pharmacology*. 79,154–161

Kuny, T., Leuenberger. H., (2003). Compression behaviour of the enzyme _-galactosidase and its mixture with microcrystalline cellulose. *Int. J. Pharm*. 260, 137–147.

Kurauchi, M., Miyazawa, Y., Sato, H. (2004). Inosine L-arginine salt and uses thereof, US0192533A.

Lai, W. G., Zahid, N., Uetrecht J. P., (1999). Metabolism of Trimethoprim to a Reactive Iminoquinone Methide by Activated Human Neutrophils and Hepatic Microsomes., *JPET* 291:292–299.

Leach, A. R., (2001). Molecular modelling: principles and applications. 2nd ed.; Prentice Hall.

Ledergerber, B., Bettex, J. D., Joos, B., Flepp, M. & Luthy, R. (1985). Effect of standard breakfast on drug absorption and multipledose pharmacokinetics of ciprofloxacin. *Antimicrobial Agents and Chemotherapy.* 27, 350–352.

Ledwidge, M.T., Corrigan, O.I., (1998). Effects of surface active characteristics and solid state forms on the pH–solubility profiles of drug–salt systems, *Int. J. Pharm*. 174, 187–200.

Lee, K., Johnson, N., Castelo., J., Sinko, P.J., Grass, G., Holme, K., Lee. Y., (2005). Effect of experimental pH on the in vitro permeability in intact rabbit intestines and Caco-2 monolayer., *Eur. J. Pharm. Sci*. 25, 193–200

Leslie, E.M., Deeley, R.G., Cole, S.P., (2001). Toxicological relevance of the multidrug resistance protein 1, MRP1 (ABCC1) and related transporters, *Toxicology.* 167 3–23.

Létourneau, I.J., Bowers, R.J., Deeley, R.G., Cole, S.P.C., (2005). Limited modulation of the transport activity of the human multidrug resitance proteins MRP1, MRP2 and MRP3 by nicotine glucuronide metabolites. *Toxicol. Lett*. 157: 9-19.

Leo, A., (2000). Octanol/Water partition coefficients. In: Boethling, R.S., Mackay, D. (Eds.), Handbook of Property Estimation Methods for Chemicals: Environmental and Health Sciences. Lewis Publishers. 89–114.

Leuenberger, H., (1982). The compressibility and compactibility of powdered systems. *Int. J. Pharm.* 12 41-55.

Leuenberger, H., (1985). Compression of binary powder mixtures and solubility parameters of solids, *Int. J. Pharm*. 27, 127– 138.

Leuner, C.; Dressman, J. (2000). Improving drug solubility for oral delivery using solid dispersions. *European Journal of Pharmaceutics and Biopharmaceutics*. 50, 47-60

Leyden, J.J., (1985). Absorption of minocycline hydrochloride and tetracycline hydrochloride, effect of food, milk, and iron, J. Am. Acad. Dermatol. 12., 308–312.

Liang, P., Pardee, A.B., (1992). Differential display of eukaryotic messenger RNA by means of the polymerase chain reaction. *Science* 257, 967–971.

Li, X., Zhi, F., Hu, Y., (2007). Investigation of excipient and processing on solid phase transformation and dissolution of ciprofloxacin. *Int. J. Pharm*. 328, 177–182

Li, N., Zhang, Y., Wu, Y., Xiong, X., Zhang, Y. (2005). Inclusion complex of trimethoprim with β-cyclodextrin. *Journal of Pharmaceutical and Biomedical Analysis*, 39, 824–829.

Li, S.; He, H.; L. Yin, P.H.; Serajuddin, A.T.M. (2005). IV–IVC considerations in the development of immediate-release oral dosage form, *J. Pharm. Sci*., 94, 1396–1417.

Li, Q., Rudolph, V., Weigl, B., Earl, A., (2004). Interparticle van der Waals force in powder flowabilityand compactibility., *Int. J. Pharm*. 280, 77–93

Li, X., Zhi, F., Hu, Y., (2007). Investigation of excipient and processing on solid phase transformation and dissolution of ciprofloxacin. *Int. J. Pharm*. 328, 177–182

Ling V., Thompson L.H. (1974). Reduced permeability in CHO cells as a mechanism`of resistance to colchicines, *J Cell Physiol*. 83, 1, 103- 116.

Lipka, E. Crison, J. Amidon, G.L., (1996). Transmembrane transport of peptide type compounds: prospects for oral delivery. *J. Control. Release*. 39, 121–129.

Liu, S., Huang, H., Lu, X., Golinski, M., Comesse, S., Watt, D. et al., (2003). Down-regulation of thiamine transporter THTR2 gene expression in breast cancer and its association with resistance to apoptosis, *Mol. Cancer Res*. 1, 665–673

Lipinski, C.A., (2000). Drug-like properties and the causes of poor solubility and poor permeability. *J. Pharmacol. Toxicol. Methods.* 44, 235–249.

Lipinski, C.A., Lombardo, F., Dominy, B.W., Feeney, P.J., (1997). Experimental and computational approaches to estimate solubility and permeability in drug discovery and development settings. *Adv. Drug Deliv. Rev*. 23, 3–25.

Lockhart, D.J., Dong, H., Byrne, M.C. et al. (1996). Expression monitoring by hybridization to high-density oligonucleotide arrays. *Nat Biotechnol*. 14: 1675-1680.

Lowes, S., Simmons, N.L., (2002). Multiple pathways for fluorochinolone secretion by human intestinal epithelial (Caco-2) cells. *Br. J. Pharmacol*. 135: 1263-1275.

Luciani, M.F. Denizot, F. Savary, S. Mattei, M.G. Chimini, G. (1994). Cloning of two novel ABC transporters mapping on human chromosome 9, *Genomics.* 21, 150-159.

Lyer, V.R., Eisen, M.B., Ross, D.T., Schuler, G., Moore, T., Lee J.C.F., Trent, J.M., Staudt, L.M., Hudson, J. Jr, Boguski, S., Lashkari, D., Shalon, D., Botstein, D., Brown, P.O. (1999). The transcriptional program in the response of human fibroblasts o serum. *Science*. 283, 83–87.

Maestrelli, F., Zerrouk, N., Chemtob, C., Mura, P., (2004). Influence of chitosan and its glutamate and hydrochloride salts on naproxen dissolution rate and permeation across Caco-2 cells. *Int. J. Pharm*. 271, 257–267.

Mahon, F.X., Belloc, F., Lagarde, V., Chollet, C., Moreau- Gaudry, F., Reiffers, J., et al., (2003). MDR1 gene overexpression confers resistance to imatinib mesylate in leukemia cell line models, *Blood*. 101, 2368–2373

Majumdar, S., Duvvuri, S., Ashim K. Mitra., S.K., (2004). Membrane transporter/receptor-targeted prodrug design: strategies for human and veterinary drug development, *Adv. Drug Deliv. Rev*. 56, 1437– 1452

Manganaro, A.M., (1997). Review of the transmucosal drug delivery, *Mil. Med*. 162, 27– 30.

Manius, G. J. (1978). Trimethoprim, In K. Florey (ed.), Analytical profiles of drug substances, vol. 7 Academic Press: New York. 445-475

Marat, M., Ni, A.L., Yu, X., Oko, Y., Smith, R., Argraves., B., (2008). ATP-binding cassette transporters ABCA1, ABCA7, and ABCG1 in mouse spermatozoa., *Biochemical and Biophysical Research Communications.* 376, 472–477

Martin, Y.C. (1981). A practitioner's perspective of the role of quantitative structure-activity analysis in medicinal chemistry. *J. Med. Chem*. 24, 229–237.

Martinez, M.N., Amidon, G.L., (2002). A mechanistic approach to understanding the factors affecting drug absorption: a review of fundamentals, *Pharmacokinet. Pharmacodyn*. 42, 620–643.

Marquez, B., Nancy, E., Caceres, Marie-Paule Mingeot-Leclercq, Paul M. Tulkens, Franc¸oise Van BambekeStudies with Ciprofloxacin-Resistant Cells Ciprofloxacin in Murine Macrophages: the Fluoroquinolone Antibiotic Identification *Antimicrob. Agents Chemother*. 2009, 5, 36.

Matter K., Balda M. S., (2003). Signalling to and from tight junctions., Nature Reviews *Molecular Cell Biology*. 4, 225-237.

McEwan, G.T., Lucas, M.L., (1990). The effect of E. coli STa enterotoxin on the absorption of weakly dissociable drugs from rat proximal jejunum in vivo. *Br. J. Pharmacol*. 101, 937–943

Mehran Yazdanian, Susan L. Glynn, James L. (1998). Wright and Amale HawiCorrelating Partitioning and Caco-2 Cell Permeability of Structurally Diverse Small Molecular Weight Compounds., *Pharm. Res*. 15, (9) 1490-1494.

Meshi, T., and Sato, Y. (1972). Studies on sulfamethoxazole-trimethoprim. Absorption, distribution, excretion and metabolism of trimethoprim in rat. *Chem. Pharm. Bull*. 20, 2079–2090.

Metz, R., Soergel, F. (1990). The gastrointestinal secretion of quinolones, Preliminary evaluation of in vivo animal model. 3rd International Symposium of New Quinolones, July 12-14, Vancouver, Canada.

Meyerhoffer, M., McGown, LB., (1990) Critical micelle concentration behavior of sodium taurocholate in water. *Langmuir*, *6* (1), pp 187–191

Miller, J. M., Dahan, A., Gupta, D., Varghese, S., Amidon, G. L. (2009). Quasi-Equilibrium Analysis of the Ion-Pair Mediated Membrane Transport of Low-Permeability Drugs. *J. Controlled Release.* 137, 31–37.

Mitchell, B.E, Jurs, P.C., (1998). Prediction of Aqueous Solubility of Organic Compounds from Molecular Structure., *J. Chem. Inf. Comput. Sci*. 38, 489-496

Mordelle, A S., Jullian, E., Costa, C., Cormet-Boyaka, E., Benamouzic, R .,Tome, D., (2000). EAAT1 is involved in transport of L-glutamate during differentiation of the Caco-2 cell line. *Am J Physiol Gastrointest Liver Physiol.* 279, 366–373.

Morales CR, Ni X, Smith CE, Inagaki N, (2012). Hermo LABCA17 mediates sterol efflux from mouse spermatozoa plasma membranes. *Histol Histopathol.* 27, 3, 317-328.

Murakami., T. Takano M. (2008). Intestinal efflux transporters and drug absorption. *Expert Opin Drug Metab Toxicol* 4, 7, 923-939

Naggar, V.F., (1981). An in vitro study of the interaction between diazepam and some antacids or excipients. *Pharmazie*. 36, 114–117.

Nakano, M., (1971). Effects of interaction with surfactants, adsorbents, and other substances on the permeation of chlorpromazine through a dimethyl polysiloxane membrane. *J. Pharm. Sci.* 60, 571–575.

Naramoto H, Uematsu T, Uchihashi T, Doto R, Matsuura T, et al. (2007). Multidrug resistance-associated protein 7 expression is involved in crossresistance to docetaxel in salivary gland adenocarcinoma cell lines. *Int J Oncol.* 30, 2, 393–401.

Neuhoff , S., Ungell, A., Zamora I., Artursson., P., (2005). pH-Dependent passive and active transport of acidic drugs across Caco-2 cell monolayers., *Eur. J. Pharm. Sci*. 25, 211–220

Neuman, M. (1988). Clinical pharmacokinetics of the newer antibacterial 4-quinolones. *Clin. Pharmacokin*. 14, 96-121

Newton, J. M., Cook, . D. T., Hollebon, C. E., (1977). The strength of tablets of mixed components. *J. Pharm. Pharmacol*. 29, 247–249.

Nimmerfall, F., Rosenthaler, J. (1980). Dependence of area under the curve on proquazone particle size and in vitro dissolution rate*. J. Pharm. Sci*. 69, 605-607.

Noyes, A.A., Whitney, W.R., (1897). The rate of solution of solid substances in their own solutions. *J. Am. Chem. Soc*. 19 930–934.

Nystrom, C. Karehill, P., (1995). Importance of intermolecular bonding forces and the concept of bonding surface area. eds Goran Alderborn and Christer Nystrom, pharmaceutical powder compaction technology, Drugs and pharmaceutical sciences; volume 71 Marcel Dekker: New York.

OECD Guidelines for the Testing of Chemicals, (1995). Test No. 107: n-Octanol/Water Partition Coefficient: Shake Flask Method. OECD Organisation for Economic Cooperation and Development.

Ogura, K., Kobayashi, M., Nakayama, M., Miho, Y., (1998). Electrochemical and in situ FTIR studies on the adsorption and oxidation of glycine and lysine in alkaline medium., *Journal of Electroanalytical Chemistry.* 449, 101–109

Olivera, M.E., Manzo, R.H., Junginger, H.E., Midha, K.K., Shah, V.P., Stavchansky, S., Dressman, J.B., Barends., D.M., (2011). Biowaiver Monographs for Immediate Release Solid Oral Dosage Forms: Ciprofloxacin Hydrochloride., *J. Pharm. Sci.*100, 1.

Pacher, P. Beckman, J. S. Liaudet., L. (2007). Nitric Oxide and Peroxynitrite in Health and Disease. *Physiol Rev*. 87, 315–424.

Palm, K., Luthman, K., Ros., J., Grasjo, J., Artursson., P., (1999). Effect of Molecular Charge on Intestinal Epithelial Drug Transport: pH-Dependent Transport of Cationic Drugs. *JPET* 291:435–443, 1999

Park, H., Kim, T., Bark. K., (2002). Physicochemical properties of quinolone antibiotics in various environments., *Eur. J. Med. Chem*. 37 443–460

Park, M. S. Leslie H. O., Benet, Z. (2011). Is Ciprofloxacin a Substrate of P-glycoprotein? *Arch Drug Info.* 4,1–9

Pappenheimer, J.R. and Reiss, K.Z. (1987). Contribution of solvent drag through intercellular junctions to absorption of nutrients by the small intestine of the rat. *J. Membr. Biol*. 100, 123–136.

Petris, M.J., (2004). The SLC31 (Ctr) copper transporter family, *Pflugers Arch*. 447, 752–755

Petrosyan, A.M. (2007). Vibrational spectra of L-histidine perchlorate and L-histidine Tetrafluoroborate. *Vibrational Spectroscopy*. 43, 284–289

Pellegata R.L., (1993). Furosamide salts, United states patent, 5,182,300

Pinto, M., Robine-Leon, S., Appay, M.-D., Kedinger, M., Triadou, N., Dussaulx, E., Lacroix, B., Simon-Assmann, P., Haffen, K., Fogh, J., Zweibaum, A., (1983). Enterocyte-like differentiation and polarization of the human colon carcinoma cell line Caco-2 in culture. *Biol. Cell* 47: 323-330.

Pistolis, G. , Andreopoulou, A. K. Malliaris, A. and Kallitsis., J. K. (2005). Direct Observation of Odd-Even Effect in Dilute Polymeric Solutions: A Time-Resolved Fluorescence Anisotropy Study., *J. Phys. Chem*. B. 109, 11538-11543

Poole, S.K., Poole, C.F., (2003). Separation methods for estimating octanol–water partition coefficients. *J. Chromatogr. B.* 797, 3–19.

Pratt, S., Chen, V., Perry, W.I., Starling, J.J., Danzig, A., (2006). Kinetic validation of the use of carboxydichlorofluorescein as a drug surrogate for MRP5-mediated transport. *Eur. J. Pharm. Sci*. 27, 524-532.

Pochopin NL, Charman WN, Stella VY (1995). Amino acid derivatives of dapsone as water soluble prodrugs. *Int J Pharm*. 121, 157 – 167

Polli, J. W. Wring, S. A. Humphereys, J. E. Huang, L. Morgan, J. B. Webester, L. O. Serabjit-Singh C., (2001). Rational Use of in Vitro P-glycoprotein Assays in Drug Discovery., *The journal of pharmacology and experimental therapeutics.* 299, 2

Quintanar-Guerrero, D., Allémann, E., Fessi, H., Doelker, E., (1997). Applications of the Ion-Pair Concept to Hydrophilic Substances with Special Emphasis on Peptides., *Pharm. Res*. 14, (2), 119-127

Raj. S., Muthiah, P. T., Rychlewska, U., Warzajtis. B. (2003). Pseudo-polymorphism and crystal engineering: hydrogen-bonded supramolecular networks in trimethoprim m-chlorobenzoate and trimethoprim m- chlorobenzoate dehydrate. *CrystEngComm*. 5,9, 48–53

Ramaswamy, C.M., Varma, Y.B.G., Venkateswarlu, D., (1970). Compaction of mixtures of materials, *Chem. Eng. J.* 1 168–171.

Rasenack, N., Muller, B.W., (2002). Crystal Habit and Tableting Behaviour, *Int. J. Pharm*. 244, 45-57.

Ratain, M.J., Cohen, E.E., (2007). The value meal: how to save $1,700 per month or more on lapatinib, *J. Clin. Oncol*. 25, 3397–3398.

Rauchwerger, D.R., Firby, P.S., Hedley, D.W., Moore, M.J., (2000). Equilibrative-sensitive nucleoside transporter and its role in gemcitabine sensitivity, *Cancer Res*. 60, 6075–6079

Rege, BD., Kao ,JP., Polli, JE., (2002). Effects of nonionic surfactants on membrane transporters in Caco-2 cell monolayers., *Eur. J. Pharm. Sci.* 16, 237–246

Reizer, J., Michotey, V., Reizer, A. & Saier, M. H., (1994). Novel phosphotransferase system genes revealed by bacterial genome analysis : unique, putative fructose- and glucoside-speci®c systems. *Protein Sci* 3, 440- 450.

Riippi, M., Antikainen, O., Niskanen, T., Yliruusi. J., (1998). The effect of compression force on surface structure, crushing strength, friability and disintegration time of erythromycin acistrate tablets., *Eur. J. Pharm. and Bio*. 46, 339–345.

Robert, P. Igo, Jr. and John F. Ash., (1998). The Na+-Dependent Glutamate and Aspartate Transporter Supports Glutathione Maintenance and Survival of CHO-K1 Cells., *Somatic Cell and Molecular Genetics*. 24, 6, 341-352

Rohwedder, R., Bergan, T., Thorsteinsson, S.B. & Scholl, H. (1990). Transintestinal elimination of ciprofloxacin. *Chemotherapy*, 36, 77 - 84.

Roma˜nuk, C.B., Garro Linck, Y., Chattah, A.K., Monti, G.A., Cuffini, S.L., Garland, M.T., Baggio, R., Manzo, R.H., Olivera,. M.E., (2010). Crystallographic, thermal and spectroscopic characterization of a ciprofloxacin saccharinate polymorph. *Int. J. Pharm*. 391 197–202

Roma˜nuk, C.B., Garro Linck, Y., Chattah, A.K., Monti, G.A., Manzo, R.H., Olivera, M.E., (2009). Characterization of the solubility and solid-state properties of saccharin salts of fluoroquinolones. *J. Pharm. Sci*. 98, 3788.

Romiti, N., Tramonti, G., Chieli., E., (2002). Influence of Different Chemicals on MDR-1 P-Glycoprotein Expression and Activity in the HK-2 Proximal Tubular Cell Line., *Toxicology and Applied Pharmacology* 183, 83–91

Rubinstein, E., St Julien, L., Ramon, J., Dautrey, S., Farinotti, R., Huneau, J.F., Carbon, C. (1994). The intestinal elimination of ciprofloxacin in the rat. *J. Infect. Dis*. 169, 218 - 221.

Rubio-Aliaga I., Daniel H. (2002). Mammalian peptide transporters as targets for drug delivery. *Trends Pharmacol Sci*. 23, 434–440.

Ruhemann, S., J. (1911). *Chem. Sot*., 99,792, 1306-1486.

Ryckaert, J. P., Ciccotti, G., Berendsen, H. J., (1977). Numerical-integration of cartesian equations of motion of a system with constrains - molecular dynamics of n-alkanes. *J Comput Phys.* 23 ,3 , 327-341.

Ryshkewitch, E., (1953). Compression strength of porous sintered alumina and zirconia*. J. Am. Cer. Soc.* 36, 65–68.

Sadeek, S. A., El-Shwiniy, W. H., Zordok, W. A., El-Didamony, A. M., (2011). Spectroscopic, structure and antimicrobial activity of new Y(III) and Zr(IV) ciprofloxacin. *Spectroc. Acta Pt. A-Molec. Biomolec. Spectr.* 78, 2, 854-867.

Sagui, C., Darden, T. A., (1999). In P3M and PME: a comparison of the two methods, Workshop on Treatment of Electrostatic Interactions in Computer Simulations of Condensed Media, Santa Fe, Nm, Jun 23-25; Pratt, L. R.; Hummer, G., Eds. Santa Fe, Nm, 104-113.

Sagui, C., Pedersen, L. G., Darden, T. A., (2004). Towards an accurate representation of electrostatics in classical force fields: Efficient implementation of multipolar interactions in biomolecular simulations. *J Chem Phys*. 120, 1, 73-87.

Saier,M.H., (2000). Families of transmembrane transporters selective for amino acids and their derivatives., *Microbiology*. 146, 1775–1795

Sahai, J., Gallicano, K., Oliveras, L., Khaliq, S., Hawley-Foss, N., Garber, G,. (1993). Cations in the didanosine tablet reduce ciprofloxacin bioavailability. *Clin. Pharmacol. Ther*. 53, 292–297.

Salama, N. Eddington, N. D. Fasano A. (2006). Tight junction modulation and its relationship to drug delivery ., *Adv. Drug Deliv. Rev*. 58, 15– 28

Sanna Siissalo, Laura Laine, Ari Tolonen, Ann M. Kaukonen, Moshe Finel , Jouni Hirvonen., (2010). Caco-2 cell monolayers as a tool to study simultaneous phase II metabolism and metabolite efflux of indomethacin, paracetamol and 1-naphthol. *Int. J. Pharm.* 383, 24–29

Sangekar, S.A., Sarli, M., Sheth, P. R, (1972). Effect of Moisture on Physical Characteristics of Tablets Prepared from Direct Compression Excipients, *J. Pharm. Sci*., 61, 939-944.

Sangster, J. (1989.) Octanol-Water Partition Coefficients of Simple Organic Compounds. *J. Phys. Chem.* 18, 3.

Santamarina-Fojo, S. Peterson, K. Knapper, C. Qiu, Y. et al., (2000). Complete genomic sequence of the human ABCA1 gene: analysis of the human and mouse ATP binding cassette A promoter, *Proc. Natl. Acad. Sci. U. S. A.* 97, 7987–7992

Sam, A.P., Fokkens, J.G., (1997). Drug Delivery System: Adding Therapeutic and Economic Value to Pharmacotherapy. Part 2, *Pharm. Tech. Eur*. 9, 58-66.

Sastry, S.V., Nyshadham,J.R., Fix., J.A., (2000). Recent technological advances in oral drug delivery – a review. *PSTT* .3 ,4.

Schinkel, A.H., Mayer, U., Wagnaar, E., et al., (1997). Normal viability and altered phamacokinetics in mice lacking mdr1-type (drug-transporting) P-glycoproteins. *Proc. Natl. Acad. Sci. U.S.A*. 94, 4028–4033.

Schwartz, D. E., Vetter, W., and Englert, G. (1970). Trimethoprim metabolites in rat, dog and man: Qualitative and quantitative studies. *Arzneimittelforschung*. 20, 1867–1871.

Segawa, H., Fukasawa, Y., Miyamoto, K., Takeda, E., Endou, H., Kanai, Y., (1999). Identification and functional characterization of a na+-independent neutral amino acid transporter with broad substrate selectivity. *J. Biol. Chem*. 274, 19745–19751

Sekiguchi, K., Obi, N. (1961). Studies on absorption of eutectic mixtures. I. A comparison of the behavior of eutectic mixtures of sulphathiazole and that of ordinary sulphathiazole in man. *Chem. Pharm. Bull*. 9, 866–872

Sekiguchi, K. and Obi, N. (1964). Studies on Absorption of Eutectic Mixture. Ii. Absorption of Fused Conglomerates of Chloramphenicol and Urea in Rabbits.
Chem. Pharm. Bull. 12, 134–144

Seelig, A., Gottschlich, R. and Devant, R.M. (1994). A method to determine the ability of drugs to diffuse through the blood-brain barrier. *Proc. Natl. Acad. Sci. USA*. 91, 68–72.

Serajuddin, A.T.M. (2007). Salt formation to improve drug solubility, *Adv. Drug Deliv. Rev*. 59, 603–616

Serajuddin, A.T.M., Mufson, D. (1985). pH–solubility profiles of organic bases and their hydrochloride salts, *Pharm. Res*. 2, 65–68.

Serajuddin, A.T.M., Jarowski, C.I. (1985). Effect of diffusion layer pH and solubility on the dissolution rate of pharmaceutical bases and their hydrochloride salts I: phenazopyridine, *J. Pharm. Sci.* 74, 142–147.

Shannon., W. Culverhouse., R. Duncan., J. (2003). Analyzing microarray data using cluster analysis., *Pharmacogenomics*. 4,1, 41–51

Shastri, S., Mroszczak, E., Prichard, R.K., Parekh, P., Nguyen, T.H., Hennessey, D.R. Schlitz, R. (1980). Relationship among particle size distribution, dissolution profile, plasma values and anthelmintic efficacy of oxfendazole. *Am. J. Vet. Res*., 41 2095-2101.

Sheikh-Salem, M., Fell, J.T. (1981). Compaction characteristics of mixtures of materials with dissimilar compaction mechanisms, *Int. J. Pharm. Tech. Prod. Mfr*. 2, 19–22.

Shiau, Y.F., Fernandez, P., Jackson, M.J., Mcmonagle, S., (1985). Mechanisms maintaining a low-pH microclimate in the intestine. *Am. J. Physiol*. 248, G608–G617.

Shibata, Y., Fujii, M., Okada, H., Noda, S., Kondoh, M., Watanabe, Y., (2005). Evaluation of the Compaction Properties of a Solid Dispersion ofIndomethacin with Crospovidone by Tableting Process Analyzer. *Chem Pharm Bull*. 53, 7, 759-763.

Shin, H., Landowski C., Sun, D., Amidon, G., (2003). transporters in the GI tract in Drug Bioavailability/Estimation of Solubility, Permeability and Absorption, Waterbeemd H., Lennernas H., Artursson. P., eds. wiley-vch: Germany.

Shih, A.Y., Erb,H., Sun, X., Toda, S., Kalivas, P., Murphy T.H., (2006). Cystine/Glutamate Exchange Modulates Glutathione Supply for Neuroprotection from Oxidative Stress and Cell Proliferation., *The Journal of Neuroscience*, 26, 41, 10514 –10523.

Shore, P.A., Brodie, B.B., Hogben, C.A.M., (1957). The gastric secretion f drugs: a pH partition hypothesis*. J. Pharmacol. Exp. Ther*. 119, 61–369.

Sichina, W.J. Characterization of Water of Hydration of Pharmaceuticals Using the Pyris 6 DSC., available at http://www.metrotec.es/metrotec/WWW_DOC/PETech-54.pdf (Accessed 23/12/2011)

Silverstein, R.M., Webster, F.X., (1998). Spectrometric Identification of Organic Compounds, 6th ed. Wiley: New York.

Simonelli, A.P. et al. (1969). Dissolution rates of high energy polyvinylpyrrolidone (PVP)-sulfathiazole coprecipitates. *J. Pharm. Sci*. 58, 538–549

Singh, B.N., (1999). Effects of food on clinical pharmacokinetics, *Clin. Pharmacokinet*. 37 213–255.

Staniforth, J.N., (2007). Powder flow, in Aulton ME (eds), Pharmaceutics – the science of dosage form design. 3rd ed., Churchill Livingstone: London, UK.

Stahl, H., Wermuth, C.G. (Eds.) (2002). Handbook of Pharmaceutical Salts: Properties, Selection and Use. Wiley-VCH: Zurich.

Stanculescu, I., Manea, M., Chiosa V., Mandravel C., (2006). A THEORETICAL APPROACH TO THE MOLECULAR INTERACTION BETWEEN CHOLESTEROL AND 2-PYRIDINE ALDOXIME METHYL CHLORIDE (2 - PAM)., *Chimie, Anul XV (serie nouă*), I, 101-105

Stella, V.J., (1996). A case for prodrugs: fosphenytoin, *Adv. Drug Deliv. Rev*. 19, 2, 311–330.

Stella, V.J., Zygmunt, J.J., Georg, I.G., Safadi, M.S., (2005). Water-soluble prodrugs of hindered alcohols or phenols, United States patent US 19980131385.

Stenberg, P., Luthman, K., Artursson., (2000). Virtual Screening of intestinal drug permeability. *Journal of Controlled Release*. 65, 231-243.

Spellman PT, Sherlock G, Zhang MQ, Iyer VR, Anders K, Eisen MB, Brown PO, Botstein D, Futcher B. (1998). omprehensive identification of cell cycle-regulated genes of the yeast

Saccharomyces cerevisiae by microarray ybridization. *Molecular Biology of the Cell*. 9, 3273–97.

Soergel, F., Naber, G., Jaedhe, U., Reiter, A., Seelmann, R. Sigl, G. (1989). Brief report: Gastrointestinal secretion of ciprofloxacin. *Am. J. Med., 87* (suppl. 5A), 62-65.

Song, X.; Lorenzi,P.L.; Landowski, C.P.; Vig, B.S.; Hilfinger, J.M.; Amidon, G. (2004). Amino Acid Ester Prodrugs of the Anticancer Agent Gemcitabine: Synthesis, Bioconversion, Metabolic Bioevasion, and hPEPT1-Mediated Transport., *Molecular Pharmaceutics*. 2, 2, 157-167

Southern E, Mir K, Shchepinov M. (1999). Molecular interactions on microarrays. *Nat Genet*. 21, 5-9.

Socrates, G. Infrared Characteristic Group Frequencies, 2nd ed. Wiley: New York, 1994.

Soppelaa, I., Airaksinenb, S., Murtomaac, M., Tenhoc, M., Hataraa, J., Räikkönena, H., Yliruusia, J. Sandlerb, N., (2010). Investigation of the powder flow behaviour of binary mixtures of microcrystalline celluloses and paracetamol., *J. Excipients and Food Chem*. 1, 1.

Sun, C., Grant, J.W., (2001). Compaction Properties of L-Lysine Salts *Pharm. Res*. 18, 3

Sun, H., Seshadri, M. Lingard, S., Monaghan, W., Faoagali, J., Chan, E., McDonald, H., Houston, King, T., Peak, I., Wilson, J. C., Haywood, A., Spencer, B., Dunn P., Grant ., G. (2011). Antibacterial Activity of b-Cyclodextrin and 2-Hydroxypropyl- b-Cyclodextrin Trimethoprim Complexes., *American Journal of Microbiology* 2, 1, 1-8.

Susana, A., Breda, F., Jimenez-Kairuz, H., Manzo, E., (2009). Solubility behavior and biopharmaceutical classification of novel high-solubility ciprofloxacin and norfloxacin pharmaceutical derivatives., *Int. J. Pharm*. 371, 106–113

Sweetman, S.C. (2005) Martindale: The Complete Drug Reference. Pharmaceutical Press. 47

Szabó-Révész, P., Göczõ. H., Pintye-Hódi K., Kása jr P., Erõs, I., Hasznos Nezdei, M. , Farkas, B., (2001). Development of spherical crystal agglomerates of an aspartic acid salt for direct tablet making., *Powder Technology.* 114, 118–124.

Tahvanainena, M., Rotkoa, T., Mäkiläb, E., Santosa, H.A., Nevesa, D., Laaksonen, T., Kallonenc, A. et al., (2012). Tablet preformulations of indomethacin-loaded mesoporous silicon Microparticles., *Intr*. *J. Pharm. Sci* 422, 125– 131

Taipalensuu, J., Rnblom, H., Lindberg, G., et al., (2001). Correlation of Gene Expression of Ten Drug Efflux Proteins of the ATP-Binding Cassette Transporter Family in Normal Human Jejunum and in Human Intestinal Epithelial Caco-2 Cell Monolayers., *The Journal of Pharmacology and Experimental therapeutics*., 299, 1.

Takanaga, H., Mackenzie, B., Peng, J., Hediger M. A. (2005). Characterization of a branched-chain amino-acid transporter SBAT1 (SLC6A15) that is expressed in human brain., *Biochemical and Biophysical Research Communications.* 337, 892–900

Takagi, M., Taki, Y., Sakane, T., Nadai, T., Sezaki, H., Oku, N., Yamashita, S., (1998). A new interpretation of salicylic acid transport across the lipid bilayer: implications of pH-

dependent but not carriermediated absorption from the gastrointestinal tract. *J. Pharmacol. Exp. Ther.* 285, 1175–1180.

Tamai, I., Yabuuchi, H., Nezu, J., Sai, Y., Oku, A., Shimane, M., Tsuji, A. (1997). Cloning and Characterization of a Novel Human pH-dependent Organic Cation Transporter, OCTN1. *FEBS Lett.* 419, 107-111.

Tamai, I. et al. (1998). Improvement of L-dopa absorption by dipeptidyl derivation, utilizing peptide transporter PepT1. *J. Pharm. Sci*. 87, 1542–1546

Tan, W. Colombini., M., (2007). VDAC closure increases calcium ion flux., *Biochimica et Biophysica Acta*. 1768, 2510–2515

Tavelin, S., Milovic, V., Ocklind, G., Olsson, S., Artursson, P., (1999). A conditionally immortalized epithelial cell line for studies of intestinal drug transport. *J. Pharm. Exp. Ther.* 290, 1212-1221.

Thiel-Demby, V. E. Humphreys, J. E. St. John Williams, L. A. Ellens, H. M. Shah, N. Ayrton, and Joseph A. D. Polli., W. (2009). Biopharmaceutics Classification System: Validation and Learnings of an in Vitro Permeability Assay., *Molecular pharmaceutics*. 6, 1, 11–18.

Thwaites, D.T., McEwan, G.T.A., Hirst, B.H., Simmons, N.L., (1995). H+-coupled α-methylaminoisobutyric acid transport in human intestinal Caco-2 cells. *Biochim. Biophys. Acta.* 1234,111-118.

Tran, C.D.H., Timmins, P., Conway, B.R., Irwin, W.J., (2002). Investigation of the coordinated functional activities of Cytochrome P450 3A4 and P-glycoprotein in limiting the absorption of xenobiotics in Caco-2 cells. *J. Pharm. Sci*. 91, 117-128.

Tsuji, A., Simanjuntak, M.T., Tamai, I., Terasaki, T., (1990). pH-Dependent intestinal transport of monocarboxylic acids: carrier-mediated and H(+)-cotransport mechanism versus pH partition hypothesis. *J. Pharm. Sci*. 79, 1123–1124.

Tsuji, A., Takanaga, H., Tamai, I., Terasaki, T., 1994. Transcellular transport of benzoic acid across Caco-2 cells by a pH-dependent and carrier-mediated transport mechanism. *Pharm. Res.* 11, 30–37.

Tsukita, S. Furuse, M. (1999). Occludin and claudins in tight junction strands: leading or supporting players, *Trends Cell Biol*. 9, 268– 273

Tong, P.; Zografi. G. (2001). A Study of Amorphous Molecular Dispersions of Indomethacin and Its Sodium Salt. *J. Pharm. Sci*, 90, 12.

Toukmaji, A., Sagui, C., Board, J., Darden, T., (2000). Efficient particle-mesh Ewald based approach to fixed and induced dipolar interactions. *J Chem Phys.* 113, 24, 10913-10927.

Tung H., Waterson S., Reynolds S.D., (1991). united states patent, 4,994, 604

Turel, I., Zivec, P., Pevec, A., Tempelaar, S., Psomas, G., (2008). Compounds of antibacterial agent ciprofloxacin and magnesium - Crystal structures and molecular modeling calculations. *Eur. J. Inorg. Chem*. 23, 3718-3727.

Uhl, G.R. Kitayama, S. Gregor, P. Nanthakumar, E. Persico, A. Shimada, S. (1992). Neurotransmitter transporter family cDNAs in a rat midbrain library: _orphan transporters_ suggest sizable structural variations, *Brain Res. Mol. Brain Res*. 16, 353–359.

Utsunomiya-Tate, N., Endou, H., Kanai, Y., (1997). Tissue specific variants of glutamate transporter GLT-1. *FEBS Lett*. 416, 312–316.

Upshall, D.G., Gouldstone, S.J., Macey, N., Maidment, M.P., West, S.J. and Yeadon, M., (1990). Conversion of a peptidoaminobenzophenone prodrug to diazepam in vitro. Enzyme isolation and characterisation. *J. Biopharm. Sci*. 1, 111-126.

Van Drooge, D.J. et al. (2006). Characterization of the molecular distribution of drugs in glassy solid dispersions at the nano-meter scale, using differential scanning calorimetry and gravimetric water vapour sorption techniques. *Int. J. Pharm*. 310, 220–229

Van, T., Klooster, G. A., Kolker, H. J., Woutersen-Van Nijnanten, F. M., Noordhoek, J., and Van Miert, A. S. (1992). Determination of trimethoprim and its oxidative metabolites in cell culture media and microsomal incubation mixtures by high performance liquid chromatography. *J. Chromatogr*. 579, 354–360.

Van Veen, B. Maarschalk, K., Bolhuis, G.K., Zuurman, K., Frijlink, H.W., (2000). Tensile strength of tablets containing two materials with a different compaction behaviour, *Int. J. Pharm.* 203, 71–79.

Van Veen, B., Maarschalk, K., Bolhuis, G.K. Frijlink, H.W., (2004). Predicting mechanical properties of compacts containing two components, *Powder Technol*. 139 156–164

Vasconcelos, T., Sarmento, B., Costa., P., (2007), Solid dispersions as strategy to improve oral bioavailability of poor water soluble drugs., *Drug Discovery Today* , 12, 23-24.

Veen, B.V., Maarschalk, V., Bolhuis, G.K., Zuurman, K., Frijlink. H.W., (2000). Tensile strength of tablets containing two materials with a different compaction behaviour., *Int. J. Pharm*. 203, 71–79.

Vromans, H., Lerk, C.F., (1988). Densification properties and compactibility of mixtures of pharmaceutical excipients with and without magnesium stearate. *Int. J. Pharm*. 46, 183–192.

Volk, E.L., Schneider, E., (2003), Wild-type breast cancer resistance protein (BCRP/ABCG2) is a methotrexate polyglutamate transporter, *Cancer Res*. 63, 5538–5543

Wacher, V.J et al., (1998). Role of P-glycoprotein and cytochrome P450 3A in limiting oral absorption of peptides and peptidomimetics. *J. Pharm. Sci*., 87, 1322- 1330.

Walter, E., Kissel, T., Amidon, G.L. , (1996). The intestinal peptide carrier: a potential system for small peptide derived drugs, *Adv. Drug Deliv. Rev*. 20, 33 58.

Wang, J. M., Wolf, R. M., Caldwell, J. W., Kollman, P. A., Case, D. A., 2005. Development and testing of a general amber force field. *Journal of Computational Chemistry*. 26, 1, 114-114.

Washington, N., Washington, C. and Wilson, C. (2001). Physiological Pharmaceutics: Barriers to Drug Absorption, 2nd Ed. Taylor & Francis: London, UK.

Watari, N., Funaki, T., Aizawa, K. and Kaneniwa, N. (1983). Nonlinear assessment of nitrofurantoin bioavailability in rabbits. J*. Pharmacokinet. Biopharm*., 11, 529-545.

Weller, S., Blum, M.R., Doucette, M., Burnette, T., Cederberg, D.M., Miranda, P., Smiley, M.L., (1993). pharmacokinetics of acyclovir prodrug valaciclovir after escalating single and multiple dose administration to normal volunteers. *Clin. Pharmacol. Ther*. 54, 595-605

Wetterich, U., Spahn-Langguth, H., Mutschler, E., Terhaag, B., Rösch, W., Langguth, P., (1996). Evidence for intestinal secretion as an additional clearance pathway of talinolol enantiomers: concentration- and dose-dependent absorption in vitro and in vivo., *Pharm Res*. 13, 4, 514-522.

Wetzstein, H., Stadler, M., Dalhoff, A., Karl, W., (1999). Degradation of Ciprofloxacin by Basidiomycetes and Identification of Metabolites Generated by the Brown Rot Fungus Gloeophyllum striatum. *Applied and environmental microbiology*. 65,4, 1556-1563

Widmaier, E. P., Raff, H. and Strang, K. T. (2011). Vander's Human Physiology: The Mechanisms of Body Function, 12th Ed. McGraw-Hill: New York.

Worth, A.P., Balls, M., ed. (2002). Alternative (non-animal) Methods for Chemicals Testing: Current Status and Future Prospects. *ATLA.* 30, 1, 125

Wu, X., George, R. L., Huang, W., Wang, H., Conway, S. J., Leibach, F. H., Ganapathy, V.(2000). Structural and Functional Characteristics and Tissue Distribution Pattern of Rat OCTN1, an Organic Cation Transporter, Cloned from Placenta. *Biochim. Biophys. Acta*. 1466, 315-327.

Wu, C., Benet, L.Z., (2005). Predicting Drug Disposition via Application of BCS: Transport/Absorption/ Elimination Interplay and Development of a Biopharmaceutics Drug Disposition Classification System., *Pharm Res*. 22, 1.

Wu, C., Best, S.M., Benthamb, A.C., Hancock, B.C., Bonfield. W. (2005). A simple predictive model for the tensile strength of binary tablets. *Eur J Pharm Sci*. 25, 331–336.

Wu, X. W., Brooks, B. R., (2003). Self-guided Langevin dynamics simulation method. *Chemical Physics Letters*. 381 ,3, 512-518.

Zakelj, S., Sturm K., Krist., A., (2006). Ciprofloxacin permeability and its active secretion through rat small intestine in vitro., *Int. J. Pharm*. 313, 175–180

Zeller, V., Janoir, C., Kitzis, M., Gutmann, L., Moreau., N.J., (1997). Active Efflux as a Mechanism of Resistance to Ciprofloxacin in Streptococcus pneumoniae., *Antimicrobial agents and chemotherapy.* 41, 9.

Zhao, Y.H., Le, J., Abraham, M.H., Hersey, A., Eddershaw, P.J., Luscombe, C.N., Boutina, D., Beck, G., Sherborne, B., Cooper, I., Platts, J.A, (2000). Evaluation of Human Intestinal

Absorption Data and Subsequent Derivation of a Quantitative Structure-Activity Relationship (QSAR) with the Abraham Descriptors. *J. Pharm. Sci*. 90,6, 749 – 784.

Yamashita, S., Furubayashi, T., Kataoka, M., Sakane, T., Sezaki, H., Tokuda, H., 2000. Optimized conditions for prediction of intestinal drug permeability using Caco-2 cells. *Eur. J. Pharm. Sci*. 10, 195–204.

Ye , D. Meurs, I. Ohigashi, M. Calpe-Berdiel, L. Habets, K. Zhao Y., et al., (2010). Macrophage ABCA5 deficiency influences cellular cholesterol efflux and increases susceptibility to atherosclerosis in female LDLr knockout mice., *Biochemical and Biophysical Research Communications.* 395, 387–394

Yee, S., (1997). In vitro permeability across Caco-2 cells (colonic) can predict in vivo (small intestinal) absorption in man – fact or myth. *Pharm. Res*. 14, 763–766.

Young, R.C., Mitchell, R.C., Brown, T.H., Ganellin, C.R., Griffiths, R., Jones, M., Rana, K.K., Saunders, D., Smith, I.R., Sore, N.E. and Wilks, T.J. (1988). Development of a new physicochemical model for brain penetration and its application to the design of centrally acting H receptor histamine antagonists. *J. Med. Chem*. 31, 656–671.

Zerangue, N., Kavanaugh, M.P., (1996). ASCT-1 is a neutral amino acid exchanger with chloride channel activity. *J. Biol. Chem*. 271, 27991– 27994.

Zheng, J., Carlson, W.B., Reed, J.S. (1995). The packing density of binary powder mixtures, *J. Eur. Ceram. Soc*. 15, 479–483.

A1.1. Validation of the HPLC method for indomethacin

Indomethacin was eluted using Acetonitrile (60%) and 0.1 M acetic acid (40%) as a mobile phase and pumped at 1.0 mL/min flow rate.

Indomethacin was first solubilised in the mobile phase and λmax was determined using scanning spectrophotometer over wavelength ranging between 200-400 nm. The maximum absorbance was 248 nm, therefore the HPLC detector was set at 248 nm to analyse indomethacin concentration.

HPLC was used as the analysis method and was validated using ICH guidelines; HPLC specificity, precision and linearity were evaluated.

Specificity was evaluated by injecting solution of the free bases (without indomethacin) into the HPLC and absence of any interference peaks at indomethacin retention time (6.5±0.12 min) was demonstrated see figure A1.1.

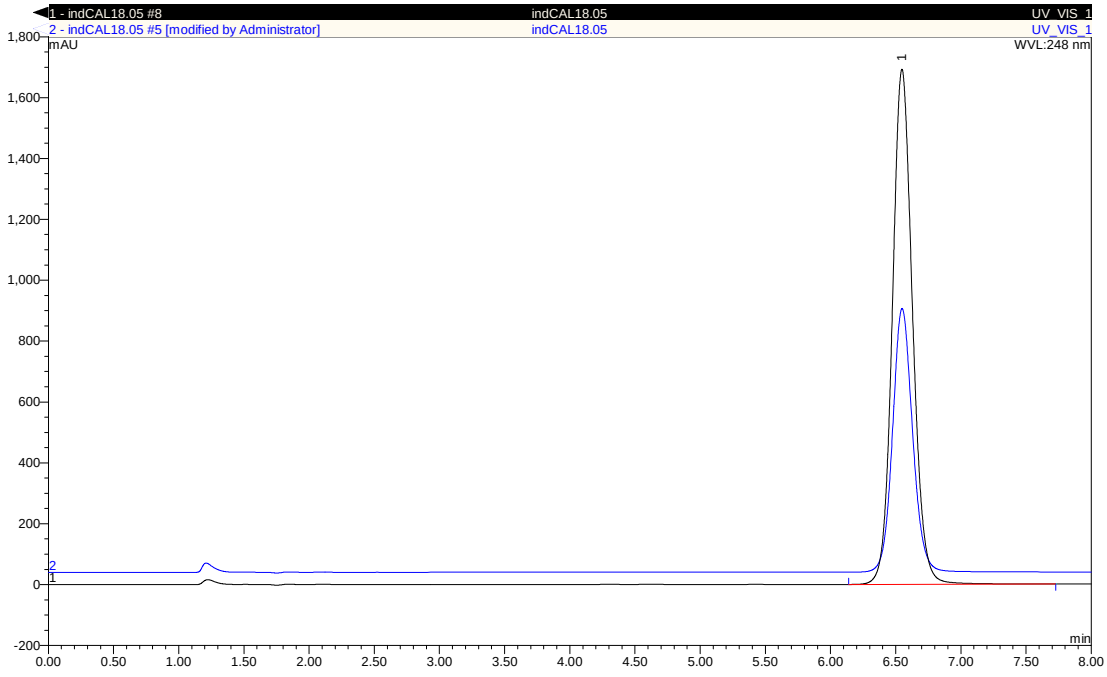

Figure A1.112:- Typical HPLC chromatogram of IND (Concentrations 50 and 100 µg/mL at 248 nm)

Repeatability (Instrumental and method precision) was also evaluated; method precision was demonstrated by preparing indomethacin samples (in concentration range between 10-500µg/mL) in triplicate and injecting them into the HPLC. The peak area R.S.D (%) ranged between 0.5- 1% which is considered acceptable. Instrumental precision was also demonstrated by injecting 100µg/mL indomethacin three times and the R.S.D (%) was 1.06% Inter-day precision was estimated from analysis of freshly prepared samples after few days and no significant difference was observed. The limit of detection (LOD) and limit of quantification (LOQ) were estimated in accordance to standard deviation of response and the slope and calculated using (Equation A1.1)

$$LOD = \frac{3.3\sigma}{S}$$ **Equation A1.65**

where σ is the standard deviation of response (0.025) and S is the slope of the calibration curve (1.54). LOD was found to be 0.05 µg.

Where as LOQ was calculated using equation (A1.2) and the LOQ was found to be 0.15 µg.

$$LOQ = \frac{10\sigma}{S}$$ **Equation 66**

Indomethacin calibration curve was constructed by plotting the peak area against indomethacin concentration over a concentration range between 10-500 µg/mL. Beer-Lambert plot was obtained with curve equation **y= 1.511 x** and correlation factor R^2 = 0.9994 which indicates the good linearity of the curve (Fig. A1.3). Therefore, the curve equation can be used to get any unknown concentration by measuring its peak area.

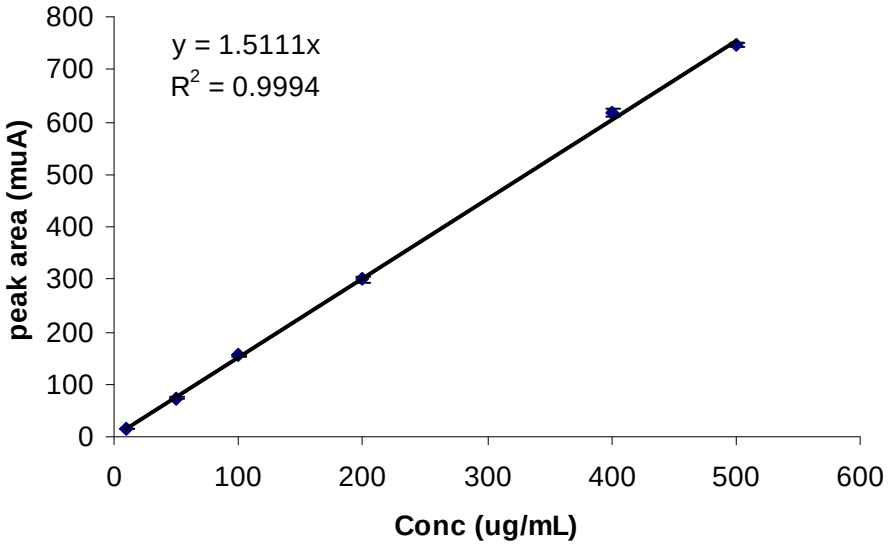

Figure A1.113:- indomethacin calibration curve (n=3)

A1.2. HPLC validation for trimethoprim

HPLC was operated at ambient temperature on RP-C18, (Phenomenex 110A, 150x4.6 mm, 5µm) column using acetonitrile-NaH_2PO_4 buffer (10 mM) (70:30, v/v) (pH 3) as mobile phase which was pumped at 1.0 mL/min flow rate using gradient pump (GP50). λ_{max} was determined by Gallego and Arroyo (2002) to be 230 nm , therefore the HPLC detector was set at 230 nm to analyse TMP concentration. HPLC was used as the analysis method and was validated using ICH guidelines; HPLC specificity, precision and linearity were evaluated as mentioned above in section (A1.1).

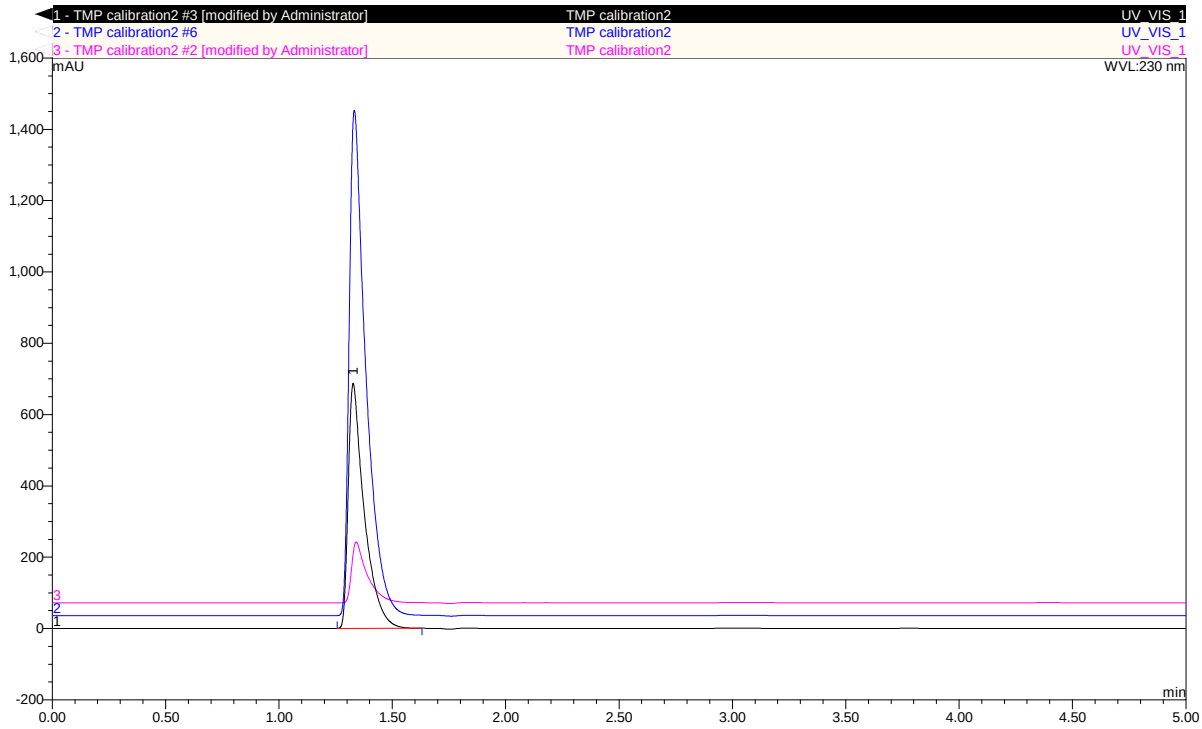

Figure 114:- Typical HPLC chromatogram of TMP (Concentrations 20, 50 and 100 µg/mL at 230 nm)

LOD and LOQ were calculated using standard deviation of response and slope using equation (A1.1 & A1.2). The standard deviation of response (σ) was found to be 0.043 and the slope of the calibration curve (S= 1.54). Applying these values to the equation above LOD and LOQ were found to be 0.109 and 0.364 respectively.

TMP calibration curve was constructed by plotting the peak area against TMP concentration over a concentration range between 10-500 µg/mL. Beer-Lambert plot was obtained with curve equation **y= 1.2 x** and correlation factor R^2 = 0.9992 (Fig. A1.4) which indicates the good linearity of the curve. Therefore, the curve equation can be used to get any unknown concentration by measuring its peak area.

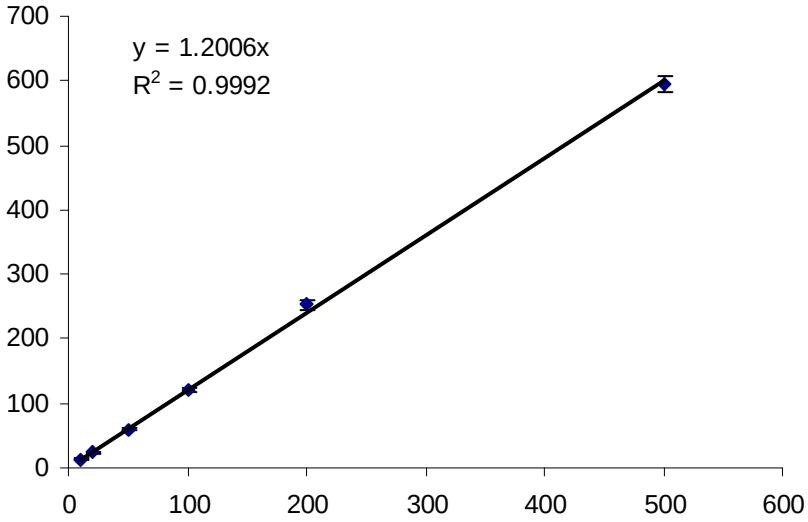

Figure A1.115:- TMP standard calibration curve (n=3)

A1.3. HPLC optimization and validation for Ciprofloxacin

CIP was assayed using HPLC method adapted from (Kmetec et al., 1999). According to Kmetec et al, the mobile phase consists of methanol: 0.02 M phosphate buffer (pH 7) at flow rate of 1mL/min. CIP was found not to be soluble in the mobile phase even at very low concentration. Therefore another method was adapted from (Husain et al., 1995) in which the mobile phase consisted of methanol: water: acetic acid (84:15.9: 0.1) with flow rate of 1 mL/min and λ_{max} of 254 nm. CIP was soluble in the mobile phase, yet a front tailing was observed (Fig. A1.5).

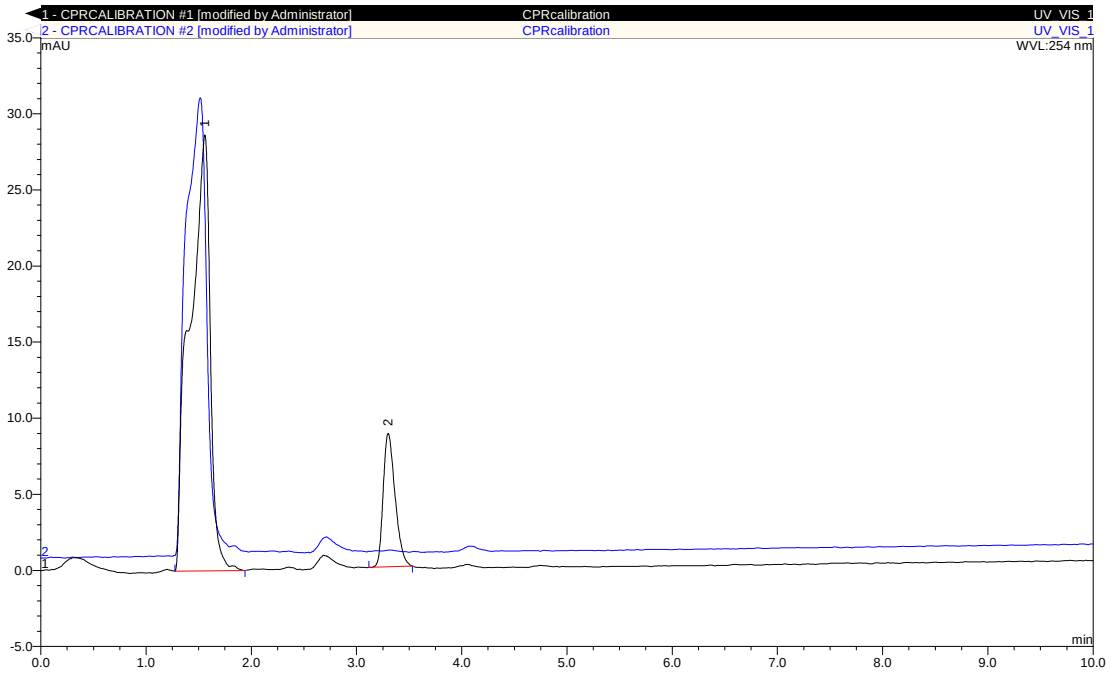

Figure A1.116:- HPLC chromatogram of CIP (concentration 20 and 50 µg/mL at 254 nm)

In order to reduce such tailing, λ_{max} was measured by UV scanning sprctrophotometer and was found to be 280 nm. The UV detector of HPLC was adjusted into the new λ_{max} and a single peak was retained at 1.24 min corresponding to CIP.

A calibration curve was constructed between 10 µg/mL to 200 µg/mL with curve equation of ***y= 1.57x+13.59*** and correlation factor R^2 = 0.996.

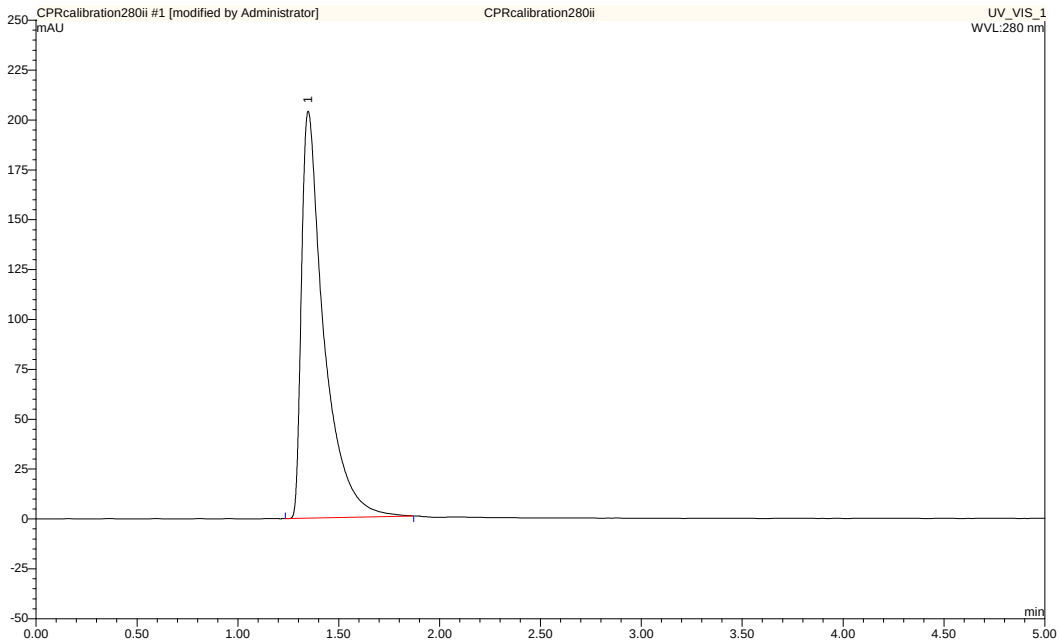

Figure A1.117:- Typical HPLC chromatogram of CIP calibration (Concentration 50µg/mL eluted at 1.24 min using methanol:water: Acetic acid (840:159:1) at 1 ml/min flow rate).

Upon studying CIP saturation solubility in water, a peak tailing was observed (Fig. A1.7). Therefore, it was a must to change the composition of the mobile phase in order to improve the affinity of CIP to the mobile phase and improve the drug retention peak characteristics. Acetic acid ratio has doubled and the new composition of the mobile phase became methanol: water: acetic acid (84:15.8: 0.2).

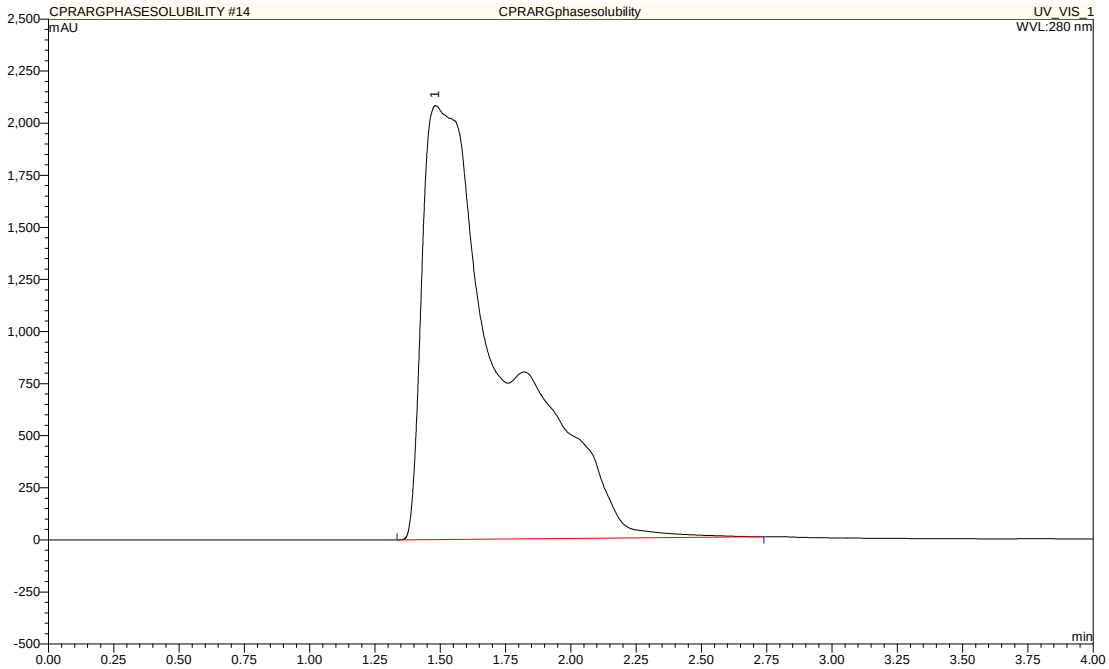

Figure A1.118:- Typical HPLC chromatogram of CIP samples solubilised in water (Saturated solubility, samples were eluted by methanol:water: Acetic acid (840:159:1) at 1 ml/min flow rate).

CIP was solubilised in the new mobile phase and a calibration curve was constructed between 10 and 200 µg/mL with curve equation of ***y=1.53x+18.9*** and R^2 of 0.998. HPLC was used as the analysis method and was validated using ICH guidelines; HPLC specificity, precision and linearity were evaluated as mentioned above in section (A1.1).

LOD and LOQ were calculated using standard deviation of response and slope using equation (A1.1 & A1.2). The standard deviation of response (σ) was found to be 0.056 and the slope of

the calibration curve (S= 1.57). Applying these values to the equation above LOD and LOQ were found to be 0.107 and 0.356 respectively.

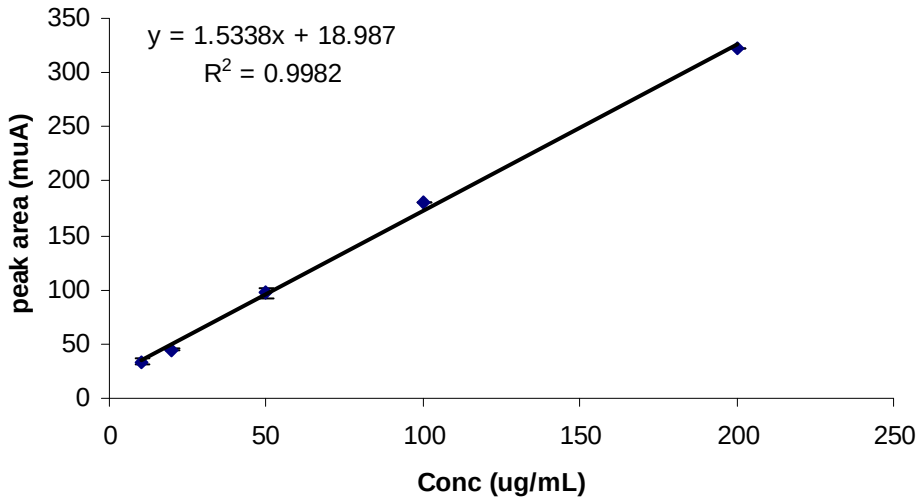

Figure 119:- CIP calibration curve (samples were eluted by methanol:water: Acetic acid (840:158:2) at 1 ml/min flow rate and λ_{max} of 280 nm).

Appendix 2

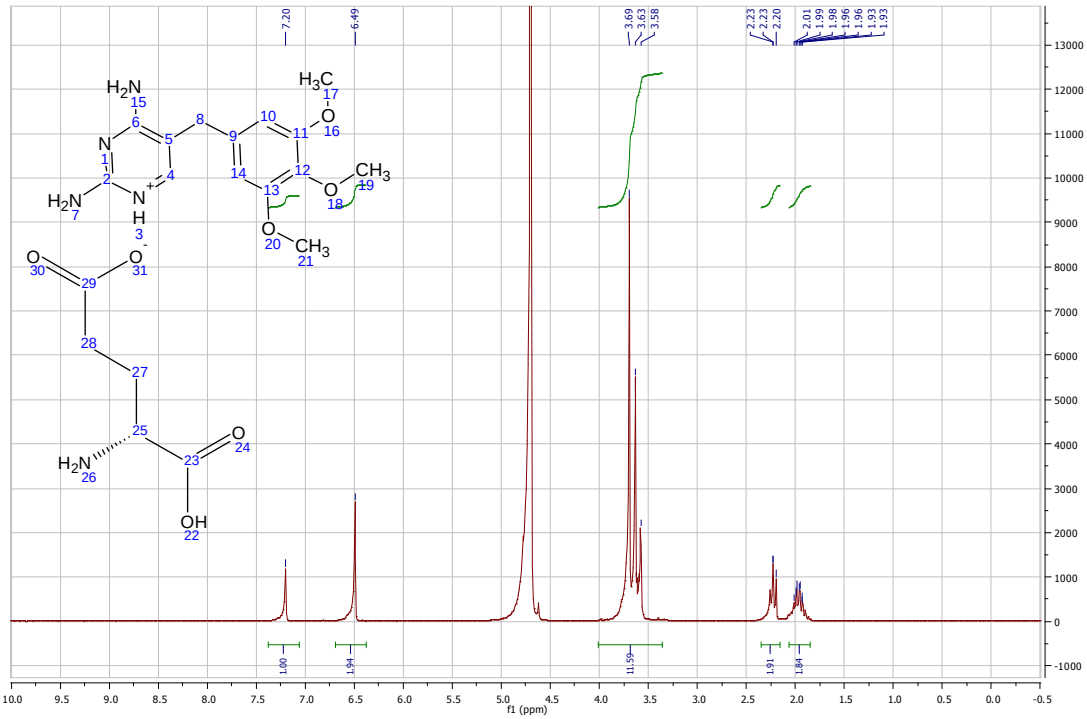

Figure A2.1:-^{1}HNMR spectra of trimethoprim D-glutamate solubilised in D2O.

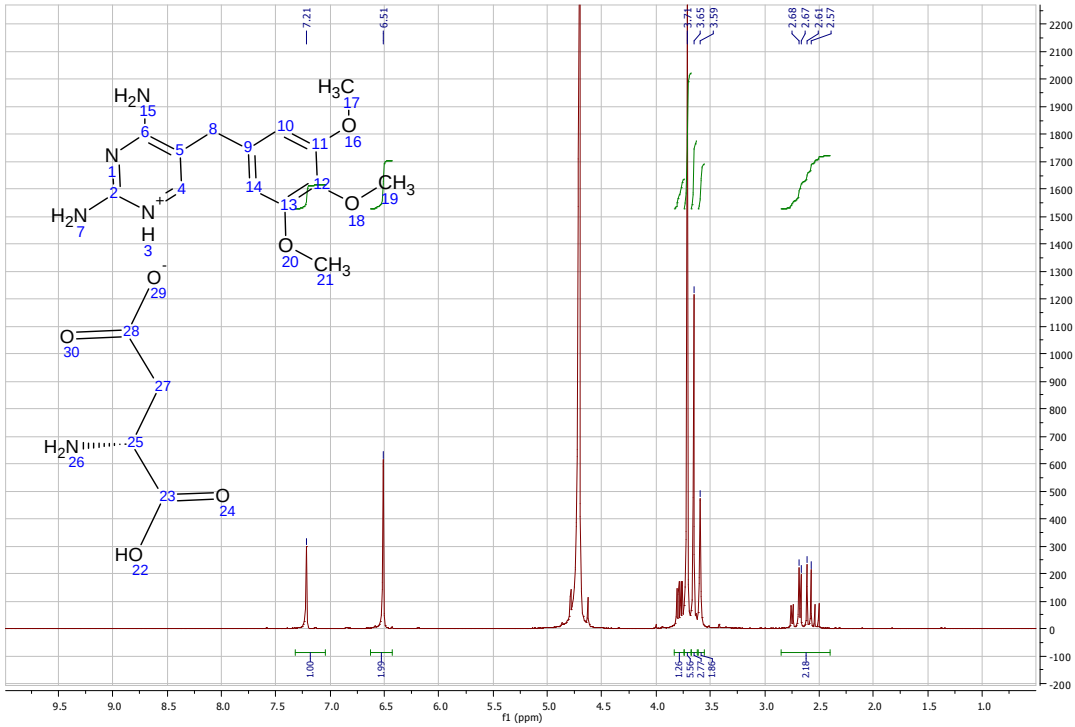

Figure A2.2:- ^{1}HNMR spectra of trimethoprim D- aspartate solubilised in D2O.